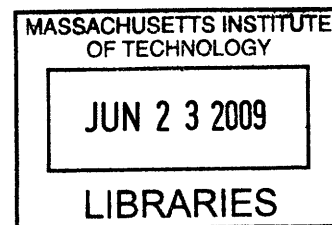# Equilibrium and Dynamics of Ionic Solutions

by

Mihai Anton

Ingénieur de l'Ecole Polytechnique
Ecole Polytechnique, 2006

M.S. Chemical Engineering Practice
Massachusetts Institute of Technology, 2006

SUBMITTED TO THE DEPARTMENT OF CHEMICAL ENGINEERING IN
PARTIAL FULFILLMENT OF THE REQUIREMENT FOR THE DEGREE OF

DOCTOR OF PHILOSOPHY IN CHEMICAL ENGINEERING PRACTICE
AT THE
MASSACHUSETTS INSTITUTE OF TECHNOLOGY

MAY 2009

ARCHIVES

Author...
Department of Chemical Engineering
May 18th, 2009

Certified by...
U (/ (/Gregory J. McRae
Hoyt C. Hottel Professor of Chemical Engineering
Thesis Supervisor

Accepted by...............................   ....
William M. Deen
Carbon P. Dubbs Professor of Chemical Engineering
Chairman, Committee of Graduate Students

Equilibrium and Dynamics of Ionic Solutions

by

Mihai Anton

ABSTRACT

The present work is motivated by the desire to understand the physical mechanism underlying the propagation of nervous influx in neurons as well as the modulation and summation of electrical signals during their progression in dendrites. The survey of existing literature shows that most studies model dendrites and axons as cables and simply ignore the physical basis of these electrical signals. Indeed in neurons as in any cell there exists a potential difference of about 70 mV across the plasmic membrane caused by differences in the concentrations of small ions between the inside and outside of the cell; nervous influx is a temporary alteration of this potential difference that can propagate along the plasmic membrane. Nervous influx is carried by ionic currents flowing both across the membrane and inside the neuron under the membrane. It propagates at velocities comprised between 0.1 m/s and 100 m/s. The present study ambitioned to build a model for the propagation of nervous influx based on ionic currents but the literature on electrolytes did not provide a good fundamental theory to construct such a model. Therefore the subject of the thesis evolved from modeling nervous influx to developing a new fundamental theory of ionic solutions and testing it against available experimental data.

The reference theory was elaborated by Debye and Hückel in the 1930's and is the only full and consistent theory but it is valid only in dilute media because it is insufficient on two points: it considers ions as infinitesimally small and ignores their correlations. Consequently a new theory of small ions is developed in which ions are treated as hard spheres and their correlations are included locally. The new theory is consistent and can be reduced to the Debye-Hückel theory when the radius of ions and the correlation length are taken to be zero.

The theory assigns to each ion an ionic radius corresponding to the extent of its electronic cloud and a hydrated radius corresponding to the extent of its shell of hydration. The solution as a whole has a correlation length determining the volume around each ion in which correlations have a significant effect. The correlation length and the hydrated radii are determined from experimental data, whereas the ionic radii have a fixed value taken from the literature.

The correlation length and the hydrated radii were determined for 75 binary electrolytes by calculating the osmotic coefficient and the mean ionic activity coefficient and by fitting the wealth of experimental data available. Usually three fits were made for each electrolyte. The general fit is always close to experimental points but underestimates the values in the semi-dilute region. The dilute fit and the semi-dilute fit approximate

experimental points very well in their respective regions but markedly stray from them in the concentrated region. The main explanation for the need for three fits is that the correlation length and the hydrated radii actually change with the concentration of ions whereas the model assumes them to be constant. The rate of change being small, the whole set of experimental points can be approximated very well with three fits.

The next step was to compare these three fits with the semi-empirical models of Meissner and Pitzer for the mean ionic activity coefficient. All three are good approximations. The Pitzer model is the most precise for almost all electrolytes; the Meissner model and the present model are equivalent in their accuracy.

Afterwards a short study was performed on multicomponent electrolytes and it confirmed the behavior observed for binary electrolytes. The osmotic coefficient and the mean ionic activity coefficient are usually well approximated in the concentrated and dilute regions and slightly underestimated in the semi-dilute region.

The last part of the present study examines the propagation of linear plane waves. In bulk solutions the propagation is generally conservative and the phase and group velocities are on the order of hundreds of meters per second. The group velocity in bulk solutions provides an upper bound for the velocity of nervous influx; the velocity resulting from diffusion provides a lower bound; the actual mechanism must be a combination of the two depending on local conditions.

In a nutshell the principal objective has been fulfilled: a new theory for ionic solutions has been developed that is valid from infinite dilution to saturation; it reproduces experimental data at equilibrium well. The theory is then applied to describe the propagation of linear waves in bulk solutions and has found group velocities on the order of hundreds of meters per second. Nevertheless the equations studied thus far cannot be applied to describe the environment under the plasmic membrane of neurons because they assume that local concentrations are small perturbations from the bulk concentrations, which is not the case. Thus the other objective of the thesis is only partially fulfilled; ionic waves are a plausible mechanism for the propagation of nervous influx and the most probable one, but the demonstration is incomplete.

Thesis Supervisor: Gregory J. McRae
                      Hoyt C. Hottel Professor of Chemical Engineering

Table of Contents

Table of Figures

Table of Tables

13

Chapter 1   Introduction

I   THESIS STATEMENT

Good models for the behavior and functions of neurons currently exist either at the level of a whole neuron or at the level of functional proteins. Models for whole neurons are derived from the Hodgkin – Huxley model and describe the electrical potential and ionic currents across the cellular membrane. They usually consist of a set of connected cables wrapped in a membrane that allows the passage of certain ionic currents under specific conditions. The equations describing the membrane are empirically determined. This high-level approach has been named Hodgkin – Huxley formalism. In present days, thanks to decades of efforts, almost every type of neuron has a precise model in this framework and current research now focuses on coupling several neurons in order to study small networks.

A second category of models aims at reconstructing a cellular function from the activity of proteins. A well known example is the signaling pathway involving membrane receptors coupled to G-proteins and kinases. Of more interest for neurons are models for individual ionic pumps and ionic channels or for kinesins and dyneins, molecular motors that transport vesicles and organelles along microtubules. Since many proteins have such a mathematical description, current research in this domain focuses on integrating these models and simulating a whole function of the neuron. This approach is known as systems biology.

Models of the dendritic arbor in the Hodgkin – Huxley formalism can accurately reproduce experimentally measured transmembrane electrical tensions and currents but they are quite complicated. Indeed the spatial and temporal variations of the underlying biological structure are captured by expanding the number of adjustable parameters and determining their values empirically. However this approach does absolutely not reflect the physical mechanisms at work in the neuron and these have remained poorly understood. Conversely a good mathematical description of nervous influx based on the actual structure of the neuron would enable real understanding of the phenomena and be predictive.

In neurons electrical signals are caused by the existence of fluctuations in the concentration of ions just under the plasmic membrane. These fluctuations can usually propagate and be summed; they can also be amplified or attenuated by the ion channels and ion pumps. Therefore the thesis aims at constructing a model for the propagation of electrical signals in neurons based on these fluctuations around the equilibrium concentration; the fluctuations are treated as ionic waves. The result would mirror neuronal workings and is expected to unveil the mechanisms for processing signals in dendrites.

Neurons are spanned by several continuous networks of scaffold proteins which constitute the cytoskeleton. The component of the cytoskeleton of interest to this thesis is the cortical network: it consists of a two dimensional mesh of actin filaments situated under the plasmic membrane and it provides support to it. The ultimate objective of the

thesis is to prove that the cortical network conducts the ionic waves that form nervous influx and to describe the mechanism mathematically.

However a consistent theory that includes both the equilibrium and the dynamics of ionic solutions exists only for dilute solutions. Therefore the principal objective of the thesis is to develop a consistent theory of ionic solutions valid for dilute, semi-dilute and concentrated solutions. The theory is to be validated by comparing its predictions of the equilibrium of binary and multicomponent electrolytes with the wealth of experimental data available. Once the equilibrium correctly described, the thesis treats the propagation of linear waves.

The final objective of the thesis, the propagation of nervous influx has not been attained in a reasonable amount of time because the elaboration of the theory of ionic solutions required considerably more efforts than anticipated.

II   MECHANISM FOR THE PROPAGATION OF NERVOUS INFLUX

The modern variants of the Hodgkin – Huxley model are short, fairly simple and reproduce the electrical signals propagating in the axon and axon hillock very well, although they completely neglect the underlying biological structure. The main reason for this success is the very role of the axon: it conducts exactly the same signals rapidly and without loss over long distances and its structure is very regular. Thus simple equations could be devised and empirically adjusted to reflect measurements because there was no need to account for variations in the physical support. Problems appeared when the Hodgkin – Huxley model was transposed to dendrites: they branch, change their diameter and their role is to transmit and process almost any kind of signal, i.e. the signal is amplified, attenuated, deformed or summated with others, whatever its form. Consequently the structure of dendrites varies considerably and models analogous to the model of the axon were too rudimentary to capture such a rich activity. In order to reproduce the behavior of dendrites, these models have kept the same formal approach but have become quite complex. In doing so, they absolutely do not reflect the underlying physical phenomena because they capture experimental data merely through a considerable increase in the number of parameters.

In any cell exists a difference in the electrical potential across the plasmic membrane, the interior being more negatively charged than the exterior. The potential difference is called the resting potential. It is created by ion pumps that selectively expel certain ions from the cell or bring others in. The result is an imbalance in the concentrations of small ions between the cytoplasm and the external medium. The electrical signals that constitute nervous influx are modifications of the resting potential caused by the sudden entry or exit of small ions through ion channels opened momentarily.

For more clarity, follow a figure with successive zooms on a neuron and the mechanism for the propagation of the nervous influx in neurons.
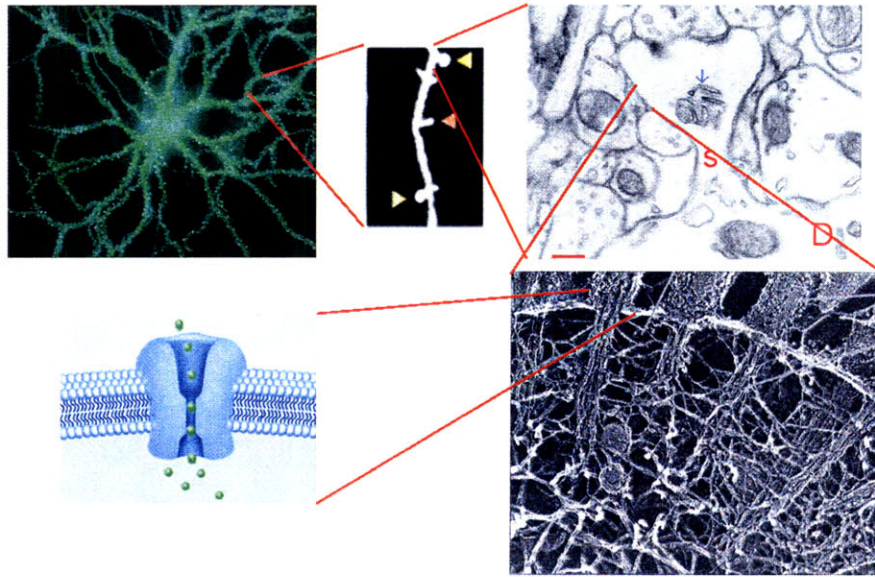
Figure 1: Successive magnifications of neuronal substructures; from the largest to the smallest: a whole neuron, a portion of dendrite, a dendritic spine, postsynaptic density, ion channel

Mechanism for the propagation of nervous influx in dendrites and soma

i. entry of ions into the dendritic spine through the ligand-gated and voltage-gated ion channels when neurotransmitters emitted by the neighboring neuron bind on their receptors

ii. electrical adhesion of these ions to the actin filaments of the postsynaptic density and creation of a local excess of positive or negative charges

iii. propagation of this charge fluctuation along actin filaments through the neck of the dendritic spine and entry into the dendrite proper; note that freely diffusive ions cannot migrate through the neck of the dendritic spine because the actin filaments obstruct it completely

iv. travel of the charge fluctuation along the dendrite then in the soma through the actin cortical network situated underneath the plasmic membrane

v. arrival in the axon hillock and firing of an action potential if the threshold is reached

Actin microfilaments form a two dimensional network under the cellular membrane named the cortical network and prevent the ionic fluctuation from entering the cytoplasm. This ensures that the fluctuation remains localized and does not perturb the activity of other proteins. It also reduces the amount of ions needed to create a significant change in the electrical potential under the membrane because the ions that enter remain confined under the membrane[58]. Last the cortical network of actin is dynamical and its reorganization consumes considerable energy [44]; this continual reorganization has been shown to coincide with variations in the electrical activity of the neuron [35].

16

III   RESEARCH PROGRAM

The research topics follow naturally from the two stated objectives and from the data available in the literature.

First we present in detail the relevant aspects of the anatomy of neurons and review all the models describing the propagation of nervous influx. Very few make use of the physiology of neurons and those that attempt to are utterly unsatisfying. They do not provide a basis for work so the thesis adopts a radically new approach.

Second we survey the theories of aqueous solutions with small ions and with polyelectrolytes to determine the one most suitable for use in the neuronal environment. Again none proves satisfying. The Poisson-Boltzmann theory is consistent but valid only in dilute solutions. However it provides a good reference point for a new theory.

Third a new theory is elaborated that improves on the Poisson-Boltzmann equations by treating ions as hard spheres instead of point charges and by including their correlations.

Fourth the theory is extensively tested against experimental data on the equilibrium of binary electrolytes. It is also compared to two of the most successful semi-empirical approaches describing the equilibrium of binary electrolytes. The new theory performs well, though not better than the semi-empirical approaches.

Fifth the theory is tested against experimental data on the equilibrium of multicomponent electrolytes. It is again compared to the two semi-empirical approaches.

Last comes the study of the propagation of linear ionic waves.

Chapter 2   Nervous system and neurons

I   INTRODUCTION

Mammalian nervous systems consist of two large organs, the brain and the spinal cord, and a vast network of nerves that reach every tissue of the body. The brain and spinal cord form the central nervous system; the nerves form the peripheral nervous system. The peripheral nervous system collects information from the sensory and body organs and, through the afferent nerves, brings it to the central nervous system, where it is duly processed, resulting in commands, that are transmitted to the rest of the body through the efferent nerves [1].

The functions of the nervous system are divided in two categories: the extraneous functions are performed in relation with other organs whereas the intraneous functions are carried out solely by the brain. The main extraneous functions are the perception of the surrounding world through the five senses, the generation of macroscopic motion through muscles, the control of homeostasis and the regulation of the endocrine and immune systems. Intraneous functions are of a higher order such as reflection, attention, memory, apperception, intuition, conscience.

The nervous system accomplishes all these tasks simultaneously, with great precision and rapidity, even in the smallest creatures. For instance the contact of a needle at the tip of a toe is felt in less than a millisecond which means that the information was propagated and processed in this short period of time. Conversely the contact of clothes is usually not felt which underscores the efficacy of selecting relevant information. These are two examples of the formidable abilities of the nervous system, and since the XIXth century scientists have endeavored to discover the physical mechanisms underlying the functioning of this wonder of nature.

II   ANATOMY OF NEURONS

II.1   General physiology

Two kinds of cells exist in the nervous system: neurons, which receive, process and transmit information, and glial cells, which provide support for neurons. Neurons have three distinct regions:

- the soma, which contains the nucleus and most organelles
- the dendritic arbor, which receives and processes electrical signals from other neurons or sensory cells; dendrites are stable protrusions that depart from the soma and regularly divide into two branches
- the axon, a long protrusion that carries electrical signals away from the soma towards other neurons.
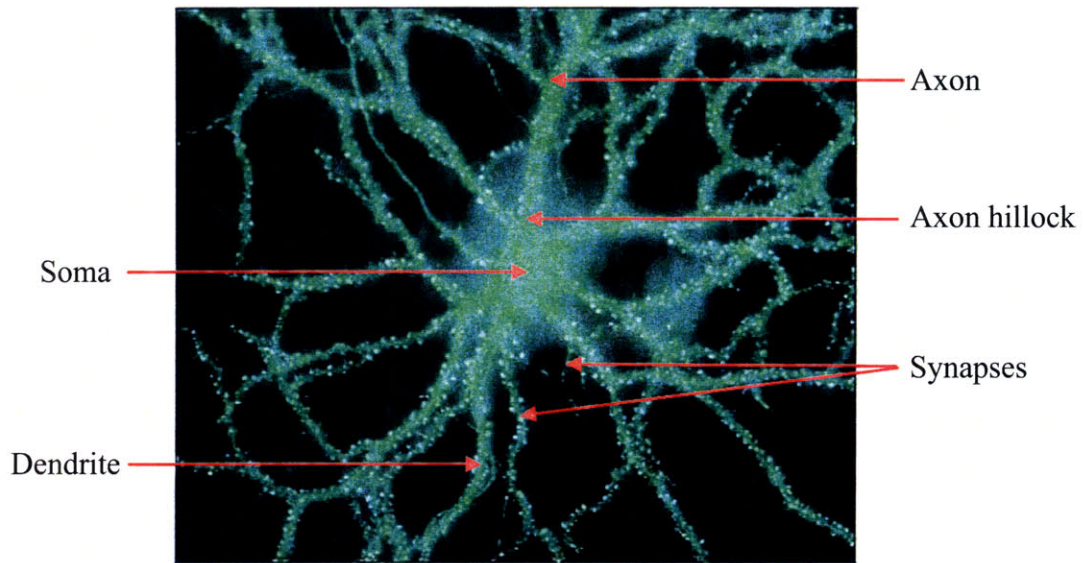
Figure 2: Neuron (from [35])

Resting neurons exhibit a difference in the electrical potential of about 70 mV across their plasmic membrane, their interior being negatively charged. Information is encoded through alterations of this resting potential. In axons, electrical signals have very regular forms and constant amplitude, and propagate without gain or loss; they are called action potentials. In dendrites and soma, the form and amplitude of electrical signals vary considerably: they are called spikes if they exhibit a sharp peak or depolarizations if they are broad; however the distinction is arbitrary [1].
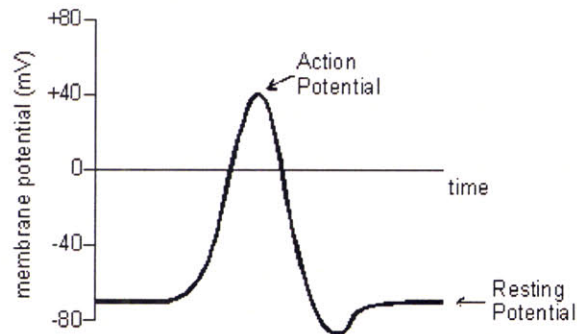
Figure 3: Action potential

In a resting neuron, the concentrations of certain ions are very different from the ones in the extracellular medium:

Table 1: Physiological concentrations of a few ions [1,2]

Ion	Intracellular concentration	Extracellular concentration
Sodium (Na^+)	12 mM	145 mM
Potassium (K^+)	139 mM	4 mM
Chlorine (Cl^-)	4 mM	116 mM
Calcium (Ca^{++})	10^{-4} mM	1.8 mM
Magnesium (Mg^{++})	0.8 mM	1.5 mM
Bicarbonate (HCO_3^-)	12 mM	29 mM
Proteins (X^-)	138 mM	9 mM

The cellular membrane is a lipid bilayer impermeable to small ions. However some membrane proteins, named ion channels, permit ions to migrate across the membrane under specific conditions. Other membrane proteins, named ionic pumps, use ATP to actively transfer ions from one side of the cellular membrane to the other. These two categories of proteins are specific to certain ions. In a resting neuron ionic pumps create large differences between the extracellular and intracellular concentrations of a few ions, as shown in Table 1. Some potassium channels are continuously open and the flow of potassium ions through the membrane generates the resting membrane potential of about – 70 mV. Other ionic channels for sodium, potassium, chlorine and calcium are voltage-gated, meaning that they open and close when the transmembrane potential reaches a threshold. Yet other ionic channels for the same ions are ligand-gated, meaning that they open or close when a specific molecule is attached to them.

When ligand-gated or voltage-gated ionic channels open, the local concentrations of ions change from their resting values, altering the transmembrane potential. If the latter increases the membrane is depolarized; if it decreases the membrane is hyperpolarized. These changes in the electrical potential across the membrane propagate, because within the neuron ions can move parallel to the cellular membrane. The precise interplay of ion channels and pumps is responsible for the conservative propagation of action potentials in the axon and for the amplification or attenuation of spikes in dendrites.

The initial and terminal parts of the axon play a considerable role in the processing of information. Electrical spikes from all parts of the neuron converge in the axon hillock, the incipient part of the axon; there they are summated and if the resulting potential is higher than a threshold, an action potential is fired through the axon. At the other extremity, the axon is divided into numerous branches with swollen tips, called axon terminals or synaptic boutons. Axon terminals are situated very close to the dendrite of another neuron but are not in contact with it, a gap of ~ 25 nm subsisting between the two. The whole structure is called a synapse and the gap, the synaptic cleft. When an action potential arrives in the axon terminals, it induces the release of small molecules, the neurotransmitters, in the synaptic cleft. These molecules diffuse and reach the surface of the neighboring neuron where they attach to specific receptors, often ligand-gated ionic channels, and induce either a depolarization or a hyperpolarization or a more complex metabolic reaction. The newly created electrical perturbation propagates and is processed in the dendrites of the second neuron.

25 neurotransmitters have been identified. The main neurotransmitters in the central nervous system are glutamate which is excitatory, and glycine and γ-aminobutyric

acid which are inhibitory. The types and quantities of neurotransmitters released after an action potential are potent modulators of the overall electric response. The synapse undergoes long term potentiation if the synaptic cleft is narrowed and abundant quantities of excitatory neurotransmitters are released; if the contrary occurs, the synapse undergoes long term depression. These phenomena are thought to play a crucial role in the persistence or vanishing of memories [1,3,4,5].

Nervous influx propagates in a single direction, from the tips of dendrites to the soma and the axon hillock, then through the axon till axon terminals. The main mechanism that enables the unidirectional propagation is the fact that neurotransmitters are released only by axon terminals and that their receptors are located only on the neighboring portion of dendrite. As a matter of fact many experiments have shown that electrical signals can propagate in the opposite direction in axon, soma and dendrites. A last observation is the important functional difference between the dendrites and axon: the role of the axon is to transmit electrical signals rapidly, 1 – 100 m/s, and without loss over long distances, 1 – 2 m; the role of dendrites is not only to transmit the signals over short distances, 0.1 – 1 mm, but also to amplify or attenuate signals, modify their extent and summate several inputs.

II.2   Neural cytoskeleton

After the general features of the neuron follows a description of the neural cytoskeleton, a set of fibers that span the whole neuron, sustain its particular shape and provide a scaffold for other proteins. The cytoskeleton in neurons is composed of three different types of fibers: microfilaments, neurofilaments and microtubules.

Microfilaments are flexible double-stranded helical polymers of actin. They form a three-dimensional network spanning the whole cell and a two-dimensional web under the plasmic membrane called the cortical network. The inner network sustains organelles and large proteins, in order to keep them distributed throughout the cytosol; the cortical network gives its shape to the cell, provides shear resistance to the membrane and supports exocytosis and endocytosis. Sometimes microfilaments assemble in bundles and contribute to the tensile strength of the cell. Microfilaments also serve as tracks for a category of molecular motor protein, the myosins [2], but these are rare in neurons.

Neurofilaments are very stable semi-rigid heteropolymers of neurofilamins. In dendrites and axons they form long axial networks which generate the characteristic cylindrical shape. In general they provide tensile strength and by their stability relieve the stress from the two other types of filaments, enabling them to be reorganized according to the needs of the neuron. Neurofilaments are especially abundant in axons where they form a very regular network responsible for the constant diameter of axons [2].

Microtubules are extremely rigid tubular polymers of the heterodimer of α/β-tubulin. In dendrites and axons they form a ladder network, consisting of long microtubules arranged in parallel and interconnected by the microtubule-associated protein 2. This network mainly provides mechanical support for neurofilaments and microfilaments. Microtubules also serve as tracks for two categories of motor proteins, the dyneins and the kinesins, which transport organelles and vesicles to and from the soma and enable the very long appendices of the neuron to function properly [2].

The three components of the cytoskeleton are intermingled, interconnected and connected to other organelles, vesicles and proteins by a horde of auxiliary proteins. They

21

form a continuous dynamic network that stretches out though the whole neuron. Microfilaments are continuously polymerized, depolymerized and reorganized; it has been estimated that this perpetual remodeling represents about half of the total energy required by neural activity [44]. A fraction of microtubules is also regularly depolymerized and repolymerized; the ladder network of microtubules appears globally stable because it is reorganized only gradually quite unlike the networks of actin. Neurofilaments are much more stable than actin filaments and microtubules but not completely inert; their dynamics have not been investigated as extensively as the behavior of their counterparts.

Table 2: Summary of the cytoskeletal fibers [2,3]

Cytoskeletal components		Characteristic dimensions
Microtubules	Unit: α/β-tubulin heterodimer Fiber: hollow tube of 13 protofilaments Networks: radial distribution around centrioles – longitudinal ladder	Outer diameter: 25 nm Inner diameter: 14 nm
Neurofilaments	Unit: 3 different neurofilamins Fiber: 4 protofilaments form a protofibril – 4 protofibrils are twisted into a semi-rigid rope Networks: cylindrical skeleton shaping the axon and dendrites	Diameter: 10 – 11 nm
Actin filaments	Unit: globular actin Fiber: double-stranded helix Networks: dense web under the plasmic membrane – bundles – sparse web spanning the cytosol	Diameter: 8 – 9 nm

II.3 Repartition of actin

The role of microtubules has been depicted above however for actin filaments a more detailed account follows.

II.3.1 Dendritic spines

In neurons, a substructure is prominent by its high concentration of actin, the dendritic spine. It is a protuberance extending out of a dendrite and connected to the dendrite by a long thin neck. The normal functional shape is similar to a mushroom. Dendritic spines may also be needle-like or hook-like but these shapes correspond to growing or contracting spines that are not fully functional [33]. A Dendritic spine is usually positioned in front of an axon terminal to form a synapse [37].
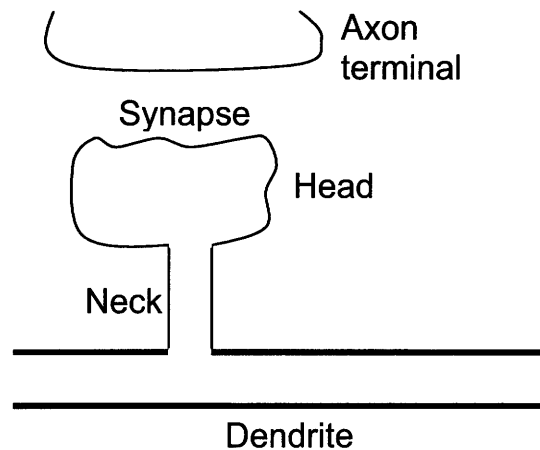
Figure 4: Mushroom-shaped dendritic spine (most common)

The membrane of dendritic spines contains a high density of ionic channels and receptors for neurotransmitters. Under the membrane, exists a very dense network of fibers, the postsynaptic density, which anchors membrane proteins [36], maintains the regular shape of the membrane and positions it with respect to the axon terminal [41]; greater proximity is thought to induce long term potentiation of the synapse, greater distance long term depression [37,38,39]. The main components of the post-synaptic density are actin microfilaments and a few specific scaffold proteins such as schank. The central part of the dendritic spine is occupied by the spinal apparatus, a local specialization of the endoplasmic reticulum; actin filaments span the whole spinal head and link the postsynaptic density to the spinal apparatus [40]. Furthermore numerous actin filaments are present in the neck of the spine and obstruct it completely, effectively preventing the diffusion of ions from the spine to the dendrite. Thus dendritic spines are isolated compartments of ions [37,42,43].

II.3.2 Cortical network in dendrites and soma

The dendrites and soma have an important cortical network that stabilizes ion channels and other membrane receptors. It has been shown that this network undergoes constant remodeling on parallel with neuronal activity [35,44]. In particular an influx of calcium generated by the opening of voltage-gated calcium channels enhances the cortical network in the soma and an influx of calcium caused by the opening of N-methy-D-aspartate channels increases the actin density in dendritic spines [35]. The role of this continuous reorganization has not been understood yet.

II.3.3 Cortical network in axon and synaptic terminals

The cortical network in axons is ordinary and it is continuously remodeled too, albeit less frantically. In synaptic boutons, actin filaments are more numerous than in the axon and have been shown to serve as tracks for myosins that transport vesicles containing neurotransmitters to a reserve pool or deliver them to their release point in the active zone. Actin is thought to play a role in the exocytosis of neurotransmitters too [32,38].

III CURRENT MODELS OF NEURONS

Intracellular measurements were made possible by the design of micropipettes in the late 1940's and the first mathematical models of the membrane and of the axon were elaborated. This led to the gradual development of abstract neural networks and computational neuroscience. Several models of the dendrites have been proposed: they are analogous to those of the axon and reproduce the behavior of dendrites but they are purely phenomenological and do not reflect the inner structure. The Hodgkin – Huxley model and its modern variants rightly capture the physical mechanism underlying conservative propagation in the axon, as well as the initial firing by the axon hillock. However its transpositions to dendrites neglect their specific mechanisms and require a considerable increase in complexity to reproduce their behavior.

III.1 Hodgkin – Huxley model (1952)

In a long series of experiments Hodgkin and Huxley determined the properties of the transmembrane ionic currents in the giant axon of squids and summarized them in a set of equations:

$$C_m \frac{\partial V}{\partial t} - \frac{\partial^2 V}{\partial z^2} = g_{Na} m^3 h \left(V - E_{Na} \right) + g_K n^4 \left(V - E_K \right) + g_L \left(V - E_L \right) + I$$

where V is the transmembrane potential

L represents the persistent leakage current, I an artificial current (μA/cm^2)

m is the activation probability of voltage-gated sodium channels

h is the inactivation probability of voltage-gated sodium channels

n is the activation probability of voltage-gated potassium channels

g_i's are the respective surface conductivities (in mS/cm^2)

E_i's are the reversal potentials of the species (in mV)

C_m is the membrane capacity (μF/cm^2)

The three gating variables are described by $\frac{dx}{dt} = \left(1 - \alpha_x \right) x - \beta_x x$, where x = m, h, n and α's and β's have empirical expressions. More detailed explanations and the numerical values of the parameters are given in appendix A. This set of equations accurately reproduces the generation of action potentials in the axon hillock and their propagation in the axon.
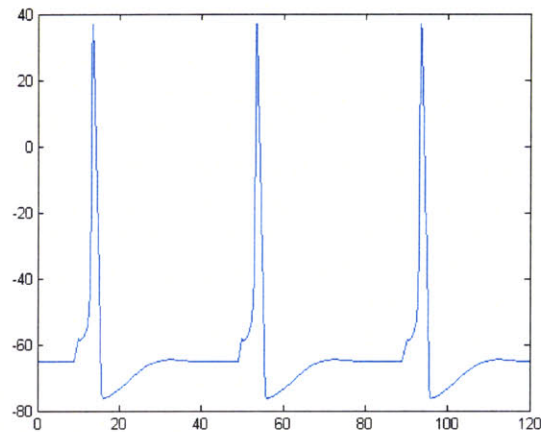
Figure 5: Action potential simulated using the Hodgkin-Huxley model

As research progressed and finer aspects of the firing in the axon hillock have been discovered, other models have sought to adapt and improve the work of Hodgkin and Huxley [3,22].

III.2   Modern developments

The first models to follow the Hodgkin – Huxley model refined it, mainly by adding new ionic currents or by adjusting the existent ones; these models sought to keep a general character. They include the Traub-Miles model, the Connor model and the Crook model. In more recent times research has focused to develop models that are specific and very accurate for a certain type of neurons, for instance hypoglossal motoneurons [24], thalamocortical relay neurons [23] or the pyramidal neurons of the visual cortex [25]. Thus most neurons in the central nervous system have now mathematical descriptions in the "Hodgkin – Huxley formalism". Because of their precision, these models begin to be used to analyze scenarios and design experiments [27]. Few elements of modeling with general purpose, such as continual adaptation [26,64], are discovered nowadays.

III.3   Neural networks

Besides being refined, the Hodgkin – Huxley model has led to development of a mathematical abstraction of the nervous system, the neural network. Such a network is composed of a set of interconnected nodes and each node performs a weighed sum of the inputs and transmits it to the nodes connected to its outputs.
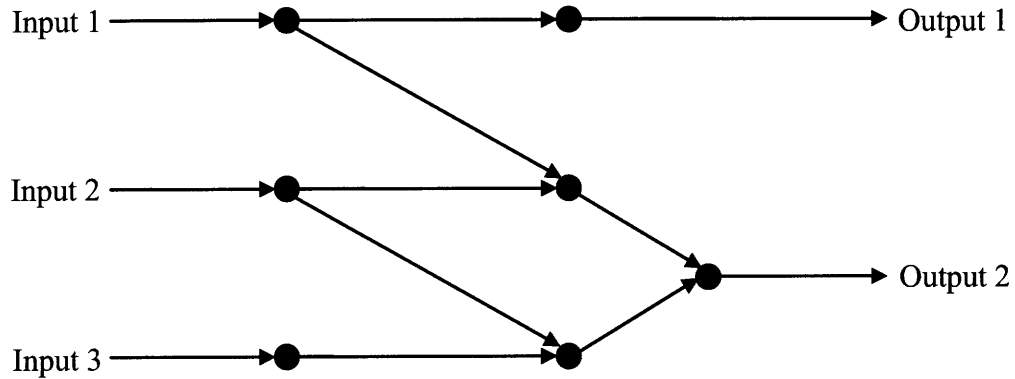
Figure 6: Example of a simple neural network

This sort of computations is thought to mimic the computations performed by the central nervous system. They have found numerous applications in applied mathematics and computer science.

III.4 Cable models for dendrites

In the first attempts the dendritic arbor was modeled as a branching sequence of passive cables [3,4].
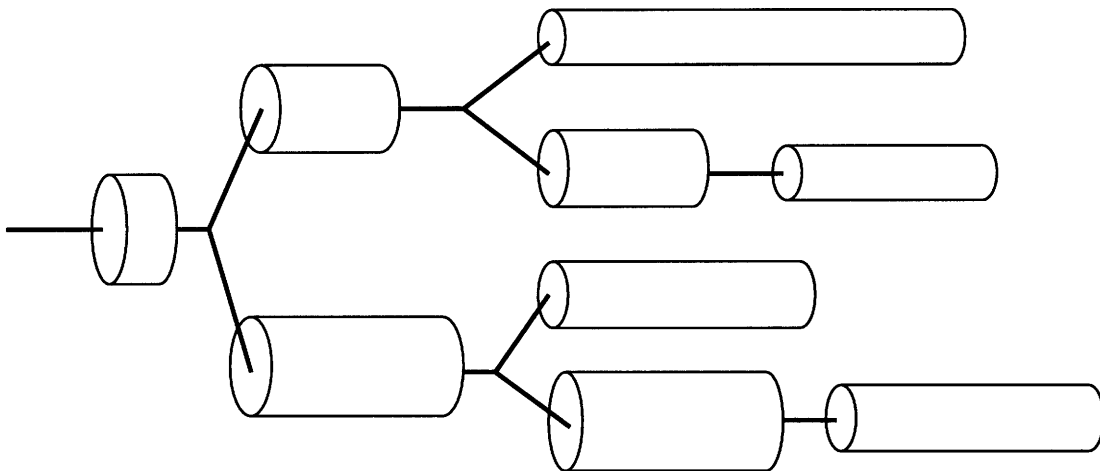
Figure 7: Cable model of a dendritic arbor

The membrane potential in each piece of cable is described by the cable equation [3]:

$$\frac{1}{r_c}\frac{\partial^2 V}{\partial z^2}(z,t) = c_m \frac{\partial V}{\partial t}(z,t) + \frac{1}{r_m}V(z,t)$$

where c_m is the capacitance of the membrane
r_m is the membrane resistance
r_c is the cytosolic resistance

The resistances r_m and r_c may be functions of the position z, the capacitance c_m is normally proportional to the radius. The three parameters can be experimentally determined for portions of dendrites.

Since the overwhelming majority of dendrites have voltage-gated ion channels, the description by passive cables is accurate only for weak depolarizations or hyperpolarizations that do not activate the voltage-gated ion channels. This is usually the case for electrical signals with an amplitude lesser than 5 mV.

III.5   Compartmental model for dendrites

In order to include the non-linear effects induced by the voltage-gated ion channels, the cable equation is discretized with respect to the space variable on a portion of dendrite where the membrane properties are assumed to be constant and an additional ionic current is introduced to account for the voltage-gated ion channels:

$$\frac{1}{r_c}\frac{V_{n+1}-2V_n+V_{n-1}}{\Delta^2}=c_m\frac{dV_n}{dt}+\frac{V_n}{r_m}+I_n$$

Usually $I_n=\sum_{ions} g_i(V_n)(V_n-E_i)$, where E_i is the reversal potential of ion I and g_i its conductance. The whole system of equations is equivalent to modeling the dendrites by a series of compartments:
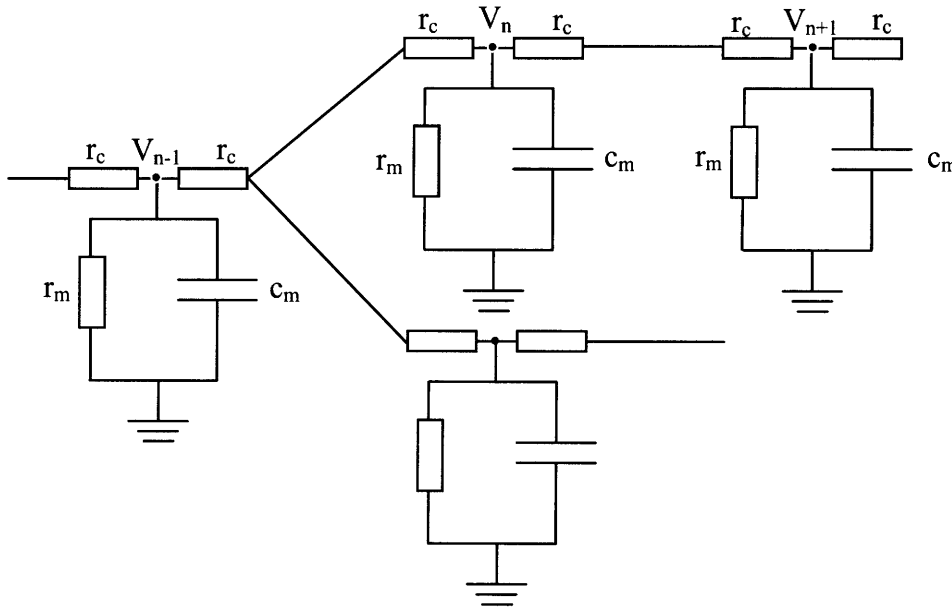
Figure 8: Compartmental model of dendrites

This approach is used to search for numerical solutions for the propagation of post-synaptic potentials in the dendritic arbor. It has been implemented in popular software packages, such as NEURON and GENESIS [3].

III.6 Models based on electrodiffusion

From the end of the 1980's, a new set of models has emerged. They aim to couple the actual variations in the concentration of ions with the transmembrane electrical potential to model the propagation of nervous influx [59,60,61,62]. They represent the state of the art. In these models a dendrite or an axon is represented by a homogenous cylinder, the radius of which may vary, and all properties are assumed to have cylindrical symmetry. Thus the inner structure of the dendrite is ignored and the models are again essentially phenomenological.

The fundamental equations are:

- Poisson equation $$\vec{\nabla}^2 V = -\frac{F}{\varepsilon \varepsilon_0} \sum_{ions} z_i C_i$$

- Transport equation $$\frac{\partial C_i}{\partial t} + \vec{\nabla} \cdot \vec{J_i} = 0 \text{ for every ion i}$$

- Nernst – Planck equation $$\vec{J_i} = -D_i \left(\vec{\nabla} C_i + \frac{z_i F}{RT} C_i \vec{\nabla} V \right) \text{ for every ion i}$$

where   V is the electrical potential   F is the faraday
C_i is the concentration of ion "i" ε_0 is the vacuum permittivity
D_i is the diffusivity of "i" in the cytosol ε is the permittivity of water
T is the temperature   R is the ideal gases constant

The properties of the membrane – capacitance, ion specific resistance, voltage-gated ion channel density – are introduced as boundary conditions. Most of the time voltage-gated ion channels are described by equations similar to those of Hodgkin and Huxley.
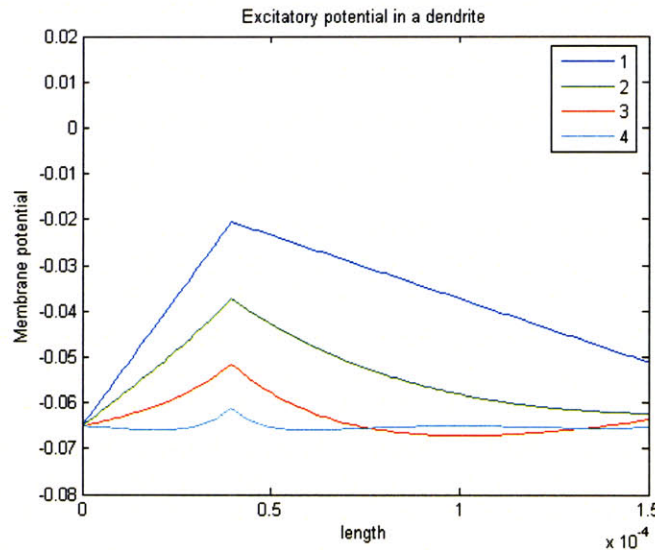
Figure 9: Signal in a dendrite modeled by electrodiffusion

The authors of electrodiffusive models have shown that their models become equivalent to cable models when the diffusivity is taken to zero and this is a criterion of coherence for this type of approach.

Chapter 3   Theories of electrolytes and polyelectrolytes

This chapter provides an overview of the current theories explaining the behavior of aqueous solutions containing small ions and polyelectrolytes. Mathematical methods vary enormously and are discussed in terms of complexity, computational requirements and explanatory power. The first sections describe very general theories; the later sections describe specific tailorings for linear polyelectrolytes and spherical macroions.

I   STANDARD MODELS FOR IONIC SOLUTIONS

A polyelectrolyte is a long linear polymer that bears electrical charges in solution. In this study the solvent is always water. The solution may contain small ions with different valences e.g. Na^+, Cl^-, Ca^{++}, and proteins are represented by negatively charged globular macroions. Concentrations are assumed to be of the same magnitude as physiological concentrations.

Water is usually modeled as a continuum with dielectric constant $\varepsilon = 78.5$ that describes the average shielding of electrical forces. In this representation the molecular character of water, the interactions between water molecules and the interactions with macroions and small ions are neglected. This assumption is reasonable for the water molecules outside the shell of hydration because they interact through dipole – dipole and ion – dipole forces which are weak and short-ranged when compared to electrical forces. The water molecules in the shell of hydration are simply assumed to be attached to the ion and constitute its hydrated radius.

Small ions are modeled as uniformly charged hard spheres, polyelectrolytes as infinitely long and rigid charged cylinders and other macroions commonly as large spheres. With a few exceptions, large ions are assumed to have negligible influence on the dielectric constant. Often all short-ranged repulsive interactions are encompassed in the definition of a distance of closest approach. The set of assumptions made until this point is known as the *primitive model* of ionic solutions. If all small ions are assumed to have the same distance of closest approach the set of assumptions is known as the *restricted primitive model* [46].

In dilute solutions polyelectrolytes and macroions are supposed to exert their influence only in their immediate vicinity and in most of the solution bulk conditions prevail. Then each polyelectrolyte is assumed to be enclosed in a cylindrical cell, each macroion in a spherical cell and these cells are supposed not to overlap. The solution outside the cells is considered to be the bulk of the solution. The sizes of the shells are not determined a priori. This representation of polyelectrolytic solutions is known as the *shell model* [7,8,46].

II   MONTE – CARLO SIMULATIONS

Monte – Carlo simulations are a simple and convenient way to obtain numerical point solutions for the electrical potential and the concentrations of the various ionic

species. They are performed within the models presented in the previous section and are compared with the results of the other theories. Since almost every other theory implicitly or explicitly uses one of the standard models and introduces more approximations for calculations, the comparison with Monte – Carlo simulations assesses the impact and the relevancy of the second set of approximations. The vast majority of studies endeavor to reach good agreement between their theory and appropriate Monte – Carlo simulations.

However very few studies have investigated the agreement of Monte – Carlo simulations with experimental results and hardly any study does compare their own theoretical findings with experimental results.

III   CORRELATION FUNCTIONS IN LIQUIDS

In a liquid containing N particles interacting with potential $U(\underline{r}_1...\underline{r}_N)$, the probability of a configuration is $dw(\underline{r}_1...\underline{r}_N) = \dfrac{e^{-\beta U}}{Z_N} d\underline{r}_1...d\underline{r}_N$. The probability to find any particle at the positions 1, 2, 3 … n is therefore:

$$\rho^{(n)}(\underline{r}_1...\underline{r}_n) = \frac{N!}{(N-n)!} \int \frac{e^{-\beta U}}{Z_N} d\underline{r}_{n+1}...d\underline{r}_N$$

$\rho^{(n)}$ is the n – particle distribution function. $\rho^{(1)}$ is the number density of the liquid. Then the n – particle correlation function is defined by:

$$g_n(\underline{r}_1...\underline{r}_n) = \frac{\rho^{(n)}(\underline{r}_1...\underline{r}_n)}{\rho^{(1)}(\underline{r}_1)...\rho^{(1)}(\underline{r}_n)}$$

For homogenous liquids the relationship simplifies to $\rho^{(n)}(\underline{r}_1...\underline{r}_n) = \rho^n g_n(\underline{r}_1...\underline{r}_n)$, where ρ is the number density. Furthermore the pair correlation function is supposed to depend only on the distance between two particles and not on their absolute position hence we can write $g_2(\underline{r}_1,\underline{r}_2) = g(|\underline{r}_1 - \underline{r}_2|) = g(r)$. The short range order of liquids is mirrored in the form of the pair correlation function:
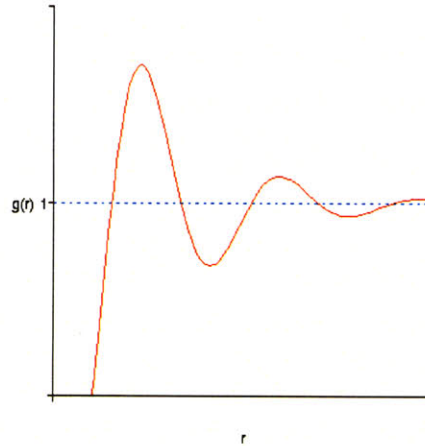
Figure 10: Typical pair correlation function for liquids

The correlation length is defined as the distance at which the oscillations in the pair correlation function vanish. It can reach several molecular diameters.

Another function named the total pair correlation function is defined by:

$$h(\underline{r}_1,\underline{r}_2) = \frac{\rho^{(2)}(\underline{r}_1,\underline{r}_2) - \rho(\underline{r}_1)\rho(\underline{r}_2)}{\rho(\underline{r}_1)\rho(\underline{r}_2)} = g(\underline{r}_1,\underline{r}_2) - 1$$

A few attempts have been made to apply this mathematical framework to ionic solutions in the primitive model, i.e. water is a continuous medium with a dielectric constant of 78.5 and ions are considered to be hard spheres. A successful one is the Pitzer model [13,14,15] and it is examined later as it requires more developments. The hypernetted chain theory [8,11] and the strongly correlated liquid derived from a molten Wigner crystal [93] are two other examples that are discussed eventually.

IV   POISSON-BOLTZMANN THEORY

In the original version of the Poisson-Boltzmann theory, the correlations between small ions were completely neglected and the only interaction taken into account was between the small ions and the closest central ion, linear polyelectrolyte or spheroidal macroion. It is valid within the frame of the shell model and the primitive model with small ions reduced to point charges [10,11]. The Poisson equation relates the mean electrostatic potential to the mean charge density:

$$\nabla^2 \langle V \rangle = -\frac{\langle \rho \rangle}{\varepsilon_0 \varepsilon} \quad \text{and} \quad \langle \rho \rangle = F \sum_{ions} z_i C_i^0 g_i$$

It is further assumed that the correlation functions of small ions are related to the mean electrostatic potential through the Boltzmann equation:

$$g_i = e^{-\frac{z_i e \langle V \rangle}{kT}}$$

Combining the three equations and writing $\langle V \rangle$ as simply V, we obtain the Poisson – Boltzmann equation:

$$\nabla^2 V = -\frac{F}{\varepsilon_0 \varepsilon} \sum_{ions} z_i C_i^0 e^{-\frac{z_i e V}{kT}}$$

V electrical potential	k Boltzmann constant
C_i^0 concentration in absence of electric field	T temperature
z_i charge of "i"	F Faraday
e elementary charge	ε_0 vacuum permittivity
ρ number charge density	ε relative permittivity

In systems without added salts, the equation possesses an analytical solution in cylindrical geometry [65,88,89] (cf. Appendix B for the derivation) and the linearized

31

equation possesses analytical solutions in planar, cylindrical and spherical geometries [11]. For systems that contain salts, approximate analytical solutions have been developed [66]. Otherwise one has to rely on numerical simulations to compute the electrical potential.

The Poisson – Boltzmann theory is a mean-field approximation and yields accurate results solely for monovalent ions and dilute solutions, i.e. for bulk concentrations lesser than 0.1 M. Significant deviations from Monte – Carlo simulations and experimental measurements appear for multivalent ions and for monovalent ions at higher concentrations [72]. The main phenomena that this theory does not capture are the overcharging of polyelectrolytes and other macroions [73], the charge oscillations in their vicinity [71] and the spontaneous bundling of polyelectrolytes [50]. These effects are caused by the existence of an excluded volume due to the finite size of small ions and by the direct electrical interactions between small ions. The excluded volume and electrical interactions between small ions are not negligible with respect to the electrical interaction between small ions and macroions. Nevertheless in the case of dilute solutions of monovalent ions they cancel each other, hence in these conditions the Poisson – Boltzmann equation yields accurate results [46].

A few studies have sought to include excluded volume and electrical interactions among small ions into the Poisson – Boltzmann equation [67,68,69,70]:

$$g_i(r) = \xi_i(r) e^{-\frac{z_i eV}{kT} + \eta_i} \quad \text{and} \quad \nabla^2 V = -\frac{F}{\varepsilon_0 \varepsilon} \sum_{ions} z_i C_i^0 \xi_i(r) e^{-\frac{z_i eV}{kT} + \eta_i}$$

where $\xi_i(r)$ accounts for the excluded volume and η_i for the electrical interactions with neighboring small ions. Both terms are usually given by very complicated ad hoc expressions and only numerical solutions have been determined. There is good agreement between these solutions and Monte – Carlo simulations so the modified Poisson – Boltzmann theory has effectively compensated the shortcomings of the original approach. Nevertheless it has been used much more rarely than the original version because of its complexity, inelegance, computational requirements and disconnect from the rest of the theory of electrochemical systems [6].

V   SEMI-EMPIRICAL THEORIES FOR THE MEAN IONIC ACTIVITY COEFFICIENT

Strong aqueous electrolytes are simple systems for which a wealth of experimental data exists. Their thermodynamic properties are modeled through the ionic activity coefficients γ_i and the mean activity coefficient $\gamma_\pm$, which can be measured experimentally [13,14].

$$\mu_i = \mu_i^0(T) + k_B T \ln \rho_i + RT \ln \gamma_i$$

$$\ln \gamma_\pm = \frac{\sum_{ions} \nu_i \ln \gamma_i}{\sum_{ions} \nu_i}$$

μ_i is the chemical potential, ρ_i is the number density of ion 'i' and v_i is the stoichiometric coefficient of the ion i.e. $\rho_i = v_i \cdot \rho$. Several methods have been developed to calculate the mean ionic activity coefficient from the individual ionic number densities ρ_i. The oldest method is the work of Debye and Hückel; it is based on the Poisson-Boltzmann equations and it is the only full theory of ionic solutions. However it is valid only in dilute solutions and it is known as the Debye- Hückel limiting law [13,14]. All other methods are extensions of the Debye- Hückel theory through semi-empirical formulae. They are focused on binary electrolytes, have arbitrary expressions and parameters to be determined from experimental data; these methods can be used for calculations involving multicomponent electrolytes through mixing rules deducing the required parameters from the binary parameters [13].

The main ones are discussed below: the Meissner model is remarkable because it uses only adjustable parameter per ionic species; the Pitzer model is the best and most widely used model; the Chen model builds on the Pitzer model to include several solvents.

V.1 Debye-Hückel theory

To determine the ionic activity coefficient for and ion α, we must compute the local distribution of ions around the ion α. The Poisson-Boltzmann equations are solved in for a hard sphere with radius R_α and charge z_α.

$$\nabla^2 V = \frac{e}{\varepsilon_0 \varepsilon_r} \sum_{i=1}^{n} z_i \rho_i \quad \text{and} \quad \rho_i = \rho_i^0 e^{-\frac{z_i e V}{k_B T}}$$

For the electrical potential alone

$$\frac{1}{r^2} \frac{d}{dr}\left(r^2 \frac{dV}{dr}\right) = \frac{e}{\varepsilon_0 \varepsilon_r} \sum_{i=1}^{n} z_i \rho_i^0 e^{-\frac{z_i e V}{k_B T}}$$

A small ion bears a charge z_α that usually takes values ± 1, ± 2, ± 3 hence the corresponding electrical field is weak and a linear approximation of the exponential can be used.

$$\frac{1}{r^2} \frac{d}{dr}\left(r^2 \frac{dV}{dr}\right) = -\frac{e^2 V}{\varepsilon_0 \varepsilon_r k_B T} \sum_{i=1}^{n} z_i^2 \rho_i^0$$

We introduce the Bjerrum length l_B and the Debye- Hückel parametrer κ.

$$l_B = \frac{e^2}{4\pi\varepsilon_0 \varepsilon_r k_B T} \qquad \kappa^2 = 4\pi l_B \sum_{i=1}^{n} z_i^2 \rho_i^0 \qquad \frac{1}{r^2} \frac{d}{dr}\left(r^2 \frac{dV}{dr}\right) + \kappa^2 V = 0$$

33

The solution to the differential equation is $V = A\dfrac{e^{\kappa r}}{r} + B\dfrac{e^{-\kappa r}}{r}$. The boundary conditions

are $\lim\limits_{r \to +\infty} V(r) = 0$ and $\dfrac{dV}{dr}(R_\alpha) = -\dfrac{z_\alpha e}{4\pi\varepsilon_0\varepsilon_r R_\alpha^2}$. Therefore A = 0 and

$$-B\left(1 + \kappa R_\alpha\right)\frac{e^{-\kappa R_\alpha}}{R_\alpha^2} = -\frac{z_\alpha e}{4\pi\varepsilon_0\varepsilon_r R_\alpha^2}$$

$$B = \frac{z_\alpha e e^{\kappa R_\alpha}}{4\pi\varepsilon_0\varepsilon_r\left(1 + \kappa R_\alpha\right)}$$

Thus

$$V(r) = \frac{z_\alpha e}{4\pi\varepsilon_0\varepsilon_r\left(1 + \kappa R_\alpha\right)}\frac{e^{-\kappa(r - R_\alpha)}}{r}$$

The ionic activity coefficient of ion α is given by the difference between the work required to charge ion α in the presence of all other ions and the work required to charge the ion α alone.

$$k_B T \ln\gamma_\alpha = \int_0^{z_\alpha} V(R_\alpha)\,e\,dz - \int_0^{z_\alpha} \frac{ze}{4\pi\varepsilon_0\varepsilon_r R_\alpha}\,e\,dz$$

$$k_B T \ln\gamma_\alpha = \frac{z_\alpha^2 e^2}{8\pi\varepsilon_0\varepsilon_r R_\alpha\left(1 + \kappa R_\alpha\right)} - \frac{z_\alpha^2 e^2}{8\pi\varepsilon_0\varepsilon_r R_\alpha}$$

$$k_B T \ln\gamma_\alpha = -\frac{z_\alpha^2 e^2 \kappa}{8\pi\varepsilon_0\varepsilon_r\left(1 + \kappa R_\alpha\right)}$$

$$\ln\gamma_\alpha = -\frac{1}{2}z_\alpha^2\frac{\kappa l_B}{1 + \kappa R_\alpha}$$

In the Poisson-Boltzmann framework, ions are assumed to be infinitely small. Therefore we must take the limit of $R_\alpha \to 0$ and the resulting formula is the only one properly valid.

$$\ln\gamma_\alpha = -\frac{1}{2}z_\alpha^2\kappa l_B$$

The mean ionic activity coefficient is

$$\ln\gamma_\pm = -\frac{\kappa l_B}{2}\frac{\displaystyle\sum_{i=1}^{n}\nu_i z_i^2}{\displaystyle\sum_{i=1}^{n}\nu_i}$$

34

We introduce the ionic strength I in the equation above.

$$I = \frac{1}{2}\sum_{i=1}^{n} z_i^2 \rho_i^0 \qquad \kappa^2 = 8\pi l_B I$$

$$\ln \gamma_\pm = -\sqrt{2\pi l_B^3}\sqrt{I}\,\frac{\sum_{i=1}^{n}\nu_i z_i^2}{\sum_{i=1}^{n}\nu_i} = -A\sqrt{I}\,\frac{\sum_{i=1}^{n}\nu_i z_i^2}{\sum_{i=1}^{n}\nu_i}$$

For an aqueous solution at room temperature, 298 K, $l_B = 7.1$ Å and $A = 1.171$ (L/mol)$^{1/2}$. This formula is the Debye-Hückel limiting law and is valid at low ionic strengths, typically less than 10^{-2} or 10^{-3} mol/L [13]. For aqueous binary electrolytes, the solution is electroneutral, $\nu_1 z_1 + \nu_2 z_2 = 0$, and the mean ionic activity coefficient is written in a more simple form

$$\ln \gamma_\pm = -A\sqrt{I}\,\frac{\nu_1 z_1^2 + \nu_2 z_2^2}{\nu_1 + \nu_2} \qquad \nu_1 z_1^2 + \nu_2 z_2^2 = -\left(\nu_1 + \nu_2\right)z_1 z_2$$

$$\ln \gamma_\pm = A z_1 z_2 \sqrt{I}$$

The osmotic coefficient ϕ is related to the mean ionic activity coefficient through a modified form of the Gibbs-Duhem identity.

$$\ln \gamma_\pm = \phi - 1 + \int_0^m \frac{\phi - 1}{m'}dm'$$

m is the molality of the solution i.e. the concentration expressed in moles per kilogram of solvent. In dilute solutions the molality and the molarity are equal. Thus the Debye-Hückel theory also provides a limiting law for the osmotic coefficient.

$$\phi = 1 + \frac{1}{3}A z_1 z_2 \sqrt{I}$$

V.2   Meissner model

Meissner et al. improved the Debye-Hückel limiting law by introducing the reduced mean ionic activity coefficient Γ, which has the same limit at infinite dilution for all binary electrolytes [13,16].

$$\ln \Gamma = \frac{1}{z_1 z_2}\ln \gamma_\pm \qquad \Gamma \underset{I \to 0}{\sim} A\sqrt{I}$$

For binary electrolytes a semi-empirical formula exists that has only one parameter per electrolyte, which makes it the most frugal model for ionic solutions.

$$\Gamma = \left[1 + B\left(1 + \frac{I}{10}\right)^q - B\right]\Gamma^*$$

$$B = \frac{3}{4} - \frac{13}{200}q \quad \ln\Gamma^* = -\frac{1.1759\sqrt{I}}{1 + C\sqrt{I}} \quad C = 1 + \frac{11}{200}qe^{-0.023I^3} \quad I = \frac{1}{2}\left(m_1 z_1^2 + m_2 z_2^2\right)$$

m_1 and m_2 are the concentrations of each ion expressed in mol/kg solvent. I is the ionic strength on a molal basis. q is a parameter determined empirically for each electrolyte. The values for q are tabulated in reference [16] and the ones used in this work are given in appendix D, Table 9.

Several methods exist to extend this approach to multicomponent electrolytes. The simplest one is a mixing rule that computes the q parameter for an electrolyte $\alpha\beta$ in a mixture of strong electrolytes [16]. By convention α is the cation and β the anion.

$$q_{ij,mix} = \frac{1}{I}\left[\sum_{cations}\frac{1}{2}m_c z_c^2 q_{c\beta}^0 + \sum_{anions}\frac{1}{2}m_a z_a^2 q_{\alpha a}^0\right]$$

q_{ij}^0 is the q parameter for electrolyte ij in a pure solution. I is again the ionic strength on a molal basis.

V.3   Pitzer model

Pitzer et al. used a third order virial expansion of the excess Gibbs free energy to derive a generic expression for the mean ionic activity coefficient of binary electrolytes then introduced semi-empirical formulae in this frame. This method is the most widely used one and one of the most reliable. We present only the final result of his work [13,14,15,16].

$$\ln\gamma_\pm = -|z_\alpha z_\beta|f^\gamma + B_\pm^\gamma \cdot m + C_\pm^\gamma \cdot m^2$$

$$f^\gamma = A_\phi\left(\frac{\sqrt{I}}{1 + b\sqrt{I}} + \frac{2}{b}\ln\left(1 + b\sqrt{I}\right)\right) \text{ with } A_\phi = 0.3915 \text{ and } b = 1.2$$

$$B_\pm^\gamma = 2\beta_0 + \frac{2\beta_1}{\alpha^2 I}\left[1 - \left(1 + \alpha\sqrt{I} - \frac{\alpha^2}{2}I\right)e^{-\alpha\sqrt{I}}\right] \text{ with } \alpha = 2.0$$

$$C_\pm^\gamma = \frac{3}{2}C_\pm^\phi$$

In the case of 2:2 electrolytes the expression of $B_\pm^\gamma$ is modified:

$$B_\pm^\gamma = 2\beta_0 + \frac{2\beta_1}{\alpha_1^2 I}\left[1 - \left(1 + \alpha_1\sqrt{I} - \frac{\alpha_1^2}{2}I\right)e^{-\alpha_1\sqrt{I}}\right] + \frac{2\beta_2}{\alpha_2^2 I}\left[1 - \left(1 + \alpha_2\sqrt{I} - \frac{\alpha_2^2}{2}I\right)e^{-\alpha_2\sqrt{I}}\right]$$

with $\alpha_1 = 1.4$ and $\alpha_2 = 12$.

Parameters β_0, β_1, β_2 and $C_\pm^\phi$ are adjusted for each electrolyte to fit experimental data.

The Pitzer model also includes similar formulae for the calculation of the osmotic coefficient. These formulae use the same empirical parameters as the mean ionic activity coefficient.

$$\phi = 1 + \left| z_\alpha z_\beta \right| f^\phi + B_\pm^\phi \cdot m + C_\pm^\phi \cdot m^2$$

$$f^\phi = -\frac{A_\phi \sqrt{I}}{1 + 1.2\sqrt{I}} \quad \text{and} \quad B_\pm^\phi = \beta_0 + \beta_1 e^{-\alpha_1 \sqrt{I}} + \beta_2 e^{-\alpha_2 \sqrt{I}}$$

The formulae for multicomponent electrolytes are extremely cumbersome and can be found in [16].

V.4 Chen model

The equations of Pitzer work very well for aqueous solutions of strong electrolytes but lose accuracy in the presence of weak electrolytes or molecular species. For instance the use of mixed solvents cannot be handled in his framework. Chen et al. have sought to extend Pitzer's model by combining the long range electrical interactions as described by Pitzer and the short range local composition interactions as described by the non-random two liquids model [13,16]. For a binary electrolyte

$$\ln \gamma_\pm = \ln f_\pm - \ln\left(1 + 0.001 M_s \left(\nu_+ + \nu_-\right) m\right)$$

$f_\pm$ is the activity coefficient on a mole fraction basis. M_s is the molecular mass of the solvent. ν_+ and ν_- are the stoichiometric coefficients. m is the molality of the electrolyte.

$$\ln f_\pm = \ln f_\pm^P + \ln f_\pm^{LC}$$

$$\ln f_\pm^P = -\sqrt{\frac{1000}{M_s}} A_\phi \left[\frac{2\left| z_+ z_- \right|}{\rho} \ln\left(1 + \rho\sqrt{I_X}\right) + \frac{\left| z_+ z_- \right| \left(\sqrt{I_X} - 2I_X^{\frac{3}{2}}\right)}{1 + \rho\sqrt{I_X}} \right]$$

$A_\phi = 0.3195 \qquad \rho = 14.9 \qquad I_X = \frac{1}{2}\sum_{i=1}^{n} x_i z_i^2 = \text{ionic strength on molar fraction basis}$

The molar fractions of the ions can be computed from the molality.

$$x_i = \frac{\nu_i m}{m + 1000/M_s}$$

The local composition part of the ionic activity coefficient follows.

$$\ln f_\pm^{LC} = \frac{\nu_+ \ln f_+^{LC} + \nu_- \ln f_-^{LC}}{\nu_+ + \nu_-}$$

37

$$\ln f_+^{LC} = \frac{x_s^2 \tau_{\pm,s} e^{-\alpha\tau_{\pm,s}}}{\left(x_+ e^{-\alpha\tau_{\pm,s}} + x_- e^{-\alpha\tau_{\pm,s}} + x_s\right)^2} - \frac{z_- x_- x_s \tau_{s,\pm} e^{-\alpha\tau_{s,\pm}}}{\left(x_+ + x_s e^{-\alpha\tau_{s,\pm}}\right)^2} + \frac{z_+ x_s \tau_{s,\pm} e^{-\alpha\tau_{s,\pm}}}{x_- + x_s e^{-\alpha\tau_{s,\pm}}} - z_+ \tau_{s,\pm} - \tau_{\pm,s} e^{-\alpha\tau_{\pm,s}}$$

$$\ln f_-^{LC} = \frac{x_s^2 \tau_{\pm,s} e^{-\alpha\tau_{\pm,s}}}{\left(x_+ e^{-\alpha\tau_{\pm,s}} + x_- e^{-\alpha\tau_{\pm,s}} + x_s\right)^2} - \frac{z_+ x_+ x_s \tau_{s,\pm} e^{-\alpha\tau_{s,\pm}}}{\left(x_- + x_s e^{-\alpha\tau_{s,\pm}}\right)^2} + \frac{z_- x_s \tau_{s,\pm} e^{-\alpha\tau_{s,\pm}}}{x_+ + x_s e^{-\alpha\tau_{s,\pm}}} - z_- \tau_{s,\pm} - \tau_{\pm,s} e^{-\alpha\tau_{\pm,s}}$$

x_+, x_- and x_s are the mole fractions of the cation, the anion and the solvent. In these expressions $\tau_{\pm,s}$ and $\tau_{s,\pm}$ are the Chen parameters, and α is a constant $\alpha = 0.2$. The Chen parameters are determined empirically.

VI   DENSITY FUNCTIONAL THEORY

Classical statistical thermodynamics describe exclusively equilibrium states. The density functional theory postulates that the thermodynamic functions can be expressed as functionals of the N – particle distribution function. If the N – particle distribution function is arbitrary, it is written $\hat{\rho}^{(N)}$; if it is the equilibrium N – particle distribution function, it is written $\rho^{(N)}$. The thermodynamic functionals have three crucial properties:

- they reach an extremum when the N – particle distribution function is the equilibrium N – particle distribution function
- the extremal values are the equilibrium values of the corresponding thermodynamic functions
- there is only one valid intrinsic Helmholtz free energy functional for a given external field.

$$\left(\frac{\delta \mathcal{B}}{\delta \hat{\rho}^{(N)}}\right)_{\hat{\rho}^{(N)} = \rho^{(N)}} \quad \text{and} \quad \mathcal{B}\left[\rho^{(N)}(\underline{r})\right] = B(\underline{r})$$

Papers investigating the behavior of solutions containing polyelectrolytes and colloids use two different but equivalent mathematical treatments. The first class [76,77,78,79,80,81] uses the Helmholz free energy F or the grand potential function Ω. For an open system with M different species enclosed in a volume $\mathcal{V}$ and interacting with an external potential $u_i^{ext}(\underline{r})$:

$$\Omega[\hat{\rho}] = F[\hat{\rho}] + \sum_{i=1}^{M} \int_{\mathcal{V}} \hat{\rho}_i(\underline{r})\left[u_i^{ext}(\underline{r}) - \mu_i\right] d\underline{r}$$

$$F[\hat{\rho}] = kT \sum_{i=1}^{M} \int_{\mathcal{V}} \hat{\rho}_i(\underline{r})\left[\ln\left(\Lambda_i^3 \hat{\rho}_i(\underline{r})\right) - 1\right] + F^{excl\,vol}[\hat{\rho}] + \frac{1}{2}\int_{\mathcal{V}}\int_{\mathcal{V}} e^2 \sum_{i,j} z_i z_j \frac{\hat{\rho}_i(\underline{r}_1)\hat{\rho}_j(\underline{r}_2)}{4\pi\varepsilon_0\varepsilon|\underline{r}_1 - \underline{r}_2|} d\underline{r}_1 d\underline{r}_2 + F^{el}[\hat{\rho}]$$

where $\Lambda_i = \sqrt{\dfrac{h^2}{2\pi m_i kT}}$ is the de Broglie wavelength of species "i", $F^{excl\,vol}$ represents the excess free energy induced by excluded volume interactions and F^{el} the excess free energy due to electrical correlations between particles. The two other terms are the

38

kinetic energy and the mean-field electric energy. If the fluid is assimilated to an ideal gas, we obtain:

$$\Omega[\hat{\rho}] = kT \sum_{i=1}^{M} \int_{V} \hat{\rho}_i(\underline{r}) \left[\ln\left(\Lambda_i^3 \hat{\rho}_i(\underline{r})\right) - 1 \right] d\underline{r} + \sum_{i=1}^{M} \int_{V} \hat{\rho}_i(\underline{r}) \left[u_i^{ext}(\underline{r}) - \mu_i \right] d\underline{r}$$

$$\frac{\delta\Omega}{\delta\hat{\rho}_i} = kT \int_{V} \left[\ln\left(\Lambda_i^3 \hat{\rho}_i(\underline{r})\right) - 1 \right] d\underline{r} + kTV + \int_{V} \left[u_i^{ext}(\underline{r}) - \mu_i \right] d\underline{r}$$

$$\frac{\delta\Omega}{\delta\hat{\rho}_i} = \int_{V} \left[kT \ln\left(\Lambda_i^3 \hat{\rho}_i(\underline{r})\right) + u_i^{ext}(\underline{r}) - \mu_i \right] d\underline{r}$$

$$\left(\frac{\delta\Omega}{\delta\hat{\rho}_i} \right)_{\hat{\rho}_i = \rho_i} = 0 \quad \Leftrightarrow \quad \int_{V} \left[kT \ln\left(\Lambda_i^3 \hat{\rho}_i(\underline{r})\right) + u_i^{ext}(\underline{r}) - \mu_i \right] d\underline{r} = 0$$

since the last equation must be valid for any system, the integrand must be equal to 0 so

$$kT \ln(\rho_i) + u_i^{ext}(\underline{r}) - \mu_i = 0$$

$$\rho_i(\underline{r}) = \frac{1}{\Lambda_i^3} e^{-\frac{u_i^{ext}}{kT} + \frac{\mu_i}{kT}}$$

which is the Boltzmann equation for the shell with small ions surrounding a polyelectrolyte or a colloid. Thus the Poisson equation, which is universally valid, combined with the ideal gas approximation for small ions results in the Poisson – Boltzmann theory. The present day research focuses on finding suitable expression for the excess free energies of excluded volume and of electrical interactions.

The second class of papers uses partition functions that are converted into functionals with the Hubbard – Stratonovich transformation [70,74,75]. This approach is equivalent to the first one, albeit mathematically more difficult. For an open system with M species in a volume V with individual particles interacting through a symmetric pair potential $u_{ij}(\underline{r})$ and interacting with an external potential $e_i(\underline{r})$:

$$\Xi = \sum_{N_1=0}^{+\infty} \cdots \sum_{N_M=0}^{+\infty} \prod_{i=1}^{M} \frac{\exp(\beta\mu_i N_i)}{N_i! \Lambda_i^{3N_i}} \int_{V} \exp\left(-\frac{\beta}{2} \sum_{ip \neq jq} u_{ij}\left(\underline{r}_{ip} - \underline{r}_{jq}\right) - \beta \sum_{ip} e_i\left(\underline{r}_{ip}\right) \right) \prod_{\substack{1 \leq i \leq M \\ 0 \leq p \leq N_i}} d\underline{r}_{ip}$$

where $\beta = \dfrac{1}{kT}$, N_i and μ_i are the number and chemical potential of particles from species "i", $\underline{r}_{ip}$ is the position of the pth particle of species "i", $\Lambda_i = \sqrt{\dfrac{h^2}{2\pi m_i kT}}$ is the de Broglie wavelength of species "i". The Hubbard – Stratonovich transformation yields

39

$$\Xi[e] = \sum_{N_1=0}^{+\infty} \cdots \sum_{N_M=0}^{+\infty} \prod_{i=1}^{M} \frac{\exp(\beta\mu_i N_i)}{N_i! \Lambda_i^{3N_i}} \int_V \exp\left[-\frac{1}{2}\sum_{i\neq j}\int_V \phi_i(\underline{r})(\beta u_{ij})^{-1}(\underline{r}-\underline{r}')\phi_j(\underline{r})d\underline{r}d\underline{r}' \right.$$

$$\left. -\beta\sum_{ip}\left(e_i(\underline{r}_{ip})-i\phi_i(\underline{r}_{ip})\right)\right]\prod_{i=1}^{M}D\phi_i(.)$$

This expression is the starting point. The objective is to construct a valid expression for the functional grand partition function. In this formulation we have:

$$\frac{\delta \ln \Xi[e]}{\delta \hat{e}(\underline{r}_1)} = \beta\rho[e](\underline{r}_1)$$

$$\frac{\delta^2 \ln \Xi[e]}{\delta \hat{e}(\underline{r}_1)\delta\hat{e}(\underline{r}_2)} = -\beta^2\left(\rho^{(2)}[e](\underline{r}_1,\underline{r}_2)-\rho[e](\underline{r}_1)\rho[e](\underline{r}_2)+\rho[e](\underline{r}_1)\delta(\underline{r}_1-\underline{r}_2)\right)$$

In both formal approaches two approximations are made to render the functional more tractable. The first one consist of assuming that the value of the functional grand free energy at a given point depends only on the values of the density at this point; or if two different density distributions coincide at a certain point, the grand free energies corresponding to these density distributions would have the same value at this point [70,76]:

$$\Omega\left[\hat{\rho}(\underline{r}')\right](\underline{r})=\Omega\left[\hat{\rho}(\underline{r})\right](\underline{r})$$

A slightly less restrictive assumption is to suppose that the value of the grand free energy at a point depends on the values of the density in the vicinity, $\mathcal{V}(r)$, of this point [77,78,79,80,81]:

$$\Omega\left[\hat{\rho}(\underline{r}')\right](\underline{r})=\Omega\left[\int_{\mathcal{V}(\underline{r})} \hat{\rho}(\underline{r}')w(\underline{r}-\underline{r}')d\underline{r}'\right](\underline{r})$$

The function w(r) is a weighting function. The next series of approximations depends on the specific geometry and on the properties investigated.

The last generic approximation technique consists in examining the behavior of the equation around the thermodynamic equilibrium values by finding a suitable small parameter and doing a perturbative expansion [74,75].

Finally the results obtained within the density functional theory are compared to Monte – Carlo simulations in order to assess the impact of the approximations; agreement is usually good for almost every phenomenon investigated. No papers present experimental results.

VII HYPERNETTED CHAIN THEORY

A second theoretical approach, based on the correlation functions of liquids, developed in parallel to the elaboration of the density functional theory. Its foundation is the Ornstein – Zernicke equation [8]:

$$h_{ij}\left(r_{ij}\right) = c_{ij}\left(r_{ij}\right) + \sum_{k \text{ species}} \rho_k \int_V c_{ik}\left(r_{ik}\right) h\left(r_{ik}\right) d\underline{r}_k$$

where r_{ij} is the distance between particles i and j, ρ_k is the number density of particles of species k, $h_{ij} = g_{ij} - 1$ is the total correlation function between particles i and j, which is decomposed is the sum of the total direct correlation function c_{ij} and the contributions through a third particle. This equation neglects interactions between particles that require two or more intermediates but, since these contributions are small, it is still very general.

A second relationship between h_{ij} (or g_{ij}) and c_{ij} is needed for the equation to be solvable. This second relationship is called a closure equation and strongly reduces the generality of the system. Five approximations are used in the study of electrolytes (u(r) is an external potential acting on the solution) [8,9]:

- Percus – Yevick approximation

$$c_{ij}\left(r_{ij}\right) = \left(1 + h_{ij}\right)\left(1 - e^{\beta u\left(r_{ij}\right)}\right)$$

it has been successfully used for hard – sphere fluids

- hypernetted chain approximation

$$c_{ij}\left(r_{ij}\right) = h_{ij}\left(r_{ij}\right) - \ln\left[1 + h_{ij}\left(r_{ij}\right)\right] - \beta u\left(r_{ij}\right)$$

it is used for fluids with long – range interactions such as electrical forces

- mean spherical approximation

$$g_{ij}\left(r_{ij}\right) = 0 \text{ for } r_{ij} < \sigma \quad \text{and} \quad c_{ij}\left(r_{ij}\right) = -\beta u\left(r_{ij}\right) \text{ for } r_{ij} > \sigma$$

where σ is the hard-core diameter of the particle; the main advantage is the simplicity and the ability to sometimes obtain analytical results

- Rogers – Young approximation

$$g_{ij}\left(r_{ij}\right) = e^{-\beta u\left(r_{ij}\right)}\left[1 + \frac{\exp\left\{\left(1 - e^{-\alpha r_{ij}}\right)\left(h_{ij}\left(r_{ij}\right) - c_{ij}\left(r_{ij}\right)\right)\right\} - 1}{1 - e^{-\alpha r_{ij}}}\right]$$

when $r_{ij} \to 0$, we obtain the Percus – Yevick approximation; when $r_{ij} \to +\infty$, we obtain the hypernetted chain approximation; it is a reasonably good compromise

- bridge graph approximation

41

$$c_{ij}\left(r_{ij}\right) = h_{ij}\left(r_{ij}\right) - \ln\left[1 + h_{ij}\left(r_{ij}\right)\right] - \beta u\left(r_{ij}\right) + B_{ij}\left(r_{ij}\right)$$

which is a generalization of the hypernetted chain approximation.

It is possible to derive the modified Poisson – Boltzmann equation and the Poisson – Boltzmann equation using the hypernetted chain approximation. The calculations are long and fastidious.

In this approach only numerical solutions can usually be obtained. The hypernetted chain approximation has been extensively used to model the behavior of polyelectrolytes and macroions [71,73,82,83,84,85]. In some papers it was used for both the polyelectrolyte and small ions but computations were heavy and few calculations converged for systems containing multivalent ions [71,82,85]. To circumvent the problem some papers combined the hypernetted chain approximation for large ions and the mean-spherical approximation for small ions; calculations were reported to be simpler and the results compared very favorably with the corresponding Monte – Carlo simulations [71,73,83,84]. The only discrepancy that consistently appears is an overestimation of small ion concentrations close to the surface of the large ion (~ 5Å); this is caused by the neglect of excluded-volume interactions in the hypernetted chain approximation [71,85].

VIII THEORIES OF COUNTERION CONDENSATION

VIII.1 Manning condensation

In the 1970's Manning introduced the notion of condensation of counterions on highly charged polyelectrolytes in order to account for several intriguing experimental observations [86,87]. He described the phenomenon in a simple and straightforward manner: polyelectrolytes were assimilated to infinitely long uniformly charged rigid rods of negligible diameter and small ions were treated in the frame of the Poisson – Boltzmann theory.

$$\vec{\nabla}^2 V = -\frac{F}{\varepsilon\varepsilon_0}\sum_{ions} z_i C_i^0 e^{-\frac{z_i eV}{kT}}$$

The polyelectrolyte has a lineic charge – e/b, b being the average distance between elementary charges. Then for small values of r the electrical potential V(r) is, as a first order approximation, given by the unscreened potential $V(r) = \dfrac{e}{4\pi\varepsilon_0\varepsilon b}\ln r + O(\ln r)$.

Therefore the partition function can be written as

$$Z = \int_0^{+\infty} 4\pi \sum_{small\ ions} e^{-\frac{z_i eV(r)}{kT}} r dr \approx \int_0^R 4\pi \sum_{small\ ions} e^{-\frac{z_i e^2 \ln r}{4\pi\varepsilon\varepsilon_0 kTb}} r dr + \int_R^{+\infty} 4\pi e^{-\frac{V(r)}{kT}} r dr$$

$$Z \approx \int_0^R 4\pi \sum_{small\ ions} r^{1-\frac{z_i e^2}{4\pi\varepsilon\varepsilon_0 kTb}} dr + \int_R^{+\infty} 4\pi e^{-\frac{V(r)}{kT}} r dr$$

42

The partition function must have a finite value therefore $\forall i$, $\dfrac{z_i e^2}{4\pi\varepsilon\varepsilon_0 kTb} \leq 1$. Using the

Bjerrum length $l_B = \dfrac{e^2}{4\pi\varepsilon\varepsilon_0 kT}$, the Manning parameter ξ is defined by $\xi = \dfrac{l_B}{b}$. If for a

species of small ions $\dfrac{1}{z} < \xi$, a fraction of these ions condense onto the polyelectrolyte

and lower its apparent lineic charge which results in $\xi_{apparent} = \dfrac{1}{z}$. Polyelectrolytes with

$\xi > 1$ are said to be highly charged and a fraction of small ions always condense on them.

Zimm et al. proposed a rigorous treatment of condensation for solutions containing a single species of counterions [88,89]. Condensed counterions were defined as the small ions that remain at finite distances from the polyelectrolyte upon infinite dilution. The calculations are detailed in appendix B. A more recent study [94] conducted a thorough analysis of the impact of the boundary conditions of the Poisson – Boltzmann equation on condensation and unveiled three different regimes: absence of condensation on weakly charged polyelectrolytes, saturated condensation on strongly charged polyelectrolytes and unsaturated condensation on strongly charged polyelectrolytes that are insufficiently insulated from the rest of the solution.

These results are similar to those of Manning and moreover have enabled the calculation of the radius delimitating the region in which condensed ions dwell. This radius is known as the Manning radius, R_M. The analysis has been further extended [45,72] to solutions containing several species of small ions by defining the condensed ions as the ions comprised within the Manning radius, the value of this radius being given by the inflexion point of the electrical potential in the graphic of the electrical potential vs. ln(r). This definition has been successfully transposed to spherical, planar and other geometries [90].

Thus condensed counterions are confined in a small region around the macroion [88]. They are not bound to a specific position but free to move. They can escape from the condensed region through an exchange with an uncondensed small ion. Counterions with the highest valence condense first, followed by others with lower valences until the apparent lineic charge is sufficiently reduced. The bond depends only on the valence of the ion and is not specific [86].

The condensation of counterions has been experimentally proven on synthetic polymers such as polyacrylate, polymethacrylate and polystyrene sulfonate and on natural polymers such as DNA and actin filaments. There is quantitative agreement for dilute solutions [87]. However the very notion of condensation is irrelevant for concentrated systems that exhibit overcharging and charge oscillations. In a nutshell counterion condensation is a useful theory for the same dilute solutions where the Poisson – Boltzmann theory is itself valid.

VIII.2 Wigner crystal model

A Wigner crystal is a 2-dimensional or 3-dimensional array of electrons. It arises when electrons are confined and forced into the ground state. These electrons are strongly

correlated to their neighbors and the crystal is structured in order to minimize the coulombic repulsions. Shklovskii et al. attempted to describe the condensation of counterions and the structure of the condensed region in highly concentrated solutions using a Wigner crystal [91,92,93].

A solution of long rigid rods with radius R and lineic charge $-e/b$ in an aqueous solution containing ions with valence z is considered. The energy per counterion in the Wigner crystal is:

$$E = -1.96 \frac{\sqrt{\sigma z^3 e^3}}{\varepsilon}$$

The two important parameters are the inverse dimensionless temperature Γ and the order parameter f.

$$\Gamma = 0.9 \frac{|E|}{kT} \qquad f = \frac{zb}{R}$$

The Wigner crystal rigorously exists only when $\Gamma > 130$. However for $\sigma = 1$ e/nm^2 (~DNA) and $z = 1, 2, 3, 4$ we have $\Gamma = 1.2, 3.5, 6.4, 9.9$. For $5 < \Gamma < 130$ a strongly correlated liquid exists i.e. the long range order of the Wigner crystal has been lost but the short range correlations persist and can be approximated using the correlation functions of the Wigner crystal. Thus for small ions of valence higher than 3, if $f \ll 1$ a two dimensional strongly correlated liquid surrounds each rod and if $f \gg 1$ rods assemble into ordered bundles which are encompassed in a three dimensional strongly correlated liquid. In the case of $f \ll 1$, the rest of the liquid is described with a modified Poisson – Boltzmann equation for which a new boundary condition is derived [91].

Modeling the condensed phase with a molten Wigner crystal improves the theory of Manning because several important experimental phenomena are captured qualitatively: the overcharging of DNA, or more generally of highly charged polyelectrolytes; the attraction of like charged polyelectrolytes; the transition in some polyelectrolyte solutions from a dispersed phase to an ordered nematic phase, when the concentration of small ions reaches an upper threshold; and the converse transition from the nematic phase to a disordered solution when the concentration of small ions reaches a lower threshold [96]. However these phenomena occur with divalent ions too, which is not included in this model since divalent ions are shown to behave like a gas not like a strongly correlated liquid. What is more, most small ions involved in living matter are either monovalent or divalent therefore direct use of this model in the study of the propagation of the nervous influx is ruled out. The strongly correlated liquid model has nevertheless applications in biology, for instance the wrapping of DNA around histones, because these involve mesoions with charges of more than 100 e [96].

Parallel to the attempt of modeling the condensed phase as a Wigner crystal, another group modeled it more simply as a two dimensional fluid in equilibrium with the three dimensional fluid of free ions [97]. The model predicts a smooth condensation for monovalent ions and an abrupt one for divalent cations. However no comparison with either Monte – Carlo simulations or experimental results has been found in the literature.

44

VIII.3 Condensation on non – uniformly charged surfaces

Using the density functional theory, Netz et al. developed a theory, named strong coupling theory that is valid in the opposite limit of the Poisson – Boltzmann theory, i.e. for highly charged macroions, high valence small ions and highly concentrated solutions [74,75]. One of the first applications was the investigation of the differences between a uniformly charged plane and a discretely charge plane with the same average charge density. Their numerical results and their Monte – Carlo simulations agree and show that the density of small ions close to the surface is higher for discretely charged surfaces with charges distributed on a regular lattice [94,95] and considerably higher for discretely charged surfaces with irregularly distributed charges [100]. But in this approach excluded volume effects are neglected which may lead to overestimate the densities of counterions close to the surface.

A second group using another density functional theory studied the impact of discrete distributions of charges in planar and cylindrical geometries in the limit of weak coupling between small ions [97,98,99]. In this approach excluded volume interactions are included and densities can reach a maximal value. The results are similar to those of Netz et al. Both Monte – Carlo simulations and the numerical results concord in predicting higher densities of counterions near discretely charged surfaces and rods [97,98]. In the cylindrical geometry, the condensation of counterions is confirmed but the expected densities are again higher than the results of Manning and his followers [99].

Last ad-hoc models for double-stranded DNA have been developed to account for electrical properties in great detail [101]. The predicted condensation of counterions is coherent with the other theories but again is confronted only with Monte-Carlo simulations.

Thus the predictions of the classical theory of counterion condensation are expected to underestimate the concentrations of counterions in the immediate vicinity of biological polymers such as DNA, actin filaments and microtubules.

VIII.4 Condensation on flexible polymers

Colby, Dobrynin and Rubinstein developed a theory for solutions of flexible polyelectrolytes inspired by the scaling framework of de Gennes [102,109]. In this approach all formulas are defined with an undetermined multiplicative constant. This value of this constant is supposed to be close to 1 and its knowledge has a limited impact on the modeling of the solution. The precise value can be computed in ideal geometries such as infinite cylinders or perfect spheres; however it is usually experimentally determined. The discussion of electrical screening in such solutions is presented with details in Appendix C. The grand merit of this theory is to agree with experimental results [102].

Other authors have used this theory to construct more realistic models of the condensation of counterions on polyelectrolytes. Some models assume that condensed ions are bound to specific sites and form dipoles with the opposite charge borne by the polymer backbone [108]. Other models keep Manning's assumption of counterions that are only territorially bound and free to move along the axis of the polyelectrolyte [103]. Their results are alike and result in smoothing Manning's results.
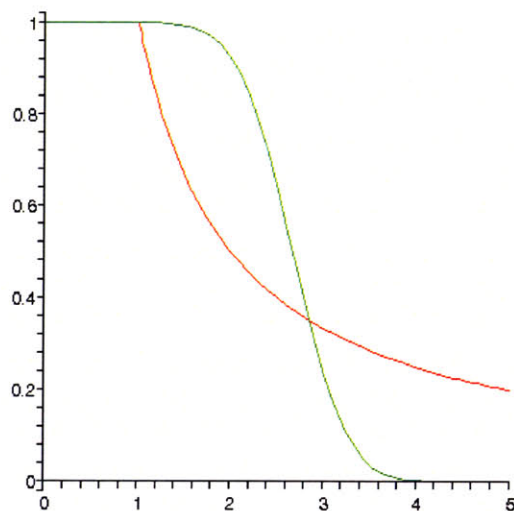
Figure 11: Fraction of uncompensated charges on the polyelectrolyte vs. Manning parameter ξ – Manning's result (red curve) vs. result from flexible polyelectrolyte (green curve)

Another group has used the scaling theory to investigate the electrical conductivity of polyelectrolytes with some success and their results recoup experimental data [105,106,107]. Polyelectrolyte molecules are assumed to be in solution and to exhibit blobs and coils, therefore they differ greatly from microtubules and actin filaments which are organized in regular networks and devoid of blobs and coils. Their approach is nevertheless a reasonably good starting point for the research on the propagation of electrical signals along polyelectrolytes.

The studies mentioned above are valid almost exclusively for monovalent small ions because they are unable to capture the spontaneous bundling of DNA or actin in the presence of divalent or trivalent small ions. These phenomena are described through specific statistical mechanical models and are in good agreement with experimental data [104].

IX   CONCLUSION

Four different fundamental theories and formalisms have been used to capture the physics of ionic solutions: Monte-Carlo simulations, the integral theory of liquids, the Poisson-Boltzmann model and the formalism of density functionals. The other theories mentioned are extensions or corrections to adapt them to specific situations.

Monte-Carlo simulations are quite versatile and cover both static and dynamic approaches but they require a considerable amount of computing power to cover a whole set of configurations and do not enable good understanding of the underlying phenomena. The integral theory of liquids is a powerful restatement of classical thermodynamics but dynamics are completely absent and the ultimate goal of the thesis is a description of ionic currents. The Poisson-Boltzmann model is implicitly linked to the Nernst-Planck equation so introducing dynamics in it is quite feasible; however it ignores the finite size of ions and their higher order interactions so its range of validity is limited to dilute solutions of monovalent ions and any simple extension is ruled out. Semi-empirical

46

extensions exist but they lose the link to the Nernst-Planck equation and dynamics cannot be included in them. Last the formalism of density functionals can be used to capture the equilibrium behavior of ions almost completely and can be extended to capture non-equilibrium states and dynamical behavior; the main objection to it is the immense complexity of the underlying mathematics.

Because working with thermodynamic functions and ionic concentrations is much easier and the interpretation of equations is straightforward, we chose not to use the too abstract density functionals. As a result we have opted for a new study of the thermodynamic functions of solutions with small ions in order to derive a new version of the Nernst-Planck equation that includes the effects of the finite size of ions and of their higher order mutual interactions.

Chapter 4   General equations for solutions containing small ions

I   FUNDAMENTAL LAWS AND ASSUMPTIONS

The solvent is water and is assumed to be a uniform medium with a relative dielectric constant ε_r. Small ions are considered to be uniformly charged hard spheres and to remain constantly hydrated. Their charge is $z_i e$ and their ionic radius is σ_i.

The electrical interaction energy between two ions is written as:

$$E_{ij} = \frac{z_i z_j e^2}{4\pi\varepsilon_0\varepsilon_r \left\| \underline{r}_i - \underline{r}_j \right\|}$$

$$\frac{E_{ij}}{kT} = \frac{z_i z_j e^2}{4\pi\varepsilon_0\varepsilon_r kT \left\| \underline{r}_i - \underline{r}_j \right\|} = z_i z_j \frac{l_B}{\left\| \underline{r}_i - \underline{r}_j \right\|}$$

where $l_B = \dfrac{e^2}{4\pi\varepsilon_0\varepsilon_r kT}$ is the Bjerrum length. For water at T = 298 K, l_B = 7.1 Å.

II   A SOLUTION WITH TWO SMALL IONS

We consider an aqueous solution in a cubic recipient with volume $\underline{W}$. There are two distinct ions in this volume, with charges z_α and z_β and radii σ_α and σ_β. We introduce their arithmetic average σ.

$$\sigma = \frac{\sigma_\alpha + \sigma_\beta}{2}$$

The solution is divided in cubes with edge 2σ. The total number of such small cubes is

$$N = \frac{W}{8\sigma^3}$$

The values of the radii of the two ions are usually close so we assume that the ions are located within these cubes and that their movement is reduced to hopping between neighboring cubes. Two cubes are neighbors if they have a face, a side or a vertex in common. Thus a cube that is not on the surface limiting the solution has 26 neighbors. The distance between the centers of any two neighboring cubes is taken to be 2σ, regardless of their respective positions.
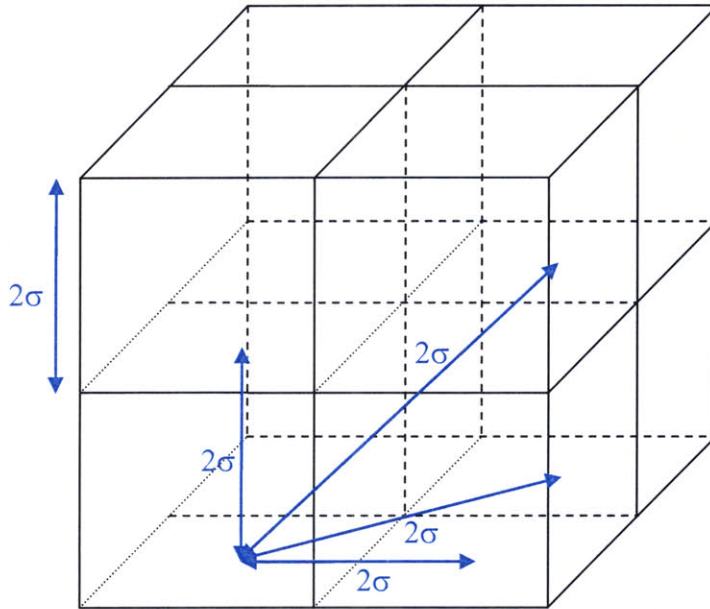
Consequently the distance between any two small cubes can be expressed in multiples of 2σ. We write it as $2\sigma \cdot d$, where d is the minimal number of hops from a cube to a neighboring cube that are necessary to go from one cube to the other. From this point on we refer to the integer d as the distance between two cubes.

The cubes situated within the distance d from a cube form a cube with edge 2d+1. The cubes situated at exactly d from a cube are the envelope of the cube with edge 2d+1. Therefore their total number is

$$(2d + 1)^3 - (2d - 1)^3 = 2(12d^2 + 1)$$

The total number of small cubes is N. We introduce p the number of cubes constituting the edge of the large cube containing the whole solution. We have $N = p^3$. The maximal distance between two small cubes is therefore $p - 1$. We enumerate the small cubes in the following way:
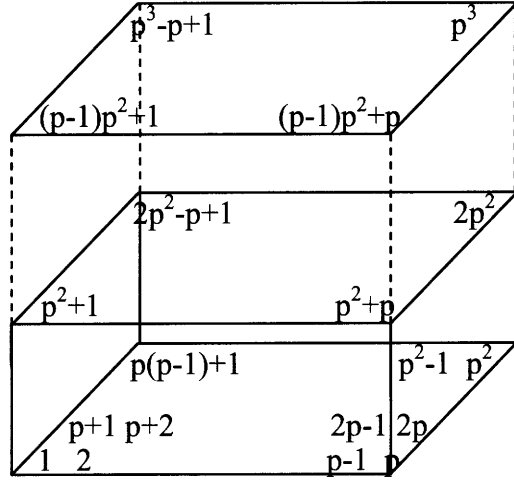
With this enumeration, the distance between the cubes i and j can be computed from

$$d(i,j) = \sup\left\{|i-j|[p], \left\lfloor\frac{|i-j|}{p^2}\right\rfloor, \left\lfloor\frac{|i-j|}{p}\right\rfloor - \left\lfloor\frac{|i-j|}{p^2}\right\rfloor p\right\}$$

|.| is the absolute value, [.] is the modulo, $\lfloor.\rfloor$ is the floor integer part and $\lceil.\rceil$ is ceiling integer part.

In the present setting, the partition function of the two ions in solution is given by

$$Q(1,1) = \sum_{(i,j)\in\Omega} \exp\left(-\frac{z_\alpha z_\beta l_B}{2\sigma d(i,j)}\right)$$

where the set Ω is defined as $([1,N]\times[1,N]) \setminus \{(i,i) ; i\in[1,N]\}$, i.e. the square of integers without its diagonal. The two ions can be distinguishable so there is no factor ½ in front of the sum. We rewrite the partition function as a sum over pairs separated by given distances:

$$Q(1,1) = \sum_{n=1}^{p-1}\sum_{\substack{(i,j)\in\Omega \\ d(i,j)=n}} \exp\left(-\frac{z_\alpha z_\beta l_B}{2\sigma n}\right) = \sum_{n=1}^{p-1} N_n \exp\left(-\frac{z_\alpha z_\beta l_B}{2\sigma n}\right)$$

We turn to the calculation of the number of positions separated by a distance of n and start with the case $n \leq p/2$. A cube far from the border has a set of $2(12n^2+1)$ cubes separated by n; this set forms the envelope of a cube with edge $2n+1$. There are $(p-2n)^3$ such internal cubes.

The cubes close to the borders have fewer correspondents at distance n. We introduce the triplet (i,j,k) representing the distances of a cube from the closest limiting surfaces; i = 0, j = 0 or k = 0 when the cube is on the border. We introduce $v_n(i,j,k)$, the number of cubes that are at distance n from the cube defined by (i,j,k).

- When $i \geq n$, $j \geq n$ and $k \geq n$, the cube is internal and $v_n(i,j,k) = 2(12n^2 + 1)$.
  There are $(p-2n)^3$ cubes of this kind.
- When $i \geq n$, $j \geq n$ and $k \leq n - 1$, the cube is close to a surface.
  There are $6(p-2n)^2$ cubes of this kind for each level k.

50

$$v_n(i,j,k) = 2(12n^2 + 1) - (2n + 1)^2 - 8n(n - k - 1)$$
$$v_n(i,j,k) = 12n^2 + 4(2k + 1)n + 1$$

- When $i \geq n$ and $j \leq n - 1$, $k \leq n - 1$, the cube is close to an edge.
  There are $12(p - 2n)$ cubes of this kind for each combination (j,k).
  $$v_n(i,j,k) = 2(n + k)(n + j) + (2n + 1)(n + k) + (2n + 1)(n + j) + 2n + 1$$
  $$v_n(i,j,k) = 6n^2 + (k + j + 1)(4n + 1) + 2kj$$
- When $i \leq n$, $j \leq n$ and $k \leq n$, the cube is close to a corner.
  There are 8 cubes of this kind for each triplet (j,j,k).
  $$v_n(i,j,k) = (n + i)(n + j) + (n + j)(n + k) + (n + k)(n + i)$$
  $$+ n + i + n + j + n + k + 1$$
  $$v_n(i,j,k) = 3n^2 + 3n + 1 + (i + k + k)(2n + 1) + ij + jk + ki$$

Thus the total number of pairs of ions at distance $n \leq p/2$ from each other is

$$N_n = 2(12n^2 + 1)(p - 2n)^3 + 6(p - 2n)^2 \left[\sum_{i=0}^{n-1} 12n^2 + 4(2i + 1)n + 1 \right]$$

$$+ 12(p - n) \left[\sum_{i=0}^{n-1} \sum_{j=0}^{n-1} 6n^2 + (i + j + 1)(4n + 1) + 2ij \right]$$

$$+ 8 \left[\sum_{i=0}^{n-1} \sum_{j=0}^{n-1} \sum_{k=0}^{n-1} 3n^2 + 3n + 1 + (2n + 1)(i + j + k) + ij + jk + ki \right]$$

$$N_n = 2(12n^2 + 1)(p - 2n)^3 + 6(p - 2n)^2 \left[12n^3 + 4n^2 + n + 4n^2(n - 1) \right]$$

$$+ 12(p - n) \left[6n^4 + (4n + 1)(n^2 + n^2(n - 1)) + \frac{n^2(n - 1)^2}{2} \right]$$

$$+ 8 \left[3n^5 + 3n^4 + n^3 + (2n + 1) \times 3 \frac{n^3(n - 1)}{2} + 3 \frac{n^3(n - 1)^2}{4} \right]$$

$$N_n = 2(12n^2 + 1)(p - 2n)^3 + 6n(16n^2 + 1)(p - 2n)^2$$
$$+ 6n^2(21n^2 + 1)(p - n) + 2n^3(27n^2 + 1)$$

When $n \geq p/2$, all cubes lose correspondents at distance n because of the borders. We use again (i,j,k) the distances of a cube from the border; i, j, $k = 0$ on the border. Then

- When $i \geq p - n$, $j \geq p - n$ and $k \geq p - n$, the cube is close to the centre.
  $v_n(i,j,k) = 0$

- When $i \geq p - n$, $j \geq p - n$ and $k \leq p - n - 1$, the cube is close to a surface.
  There are $6(2n - p)^2$ such cubes for each level k.
  $$v_n(i,j,k) = p^2$$

- When $i \geq p - n$ and $j \leq p - n - 1$, $k \leq p - n - 1$, the cube is close to an edge.

There are 12(2n – p) such cubes for each combination (j,k).

$$v_n\left(i,j,k\right) = p\left(n+k+1\right) + p\left(n+j+1\right) - p$$
$$v_n\left(i,j,k\right) = \left(2n+1+j+k\right)p$$

- When $i \le p - n$, $j \le p - n - 1$ and $k \le p - n - 1$, the cube is close to a corner. There are 8 such cubes for each triplet (i,j,k).

$$v_n\left(i,j,k\right) = \left(n+1+i\right)\left(n+1+j\right) + \left(n+1+j\right)\left(n+1+k\right)$$
$$+ \left(n+1+k\right)\left(n+1+i\right)$$
$$- \left(n+1+i\right) - \left(n+1+j\right) - \left(n+1+k\right) + 1$$
$$v_n\left(i,j,k\right) = 3n^2 + 3n + 1 + \left(2n+1\right)\left(i+j+k\right) + ij + jk + ki$$

Thus the total number of pairs of ions at distance $n \ge p/2$ from each other is

$$N_n = 6\left(2n-p\right)^2 \sum_{k=0}^{p-n-1} p^2 + 12\left(2n-p\right) \sum_{i=0}^{p-n-1}\sum_{j=0}^{p-n-1} p\left(2n+1+i+j\right)$$
$$+ 8 \sum_{i=0}^{p-n-1}\sum_{j=0}^{p-n-1}\sum_{k=0}^{p-n-1} 3n^2 + 3n + 1 + \left(2n+1\right)\left(i+j+k\right) + ij + jk + ki$$

$$N_n = 6p^2\left(p-n\right)\left(2n-p\right)^2 + 12p\left(2n-p\right)\begin{bmatrix}\left(2n+1\right)\left(p-n\right)+ \\ \left(p-n\right)^2\left(p-n-1\right)\end{bmatrix}$$
$$+ 8\begin{bmatrix}\left(3n^2+3n+1\right)\left(p-n\right)^3 + \dfrac{3}{2}\left(2n+1\right)\left(p-n-1\right)\left(p-n\right)^3 \\ +\dfrac{3}{4}\left(p-n-1\right)^2\left(p-n\right)^3\end{bmatrix}$$

$$N_n = 6p^2\left(p-n\right)\left(2n-p\right)^2 + 12p\left(p-n\right)^2\left(p+n\right)\left(2n-p\right)$$
$$+ 2\left(p-n\right)^3\left[3\left(p+n\right)^2+1\right]$$

$$N_n = 2\left(p-n\right)\left[3n^2\left(p+n\right)^2 + \left(p-n\right)^2 - 9pn^2\left(2n-p\right)\right]$$

Summary

- When n < p/2

$$N_n = 2\left(12n^2+1\right)\left(p-2n\right)^3 + 6n\left(16n^2+1\right)\left(p-2n\right)^2$$
$$+6n^2\left(21n^2+1\right)\left(p-n\right) + 2n^3\left(27n^2+1\right)$$

- When n > p/2

$$N_n = 2\left(p-n\right)\left[3n^2\left(p+n\right)^2 + \left(p-n\right)^2 - 9pn^2\left(2n-p\right)\right]$$

- When n = p/2

$$N_{p/2} = \frac{p^3}{16}\left(27p^2+4\right)$$

- Check

$$\sum_{n=1}^{p-1} N_n = p^6 - p^3 = N(N-1) \text{ as expected}$$

These formulas are valid when the two ions are distinct. If they are identical, one ought to divide the numbers by 2 to avoid double counting.

Since we know the N_n's we can now determine the partition function.

$$Q(1,1) = \sum_{n=1}^{p-1} N_n \exp\left(-\frac{z_\alpha z_\beta l_B}{2\sigma n}\right)$$

$$Q(1,1) = \sum_{n=1}^{p-1} N_n \sum_{k=0}^{+\infty} \frac{1}{k!}\left(-\frac{z_\alpha z_\beta l_B}{2\sigma n}\right)^k = \sum_{k=0}^{+\infty} \frac{1}{k!}\left(-\frac{z_\alpha z_\beta l_B}{2\sigma}\right)^k \sum_{n=1}^{p-1} \frac{N_n}{n^k}$$

The development has the following terms:

$$\sum_{n=1}^{p-1} N_n = p^6 - p^3$$

$$\sum_{n=1}^{p-1} \frac{N_n}{n} = \frac{23}{10}p^5 + 2p^3 \ln p + \left(2\gamma - \frac{37}{6}\right)p^3 + O(p^2)$$

$$\sum_{n=1}^{p-1} \frac{N_n}{n^2} = \frac{17}{2}p^4 + \left(\frac{\pi^2}{3} - 12\right)p^3 - 6p^2 \ln p + O(p^2)$$

$$\sum_{n=1}^{p-1} \frac{N_n}{n^3} = 24p^3 \ln p + (24\gamma + 2\zeta(3) - 35)p^3 + O(p^2)$$

$$\sum_{n=1}^{p-1} \frac{N_n}{n^4} = \left(\frac{\pi^4}{45} + 4\pi^2\right)p^3 - 48p^2 \ln p + O(p^2)$$

$$\sum_{n=1}^{p-1} \frac{N_n}{n^k} = 2(\zeta(k) - 12\zeta(k-2))p^3 + O(p^2) \qquad \text{for all } k \geq 5$$

γ is the Euler-Mascheroni constant; $\gamma = \lim_{n \to +\infty}\left(\ln n - \sum_{k=1}^{n}\frac{1}{k}\right)$. ζ is the Riemann Zeta function usually defined by $\zeta(n) = \sum_{k=1}^{+\infty}\frac{1}{k^n}$.

We rewrite these terms using the extension of ζ defined below:

$$\tilde{\zeta}(-1) = 0 \qquad \tilde{\zeta}(0) = -\frac{1}{2} \qquad \tilde{\zeta}(1) = \gamma + \ln p \qquad \text{and} \qquad \tilde{\zeta}(n) = \zeta(n) \text{ for } n \geq 2$$

$$\sum_{n=1}^{p-1} \frac{N_n}{n} = \frac{23}{10}p^5 - \frac{37}{6}p^3 + 2(\tilde{\zeta}(1) - 12\tilde{\zeta}(-1))p^3 + O(p^2)$$

$$\sum_{n=1}^{p-1} \frac{N_n}{n^2} = \frac{17}{2} p^4 + 2(\tilde{\zeta}(2) - 12\tilde{\zeta}(0)) p^3 - 6p^2 \ln p + O(p^2)$$

$$\sum_{n=1}^{p-1} \frac{N_n}{n^3} = -35p^3 + 2(\tilde{\zeta}(3) + 12\tilde{\zeta}(1)) p^3 + O(p^2)$$

$$\sum_{n=1}^{p-1} \frac{N_n}{n^4} = 2(\tilde{\zeta}(4) + 12\tilde{\zeta}(2)) p^3 - 48p^2 \ln p + O(p^2)$$

$$\sum_{n=1}^{p-1} \frac{N_n}{n^k} = 2(\tilde{\zeta}(k) - 12\tilde{\zeta}(k-2)) p^3 + O(p^2) \qquad \text{for all } k \geq 5$$

The resulting development of the partition function is

$$Q(1,1) = \sum_{k=0}^{+\infty} \frac{1}{k!} \left(-\frac{z_\alpha z_\beta l_B}{2\sigma} \right)^k \sum_{n=1}^{p-1} \frac{N_n}{n^k}$$

$$Q(1,1) = p^6 - \frac{23}{10} \frac{z_\alpha z_\beta l_B}{2\sigma} p^5 + \frac{17}{4} \left(\frac{z_\alpha z_\beta l_B}{2\sigma} \right)^2 p^4 - \frac{z_\alpha z_\beta l_B}{2\sigma} \left(\frac{37}{6} - \frac{35}{6} \left(\frac{z_\alpha z_\beta l_B}{2\sigma} \right)^2 \right) p^3$$

$$+ 2p^3 \sum_{k=1}^{+\infty} \frac{\tilde{\zeta}(k) + 12\tilde{\zeta}(k-2)}{k!} \left(-\frac{z_\alpha z_\beta l_B}{2\sigma} \right)^k + O(p^2 \ln p)$$

III   A SOLUTION WITH TWO SPECIES OF SMALL IONS

We consider an aqueous solution in a cubic recipient with volume $\underline{W}$. There are two species ions in this volume with number densities ρ_α and ρ_β, with charges z_α and z_β and with ionic radii σ_α and σ_β. The total number of ions of each species present in solution are $N_\alpha = \rho_\alpha \underline{W}$ and $N_\beta = \rho_\beta \underline{W}$. The arithmetic average of the two radii is σ.

We adopt the same geometrical setting as in the previous paragraph. The partition function has a more complicated form.

$$Q(N_\alpha, N_\beta) = \frac{1}{N_\alpha! N_\beta! (N - N_\alpha - N_\beta)!} \sum_{s \in \mathbb{S}_N} \prod_{(i,j) \in \Omega} \exp\left(-\frac{z_{s(i)} z_{s(j)} l_B}{2 \times 2\sigma d(i,j)} \right)$$

where $\mathbb{S}_N$ is the symmetric group of order N $\Omega = ([1,N] \times [1,N]) \setminus \{(i,i) ; i \in [1,N]\}$

$z_i = z_\alpha$ if the position i is occupied by an ion of species α
$z_i = z_\beta$ if the position i is occupied by an ion of species β
$z_i = 0$ if the position i is not occupied

The additional division by 2 is introduced to avoid counting the interactions twice. We rewrite the partition function as

$$Q(N_\alpha, N_\beta) = \frac{N!}{N_\alpha! N_\beta! (N - N_\alpha - N_\beta)!} \tilde{Q}(N_\alpha, N_\beta)$$

$$\tilde{Q}(N_\alpha, N_\beta) = \frac{1}{N!} \sum_{s \in \mathbb{S}_N} \prod_{(i,j) \in \Omega} \exp\left(-\frac{z_{s(i)} z_{s(j)} l_B}{4\sigma d(i,j)}\right)$$

Thence we move the summation from the permutations of ions to the permutation of the positions and choose to place the ions of species α in the small cubes numbered from 1 to N_α and the ions of species β in the small cubes numbered from $N_\alpha + 1$ to $N_\alpha + N_\beta$.

$$\tilde{Q}(N_\alpha, N_\beta) = \frac{1}{N!} \sum_{s \in \mathbb{S}_N} \prod_{(i,j) \in \Omega} \exp\left(-\frac{z_i z_j l_B}{4\sigma d(s(i), s(j))}\right)$$

$$\tilde{Q}(N_\alpha, N_\beta) = \frac{1}{N!} \sum_{s \in \mathbb{S}_N} \prod_{i=1}^{N_\alpha} \prod_{j=i+1}^{N_\alpha} \exp\left(-\frac{z_\alpha^2 l_B}{2\sigma d(s(i), s(j))}\right)$$

$$\times \prod_{i=N_\alpha+1}^{N_\alpha+N_\beta} \prod_{j=i+1}^{N_\alpha+N_\beta} \exp\left(-\frac{z_\beta^2 l_B}{2\sigma d(s(i), s(j))}\right)$$

$$\times \prod_{i=1}^{N_\alpha} \prod_{j=N_\alpha+1}^{N_\alpha+N_\beta} \exp\left(-\frac{z_\alpha z_\beta l_B}{2\sigma d(s(i), s(j))}\right)$$

In the rewriting of the sum, we limit the summation to the upper half of $[1, N_\alpha + N_\beta]^2$ therefore we do not need the additional division by 2 in the exponential.

We interpret the summation over the symmetric group as the expectation of a random variable X defined from a set of random variables X_{ij}.

$$\tilde{Q}(N_\alpha, N_\beta) = E[X]$$

$$X = \prod_{\substack{i=1 \\ j=i+1}}^{N_\alpha} e^{-\frac{z_\alpha^2 l_B}{2\sigma} X_{ij}} \times \prod_{\substack{i=N_\alpha+1 \\ j=i+1}}^{N_\alpha+N_\beta} e^{-\frac{z_\beta^2 l_B}{2\sigma} X_{ij}} \times \prod_{\substack{i=1 \\ j=N_\alpha+1}}^{N_\alpha+N_\beta} e^{-\frac{z_\alpha z_\beta l_B}{2\sigma} X_{ij}}$$

$$X_{ij} : \mathbb{S}_N \to \mathbb{Q}_+$$

$$s \to \frac{1}{d(s(i), s(j))}$$

Note that $X_{ij} = X_{ji}$. Moreover the X_{ij}'s are essentially the same random variable because the action of the whole symmetric group on a pair of integers yields identical results. The X_{ij}'s have the same probability density function and the same moments, $E[X_{ij}^n] = E[X_{kl}^n]$ for all i, j, k, l.

- If i, j, k, l are four different integers comprised between 1 and N, then X_{ij} and X_{kl} are independent because the permutations act on (i,j) independently from (k,l); for any permutation s, knowing $d(s(i),s(j)) = n$ does not give any information about $d(s(k),s(l))$.
- If k = i and l = j or k = j and l = i, then $X_{ij} = X_{kl}$.
- The case l = i and k $\neq$ i, j is more complicated because X_{ij} and X_{ik} are not independent.

$$\Pr\left[X_{ij} = \frac{1}{n}, X_{ik} = \frac{1}{m}\right] = \Pr\left[X_{ik} = \frac{1}{m} \middle| X_{ij} = \frac{1}{n}\right] \Pr\left[X_{ij} = \frac{1}{n}\right]$$

$$\Pr\left[X_{ij} = \frac{1}{n}, X_{ik} = \frac{1}{m}\right] = \Pr\left[X_{ik} = \frac{1}{m} \middle| X_{ij} = \frac{1}{n}\right] \Pr[d(s(i), s(j)) = n)]$$

$$\Pr\left[X_{ij} = \frac{1}{n}, X_{ik} = \frac{1}{m}\right] = \frac{N_n}{N(N-1)} \Pr\left[X_{ik} = \frac{1}{m} \middle| X_{ij} = \frac{1}{n}\right]$$

N_n is the number of pairs of cubes at distance n from each other; it is calculated above.

$$\Pr\left[X_{ik} = \frac{1}{n} \middle| X_{ij} = \frac{1}{n}\right] = \frac{N_n - N}{N(N-2)}$$

$$\Pr\left[X_{ik} = \frac{1}{m} \middle| X_{ij} = \frac{1}{n}\right] = \frac{N_m}{N(N-2)} \quad \text{for } m \neq n$$

- the presence of s(j) reduces the available positions for s(k) by one for every position of s(i) so the total number of injections of (i,k) into [1,N] is N(N − 2), not N(N − 1)
- when m = n, for every position of s(i), the number of positions possible for s(k) is reduced by one hence the total number of possible combinations (i,k) is N_n − N
- when m ≠ n, the presence of s(j) does not reduce the number of positions possible for s(k) hence the total number of possible combinations (i,k) is N_m

The resulting joint probability density function is

$$\Pr\left[X_{ij} = \frac{1}{n}, X_{ik} = \frac{1}{m}\right] = \frac{N_n\left(N_m - N\delta_{n,m}\right)}{N^2(N-1)(N-2)}$$

where δ_{nm} = 1 if n = m and 0 otherwise (Kronecker's delta function).

Using a similar reasoning we can construct the joint probability density function for all X_{ij}'s of interest and compute E[X]. But this would be a hugely complicated calculation. Instead let us compute the difference between the joint probability density function and the product of the separate probability density functions.

$$\Delta\Pr = \Pr\left[X_{ij} = \frac{1}{n}, X_{ik} = \frac{1}{m}\right] - \Pr\left[X_{ij} = \frac{1}{n}\right]\Pr\left[X_{ik} = \frac{1}{m}\right]$$

$$\Delta\Pr = \frac{N_n\left(N_m - N\delta_{n,m}\right)}{N^2(N-1)(N-2)} - \frac{N_n}{N(N-1)}\frac{N_m}{N(N-1)}$$

$$\Delta\Pr = \frac{N_n}{N^2(N-1)}\left[\frac{N_m - N\delta_{n,m}}{N-2} - \frac{N_m}{N-1}\right]$$

$$\Delta\Pr = \frac{N_n}{N^2(N-1)}\left[\frac{N_m}{(N-1)(N-2)} - \frac{N\delta_{n,m}}{N-2}\right]$$

$$\Delta\Pr = \frac{1}{N-2}\left[\frac{N_n N_m}{N^2(N-1)^2} - \frac{N_n\delta_{n,m}}{N(N-1)}\right]$$

Thus it appears that approximating of the joint probability density function of the X_{ij}'s with the product of their single probability density functions yields an error that is on the order of 1/N or $1/p^3$. The X_{ij}'s are independent to the order $1/p^2$. We continue with the approximation of X_{ij}'s being independent.

$$E[X] = E\left[\prod_{\substack{i=1 \\ j=i+1}}^{\substack{N_\alpha \\ N_\alpha}} e^{-\frac{z_\alpha^2 l_B}{2\sigma}X_{ij}} \times \prod_{\substack{i=N_\alpha+1 \\ j=i+1}}^{\substack{N_\alpha+N_\beta \\ N_\alpha+N_\beta}} e^{-\frac{z_\beta^2 l_B}{2\sigma}X_{ij}} \times \prod_{\substack{i=1 \\ j=N_\alpha+1}}^{\substack{N_\alpha \\ N_\alpha+N_\beta}} e^{-\frac{z_\alpha z_\beta l_B}{2\sigma}X_{ij}}\right]$$

$$E[X] = \prod_{\substack{i=1 \\ j=i+1}}^{\substack{N_\alpha \\ N_\alpha}} E\left[e^{-\frac{z_\alpha^2 l_B}{2\sigma}X_{ij}}\right] \times \prod_{\substack{i=N_\alpha+1 \\ j=i+1}}^{\substack{N_\alpha+N_\beta \\ N_\alpha+N_\beta}} E\left[e^{-\frac{z_\beta^2 l_B}{2\sigma}X_{ij}}\right] \times \prod_{\substack{i=1 \\ j=N_\alpha+1}}^{\substack{N_\alpha \\ N_\alpha+N_\beta}} E\left[e^{-\frac{z_\alpha z_\beta l_B}{2\sigma}X_{ij}}\right]$$

$$E[X] = E\left[e^{-\frac{z_\alpha^2 l_B}{2\sigma}X_{ij}}\right]^{\frac{N_\alpha(N_\alpha-1)}{2}} \times E\left[e^{-\frac{z_\beta^2 l_B}{2\sigma}X_{ij}}\right]^{\frac{N_\beta(N_\beta-1)}{2}} \times E\left[e^{-\frac{z_\alpha z_\beta l_B}{2\sigma}X_{ij}}\right]^{N_\alpha N_\beta}$$

Then

$$E\left[e^{-\frac{z_\alpha^2 l_B}{2\sigma}X_{ij}}\right] = E\left[\sum_{n=0}^{+\infty}\frac{1}{n!}\left(-\frac{z_\alpha^2 l_B}{2\sigma}X_{ij}\right)^n\right] = \sum_{n=0}^{+\infty}\frac{1}{n!}\left(-\frac{z_\alpha^2 l_B}{2\sigma}\right)^n E\left[X_{ij}^n\right]$$

Since $E\left[X_{ij}^n\right] = \frac{1}{N(N-1)}\sum_{k=1}^{p-1}\frac{N_k}{k^n}$, we can write $E\left[e^{-\frac{z_\alpha^2 l_B}{2\sigma}X_{ij}}\right] = \frac{\tilde{Q}(2)}{p^3(p^3-1)}$ the partition

function of two ions of the same species calculated previously. Therefore

$$E\left[e^{-\frac{z_\alpha^2 l_B}{2\sigma}X_{ij}}\right] = \frac{\tilde{Q}(2)}{p^3(p^3-1)} = \frac{\tilde{Q}(2)}{p^6}\left(1 + O\left(\frac{1}{p^3}\right)\right)$$

$$E\left[e^{-\frac{z_\alpha^2 l_B}{2\sigma}X_{ij}}\right] = 1 - \frac{23}{10}\frac{z_\alpha^2 l_B}{2\sigma}\frac{1}{p} + \frac{17}{4}\left(\frac{z_\alpha^2 l_B}{2\sigma}\right)^2\frac{1}{p^2} + O\left(\frac{1}{p^3}\right)$$

The terms of order $1/p^3$ and smaller are not relevant because the approximation of mutually independent X_{ij}'s entails an error of order $1/N = 1/p^3$. Next

$$E\left[e^{-\frac{z_\alpha^2 l_B}{2\sigma}X_{ij}}\right]^{\frac{N_\alpha(N_\alpha-1)}{2}} = \left(1 - \frac{23}{10}\frac{z_\alpha^2 l_B}{2\sigma}\frac{1}{p} + \frac{17}{4}\left(\frac{z_\alpha^2 l_B}{2\sigma}\right)^2\frac{1}{p^2} + O\left(\frac{1}{p^3}\right)\right)^{\frac{N_\alpha(N_\alpha-1)}{2}}$$

$$E\left[e^{-\frac{z_\alpha^2 l_B}{2\sigma}X_{ij}}\right]^{\frac{N_\alpha(N_\alpha-1)}{2}} = 1 - \frac{23}{10}\frac{z_\alpha^2 l_B}{2\sigma}\frac{N_\alpha(N_\alpha-1)}{2}\frac{1}{p} + \frac{17}{4}\left(\frac{z_\alpha^2 l_B}{2\sigma}\right)^2\frac{N_\alpha(N_\alpha-1)}{2}\frac{1}{p^2}$$

$$+ \frac{N_\alpha(N_\alpha-1)\left[N_\alpha(N_\alpha-1)/2-1\right]}{2\times 2}\left(\frac{23}{10}\frac{z_\alpha^2 l_B}{2\sigma}\frac{1}{p}\right)^2\frac{1}{p^2} + O\left(\frac{1}{p^3}\right)$$

The two other terms $E\left[e^{-\frac{z_\beta^2 l_B}{2\sigma}X_{ij}}\right]^{\frac{N_\beta(N_\beta-1)}{2}}$ and $E\left[e^{-\frac{z_\alpha z_\beta l_B}{2\sigma}X_{ij}}\right]^{N_\alpha N_\beta}$ have similar expressions. The next step is multiplying them and determining first two terms of the series.

57

$$\tilde{Q} = E[X] = E\left[e^{-\frac{z_\alpha^2 l_B}{2\sigma} X_{ij}}\right]^{\frac{N_\alpha(N_\alpha-1)}{2}} \times E\left[e^{-\frac{z_\beta^2 l_B}{2\sigma} X_{ij}}\right]^{\frac{N_\beta(N_\beta-1)}{2}} \times E\left[e^{-\frac{z_\alpha z_\beta l_B}{2\sigma} X_{ij}}\right]^{N_\alpha N_\beta}$$

$$\tilde{Q} = 1 - \frac{23}{20}\frac{l_B}{2\sigma}\frac{1}{p}\left[z_\alpha^2 N_\alpha\left(N_\alpha - 1\right) + z_\beta^2 N_\beta\left(N_\beta - 1\right) + 2z_\alpha z_\beta N_\alpha N_\beta\right] +$$

$$+ \frac{17}{8}\left(\frac{l_B}{2\sigma}\right)^2 \frac{1}{p^2}\left[z_\alpha^2 N_\alpha\left(N_\alpha - 1\right) + z_\beta^2 N_\beta\left(N_\beta - 1\right) + 2z_\alpha z_\beta N_\alpha N_\beta\right] +$$

$$+ \frac{1}{8}\left(\frac{23}{10}\frac{l_B}{2\sigma}\frac{1}{p}\right)^2 \left[\begin{matrix} z_\alpha^4 N_\alpha^2\left(N_\alpha - 1\right)^2 + z_\beta^4 N_\beta^2\left(N_\beta - 1\right)^2 + 4z_\alpha^2 z_\beta^2 N_\alpha^2 N_\beta^2 \\ -2z_\alpha^4 N_\alpha\left(N_\alpha - 1\right) - 2z_\beta^4 N_\beta\left(N_\beta - 1\right) - 4z_\alpha^2 z_\beta^2 N_\alpha N_\beta \end{matrix}\right]$$

$$+ \frac{1}{4}\left(\frac{23}{10}\frac{l_B}{2\sigma}\frac{1}{p}\right)^2 \left[\begin{matrix} z_\alpha^2 z_\beta^2 N_\alpha N_\beta\left(N_\alpha - 1\right)\left(N_\beta - 1\right) \\ +2z_\alpha^3 z_\beta N_\alpha^2 N_\beta\left(N_\alpha - 1\right) + 2z_\alpha z_\beta^3 N_\alpha N_\beta^2\left(N_\beta - 1\right) \end{matrix}\right]$$

This formula can be transformed into something simpler by introducing a new family of variables: $\tilde{I}_n = \frac{1}{n}\left(N_\alpha z_\alpha^n + N_\beta z_\beta^n\right)$

- $\tilde{I}_1$ is the net density of the solution; e·$\tilde{I}_1$ is the net charge present in the solution; when $\tilde{I}_1 = 0$ the solution is electroneutral.
- $\tilde{I}_2$ is the ionic strength of the solution.
- The other variables do not have classical names.

$$\tilde{Q} = 1 - \frac{23}{20}\frac{l_B}{2\sigma}\frac{\tilde{I}_1^2 - 2\tilde{I}_2}{p} + \frac{17}{8}\left(\frac{l_B}{2\sigma}\right)^2 \frac{\tilde{I}_1^2 - 2\tilde{I}_2}{p^2} + \frac{1}{2}\left(\frac{23}{20}\frac{l_B}{2\sigma}\right)^2 \frac{8\tilde{I}_4 - 4\tilde{I}_2^2 - 4\tilde{I}_1^2\tilde{I}_2 + \tilde{I}_1^4}{p^2}$$

The complete partition function is therefore

$$Q\left(N_\alpha, N_\beta\right) = \frac{N!}{N_\alpha! N_\beta!\left(N - N_\alpha - N_\beta\right)!}\tilde{Q}\left(N_\alpha, N_\beta\right)$$

$$\tilde{Q}\left(N_\alpha, N_\beta\right) = 1 - \frac{23}{20}\frac{l_B}{2\sigma}\frac{\tilde{I}_1^2 - 2\tilde{I}_2}{p} + \frac{1}{8}\left(\frac{l_B}{2\sigma}\right)^2 \frac{1}{p^2}\left[\begin{matrix} \left(\frac{23}{10}\right)^2\left(8\tilde{I}_4 - 4\tilde{I}_2^2 - 4\tilde{I}_1^2\tilde{I}_2 + \tilde{I}_1^4\right) \\ +17\left(\tilde{I}_1^2 - 2\tilde{I}_2\right) \end{matrix}\right]$$

Note that the first and second orders in $1/p$ are very general. From the third order on, the terms are much more complicated, include elements that are peculiar to the geometrical setting chosen and cannot be expressed as simple functions of N_α and N_β.

58

IV GENERALIZATION TO A SOLUTION WITH MANY SPECIES OF SMALL IONS

We consider an aqueous solution in a cubic recipient with volume $\underline{W}$. There are m species ions in this volume with number densities ρ_i, with charges z_i and with ionic radii σ_i, $i \in [1,m]$. The total number of ions of each species present in solution is $N_i = \rho_i \underline{W}$. The arithmetic average of the ionic radii is σ.

We adopt the same geometrical setting as in the two previous paragraphs. The partition function is derived by similar calculations.

$$Q\left(N_1, \cdots, N_m\right) = \frac{N!}{\left(N - \sum_{i=1}^{m} N_i\right)! \prod_{i=1}^{m} N_i!} \tilde{Q}\left(N_1, \cdots, N_m\right)$$

$$\tilde{Q}\left(N_1, \cdots, N_m\right) = 1 - \frac{23}{20}\frac{l_B}{2\sigma}\frac{\tilde{I}_1^2 - 2\tilde{I}_2}{p} + \frac{1}{8}\left(\frac{l_B}{2\sigma}\right)^2 \frac{1}{p^2}\left[\begin{array}{l}\left(\frac{23}{20}\right)^2\left(8\tilde{I}_4 - 4\tilde{I}_2^2 - 4\tilde{I}_1^2\tilde{I}_2 + \tilde{I}_1^4\right) \\ +17\left(\tilde{I}_1^2 - 2\tilde{I}_2\right)\end{array}\right]$$

Where $\tilde{I}_n = \frac{1}{n}\sum_{i=1}^{m} N_i z_i^n = \frac{W}{n}\sum_{i=1}^{m} \rho_i z_i^n$ are the ionic moments of the solution, i.e. a generalization of the net density and the ionic strength.

V THERMODYNAMIC FUNCTIONS OF A UNIFORM HOMOGENOUS SOLUTION WITH TWO SPECIES OF SMALL IONS

We work in the same setting as before and derive a few thermodynamic functions, namely the internal energy $\underline{U}$, the entropy $\underline{S}$, the Gibbs free energy $\underline{G}$ and the chemical potential $\underline{\mu}$. We treat the case of a binary solute in order to keep the derivation simple and readable; the generalization is straightforward.

V.1 Partition function

Starting with the partition function derived earlier, we use the approximation of ln(N!) determined from Stirling's formula.

$$Q\left(N_\alpha, N_\beta\right) = \frac{N!}{N_\alpha! N_\beta! \left(N - N_\alpha - N_\beta\right)!} \tilde{Q}\left(N_\alpha, N_\beta\right)$$

$$\ln Q = \ln \tilde{Q} + \ln\left(N!\right) - \ln\left(N_\alpha!\right) - \ln\left(N_\beta!\right) - \ln\left(\left(N - N_\alpha - N_\beta\right)!\right)$$

$$\ln Q = \ln \tilde{Q} + N\ln N - N_\alpha \ln N_\alpha - N_\beta \ln N_\beta - \left(N - N_\alpha - N_\beta\right)\ln\left(N - N_\alpha - N_\beta\right)$$

$$\ln Q = \ln \tilde{Q} + N\left[\ln N - \frac{N_\alpha}{N}\ln N_\alpha - \frac{N_\beta}{N}\ln N_\beta - \left(1 - \frac{N_\alpha}{N} - \frac{N_\beta}{N}\right)\ln\left(N - N_\alpha - N_\beta\right)\right]$$

$$\ln Q = \ln \tilde{Q} - N\left[\frac{N_\alpha}{N}\ln \frac{N_\alpha}{N} + \frac{N_\beta}{N}\ln \frac{N_\beta}{N} + \left(1 - \frac{N_\alpha}{N} - \frac{N_\beta}{N}\right)\ln\left(1 - \frac{N_\alpha}{N} - \frac{N_\beta}{N}\right)\right]$$

We also have $\sigma = \dfrac{\sigma_\alpha + \sigma_\beta}{2}$, $N = \dfrac{W}{8\sigma^3}$, $N_\alpha = \rho_\alpha W$ and $N_\beta = \rho_\beta W$. Hence

$$\frac{N_\alpha}{N} = 8\sigma^3 \rho_\alpha \simeq 8\sigma_\alpha^3 \rho_\alpha \qquad\qquad \frac{N_\beta}{N} = 8\sigma^3 \rho_\beta \simeq 8\sigma_\beta^3 \rho_\beta$$

And

$$\ln Q = \ln \tilde{Q} - \frac{W}{8\sigma^3}\left[\begin{array}{l} 8\sigma_\alpha^3 \rho_\alpha \ln\left(8\sigma_\alpha^3 \rho_\alpha\right) + 8\sigma_\beta^3 \rho_\beta \ln 8\sigma_\beta^3 \rho_\beta \\ +\left(1 - 8\sigma_\alpha^3 \rho_\alpha - 8\sigma_\beta^3 \rho_\beta\right)\ln\left(1 - 8\sigma_\alpha^3 \rho_\alpha - 8\sigma_\beta^3 \rho_\beta\right)\end{array}\right]$$

Next using $N = p^3$

$$\ln \tilde{Q} = \ln\left(1 - \frac{A}{p} + \frac{B}{p^2}\right) = -\frac{A}{p} + \frac{B}{p^2} - \frac{1}{2}\frac{A^2}{p^2}$$

$$\ln \tilde{Q} = -1.15\frac{l_B}{2\sigma}\frac{\tilde{I}_1^2 - 2\tilde{I}_2}{p} + \frac{1}{8}\left(\frac{l_B}{2\sigma}\right)^2 \frac{1}{p^2}\left[\begin{array}{l} 5.29\left(8\tilde{I}_4 - 4\tilde{I}_2^2 - 4\tilde{I}_1^2\tilde{I}_2 + \tilde{I}_1^4\right) \\ -5.29\left(\tilde{I}_1^2 - 2\tilde{I}_2\right)^2 + 17\left(\tilde{I}_1^2 - 2\tilde{I}_2\right)\end{array}\right]$$

$$\ln \tilde{Q} = -1.15\frac{l_B}{2\sigma}\frac{\tilde{I}_1^2 - 2\tilde{I}_2}{p} + \frac{1}{8}\left(\frac{l_B}{2\sigma}\right)^2 \frac{1}{p^2}\left[5.29\left(8\tilde{I}_4 - 8\tilde{I}_2^2\right) + 17\left(\tilde{I}_1^2 - 2\tilde{I}_2\right)\right]$$

$$\ln \tilde{Q} = -\frac{23}{20}\frac{l_B}{2\sigma}\frac{\tilde{I}_1^2 - 2\tilde{I}_2}{p} + \frac{1}{8}\left(\frac{l_B}{2\sigma}\right)^2 \frac{1}{p^2}\left[\left(\frac{23}{10}\right)^2\left(8\tilde{I}_4 - 8\tilde{I}_2^2\right) + 17\left(\tilde{I}_1^2 - 2\tilde{I}_2\right)\right]$$

$$\ln \tilde{Q} = -\frac{23}{20}\frac{l_B}{2\sigma}\frac{\tilde{I}_1^2 - 2\tilde{I}_2}{p} + \frac{1}{8}\left(\frac{l_B}{2\sigma}\right)^2 \frac{2\left(23/5\right)^2\left(\tilde{I}_4 - \tilde{I}_2^2\right) + 17\left(\tilde{I}_1^2 - 2\tilde{I}_2\right)}{p^2}$$

We have $p^3 = N = \dfrac{W}{8\sigma^3}$ and we define $I_n = \dfrac{1}{n}\left(\rho_\alpha z_\alpha^n + \rho_\beta z_\beta^n\right) = \dfrac{\tilde{I}_n}{W}$. Thence

$$\ln \tilde{Q} = -\frac{23}{20}\frac{l_B}{W^{1/3}}\left(WI_1^2 - 2I_2\right)W + \frac{1}{8}\left(\frac{l_B}{W^{1/3}}\right)^2\left[\begin{array}{l} 2\left(23/5\right)^2\left(I_4 - I_2^2 W\right) \\ +17\left(I_1^2 W - 2I_2\right)\end{array}\right]W$$

$$\ln \tilde{Q} = -\frac{23}{20}l_B\left(WI_1^2 - 2I_2\right)W^{2/3} + \frac{1}{8}l_B^2\left[\begin{array}{l} 2\left(23/5\right)^2\left(I_4 - I_2^2 W\right) \\ +17\left(I_1^2 W - 2I_2\right)\end{array}\right]W^{1/3}$$

Summary

$$\ln Q = \ln \tilde{Q} - \frac{W}{8\sigma^3}\left[\begin{array}{l} 8\sigma_\alpha^3 \rho_\alpha \ln\left(8\sigma_\alpha^3 \rho_\alpha\right) + 8\sigma_\beta^3 \rho_\beta \ln 8\sigma_\beta^3 \rho_\beta \\ +\left(1 - 8\sigma_\alpha^3 \rho_\alpha - 8\sigma_\beta^3 \rho_\beta\right)\ln\left(1 - 8\sigma_\alpha^3 \rho_\alpha - 8\sigma_\beta^3 \rho_\beta\right)\end{array}\right]$$

$$\ln \tilde{Q} = -\frac{23}{20}l_B\left(WI_1^2 - 2I_2\right)W^{2/3} + \frac{1}{8}l_B^2\left[\begin{array}{l} 2\left(23/5\right)^2\left(I_4 - I_2^2 W\right) \\ +17\left(I_1^2 W - 2I_2\right)\end{array}\right]W^{1/3}$$

V.2 Internal energy and entropy

$$\underline{U} = kT^2 \frac{\partial \ln Q}{\partial T} = 0$$

$$\underline{S} = k \ln Q + kT \frac{\partial \ln Q}{\partial T}$$

$$\frac{\underline{S}}{k\underline{W}} = \frac{\tilde{S}}{k\underline{W}} - \frac{1}{8\sigma^3}\left[\begin{array}{l} 8\sigma_\alpha^3 \rho_\alpha \ln\left(8\sigma_\alpha^3 \rho_\alpha\right) + 8\sigma_\beta^3 \rho_\beta \ln 8\sigma_\beta^3 \rho_\beta \\ +\left(1 - 8\sigma_\alpha^3 \rho_\alpha - 8\sigma_\beta^3 \rho_\beta\right)\ln\left(1 - 8\sigma_\alpha^3 \rho_\alpha - 8\sigma_\beta^3 \rho_\beta\right) \end{array}\right]$$

$$\frac{\tilde{S}}{k\underline{W}} = -\frac{23}{20}\frac{l_B}{\underline{W}^{1/3}}\left(\underline{W}I_1^2 - 2I_2\right) + \frac{1}{8}\left(\frac{l_B}{\underline{W}^{1/3}}\right)^2 \left[\begin{array}{l} 2\left(23/5\right)^2\left(I_4 - I_2^2\underline{W}\right) \\ +17\left(I_1^2\underline{W} - 2I_2\right) \end{array}\right]$$

V.3 Gibbs free energy and electrical potential

$$\underline{G} = \underline{U} + P\underline{W} - T\underline{S} = P\underline{W} - k_B T \ln Q$$

$$\frac{\underline{G}}{\underline{W}} = \frac{\tilde{G}}{\underline{W}} + P + \frac{kT}{8\sigma^3}\left[\begin{array}{l} 8\sigma_\alpha^3 \rho_\alpha \ln\left(8\sigma_\alpha^3 \rho_\alpha\right) + 8\sigma_\beta^3 \rho_\beta \ln 8\sigma_\beta^3 \rho_\beta \\ +\left(1 - 8\sigma_\alpha^3 \rho_\alpha - 8\sigma_\beta^3 \rho_\beta\right)\ln\left(1 - 8\sigma_\alpha^3 \rho_\alpha - 8\sigma_\beta^3 \rho_\beta\right) \end{array}\right]$$

$$\frac{\tilde{G}}{kT\underline{W}} = \frac{23}{20}\frac{l_B}{\underline{W}^{1/3}}\left(\underline{W}I_1^2 - 2I_2\right) - \frac{1}{8}\left(\frac{l_B}{\underline{W}^{1/3}}\right)^2 \left[\begin{array}{l} 2\left(23/5\right)^2\left(I_4 - \underline{W}I_2^2\right) \\ +17\left(\underline{W}I_1^2 - 2I_2\right) \end{array}\right]$$

$$\mu_\alpha = \left(\frac{\partial \underline{G}}{\partial N_\alpha}\right)_{T,P,N_\beta} = \frac{1}{\underline{W}}\left(\frac{\partial \underline{G}}{\partial \rho_\alpha}\right)_{T,P,\rho_\beta} \qquad \text{because } \underline{W} \text{ is fixed}$$

$$\mu_\alpha = \frac{1}{\underline{W}}\frac{\partial \tilde{G}}{\partial \rho_\alpha} + \frac{kT}{8\sigma^3}\left[\begin{array}{l} 8\sigma_\alpha^3 \ln\left(8\sigma_\alpha^3 \rho_\alpha\right) + 8\sigma_\alpha^3 - \\ 8\sigma_\alpha^3 \ln\left(1 - 8\sigma_\alpha^3 \rho_\alpha - 8\sigma_\beta^3 \rho_\beta\right) - 8\sigma_\alpha^3 \end{array}\right]$$

$$\frac{1}{kT\underline{W}}\frac{\partial \tilde{G}}{\partial \rho_\alpha} = \frac{23}{20}\frac{l_B}{\underline{W}^{1/3}}\left(2z_\alpha \underline{W}I_1 - z_\alpha^2\right) - \frac{1}{8}\left(\frac{l_B}{\underline{W}^{1/3}}\right)^2 \left[\begin{array}{l} 2\left(23/5\right)^2\left(\frac{1}{4}z_\alpha^4 - z_\alpha^2\underline{W}I_2\right) \\ +17\left(2z_\alpha \underline{W}I_1 - z_\alpha^2\right) \end{array}\right]$$

$$\frac{\mu_\alpha}{kT} = \frac{1}{kT\underline{W}}\frac{\partial \tilde{G}}{\partial \rho_\alpha} + \ln\left(\frac{8\sigma_\alpha^3 \rho_\alpha}{1 - 8\sigma_\alpha^3 \rho_\alpha - 8\sigma_\beta^3 \rho_\beta}\right)$$

$$\frac{1}{kT\underline{W}}\frac{\partial \tilde{G}}{\partial \rho_\alpha} = \frac{23}{20}\frac{z_\alpha l_B}{\underline{W}^{1/3}}\left(2\underline{W}I_1 - z_\alpha\right) - \frac{1}{8}\left(\frac{l_B}{\underline{W}^{1/3}}\right)^2 \left[\begin{array}{l} 2\left(23/10\right)^2 z_\alpha^2\left(z_\alpha^2 - 4\underline{W}I_2\right) \\ +17z_\alpha\left(2\underline{W}I_1 - z_\alpha\right) \end{array}\right]$$

VI IONIC SOLUTION UNDER AN EXTERNAL ELECTRICAL FIELD

VI.1 Solution containing two species of small ions

We have solution containing two species of ions. Their charges are z_α and z_β, the number densities are ρ_α and ρ_β, their ionic radii are σ_α and σ_β. The external electrical field is $\underline{E}$ and derives from the electrical potential V. We consider a particle of fluid of small but finite size, in which the number densities of the ions and the electrical potential are considered to be constant. The volume of this particle of fluid is expressed as a multiple of the Bjerrum length l_B.

$$\underline{W} = \left(w l_B\right)^3$$

The particle of fluid is examined in isolation. It constitutes a homogenous ionic solution and we apply to it the analysis done above. Note that the size of this particle of fluid constitutes the length scale at which we take into account the local inter-ionic correlations and the effects of excluded volume; in this mathematical framework, there are no such correlations between ions in different particles of fluid.

$$\underline{U} = \left(z_\alpha \rho_\alpha + z_\beta \rho_\beta\right) e V \underline{W}$$

$$\frac{\underline{U}}{\underline{W}} = e I_1 V$$

$$\frac{\mu_\alpha}{kT} = \frac{z_\alpha e V}{kT} + \ln\left(\frac{8\sigma_\alpha^3 \rho_\alpha}{1 - 8\sigma_\alpha^3 \rho_\alpha - 8\sigma_\beta^3 \rho_\beta}\right)$$
$$+ \frac{23}{20}\frac{1}{w} z_\alpha \left(2 w^3 l_B^3 I_1 - z_\alpha\right) - \frac{1}{8}\frac{1}{w^2}\left[\begin{array}{l} 2\left(23/10\right)^2 z_\alpha^2 \left(z_\alpha^2 - 4 w^3 l_B^3 I_2\right) \\ + 17 z_\alpha \left(2 w^3 l_B^3 I_1 - z_\alpha\right) \end{array}\right]$$

The chemical potential depends on the volume of the particle of fluid. We assume w to remain constant throughout the analysis.

The local flux of an ionic species J_α is derived from its chemical potential.

$$J_\alpha = -\frac{\rho_\alpha}{f_\alpha} \nabla \mu_\alpha$$

$$\frac{J_\alpha}{kT} = -\frac{\rho_\alpha}{f_\alpha}\left[\begin{array}{l} \dfrac{z_\alpha e}{kT}\nabla V + \dfrac{\nabla \rho_\alpha}{\rho_\alpha} + \dfrac{8\sigma_\alpha^3 \nabla \rho_\alpha + 8\sigma_\beta^3 \nabla \rho_\beta}{1 - 8\sigma_\alpha^3 \rho_\alpha - 8\sigma_\beta^3 \rho_\beta} + \\[2ex] \dfrac{23}{10} w^2 l_B^3 z_\alpha \left(z_\alpha \nabla \rho_\alpha + z_\beta \nabla \rho_\beta\right) - \dfrac{w l_B^3}{4}\left[\begin{array}{l} -2\left(\dfrac{23}{10}\right)^2 z_\alpha^2 \left(z_\alpha^2 \nabla \rho_\alpha + z_\beta^2 \nabla \rho_\beta\right) \\ + 17 z_\alpha \left(z_\alpha \nabla \rho_\alpha + z_\beta \nabla \rho_\beta\right) \end{array}\right] \end{array}\right]$$

This equation takes a more general form than the Nernst-Planck equation which has only the first two terms. Note that $J_\alpha \to 0$ as $w \to 0$ whereas the previous thermodynamic functions per volume had a singularity in $w = 0$, because they cannot be properly defined per volume for infinitely small volumes. Last by comparison with the diffusion equation we observe that

$$\frac{k_B T}{f_\alpha} = D_\alpha \text{ where } D_\alpha \text{ is the normal diffusion coefficient of the species } \alpha$$

$$J_\alpha = -D_\alpha \rho_\alpha \left[\begin{array}{l} \dfrac{z_\alpha e}{k_B T}\nabla V + \dfrac{\nabla\rho_\alpha}{\rho_\alpha} + \dfrac{8\sigma_\alpha^3\nabla\rho_\alpha + 8\sigma_\beta^3\nabla\rho_\beta}{1 - 8\sigma_\alpha^3\rho_\alpha - 8\sigma_\beta^3\rho_\beta} + \\[3mm] 2.3w^2 l_B^3 z_\alpha \left(z_\alpha\nabla\rho_\alpha + z_\beta\nabla\rho_\beta \right) - \dfrac{w l_B^3}{4}\left[\begin{array}{l} -2(2.3)^2 z_\alpha^2 \left(z_\alpha^2\nabla\rho_\alpha + z_\beta^2\nabla\rho_\beta \right) \\[2mm] +17z_\alpha \left(z_\alpha\nabla\rho_\alpha + z_\beta\nabla\rho_\beta \right) \end{array} \right] \end{array} \right]$$

The corresponding equations for the electrical field and the electrical potential follow.

$$-\nabla \cdot E = \Delta V = -\frac{e}{\varepsilon_0\varepsilon_r}\left(z_\alpha\rho_\alpha + z_\beta\rho_\beta \right)$$

VI.2 Solution containing several species of small ions

We have solution containing m species of ions. The charges are z_i, the number densities are ρ_i, the ionic radii are σ_i. The external electrical field is $\underline{E}$ and derives from the electrical potential V. The volume of a particle of fluid is $\underline{W}$. The correlation parameter is defined as

$$w = \left(\frac{\underline{W}}{l_B} \right)^{1/3}$$

The flux of an ionic species is expressed using the net number density $\rho_\pm$, the ionic strength I and the volume proportion of the ions ψ.

$$\rho_\pm = \sum_{i=1}^{n} z_i\rho_i \qquad I = \frac{1}{2}\sum_{i=1}^{n} z_i^2\rho_i \qquad \psi = \sum_{i=1}^{n} 8\sigma_i^3\rho_i$$

$$J_\alpha = -D_\alpha\rho_\alpha \left[\frac{\nabla\rho_\alpha}{\rho_\alpha} + \frac{z_\alpha e}{k_B T}\nabla V + \frac{\nabla\psi}{1-\psi} + 2.3w^2 l_B^3\nabla\rho_\pm - w l_B^3\left[\frac{17}{4}\nabla\rho_\pm - (2.3)^2\nabla I \right] \right]$$

The electrical field and the electrical potential are determined from

$$-\nabla \cdot E = \Delta V = -\frac{e}{\varepsilon_0\varepsilon_r}\sum_{i=1}^{m} z_i\rho_i = -\frac{e\rho_\pm}{\varepsilon_0\varepsilon_r}$$

Chapter 5   Dielectric permittivity and ionic strength

I   DIELECTRIC PERMITTIVITY

The relative dielectric permittivity is a lowering of the electrical forces induced by the medium. Pure water has a relative dielectric permittivity of 78.5. A molecule of water is has a permanent dipole and the free rotation of water molecules creates an additional screening of electrical forces that is responsible for the high value of the dielectric permittivity. The introduction of a charged solute modifies the ability of water molecules to rotate freely and induces usually a reduction, but sometimes an increase, in the dielectric permittivity of the solution.

Experimental data has been taken from two sources:

- "Dielectric properties of binary solutions – A data handbook" by Y.Y. Akhadov, Pergamon Press, 1981 [17]
- "Electrolyte data collection – Dielectric properties of water and aqueous electrolyte solutions" by J. Barthel, R. Buchner, M. Münsterer, DECHEMA Chemistry Data Series, vol. XII, part 2 [18]

The data has been collected from the 1930's to the 1980's. However the measurements made before the 1960's were poor and often contradicted by later ones. As a result only data resulting from measurements made after 1960 was used. Moreover when the dielectric permittivity of a solution was available from several sources, the most recent measurements were kept and averaged.

Overall experimental data on the dielectric permittivity of electrolytic solutions is scarce therefore measurements at two different concentrations were found for only 54 electrolytes. The values measured at a few different concentrations were used to find the parameters in an empirical equation that has been shown to accurately reproduce the variations of the dielectric permittivity for a few common electrolytes [110].

$$\varepsilon_r = \frac{\varepsilon_r^0}{1 + \left(A_{anion} x_{anion} + A_{cation} x_{cation} \right) \ln\left(1 + B\sqrt{I_x}\right)}$$

Where $\varepsilon_r^0 = 78.5$ dielectric permittivity of pure water at T = 298 K

x_i = mole fraction of i

I_x = ionic strength based on mole fractions

B = 1,027,752 at T = 298 K

A_i = constants to be adjusted for each electrolyte

This empirical equation is not suitable to reproduce the experimental data of the 2:2 and 3:2 electrolytes examined. It has been modified to include them. The constants A_{anion} and A_{cation} are taken to be equal and written as A_1. An additional constant A_2 is introduced for 2:2 and 3:2 electrolytes; $A_2 = 0$ if one of the ionic species is univalent.

$$\varepsilon_r = \varepsilon_r^0 \frac{1 + A_2 \ln\left(1 + A_1 \left(x_{anion} + x_{cation} \right)\right)}{1 + A_1 \left(x_{anion} + x_{cation} \right) \ln\left(1 + B\sqrt{I_x}\right)}$$

The curves of the dielectric permittivity of the 53 electrolytes examined are grouped in series by anion and displayed below.
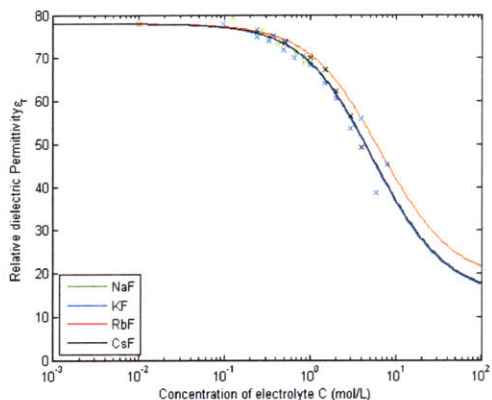
Figure 12: Dielectric permittivity of alkali fluorides
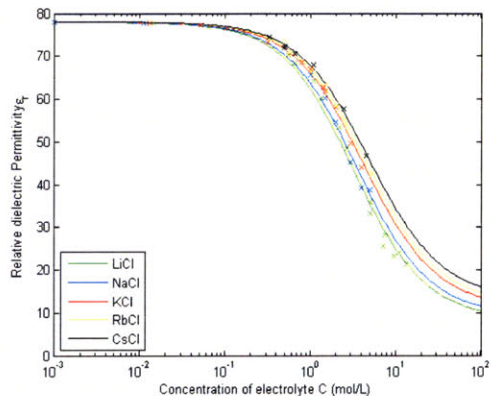
Figure 13: Dielectric permittivity of alkali chlorides
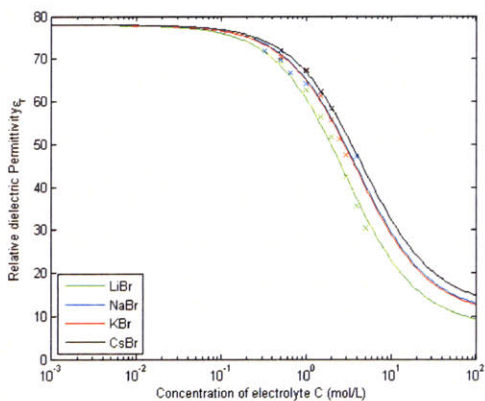
Figure 14: Dielectric permittivity of alkali bromides
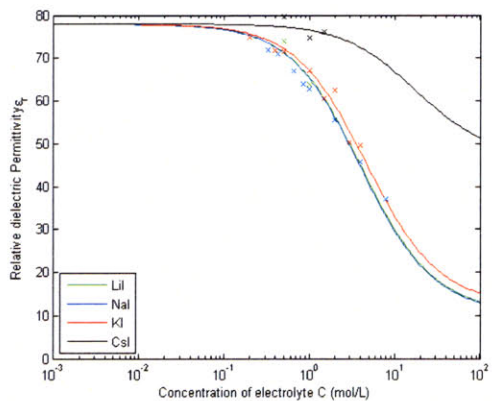
Figure 15: Dielectric permittivity of alkali iodides
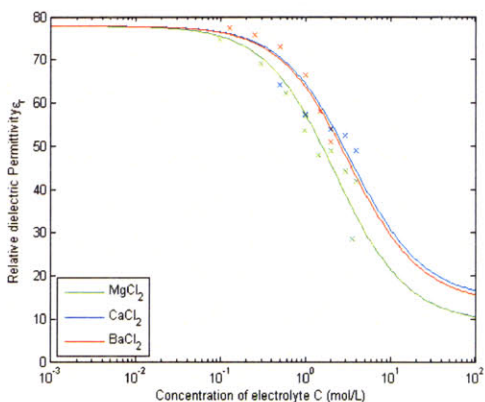
Figure 16: Dielectric permittivity of alkaline metal chlorides
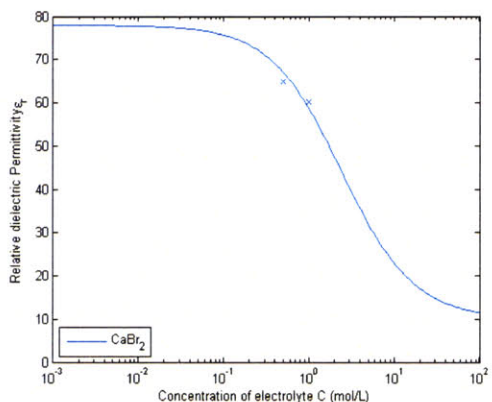
Figure 17: Dielectric permittivity of calcium bromide
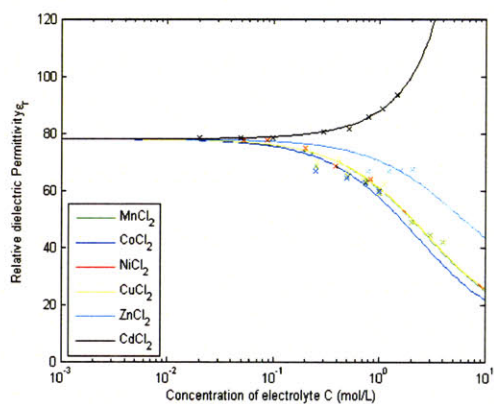
Figure 18: Dielectric permittivity of metal dichlorides
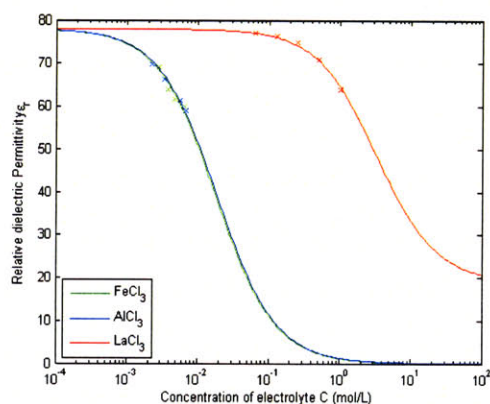
Figure 19: Dielectric permittivity of metal trichlorides
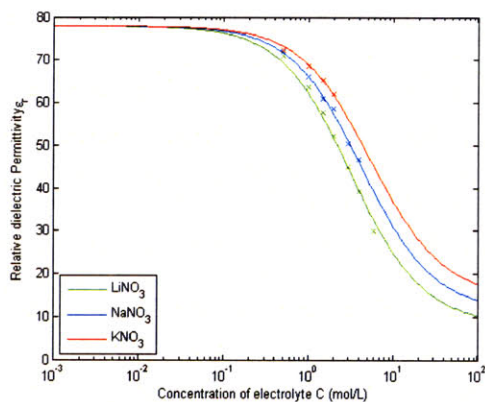
Figure 20: Dielectric permittivity of alkali nitrates
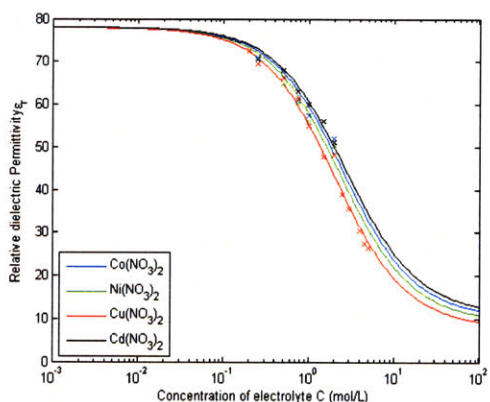
Figure 21: Dielectric permittivity of metal dinitrates
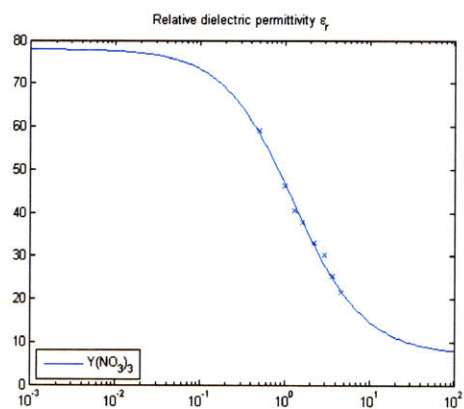
Figure 22: Dielectric permittivity of yttrium nitrate
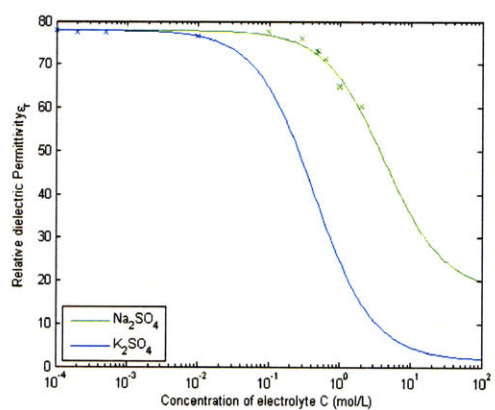
Figure 23: Dielectric permittivity of alkali sulfates

66
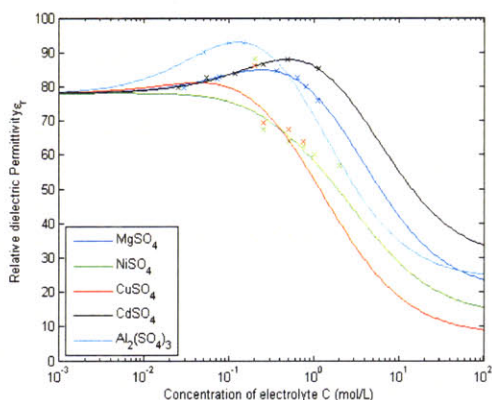
Figure 24: Dielectric permittivity of metal sulfates
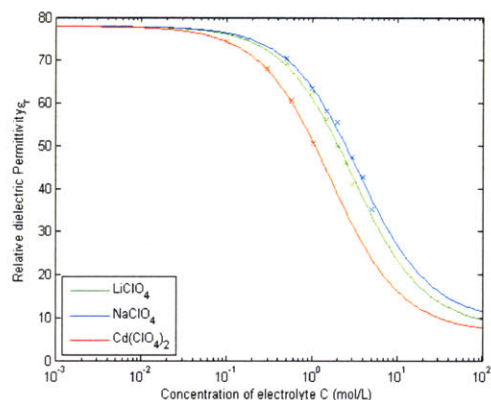
Figure 25: Dielectric permittivity of perchlorates
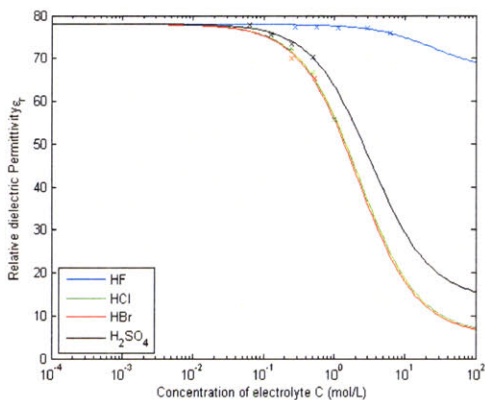
Figure 26: Dielectric permittivity of acids
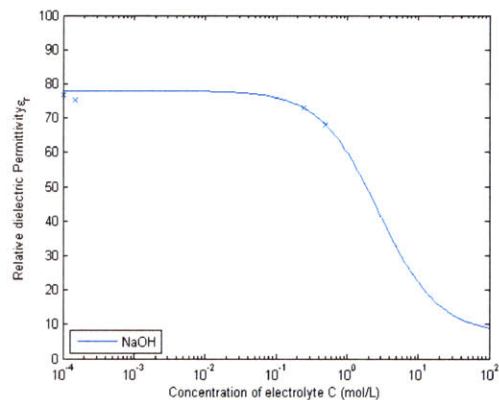
Figure 27: Dielectric permittivity of sodium hydroxide

The dielectric permittivity of most electrolytes exhibits the same pattern:
- Effectively constant at low concentrations, the value being that of pure water, i.e. 78.5
- Linear decrease in the logarithm of the concentration over a range usually comprised between 0.1 mol/L and 10 mol/L
- Effectively constant at very high concentrations, the value depending on the electrolyte and being around 10.

For a few electrolytes, the dielectric permittivity has a completely different behavior:
- For cesium iodide (CsI), lanthanum chloride (LaCl$_3$) and the hydrofluoric acid (HF), it remains constant until much higher concentrations and the decrease is much slower.
- For cadmium chloride (CdCl$_2$), it increases instead of decreasing; it is the only electrolyte with a negative constant A$_1$
- For magnesium sulfate (MgSO$_4$), cadmium sulfate (CdSO$_4$) and aluminum sulfate (Al$_2$(SO$_4$)$_3$), it increases first then decreases linearly in the logarithm of the concentration and stabilizes at much higher values.
  The numerical values of parameters A$_1$ and A$_2$ are given in Appendix D.

Since in most of the series shown above, the dielectric permittivities of chemically similar electrolytes exhibit similar behavior, we studied more than the 53 electrolytes for which

67

enough experimental data was available. For these other electrolytes, we used the dielectric permittivity of nearby electrolytes in the periodic table. These substitutions are given in the table below.

Table 3: Electrolyte substitutions for the dielectric permittivity

Electrolyte	Substitute	Electrolyte	Substitute	Electrolyte	Substitute
$SrCl_2$	$CaCl_2$	$MgBr_2$	$CaBr_2$	MgI_2	$CaBr_2$
$FeCl_2$	$MnCl_2$	$MnBr_2$	$CaBr_2$	CaI_2	$CaBr_2$
$CeCl_3$	$LaCl_3$	$CuBr_2$	$CaBr_2$	HI	HBr
RbBr	KBr	$ZnBr_2$	$CaBr_2$	HNO_3	HBr
RbI	KI	Li_2SO_4	Na_2SO_4	KOH	NaOH
$Zn(NO_3)_2$	$Cu(NO_3)_2$	Rb_2SO_4	K_2SO_4	YCl_3	$Y(NO_3)_3$
$ZnSO_4$	$CuSO_4$	Cs_2SO_4	K_2SO_4	$KClO_4$	$NaClO_4$

II   IONIC STRENGTH

Extensive experimental data for 74 electrolytes was collected. In the literature the concentration was given as molality, i.e. moles of solute per kilogram of water. However the ionic strength present in the equations is in terms of molarity, i.e. moles of solute per liter of solution. The relationship between the two measures of concentration is [14]

$$c = m\frac{1000d}{1000 + mM} \qquad m = c\frac{1000}{1000d - cM}$$

Where   c = concentration in mol of solute/L solution
m = concentration in mol of solute/kg solvent
d = density of solution (kg/L)
M = molecular mass of salt (g/mol)

In order to convert from molality to molarity, the density of the solution is needed. Experimental data on the density of electrolyte solutions was gathered from [20].

− Density of pure water

$$d_w(t) = 0.99965 + 2.0438 \cdot 10^{-4}t - 6.1744 \cdot 10^{-5}t^{3/2}$$

t = temperature in °C d_w in kg/L
d_w(4°C) = 1.0 kg/L d_w(25°C) = 0.997 kg/L

− Density of a saline solution
■ At a given temperature $d = d_w(t) + G \cdot c + H \cdot c^{3/2}$

■ In general $d = d_w(t) + A \cdot c + B \cdot c \cdot t + C \cdot c \cdot t^2 + D \cdot c^{3/2} + E \cdot c^{3/2} \cdot t + F \cdot c^{3/2} \cdot t^2$

Where t = temperature in °C and c = concentration in mol/L of solution.

The sets of parameters {G,H} or {A,B,C,D,E,F} were given in the literature [20]. Sometimes no set of parameters was available at room temperature, t = 25°C, and in this case the set of parameters at the closest temperature was used.

The computation of the molarity from the molality was performed numerically by solving the equation

$$\frac{1000c}{1000d - cM} = m$$

where the density d is itself a function of c. The solver was initialized with $c_0 = m$ and the resolution took place in the interval $\left[\frac{1}{2}m, \frac{17}{10}m\right]$.

The ionic strength is given by $I = \frac{1}{2}\left(\nu_\alpha z_\alpha^2 + \nu_\beta z_\beta^2\right)\rho^0$. ρ^0 is the concentration expressed as number of ions per Å^3; $\rho^0 = N_A \cdot 10^{-27} \cdot c$.

Chapter 6   Equilibrium of solutions containing binary electrolytes

I   GENERAL EQUATIONS FOR A BINARY SOLUTE

A binary solute $A_{v\alpha}B_{v\beta}$ is dissolved in water. The global bulk concentrations are $\rho_\alpha{}^0$ and $\rho_\beta{}^0$; the solution is overall electroneutral i.e. $z_\alpha\rho_\alpha{}^0 + z_\beta\rho_\beta{}^0 = 0$. The system is in equilibrium. For the two chemical species

$$J_\alpha = 0$$

$$\frac{z_\alpha e}{k_B T}\nabla V + \frac{\nabla\rho_\alpha}{\rho_\alpha} + \frac{8\sigma_\alpha^3\nabla\rho_\alpha + 8\sigma_\beta^3\nabla\rho_\beta}{1 - 8\sigma_\alpha^3\rho_\alpha - 8\sigma_\beta^3\rho_\beta}$$
$$+2.3w^2 l_B^3 z_\alpha\left(z_\alpha\nabla\rho_\alpha + z_\beta\nabla\rho_\beta\right) \qquad = 0$$
$$-\frac{w l_B^3}{4}\begin{bmatrix} -10.58z_\alpha^2\left(z_\alpha^2\nabla\rho_\alpha + z_\beta^2\nabla\rho_\beta\right) \\ +17z_\alpha\left(z_\alpha\nabla\rho_\alpha + z_\beta\nabla\rho_\beta\right) \end{bmatrix}$$

$$J_\beta = 0$$

$$\frac{z_\beta e}{k_B T}\nabla V + \frac{\nabla\rho_\beta}{\rho_\beta} + \frac{8\sigma_\alpha^3\nabla\rho_\alpha + 8\sigma_\beta^3\nabla\rho_\beta}{1 - 8\sigma_\alpha^3\rho_\alpha - 8\sigma_\beta^3\rho_\beta}$$
$$+2.3w^2 l_B^3 z_\beta\left(z_\alpha\nabla\rho_\alpha + z_\beta\nabla\rho_\beta\right) \qquad = 0$$
$$-\frac{w l_B^3}{4}\begin{bmatrix} -10.58z_\beta^2\left(z_\alpha^2\nabla\rho_\alpha + z_\beta^2\nabla\rho_\beta\right) \\ +17z_\beta\left(z_\alpha\nabla\rho_\alpha + z_\beta\nabla\rho_\beta\right) \end{bmatrix}$$

For the electrical field

$$\nabla\cdot E = \frac{e}{\varepsilon_0\varepsilon_r}\left(z_\alpha\rho_\alpha + z_\beta\rho_\beta\right)$$

We consider a hard sphere with radius R and total charge Ze. The ionic solution surrounding the sphere has on average spherical symmetry and the different quantities studied depend only on the radial coordinate r. The electrical field is inferred from the theorem of Gauss for $r \geq R$.

$$4\pi r^2 E(r) = \frac{e}{\varepsilon_0\varepsilon_r}\left[Z + 4\pi\int_R^r\left(z_\alpha\rho_\alpha(r') + z_\beta\rho_\beta(r')\right)r'^2\,dr'\right]$$

$$E(r) = \frac{e}{4\pi\varepsilon_0\varepsilon_r r^2}\left[Z + 4\pi\int_R^r\left(z_\alpha\rho_\alpha(r') + z_\beta\rho_\beta(r')\right)r'^2\,dr'\right]$$

$$\frac{eE(r)}{k_B T} = \frac{e^2}{4\pi\varepsilon_0\varepsilon_r k_B T r^2}\left[Z + 4\pi\int_R^r\left(z_\alpha\rho_\alpha(r') + z_\beta\rho_\beta(r')\right)r'^2\,dr'\right]$$

$$\frac{eE(r)}{k_B T} = \frac{Z l_B}{r^2} + \frac{4\pi l_B}{r^2}\int_R^r\left(z_\alpha\rho_\alpha(r') + z_\beta\rho_\beta(r')\right)r'^2\,dr'$$

Substituting this expression of the electrical field in the previous differential equations yields

$$-\frac{4\pi z_\alpha l_B}{r^2}\int_R^r \left(z_\alpha\rho_\alpha\left(r'\right)+z_\beta\rho_\beta\left(r'\right)\right)r'^2\,dr'$$

$$-\frac{Zz_\alpha l_B}{r^2}+\frac{\rho_\alpha'}{\rho_\alpha}+\frac{8\sigma_\alpha^3\rho_\alpha'+8\sigma_\beta^3\rho_\beta'}{1-8\sigma_\alpha^3\rho_\alpha-8\sigma_\beta^3\rho_\beta}\qquad=0$$

$$+2.3w^2l_B^3z_\alpha\left(z_\alpha\rho_\alpha'+z_\beta\rho_\beta'\right)$$

$$-\frac{wl_B^3}{4}\left[\begin{array}{l}-10.58z_\alpha^2\left(z_\alpha^2\rho_\alpha'+z_\beta^2\rho_\beta'\right)\\+17z_\alpha\left(z_\alpha\rho_\alpha'+z_\beta\rho_\beta'\right)\end{array}\right]$$

$$-\frac{4\pi z_\beta l_B}{r^2}\int_R^r \left(z_\alpha\rho_\alpha\left(r'\right)+z_\beta\rho_\beta\left(r'\right)\right)r'^2\,dr'$$

$$-\frac{Zz_\beta l_B}{r^2}+\frac{\rho_\beta'}{\rho_\beta}+\frac{8\sigma_\alpha^3\rho_\alpha'+8\sigma_\beta^3\rho_\beta'}{1-8\sigma_\alpha^3\rho_\alpha-8\sigma_\beta^3\rho_\beta}\qquad=0$$

$$+2.3w^2l_B^3z_\beta\left(z_\alpha\rho_\alpha'+z_\beta\rho_\beta'\right)$$

$$-\frac{wl_B^3}{4}\left[\begin{array}{l}-10.58z_\beta^2\left(z_\alpha^2\rho_\alpha'+z_\beta^2\rho_\beta'\right)\\+17z_\beta\left(z_\alpha\rho_\alpha'+z_\beta\rho_\beta'\right)\end{array}\right]$$

II   SOLUTION OF THE LINEARIZED DIFFERENTIAL EQUATIONS

When the charge of the sphere is low, typically $Z = \pm1, \pm2, \pm3$, or when the radius of the sphere is large, the electrical fields generated are small so the local deviation from the bulk concentrations is small. To study this case we linearize the two differential equations by writing

$$\rho_\alpha = \rho_\alpha^0 + \rho_\alpha^\varepsilon \quad\text{and}\quad \rho_\beta = \rho_\beta^0 + \rho_\beta^\varepsilon$$

$$\left|\frac{\rho_\alpha^\varepsilon}{\rho_\alpha^0}\right| \ll 1 \quad\text{and}\quad \left|\frac{\rho_\alpha^\varepsilon}{\rho_\alpha^0}\right| \ll 1$$

and by introducing $\rho_\pm = z_\alpha\rho_\alpha + z_\beta\rho_\beta = z_\alpha\rho_\alpha^\varepsilon + z_\beta\rho_\beta^\varepsilon$ the net charge (identical to I_1).

Approximating the equations to the first order yields

$$-\frac{4\pi z_\alpha l_B}{r^2}\int_R^r \rho_\pm\left(r'\right)r'^2\,dr'-\frac{Zz_\alpha l_B}{r^2}+$$

$$\frac{\rho_\alpha'^\varepsilon}{\rho_\alpha^0}+\frac{8\sigma_\alpha^3\rho_\alpha'^\varepsilon+8\sigma_\beta^3\rho_\beta'^\varepsilon}{1-8\sigma_\alpha^3\rho_\alpha^0-8\sigma_\beta^3\rho_\beta^0}+2.3w^2l_B^3z_\alpha\rho_\pm'\qquad=0$$

$$-\frac{wl_B^3}{4}\left[\begin{array}{l}-10.58z_\alpha^2\left(z_\alpha^2\rho_\alpha'^\varepsilon+z_\beta^2\rho_\beta'^\varepsilon\right)\\+17z_\alpha\rho_\pm'\end{array}\right]$$

$$-\frac{4\pi z_\beta l_B}{r^2}\int_R^r \rho_\pm\left(r'\right)r'^2\,dr'-\frac{Zz_\beta l_B}{r^2}+$$

$$\frac{\rho_\beta'^\varepsilon}{\rho_\beta^0}+\frac{8\sigma_\alpha^3\rho_\alpha'^\varepsilon+8\sigma_\beta^3\rho_\beta'^\varepsilon}{1-8\sigma_\alpha^3\rho_\alpha^0-8\sigma_\beta^3\rho_\beta^0}+2.3w^2l_B^3z_\beta\rho_\pm'\qquad=0$$

$$-\frac{wl_B^3}{4}\left[\begin{array}{l}-10.58z_\beta^2\left(z_\alpha^2\rho_\alpha'^\varepsilon+z_\beta^2\rho_\beta'^\varepsilon\right)\\+17z_\beta\rho_\pm'\end{array}\right]$$

A simple relationship between ρ_α^ε and ρ_β^ε exists

$$\frac{1}{z_\alpha}\frac{\rho_\alpha'^\varepsilon}{\rho_\alpha^0}+\frac{1}{z_\alpha}\frac{8\sigma_\alpha^3\rho_\alpha'^\varepsilon+8\sigma_\beta^3\rho_\beta'^\varepsilon}{1-8\sigma_\alpha^3\rho_\alpha^0-8\sigma_\beta^3\rho_\beta^0}$$

$$+\frac{10.58}{4}z_\alpha wl_B^3\left(z_\alpha^2\rho_\alpha'^\varepsilon+z_\beta^2\rho_\beta'^\varepsilon\right)$$

$$=\frac{1}{z_\beta}\frac{\rho_\beta'^\varepsilon}{\rho_\beta^0}+\frac{1}{z_\beta}\frac{8\sigma_\alpha^3\rho_\alpha'^\varepsilon+8\sigma_\beta^3\rho_\beta'^\varepsilon}{1-8\sigma_\alpha^3\rho_\alpha^0-8\sigma_\beta^3\rho_\beta^0}$$

$$+\frac{10.58}{4}z_\beta wl_B^3\left(z_\alpha^2\rho_\alpha'^\varepsilon+z_\beta^2\rho_\beta'^\varepsilon\right)$$

That can be integrated into

$$\frac{1}{z_\alpha}\frac{\rho_\alpha^\varepsilon}{\rho_\alpha^0}+\frac{1}{z_\alpha}\frac{8\sigma_\alpha^3\rho_\alpha^\varepsilon+8\sigma_\beta^3\rho_\beta^\varepsilon}{1-8\sigma_\alpha^3\rho_\alpha^0-8\sigma_\beta^3\rho_\beta^0}$$

$$+2.645z_\alpha wl_B^3\left(z_\alpha^2\rho_\alpha^\varepsilon+z_\beta^2\rho_\beta^\varepsilon\right)$$

$$=\frac{1}{z_\beta}\frac{\rho_\beta^\varepsilon}{\rho_\beta^0}+\frac{1}{z_\beta}\frac{8\sigma_\alpha^3\rho_\alpha^\varepsilon+8\sigma_\beta^3\rho_\beta^\varepsilon}{1-8\sigma_\alpha^3\rho_\alpha^0-8\sigma_\beta^3\rho_\beta^0}$$

$$+2.645z_\beta wl_B^3\left(z_\alpha^2\rho_\alpha^\varepsilon+z_\beta^2\rho_\beta^\varepsilon\right)$$

71

Thence

$$
\rho_\alpha^\varepsilon \left[\frac{1}{z_\alpha}\frac{1}{\rho_\alpha^0} + \frac{8\sigma_\alpha^3\left(\dfrac{1}{z_\alpha}-\dfrac{1}{z_\beta}\right)}{1-8\sigma_\alpha^3\rho_\alpha^0-8\sigma_\beta^3\rho_\beta^0} +2.645 w l_B^3 z_\alpha^2 \left(z_\alpha - z_\beta\right) \right]
= \rho_\beta^\varepsilon \left[\frac{1}{z_\beta}\frac{1}{\rho_\beta^0} + \frac{8\sigma_\beta^3\left(\dfrac{1}{z_\beta}-\dfrac{1}{z_\alpha}\right)}{1-8\sigma_\alpha^3\rho_\alpha^0-8\sigma_\beta^3\rho_\beta^0} +2.645 w l_B^3 z_\beta^2 \left(z_\beta - z_\alpha\right) \right]
$$

We introduce three constants K_α, K_β and K to make the calculations simpler. They are homogenous to the inverse of a length.

$$
K_\alpha^2 = \frac{4\pi l_B z_\alpha^2 \rho_\alpha^0}{1+\left(1-\dfrac{z_\alpha}{z_\beta}\right)\dfrac{8\sigma_\alpha^3\rho_\alpha^0}{1-8\sigma_\alpha^3\rho_\alpha^0-8\sigma_\beta^3\rho_\beta^0}+2.645 w l_B^3 \rho_\alpha^0 z_\alpha^4 \left(1-\dfrac{z_\beta}{z_\alpha}\right)}
$$

$$
K_\beta^2 = \frac{4\pi l_B z_\beta^2 \rho_\beta^0}{1+\left(1-\dfrac{z_\beta}{z_\alpha}\right)\dfrac{8\sigma_\beta^3\rho_\beta^0}{1-8\sigma_\alpha^3\rho_\alpha^0-8\sigma_\beta^3\rho_\beta^0}+2.645 w l_B^3 \rho_\beta^0 z_\beta^4 \left(1-\dfrac{z_\alpha}{z_\beta}\right)}
$$

$$
K^2 = K_\alpha^2 + K_\beta^2
$$

The solution is electroneutral overall i.e. $z_\alpha\rho_\alpha^0 + z_\beta\rho_\beta^0 = 0$. The following formulae result from it

$$
\left(1-\frac{z_\alpha}{z_\beta}\right)\rho_\alpha^0 = \rho_\alpha^0 + \rho_\beta^0 \qquad z_\alpha^4\left(1-\frac{z_\beta}{z_\alpha}\right)\rho_\alpha^0 = -z_\alpha^3 z_\beta\left(\rho_\alpha^0 + \rho_\beta^0\right)
$$

$$
\left(1-\frac{z_\beta}{z_\alpha}\right)\rho_\beta^0 = \rho_\alpha^0 + \rho_\beta^0 \qquad z_\beta^4\left(1-\frac{z_\alpha}{z_\beta}\right)\rho_\beta^0 = -z_\beta^3 z_\alpha\left(\rho_\alpha^0 + \rho_\beta^0\right)
$$

Thus the constants can be rewritten as

$$
K_\alpha^2 = \frac{4\pi l_B z_\alpha^2 \rho_\alpha^0}{1+\dfrac{8\sigma_\alpha^3\left(\rho_\alpha^0 + \rho_\beta^0\right)}{1-8\sigma_\alpha^3\rho_\alpha^0-8\sigma_\beta^3\rho_\beta^0}-2.645 w l_B^3 z_\alpha^3 z_\beta\left(\rho_\alpha^0 + \rho_\beta^0\right)}
$$

$$
K_\beta^2 = \frac{4\pi l_B z_\beta^2 \rho_\beta^0}{1+\dfrac{8\sigma_\beta^3\left(\rho_\alpha^0 + \rho_\beta^0\right)}{1-8\sigma_\alpha^3\rho_\alpha^0-8\sigma_\beta^3\rho_\beta^0}-2.645 w l_B^3 z_\beta^3 z_\alpha\left(\rho_\alpha^0 + \rho_\beta^0\right)}
$$

The previous equation between ρ_α^ε and ρ_β^ε can rewritten as $\dfrac{z_\alpha\rho_\alpha^\varepsilon}{K_\alpha^2} = \dfrac{z_\beta\rho_\beta^\varepsilon}{K_\beta^2}$. The net ionic

density $\rho_\pm = z_\alpha\rho_\alpha^\varepsilon + z_\beta\rho_\beta^\varepsilon$ is transformed into

$$
\rho_\pm = \frac{z_\alpha\rho_\alpha^\varepsilon}{K_\alpha^2}\left(K_\alpha^2 + K_\beta^2\right) = \frac{z_\beta\rho_\beta^\varepsilon}{K_\beta^2}\left(K_\alpha^2 + K_\beta^2\right)
$$

$$\rho_{\pm} = z_\alpha \frac{K^2}{K_\alpha^2} \rho_\alpha^\varepsilon = z_\beta \frac{K^2}{K_\beta^2} \rho_\beta^\varepsilon$$

$$\rho_\alpha^\varepsilon = \frac{1}{z_\alpha} \frac{K_\alpha^2}{K^2} \rho_{\pm} \quad \text{and} \quad \rho_\beta^\varepsilon = \frac{1}{z_\beta} \frac{K_\beta^2}{K^2} \rho_{\pm}$$

We substitute $\rho_{\pm}$ to ρ_α and ρ_β in the previous two differential equations.

$$-\frac{4\pi z_\alpha l_B}{r^2} \int_R^r \rho_{\pm}(r')r'^2 \, dr' - \frac{Zz_\alpha l_B}{r^2} + \frac{1}{z_\alpha}\frac{1}{\rho_\alpha^0}\frac{K_\alpha^2}{K^2}\rho_{\pm}'$$
$$+\frac{\rho_{\pm}'}{K^2}\frac{8K_\alpha^2\sigma_\alpha^3/z_\alpha + 8K_\beta^2\sigma_\beta^3/z_\beta}{1 - 8\sigma_\alpha^3\rho_\alpha^0 - 8\sigma_\beta^3\rho_\beta^0} + 2.3w^2 l_B^3 z_\alpha \rho_{\pm}' \qquad = \quad 0$$
$$+\frac{wl_B^3}{4}\left[\frac{10.58z_\alpha^2}{K^2}\left(z_\alpha K_\alpha^2 + z_\beta K_\beta^2\right) - 17z_\alpha\right]\rho_{\pm}'$$

$$-\frac{4\pi z_\beta l_B}{r^2} \int_R^r \rho_{\pm}(r')r'^2 \, dr' - \frac{Zz_\beta l_B}{r^2} + \frac{1}{z_\beta}\frac{1}{\rho_\beta^0}\frac{K_\beta^2}{K^2}\rho_{\pm}'$$
$$+\frac{\rho_{\pm}'}{K^2}\frac{8K_\alpha^2\sigma_\alpha^3/z_\alpha + 8K_\beta^2\sigma_\beta^3/z_\beta}{1 - 8\sigma_\alpha^3\rho_\alpha^0 - 8\sigma_\beta^3\rho_\beta^0} + 2.3w^2 l_B^3 z_\beta \rho_{\pm}' \qquad = \quad 0$$
$$+\frac{wl_B^3}{4}\left[\frac{10.58z_\beta^2}{K^2}\left(z_\alpha K_\alpha^2 + z_\beta K_\beta^2\right) - 17z_\beta\right]\rho_{\pm}'$$

We divide the equations respectively by z_α and z_β and add them and divide the resulting equation by 2.

$$-\frac{4\pi l_B}{r^2} \int_R^r \rho_{\pm}(r')r'^2 \, dr' - \frac{Zl_B}{r^2} + \frac{1}{2}\left(\frac{1}{z_\alpha^2}\frac{K_\alpha^2}{\rho_\alpha^0} + \frac{1}{z_\beta^2}\frac{K_\beta^2}{\rho_\beta^0}\right)\frac{\rho_{\pm}'}{K^2}$$
$$+\frac{1}{2}\frac{\rho_{\pm}'}{K^2}\left(\frac{1}{z_\alpha} + \frac{1}{z_\beta}\right)\frac{8K_\alpha^2\sigma_\alpha^3/z_\alpha + 8K_\beta^2\sigma_\beta^3/z_\beta}{1 - 8\sigma_\alpha^3\rho_\alpha^0 - 8\sigma_\beta^3\rho_\beta^0} + 2.3w^2 l_B^3 \rho_{\pm}' \quad = \quad 0$$
$$+\frac{wl_B^3}{4}\left[\frac{10.58}{2K^2}\left(z_\alpha + z_\beta\right)\left(z_\alpha K_\alpha^2 + z_\beta K_\beta^2\right) - 17\right]\rho_{\pm}'$$

We introduce a new constant κ in order to simplify the equation; κ has the dimension of inverse length.

$$\frac{4\pi l_B}{\kappa^2} = \frac{1}{2K^2}\left(\frac{1}{z_\alpha^2}\frac{K_\alpha^2}{\rho_\alpha^0} + \frac{1}{z_\beta^2}\frac{K_\beta^2}{\rho_\beta^0}\right) + \frac{1}{2}\frac{1}{K^2}\left(\frac{1}{z_\alpha} + \frac{1}{z_\beta}\right)\frac{8K_\alpha^2\sigma_\alpha^3/z_\alpha + 8K_\beta^2\sigma_\beta^3/z_\beta}{1 - 8\sigma_\alpha^3\rho_\alpha^0 - 8\sigma_\beta^3\rho_\beta^0}$$
$$+ 2.3w^2 l_B^3 + \frac{wl_B^3}{4}\left[\frac{10.58}{2K^2}\left(z_\alpha + z_\beta\right)\left(z_\alpha K_\alpha^2 + z_\beta K_\beta^2\right) - 17\right]$$

73

Transforming the expression of κ to a more direct form yields

$$\frac{1}{\kappa^2} = \frac{1}{K^2} + \frac{2.3}{4\pi} w^2 l_B^2 - \frac{17}{16\pi} w l_B^2 + \frac{1}{K^2} \frac{\dfrac{z_\alpha}{z_\beta} \dfrac{8\sigma_\alpha^3 \rho_\alpha^0}{1 - 8\sigma_\alpha^3 \rho_\alpha^0 - 8\sigma_\beta^3 \rho_\beta^0} + 2.645 w l_B^3 \rho_\alpha^0 z_\alpha^3 z_\beta}{1 + \left(1 - \dfrac{z_\alpha}{z_\beta}\right) \dfrac{8\sigma_\alpha^3 \rho_\alpha^0}{1 - 8\sigma_\alpha^3 \rho_\alpha^0 - 8\sigma_\beta^3 \rho_\beta^0} + 2.645 w l_B^3 \rho_\alpha^0 z_\alpha^4 \left(1 - \dfrac{z_\beta}{z_\alpha}\right)}$$

$$+ \frac{1}{K^2} \frac{\dfrac{z_\beta}{z_\alpha} \dfrac{8\sigma_\beta^3 \rho_\beta^0}{1 - 8\sigma_\alpha^3 \rho_\alpha^0 - 8\sigma_\beta^3 \rho_\beta^0} + 2.645 w l_B^3 \rho_\beta^0 z_\beta^3 z_\alpha}{1 + \left(1 - \dfrac{z_\beta}{z_\alpha}\right) \dfrac{8\sigma_\beta^3 \rho_\beta^0}{1 - 8\sigma_\alpha^3 \rho_\alpha^0 - 8\sigma_\beta^3 \rho_\beta^0} + 2.645 w l_B^3 \rho_\beta^0 z_\beta^4 \left(1 - \dfrac{z_\alpha}{z_\beta}\right)}$$

Or

$$\frac{1}{\kappa^2} = \frac{1}{K^2} + \frac{2.3}{4\pi} w^2 l_B^2 - \frac{17}{16\pi} w l_B^2 - \frac{1}{K^2} \frac{\dfrac{8\sigma_\alpha^3 \rho_\beta^0}{1 - 8\sigma_\alpha^3 \rho_\alpha^0 - 8\sigma_\beta^3 \rho_\beta^0} - 2.645 w l_B^3 z_\alpha^3 z_\beta \rho_\alpha^0}{1 + \dfrac{8\sigma_\alpha^3 \left(\rho_\alpha^0 + \rho_\beta^0\right)}{1 - 8\sigma_\alpha^3 \rho_\alpha^0 - 8\sigma_\beta^3 \rho_\beta^0} - 2.645 w l_B^3 z_\alpha^3 z_\beta \left(\rho_\alpha^0 + \rho_\beta^0\right)}$$

$$- \frac{1}{K^2} \frac{\dfrac{8\sigma_\beta^3 \rho_\alpha^0}{1 - 8\sigma_\alpha^3 \rho_\alpha^0 - 8\sigma_\beta^3 \rho_\beta^0} - 2.645 w l_B^3 \rho_\beta^0 z_\beta^3 z_\alpha}{1 + \dfrac{8\sigma_\beta^3 \left(\rho_\alpha^0 + \rho_\beta^0\right)}{1 - 8\sigma_\alpha^3 \rho_\alpha^0 - 8\sigma_\beta^3 \rho_\beta^0} - 2.645 w l_B^3 z_\beta^3 z_\alpha \left(\rho_\alpha^0 + \rho_\beta^0\right)}$$

The differential equation takes the simple form

$$-\frac{4\pi l_B}{r^2} \int_R^r \rho_\pm (r') r'^2 \, dr' - \frac{Z l_B}{r^2} + \frac{4\pi l_B}{\kappa^2} \rho'_\pm \; = \; 0$$

Now we substitute the variable u = 1/r in the differential equation.

$$-4\pi l_B u^2 \int_u^{1/R} \rho_\pm (u') \frac{du'}{u'^4} - Z l_B u^2 - \frac{4\pi l_B}{\kappa^2} u^2 \frac{d\rho_\pm}{du} \; = \; 0$$

$$4\pi l_B \int_u^{1/R} \rho_\pm (u') \frac{du'}{u'^4} + Z l_B + \frac{4\pi l_B}{\kappa^2} \frac{d\rho_\pm}{du} \; = \; 0$$

We differentiate the equation and obtain a simple second order differential equation.

$$-4\pi l_B \frac{\rho_\pm}{u^4} + \frac{4\pi l_B}{\kappa^2} \frac{d^2 \rho_\pm}{du^2} \; = \; 0$$

$$\frac{\rho_\pm}{u^4} - \frac{1}{\kappa^2} \frac{d^2 \rho_\pm}{du^2} \; = \; 0$$

74

We reintroduce the variable r = 1/u.

$$\rho_\pm - \frac{1}{\kappa^2 r^2} \frac{d}{dr}\left(r^2 \frac{d\rho_\pm}{dr}\right) = 0$$

The solution to the differential equation is $\rho_\pm(r) = A\dfrac{e^{-\kappa r}}{r} + B\dfrac{e^{\kappa r}}{r}$. The boundary conditions

are $\dfrac{d\rho_\pm}{dr}(R) = \dfrac{\kappa^2 Z}{4\pi R^2}$ and $\rho_\pm(r)\xrightarrow[r\to+\infty]{}0$. Thus B = 0 and $A = -Z\dfrac{e^{\kappa R}}{4\pi}\dfrac{\kappa^2}{1+\kappa R}$ hence

$$\rho_\pm(r) = \frac{-Z\kappa^2}{4\pi(1+\kappa R)}\frac{e^{\kappa(R-r)}}{r}$$

$$\rho_\pm(r) = -\frac{Z}{4\pi}\frac{\kappa^2 e^{\kappa R}}{1+\kappa R}\frac{e^{-\kappa r}}{r}$$

III OSMOTIC COEFFICIENT

III.1 Definition

Two osmotic coefficients have been introduced. The first one is the practical osmotic coefficient ϕ_s and is defined in terms of the activity of the solvent a_s.

$$\phi_s = \frac{-1000\ln a_s}{m_s(m_\alpha + m_\beta)}$$

where m_α and m_β are the molalities of ions α and β, and m_s is the molecular mass of the solvent in g/mol. $m_s = 18.015$ g/mol for water. The relationships with the osmotic pressure Π and with the mean ionic activity coefficient are

$$\Pi = \frac{RT}{\overline{V}_s}\frac{(m_\alpha + m_\beta)m_s}{1000}\phi_s \qquad\qquad \ln\gamma_\pm = \phi_s - 1 + \int_0^m \frac{\phi_s - 1}{m'}dm'$$

The second one is the rational osmotic coefficient ϕ_{MM} and is defined from the theory of McMillan and Mayer.

$$\phi_{MM} = \frac{\Pi}{(\rho_\alpha + \rho_\beta)k_B T}$$

The relationship between the two is derived from the expression of the osmotic pressure.

$$\phi_s = \frac{1000\overline{V}_s(\rho_\alpha + \rho_\beta)}{m_s(m_\alpha + m_\beta)}\phi_{MM}$$

In the remainder of the chapter, we describe the osmotic pressure so we use the rational osmotic coefficient and for simplicity we write $\phi_{MM} = \phi$.

III.2 Calculation

From the net charge density $\rho_\pm$, we can compute the osmotic coefficient ϕ. Indeed from the integral theory of liquids, we have the following expression:

$$\phi = 1 - \frac{1}{6\left(\rho_\alpha^0 + \rho_\beta^0\right)k_B T} \sum_{i \in \{\alpha,\beta\}} \sum_{j \in \{\alpha,\beta\}} \rho_i^0 \rho_j^0 \int_0^{+\infty} r \frac{\partial u_{ij}}{\partial r} g_{ij}(r) 4\pi r^2 dr$$

$$\phi = 1 - \frac{2\pi}{3\left(\rho_\alpha^0 + \rho_\beta^0\right)k_B T} \sum_{i \in \{\alpha,\beta\}} \sum_{j \in \{\alpha,\beta\}} \rho_i^0 \rho_j^0 \int_0^{+\infty} \frac{\partial u_{ij}}{\partial r} g_{ij}(r) r^3 dr$$

'i' and 'j' are two indexes that both take values α and β. Four ij combinations exist: $\alpha\alpha$, $\alpha\beta$, $\beta\alpha$ and $\beta\beta$. The two functions to be integrated are

- u_{ij} = potential of the interaction between central ion i and surrounding ions of species j

$$\frac{u_{ij}}{k_B T} = \begin{vmatrix} +\infty \ for \ r < \lambda_i \\ z_i z_j \dfrac{l_B}{r} \ for \ r \geq \lambda_i \end{vmatrix}$$

- g_{ij} = correlation function between central ion i and surrounding ions of species j

$$g_{ij} = \begin{vmatrix} 0 \ for \ r < \lambda_i \\ \dfrac{\rho_j}{\rho_j^0} = \dfrac{\rho_j^0 + \rho_j^\varepsilon}{\rho_j^0} = 1 + \dfrac{\rho_j^\varepsilon}{\rho_j^0} = 1 + \dfrac{1}{z_j} \dfrac{K_j^2}{K^2} \dfrac{\rho_\pm\left(Z = z_i, R = \sigma_i\right)}{\rho_j^0} \ for \ r \geq \lambda_i \end{vmatrix}$$

$$g_{ij} = \begin{vmatrix} 0 \ for \ r < \lambda_i \\ 1 - \dfrac{1}{z_j} \dfrac{z_i}{4\pi\rho_j^0} \dfrac{K_j^2}{K^2} \dfrac{\kappa^2 e^{\kappa\sigma_i}}{1+\kappa\sigma_i} \dfrac{e^{-\kappa r}}{r} \ for \ r \geq \lambda_i \end{vmatrix}$$

λ_i is stricto sensu the distance of closest approach to an ion of species i. We distinguish between the ionic radius σ_i that is the extent of the electronic cloud and the distance of closest approach λ_i that corresponds to the hydrated radius of the ion. The ionic radius is a characteristic of the ionic species and remains constant, whereas the hydrated radius can vary depending on the counterion and its ability to retain and displace water molecules.

The correlation function g_{ij} is 0 for r < λ_i because two ions cannot be closer than allowed by the distance of closest approach.

Then, using the step function of Heaviside, Hv(.), and the delta function of Dirac, $\delta(.)$,

$$\phi = 1 - \frac{2\pi}{3\left(\rho_\alpha^0 + \rho_\beta^0\right)k_B T} \sum_{i \in \{\alpha,\beta\}} \sum_{j \in \{\alpha,\beta\}} \rho_i^0 \rho_j^0 \int_0^{+\infty} \frac{\partial u_{ij}}{\partial r} g_{ij}(r) r^3 dr$$

$$\phi = 1 - \frac{2\pi}{3\left(\rho_\alpha^0 + \rho_\beta^0\right)} \sum_{i \in \{\alpha,\beta\}} \sum_{j \in \{\alpha,\beta\}} \rho_i^0 \rho_j^0 \int_0^{+\infty} -\frac{\partial}{\partial r}\left[e^{-\frac{u_{ij}}{k_B T}}\right] e^{\frac{u_{ij}}{k_B T}} g_{ij}(r) r^3 dr$$

$$\phi = 1 - \frac{2\pi}{3\left(\rho_\alpha^0 + \rho_\beta^0\right)} \sum_{i \in \{\alpha,\beta\}} \sum_{j \in \{\alpha,\beta\}} \rho_i^0 \rho_j^0 \int_0^{+\infty} -\frac{\partial}{\partial r}\left[Hv(r - \lambda_i) e^{-z_i z_j \frac{l_B}{r}}\right] e^{\frac{u_{ij}}{k_B T}} g_{ij}(r) r^3 dr$$

$$\phi = 1 + \frac{2\pi}{3\left(\rho_\alpha^0 + \rho_\beta^0\right)} \sum_{i\in\{\alpha,\beta\}} \sum_{j\in\{\alpha,\beta\}} \rho_i^0 \rho_j^0 \int_0^{+\infty} \left[z_i z_j \frac{l_B}{r^2} Hv\left(r-\lambda_i\right) e^{-z_i z_j \frac{l_B}{r}} + \delta\left(r-\lambda_i\right) e^{-z_i z_j \frac{l_B}{r}} \right] e^{\frac{u_{ij}}{k_B T}} g_{ij}\left(r\right) r^3 dr$$

$$\phi = 1 + \frac{2\pi}{3\left(\rho_\alpha^0 + \rho_\beta^0\right)} \sum_{i\in\{\alpha,\beta\}} \sum_{j\in\{\alpha,\beta\}} \rho_i^0 \rho_j^0 \left[\begin{array}{l} \displaystyle\int_{\lambda_i}^{+\infty} z_i z_j \frac{l_B}{r^2} e^{-z_i z_j \frac{l_B}{r}} \times e^{z_i z_j \frac{l_B}{r}} g_{ij}\left(r\right) r^3 dr + \\[2ex] \displaystyle\int_0^{+\infty} \delta\left(r-\lambda_i\right) e^{-z_i z_j \frac{l_B}{r}} \times e^{\frac{u_{ij}}{k_B T}} g_{ij}\left(r\right) r^3 dr \end{array} \right]$$

$$\phi = 1 + \frac{2\pi}{3\left(\rho_\alpha^0 + \rho_\beta^0\right)} \sum_{i\in\{\alpha,\beta\}} \sum_{j\in\{\alpha,\beta\}} \rho_i^0 \rho_j^0 \left[z_i z_j l_B \int_{\lambda_i}^{+\infty} g_{ij}\left(r\right) r dr + g_{ij}\left(\lambda_i\right) \lambda_i^3 \right]$$

The two pieces are calculated separately.

- $g_{ij}\left(\lambda_i\right)\lambda_i^3 = \lambda_i^3 \left(1 - \frac{1}{z_j} \frac{z_i}{4\pi\rho_j^0} \frac{K_j^2}{K^2} \frac{\kappa^2 e^{\kappa\sigma_i}}{1+\kappa\sigma_i} \frac{e^{-\kappa\lambda_i}}{\lambda_i}\right) = \lambda_i^3 - \frac{1}{z_j} \frac{z_i}{4\pi\rho_j^0} \frac{K_j^2}{K^2} \frac{\kappa^2 \lambda_i^2}{1+\kappa\sigma_i} e^{-\kappa(\lambda_i-\sigma_i)}$

- $\displaystyle\int_{\lambda_i}^{+\infty} g_{ij}\left(r\right) r dr = \int_{\lambda_i}^{+\infty} \left(1 - \frac{1}{z_j} \frac{z_i}{4\pi\rho_j^0} \frac{K_j^2}{K^2} \frac{\kappa^2 e^{\kappa\sigma_i}}{1+\kappa\sigma_i} \frac{e^{-\kappa r}}{r}\right) r dr = \lim_{\varsigma\to+\infty} \int_{\lambda_i}^{\varsigma} r dr - \frac{1}{z_j} \frac{z_i}{4\pi\rho_j^0} \frac{K_j^2}{K^2} \frac{\kappa^2 e^{\kappa\sigma_i}}{1+\kappa\sigma_i} \int_{\lambda_i}^{+\infty} e^{-\kappa r} dr$

$$\int_{\lambda_i}^{+\infty} g_{ij}\left(r\right) r dr = Lim - \frac{1}{z_j} \frac{z_i}{4\pi\rho_j^0} \frac{K_j^2}{K^2} \frac{\kappa^2 e^{\kappa\sigma_i}}{1+\kappa\sigma_i} \frac{e^{-\kappa\lambda_i}}{\kappa} = Lim - \frac{1}{z_j} \frac{z_i}{4\pi\rho_j^0} \frac{K_j^2}{K^2} \frac{\kappa e^{\kappa(\sigma_i-\lambda_i)}}{1+\kappa\sigma_i}$$

Thus

$$\phi = 1 + \frac{2\pi}{3\left(\rho_\alpha^0 + \rho_\beta^0\right)} \left(\lambda_\alpha^3 \rho_\alpha^0 + \lambda_\beta^3 \rho_\beta^0\right)\left(\rho_\alpha^0 + \rho_\beta^0\right)$$

$$- \frac{2\pi}{3\left(\rho_\alpha^0 + \rho_\beta^0\right)} \frac{1}{K^2} \left(\frac{z_\alpha \rho_\alpha^0}{4\pi} \frac{\kappa^2 \lambda_\alpha^2}{1+\kappa\sigma_\alpha} e^{-\kappa(\lambda_\alpha-\sigma_\alpha)} + \frac{z_\beta \rho_\beta^0}{4\pi} \frac{\kappa^2 \lambda_\beta^2}{1+\kappa\sigma_\beta} e^{-\kappa(\lambda_\beta-\sigma_\beta)} \right)\left(\frac{K_\alpha^2}{z_\alpha} + \frac{K_\beta^2}{z_\beta} \right)$$

$$+ \frac{2\pi l_B Lim}{3\left(\rho_\alpha^0 + \rho_\beta^0\right)} \left(z_\alpha \rho_\alpha^0 + z_\beta \rho_\beta^0\right)^2 - \frac{2\pi\kappa l_B}{3\left(\rho_\alpha^0 + \rho_\beta^0\right)} \left(\frac{z_\alpha^2 \rho_\alpha^0}{4\pi} \frac{1}{K^2} \frac{e^{\kappa(\sigma_\alpha-\lambda_\alpha)}}{1+\kappa\sigma_\alpha} + \frac{z_\beta^2 \rho_\beta^0}{4\pi} \frac{1}{K^2} \frac{e^{\kappa(\sigma_\beta-\lambda_\beta)}}{1+\kappa\sigma_\beta} \right)\left(K_\alpha^2 + K_\beta^2\right)$$

The solution is electroneutral, i.e. $z_\alpha \rho_\alpha^0 + z_\beta \rho_\beta^0 = 0$, which eliminates the term with an infinite value. Moreover $K_\alpha^2 + K_\beta^2 = K^2$. The expression of the osmotic coefficient can be simplified to

$$\phi = 1 + \frac{2\pi}{3}\left(\lambda_\alpha^3 \rho_\alpha^0 + \lambda_\beta^3 \rho_\beta^0\right) - \frac{\kappa l_B}{6\left(\rho_\alpha^0 + \rho_\beta^0\right)} \left(\frac{z_\alpha^2 \rho_\alpha^0}{1+\kappa\sigma_\alpha} e^{-\kappa(\lambda_\alpha-\sigma_\alpha)} + \frac{z_\beta^2 \rho_\beta^0}{1+\kappa\sigma_\beta} e^{-\kappa(\lambda_\beta-\sigma_\beta)} \right)$$

$$- \frac{\kappa^2/K^2}{6\left(\rho_\alpha^0 + \rho_\beta^0\right)} \left(\frac{z_\alpha}{\sigma_\alpha} \frac{\rho_\alpha^0 \lambda_\alpha^3}{1+\kappa\sigma_\alpha} e^{-\kappa(\lambda_\alpha-\sigma_\alpha)} + \frac{z_\beta}{\sigma_\beta} \frac{\rho_\beta^0 \lambda_\beta^3}{1+\kappa\sigma_\beta} e^{-\kappa(\lambda_\beta-\sigma_\beta)} \right)\left(\frac{K_\alpha^2}{z_\alpha} + \frac{K_\beta^2}{z_\beta} \right)$$

Using the concentration of solute ρ_0, we have $\rho_\alpha^0 = \nu_\alpha \rho^0$, $\rho_\beta^0 = \nu_\beta \rho^0$ and

$$\phi = 1 + \frac{2\pi\rho^0}{3}\left(v_\alpha\lambda_\alpha^3 + v_\beta\lambda_\beta^3\right) - \frac{\kappa l_B}{6\left(v_\alpha + v_\beta\right)}\left(\frac{z_\alpha^2 v_\alpha}{1+\kappa\sigma_\alpha}e^{-\kappa(\lambda_\alpha - \sigma_\alpha)} + \frac{z_\beta^2 v_\beta}{1+\kappa\sigma_\beta}e^{-\kappa(\lambda_\beta - \sigma_\beta)}\right)$$

$$-\frac{\kappa^2/K^2}{6\left(v_\alpha + v_\beta\right)}\left(\frac{z_\alpha}{\sigma_\alpha}\frac{v_\alpha\lambda_\alpha^3}{1+\kappa\sigma_\alpha}e^{-\kappa(\lambda_\alpha - \sigma_\alpha)} + \frac{z_\beta}{\sigma_\beta}\frac{v_\beta\lambda_\beta^3}{1+\kappa\sigma_\beta}e^{-\kappa(\lambda_\beta - \sigma_\beta)}\right)\left(\frac{K_\alpha^2}{z_\alpha} + \frac{K_\beta^2}{z_\beta}\right)$$

IV   MEAN IONIC ACTIVITY COEFFICIENT

IV.1   Calculation

The mean ionic activity coefficient can be calculated using the integral theory of liquids from the following expression:

$$k_B T \ln\gamma_\pm = \frac{1}{\rho_\alpha^0 + \rho_\beta^0}\sum_{i\in\{\alpha,\beta\}}\sum_{j\in\{\alpha,\beta\}}\rho_i^0\rho_j^0\int_{\zeta=0}^{1}\int_{\xi=0}^{1}\int_{r=0}^{+\infty}u_{ij}(r)g_{ij}(r;\xi,\zeta)4\pi r^2 dr d\xi d\zeta$$

'i' and 'j' are two indexes that both take values α and β. Four ij combinations exist: $\alpha\alpha$, $\alpha\beta$, $\beta\alpha$ and $\beta\beta$. The two functions to be integrated are the same as for the osmotic coefficient:

- u_{ij} = potential of the interaction between central ion i and surrounding ions of species j

$$\frac{u_{ij}}{k_B T} = \begin{vmatrix} +\infty \ for \ r < \xi\cdot\lambda_i \\ z_i z_j \dfrac{l_B}{r} \ for \ r \geq \xi\cdot\lambda_i \end{vmatrix}$$

- g_{ij} = correlation function between central ion i and surrounding ions of species j

$$g_{ij} = \begin{vmatrix} 0 \ for \ r < \xi\cdot\lambda_i \\ \dfrac{\rho_j}{\rho_j^0} = \dfrac{\rho_j^0 + \rho_j^\varepsilon}{\rho_j^0} = 1 + \dfrac{\rho_j^\varepsilon}{\rho_j^0} = 1 + \dfrac{1}{z_j}\dfrac{K_j^2}{K^2}\dfrac{\rho_\pm\left(Z=\zeta\cdot z_i, R=\xi\cdot\sigma_i\right)}{\rho_j^0} \ for \ r \geq \xi\cdot\lambda_i \end{vmatrix}$$

$$g_{ij} = \begin{vmatrix} 0 \ for \ r < \xi\cdot\lambda_i \\ 1 - \dfrac{1}{z_j}\dfrac{\zeta\cdot z_i}{4\pi\rho_j^0}\dfrac{K_j^2}{K^2}\dfrac{\kappa^2 e^{\xi\cdot\kappa\sigma_i}}{1+\xi\cdot\kappa\sigma_i}\dfrac{e^{-\kappa r}}{r} \ for \ r \geq \xi\cdot\lambda_i \end{vmatrix}$$

The two parameters, ξ and ζ, are used to describe the progressive introduction of the central ion in the solution; ξ describes the introduction of a hard sphere of radius σ_i and ζ describes the charging from 0 to z_i.

λ_i is again the distance of closest approach to an ion of species i. We have $g_{ij} = 0$ for $r < \lambda_i$ because two ions cannot be closer than allowed by the distance of closest approach. Thus the product $u_{ij}\cdot g_{ij}$ is undefined for $r < \lambda_i$; we assign the value 4 to the product $u_{ij}\cdot g_{ij}$ in order to recover the usual term representing the excluded volume of a hard sphere.

$$\ln \gamma_\pm = \sum_{i \in \{\alpha,\beta\}} \sum_{j \in \{\alpha,\beta\}} \frac{\rho_i^0 \rho_j^0}{\rho_\alpha^0 + \rho_\beta^0} \int\limits_{\zeta=0}^{1} \int\limits_{\xi=0}^{1} \int\limits_{r=\xi \cdot \lambda_i}^{+\infty} \zeta \cdot z_i z_j \frac{l_B}{r} \left[1 - \frac{1}{z_j} \frac{\zeta \cdot z_i}{4\pi \rho_j^0} \frac{K_j^2}{K^2} \frac{\kappa^2 e^{\xi \cdot \kappa \sigma_i}}{1 + \xi \cdot \kappa \sigma_i} \frac{e^{-\kappa r}}{r} \right] 4\pi r^2 \, dr \, d\xi \, d\zeta$$

$$+ \frac{1}{\rho_\alpha^0 + \rho_\beta^0} \sum_{i \in \{\alpha,\beta\}} \sum_{j \in \{\alpha,\beta\}} \rho_i^0 \rho_j^0 \int\limits_{\zeta=0}^{1} \int\limits_{\xi=0}^{1} \int\limits_{r=0}^{\xi \cdot \lambda_i} 4 \times 4\pi r^2 \, dr \, d\xi \, d\zeta$$

$$\ln \gamma_\pm = \frac{1}{\rho_\alpha^0 + \rho_\beta^0} \sum_{i \in \{\alpha,\beta\}} \sum_{j \in \{\alpha,\beta\}} \rho_i^0 \rho_j^0 \int\limits_{\xi=0}^{1} \int\limits_{r=\xi \cdot \lambda_i}^{+\infty} z_i z_j \frac{l_B}{r} \left[1 - \frac{1}{z_j} \frac{z_i}{8\pi \rho_j^0} \frac{K_j^2}{K^2} \frac{\kappa^2 e^{\xi \cdot \kappa \sigma_i}}{1 + \xi \cdot \kappa \sigma_i} \frac{e^{-\kappa r}}{r} \right] 4\pi r^2 \, dr \, d\xi$$

$$+ \frac{1}{\rho_\alpha^0 + \rho_\beta^0} \sum_{i \in \{\alpha,\beta\}} \sum_{j \in \{\alpha,\beta\}} \rho_i^0 \rho_j^0 \int\limits_{\xi=0}^{1} \int\limits_{r=0}^{\xi \cdot \lambda_i} 4 \times 4\pi r^2 \, dr \, d\xi$$

$$\ln \gamma_\pm = \frac{4\pi l_B}{\rho_\alpha^0 + \rho_\beta^0} \sum_{i \in \{\alpha,\beta\}} \sum_{j \in \{\alpha,\beta\}} \rho_i^0 \rho_j^0 \int\limits_{\xi=0}^{1} \int\limits_{r=\xi \cdot \lambda_i}^{+\infty} z_i z_j \left[1 - \frac{1}{z_j} \frac{z_i}{8\pi \rho_j^0} \frac{K_j^2}{K^2} \frac{\kappa^2 e^{\xi \cdot \kappa \sigma_i}}{1 + \xi \cdot \kappa \sigma_i} \frac{e^{-\kappa r}}{r} \right] r \, dr \, d\xi$$

$$+ \frac{4\pi}{\rho_\alpha^0 + \rho_\beta^0} \sum_{i \in \{\alpha,\beta\}} \sum_{j \in \{\alpha,\beta\}} \rho_i^0 \rho_j^0 \int\limits_{\xi=0}^{1} \int\limits_{r=0}^{\xi \cdot \lambda_i} 4 r^2 \, dr \, d\xi$$

The solution is electroneutral, $z_\alpha \rho_\alpha^0 + z_\beta \rho_\beta^0 = 0$, which enables us to simplify the first integral.

$$\ln \gamma_\pm = -\frac{l_B}{\rho_\alpha^0 + \rho_\beta^0} \sum_{i \in \{\alpha,\beta\}} \sum_{j \in \{\alpha,\beta\}} \rho_i^0 \int\limits_{\xi=0}^{1} \int\limits_{r=\xi \cdot \lambda_i}^{+\infty} \frac{z_i^2}{2} \frac{K_j^2}{K^2} \frac{\kappa^2 e^{\xi \cdot \kappa \sigma_i}}{1 + \xi \cdot \kappa \sigma_i} e^{-\kappa r} \, dr \, d\xi$$

$$+ \frac{4\pi}{\rho_\alpha^0 + \rho_\beta^0} \sum_{i \in \{\alpha,\beta\}} \sum_{j \in \{\alpha,\beta\}} \rho_i^0 \rho_j^0 \int\limits_{\xi=0}^{1} \int\limits_{r=0}^{\xi \cdot \lambda_i} 4 r^2 \, dr \, d\xi$$

We integrate with respect to r.

$$\ln \gamma_\pm = -\frac{l_B}{\rho_\alpha^0 + \rho_\beta^0} \sum_{i \in \{\alpha,\beta\}} \sum_{j \in \{\alpha,\beta\}} \rho_i^0 \int\limits_{\xi=0}^{1} \frac{z_i^2}{2} \frac{K_j^2}{K^2} \frac{\kappa e^{\xi \cdot \kappa \sigma_i}}{1 + \xi \cdot \kappa \sigma_i} e^{-\xi \cdot \kappa \lambda_i} \, d\xi$$

$$+ \frac{4\pi}{\rho_\alpha^0 + \rho_\beta^0} \sum_{i \in \{\alpha,\beta\}} \sum_{j \in \{\alpha,\beta\}} \rho_i^0 \rho_j^0 \int\limits_{\xi=0}^{1} \frac{4}{3} (\xi \cdot \lambda_i)^3 \, d\xi$$

We simplify the first integral using the formula $K_\alpha^2 + K_\beta^2 = K^2$ and integrate the second integral.

$$\ln \gamma_\pm = -\frac{l_B}{\rho_\alpha^0 + \rho_\beta^0} \sum_{i \in \{\alpha,\beta\}} \frac{1}{2} z_i^2 \rho_i^0 \int\limits_{\xi=0}^{1} \frac{\kappa e^{\xi \cdot \kappa (\sigma_i - \lambda_i)}}{1 + \xi \cdot \kappa \sigma_i} \, d\xi + \frac{1}{\rho_\alpha^0 + \rho_\beta^0} \sum_{i \in \{\alpha,\beta\}} \sum_{j \in \{\alpha,\beta\}} \rho_i^0 \rho_j^0 \times \frac{4\pi}{3} \lambda_i^3$$

$$\ln \gamma_\pm = \frac{4\pi}{3} \left(\rho_\alpha^0 \lambda_\alpha^3 + \rho_\beta^0 \lambda_\beta^3 \right) - \frac{1}{2} \frac{\kappa l_B}{\rho_\alpha^0 + \rho_\beta^0} \sum_{i \in \{\alpha,\beta\}} z_i^2 \rho_i^0 \int\limits_{\xi=0}^{1} \frac{e^{\xi \cdot \kappa (\sigma_i - \lambda_i)}}{1 + \xi \cdot \kappa \sigma_i} \, d\xi$$

We isolate the integral and proceed to calculate it.

79

$$\int_{\xi=0}^{1} \frac{e^{\xi \cdot \kappa(\sigma_i - \lambda_i)}}{1 + \xi \cdot \kappa \sigma_i} d\xi = \frac{1}{\kappa \sigma_i} \int_{x=0}^{\kappa \sigma_i} \frac{e^{x \frac{\sigma_i - \lambda_i}{\sigma_i}}}{1 + x} dx = \frac{1}{\kappa \sigma_i} \int_{y=1}^{1 + \kappa \sigma_i} \frac{1}{y} e^{(y-1)\frac{\sigma_i - \lambda_i}{\sigma_i}} dy$$

$$\int_{\xi=0}^{1} \frac{e^{\xi \cdot \kappa(\sigma_i - \lambda_i)}}{1 + \xi \cdot \kappa \sigma_i} d\xi = \frac{1}{\kappa \sigma_i} e^{\frac{\lambda_i - \sigma_i}{\sigma_i}} \int_{y=1}^{1 + \kappa \sigma_i} \frac{1}{y} e^{y \frac{\sigma_i - \lambda_i}{\sigma_i}} dy = \frac{1}{\kappa \sigma_i} e^{\frac{\lambda_i - \sigma_i}{\sigma_i}} \int_{z=\frac{\lambda_i - \sigma_i}{\sigma_i}}^{(1+\kappa\sigma_i)\frac{\lambda_i - \sigma_i}{\sigma_i}} \frac{e^{-z}}{z} dz$$

$$\int_{\xi=0}^{1} \frac{e^{\xi \cdot \kappa(\sigma_i - \lambda_i)}}{1 + \xi \cdot \kappa \sigma_i} d\xi = \frac{1}{\kappa \sigma_i} e^{\frac{\lambda_i - \sigma_i}{\sigma_i}} \left[Ei\left(\frac{\lambda_i - \sigma_i}{\sigma_i}\right) - Ei\left((1+\kappa\sigma_i)\frac{\lambda_i - \sigma_i}{\sigma_i}\right) \right]$$

$$\int_{\xi=0}^{1} \frac{e^{\xi \cdot \kappa(\sigma_i - \lambda_i)}}{1 + \xi \cdot \kappa \sigma_i} d\xi = \frac{1}{\kappa \sigma_i} e^{\frac{\lambda_i}{\sigma_i}-1} \left[Ei\left(\frac{\lambda_i}{\sigma_i} - 1\right) - Ei\left((1+\kappa\sigma_i)\left(\frac{\lambda_i}{\sigma_i} - 1\right)\right) \right]$$

In this expression $Ei(x) = \int_{x}^{+\infty} \frac{e^{-t}}{t} dt$ is the exponential integral. Thus we obtain

$$\ln \gamma_{\pm} = \frac{4\pi}{3} \left(\rho_\alpha^0 \lambda_\alpha^3 + \rho_\beta^0 \lambda_\beta^3 \right) - \frac{1}{2} \frac{l_B}{\rho_\alpha^0 + \rho_\beta^0} \sum_{i \in \{\alpha, \beta\}} \frac{z_i^2 \rho_i^0}{\sigma_i} e^{\frac{\lambda_i}{\sigma_i}-1} \left[Ei\left(\frac{\lambda_i}{\sigma_i} - 1\right) - Ei\left((1+\kappa\sigma_i)\left(\frac{\lambda_i}{\sigma_i} - 1\right)\right) \right]$$

We can simplify this expression by introducing an approximation to the exponential integral.

$$Ei(x) = e^{-x} \ln\left[1 + e^{-\gamma}\left(\frac{1}{x} + \frac{1}{2\sqrt{x}}\right) \right]$$

The maximum error is 0.015 and is close to x = 0.01. For x > 0.035 and x < 0.001, the error is less than 0.01. For x > 4, the error is less than 0.001. We deem the approximation to be suitable and induce negligible errors when compared to the other approximations. Thus

$$e^{\frac{\lambda_i}{\sigma_i}-1} Ei\left(\frac{\lambda_i}{\sigma_i} - 1\right) = e^{\frac{\lambda_i}{\sigma_i}-1} \times e^{1-\frac{\lambda_i}{\sigma_i}} \ln\left[1 + e^{-\gamma}\left(\frac{\sigma_i}{\lambda_i - \sigma_i} + \frac{1}{2}\sqrt{\frac{\sigma_i}{\lambda_i - \sigma_i}}\right) \right]$$

$$e^{\frac{\lambda_i}{\sigma_i}-1} Ei\left(\frac{\lambda_i}{\sigma_i} - 1\right) = \ln\left[1 + e^{-\gamma}\left(\frac{\sigma_i}{\lambda_i - \sigma_i} + \frac{1}{2}\sqrt{\frac{\sigma_i}{\lambda_i - \sigma_i}}\right) \right]$$

$$e^{\frac{\lambda_i}{\sigma_i}-1} Ei\left((1+\kappa\sigma_i)\left(\frac{\lambda_i}{\sigma_i} - 1\right)\right) = e^{\frac{\lambda_i}{\sigma_i}-1} \times e^{(1+\kappa\sigma_i)\left(1-\frac{\lambda_i}{\sigma_i}\right)} \ln\left[1 + e^{-\gamma}\left(\frac{1}{1+\kappa\sigma_i}\frac{\sigma_i}{\lambda_i - \sigma_i} + \frac{1}{2\sqrt{1+\kappa\sigma_i}}\sqrt{\frac{\sigma_i}{\lambda_i - \sigma_i}}\right) \right]$$

$$e^{\frac{\lambda_i}{\sigma_i}-1} Ei\left((1+\kappa\sigma_i)\left(\frac{\lambda_i}{\sigma_i} - 1\right)\right) = e^{-\kappa(\lambda_i - \sigma_i)} \ln\left[1 + e^{-\gamma}\left(\frac{1}{1+\kappa\sigma_i}\frac{\sigma_i}{\lambda_i - \sigma_i} + \frac{1}{2\sqrt{1+\kappa\sigma_i}}\sqrt{\frac{\sigma_i}{\lambda_i - \sigma_i}}\right) \right]$$

The final expression of the mean ionic activity coefficient is

$$\ln \gamma_{\pm} = \frac{4\pi}{3}\left(\rho_{\alpha}^{0}\lambda_{\alpha}^{3} + \rho_{\beta}^{0}\lambda_{\beta}^{3}\right)$$

$$-\frac{1}{2}\frac{l_{B}}{\sigma_{\alpha}}\frac{z_{\alpha}^{2}\rho_{\alpha}^{0}}{\rho_{\alpha}^{0}+\rho_{\beta}^{0}}\left[\begin{array}{l}\ln\left(1+\dfrac{e^{-\gamma}\sigma_{\alpha}}{\lambda_{\alpha}-\sigma_{\alpha}}+\dfrac{e^{-\gamma}}{2}\sqrt{\dfrac{\sigma_{\alpha}}{\lambda_{\alpha}-\sigma_{\alpha}}}\right)\\ -e^{-\kappa(\lambda_{\alpha}-\sigma_{\alpha})}\ln\left(1+\dfrac{e^{-\gamma}}{1+\kappa\sigma_{\alpha}}\dfrac{\sigma_{i}}{\lambda_{\alpha}-\sigma_{\alpha}}+\dfrac{e^{-\gamma}}{2}\dfrac{1}{\sqrt{1+\kappa\sigma_{\alpha}}}\sqrt{\dfrac{\sigma_{\alpha}}{\lambda_{\alpha}-\sigma_{\alpha}}}\right)\end{array}\right]$$

$$-\frac{1}{2}\frac{l_{B}}{\sigma_{\beta}}\frac{z_{\beta}^{2}\rho_{\beta}^{0}}{\rho_{\alpha}^{0}+\rho_{\beta}^{0}}\left[\begin{array}{l}\ln\left(1+\dfrac{e^{-\gamma}\sigma_{\beta}}{\lambda_{\beta}-\sigma_{\beta}}+\dfrac{e^{-\gamma}}{2}\sqrt{\dfrac{\sigma_{\beta}}{\lambda_{\beta}-\sigma_{\beta}}}\right)\\ -e^{-\kappa(\lambda_{\beta}-\sigma_{\beta})}\ln\left(1+\dfrac{e^{-\gamma}}{1+\kappa\sigma_{\beta}}\dfrac{\sigma_{\beta}}{\lambda_{\beta}-\sigma_{\beta}}+\dfrac{e^{-\gamma}}{2}\dfrac{1}{\sqrt{1+\kappa\sigma_{\beta}}}\sqrt{\dfrac{\sigma_{\beta}}{\lambda_{\beta}-\sigma_{\beta}}}\right)\end{array}\right]$$

We can rewrite this expression using $\rho_{\alpha}^{0} = \nu_{\alpha}\rho^{0}$ and $\rho_{\beta}^{0} = \nu_{\beta}\rho^{0}$.

$$\ln \gamma_{\pm} = \frac{4\pi}{3}\left(\nu_{\alpha}\lambda_{\alpha}^{3} + \nu_{\beta}\lambda_{\beta}^{3}\right)\rho^{0}$$

$$-\frac{1}{2}\frac{l_{B}}{\sigma_{\alpha}}\frac{z_{\alpha}^{2}\nu_{\alpha}}{\nu_{\alpha}+\nu_{\beta}}\left[\begin{array}{l}\ln\left(1+\dfrac{e^{-\gamma}\sigma_{\alpha}}{\lambda_{\alpha}-\sigma_{\alpha}}+\dfrac{e^{-\gamma}}{2}\sqrt{\dfrac{\sigma_{\alpha}}{\lambda_{\alpha}-\sigma_{\alpha}}}\right)\\ -e^{-\kappa(\lambda_{\alpha}-\sigma_{\alpha})}\ln\left(1+\dfrac{e^{-\gamma}}{1+\kappa\sigma_{\alpha}}\dfrac{\sigma_{i}}{\lambda_{\alpha}-\sigma_{\alpha}}+\dfrac{e^{-\gamma}}{2}\dfrac{1}{\sqrt{1+\kappa\sigma_{\alpha}}}\sqrt{\dfrac{\sigma_{\alpha}}{\lambda_{\alpha}-\sigma_{\alpha}}}\right)\end{array}\right]$$

$$-\frac{1}{2}\frac{l_{B}}{\sigma_{\beta}}\frac{z_{\beta}^{2}\nu_{\beta}}{\nu_{\alpha}+\nu_{\beta}}\left[\begin{array}{l}\ln\left(1+\dfrac{e^{-\gamma}\sigma_{\beta}}{\lambda_{\beta}-\sigma_{\beta}}+\dfrac{e^{-\gamma}}{2}\sqrt{\dfrac{\sigma_{\beta}}{\lambda_{\beta}-\sigma_{\beta}}}\right)\\ -e^{-\kappa(\lambda_{\beta}-\sigma_{\beta})}\ln\left(1+\dfrac{e^{-\gamma}}{1+\kappa\sigma_{\beta}}\dfrac{\sigma_{\beta}}{\lambda_{\beta}-\sigma_{\beta}}+\dfrac{e^{-\gamma}}{2}\dfrac{1}{\sqrt{1+\kappa\sigma_{\beta}}}\sqrt{\dfrac{\sigma_{\beta}}{\lambda_{\beta}-\sigma_{\beta}}}\right)\end{array}\right]$$

IV.2   Reduction to the Debye-Hückel limiting law

In the limit of small ionic radii and small hydrated radii, we recover the usual Debye-Hückel formula. First $\lambda_{i} \to \sigma_{i}$ and we obtain

$$Ei\left(\frac{\lambda_{i}}{\sigma_{i}}-1\right)-Ei\left((1+\kappa\sigma_{i})\left(\frac{\lambda_{i}}{\sigma_{i}}-1\right)\right)=-\gamma-\ln\left(\frac{\lambda_{i}}{\sigma_{i}}-1\right)+\gamma+\ln\left((1+\kappa\sigma_{i})\left(\frac{\lambda_{i}}{\sigma_{i}}-1\right)\right)+O\left(\frac{\lambda_{i}}{\sigma_{i}}-1\right)$$

$$Ei\left(\frac{\lambda_{i}}{\sigma_{i}}-1\right)-Ei\left((1+\kappa\sigma_{i})\left(\frac{\lambda_{i}}{\sigma_{i}}-1\right)\right)=\ln(1+\kappa\sigma_{i})+O\left(\frac{\lambda_{i}}{\sigma_{i}}-1\right)$$

So at at the limit we have $\ln\gamma_{\pm} = \dfrac{4\pi}{3}\left(\rho_{\alpha}^{0}\sigma_{\alpha}^{3}+\rho_{\beta}^{0}\sigma_{\beta}^{3}\right)-\dfrac{1}{2}\dfrac{l_{B}}{\rho_{\alpha}^{0}+\rho_{\beta}^{0}}\displaystyle\sum_{i\in\{\alpha,\beta\}}\dfrac{z_{i}^{2}\rho_{i}^{0}}{\sigma_{i}}\ln(1+\kappa\sigma_{i})$

Second $\lambda_i = \sigma_i \to 0$ and we obtain

$$\ln \gamma_{\pm} = \frac{4\pi}{3}\left(\rho_{\alpha}^0 \sigma_{\alpha}^3 + \rho_{\beta}^0 \sigma_{\beta}^3\right) - \frac{1}{2}\frac{l_B}{\rho_{\alpha}^0 + \rho_{\beta}^0} \sum_{i \in \{\alpha,\beta\}} \frac{z_i^2 \rho_i^0}{\sigma_i} \times \left(\kappa\sigma_i + O\left(\sigma_i^2\right)\right)$$

$$\ln \gamma_{\pm} = \frac{4\pi}{3}\left(\rho_{\alpha}^0 \sigma_{\alpha}^3 + \rho_{\beta}^0 \sigma_{\beta}^3\right) - \frac{1}{2}\frac{\kappa l_B}{\rho_{\alpha}^0 + \rho_{\beta}^0} \sum_{i \in \{\alpha,\beta\}} z_i^2 \rho_i^0 \times \left(1 + O(\sigma_i)\right)$$

So at the limit we have

$$\ln \gamma_{\pm} = -\frac{1}{2}\frac{\kappa l_B}{\rho_{\alpha}^0 + \rho_{\beta}^0} \sum_{i \in \{\alpha,\beta\}} z_i^2 \rho_i^0$$

$$\ln \gamma_{\pm} = -\frac{1}{2}\frac{\kappa l_B}{\rho_{\alpha}^0 + \rho_{\beta}^0}\left(z_{\alpha}^2 \rho_{\alpha}^0 + z_{\beta}^2 \rho_{\beta}^0\right)$$

$$\ln \gamma_{\pm} = -\frac{1}{2}\frac{\kappa l_B}{v_{\alpha} + v_{\beta}}\left(v_{\alpha} z_{\alpha}^2 + v_{\beta} z_{\beta}^2\right) = -\frac{1}{2}\left|z_{\alpha} z_{\beta}\right| \kappa l_B$$

Moreover if we eliminate the correlation between ions, i.e. $w \to 0$, $\kappa = \kappa_{DH}$. Hence in the limit of point ions and no interionic correlations, we recover the Debye-Hückel law.

V   COMPARISON OF THE OSMOTIC COEFFICIENT WITH EXPERIMENTAL DATA

Extensive experimental data for 70 electrolytes was collected from reference [19] and grouped in series by anion. The equation describing the osmotic coefficient is

$$\phi = 1 + \frac{2\pi\rho^0}{3}\left(v_{\alpha}\lambda_{\alpha}^3 + v_{\beta}\lambda_{\beta}^3\right) - \frac{\kappa l_B}{6\left(v_{\alpha} + v_{\beta}\right)}\left(\frac{v_{\alpha} z_{\alpha}^2}{1 + \kappa\sigma_{\alpha}}e^{-\kappa(\lambda_{\alpha}-\sigma_{\alpha})} + \frac{v_{\beta} z_{\beta}^2}{1 + \kappa\sigma_{\beta}}e^{-\kappa(\lambda_{\beta}-\sigma_{\beta})}\right)$$

$$- \frac{\kappa^2/K^2}{6\left(v_{\alpha} + v_{\beta}\right)}\left(\frac{z_{\alpha}}{\sigma_{\alpha}}\frac{v_{\alpha}\lambda_{\alpha}^3}{1 + \kappa\sigma_{\alpha}}e^{-\kappa(\lambda_{\alpha}-\sigma_{\alpha})} + \frac{z_{\beta}}{\sigma_{\beta}}\frac{v_{\beta}\lambda_{\beta}^3}{1 + \kappa\sigma_{\beta}}e^{-\kappa(\lambda_{\beta}-\sigma_{\beta})}\right)\left(\frac{K_{\alpha}^2}{z_{\alpha}} + \frac{K_{\beta}^2}{z_{\beta}}\right)$$

ρ^0 is the concentration of the electrolyte; v_{α} and v_{β} are the multiplicity of the cation and anion; z_{α} and z_{β} are their charges; σ_{α} and σ_{β} are their ionic radii; λ_{α} and λ_{β} are their hydrated radii. K_{α}, K_{β}, K and κ are constants given by the formulae above; they are all homogenous to the inverse of a length.

The ionic radii of each species were taken from the literature [111,112]; the values used are summarized in Appendix D, Table 8. Therefore each electrolyte has three free parameters the values of which are to be determined by fitting the curve to the experimental points. They are the correlation parameter w, linked to the correlation length $W = w \cdot l_B$; and the hydrated radii, λ_{α} and λ_{β}, of the anion and cation. These parameters depend on the concentration of electrolyte; however their values change only slowly and are taken to be constant over a range. Therefore we distinguish three different regions for most electrolytes and have computed the pertaining sets of parameters:

- The concentrated region corresponds to ionic strengths above 7 – 10 mol/L. The general set of parameters, computed with the integrality of the dataset, usually yields a curve in good agreement with the data over the concentrated region. In a few cases, a separate set of parameters has been computed to fit the data at high ionic strengths.

82

- The dilute region corresponds to ionic strengths below 0.7 – 1 mol/L. The set of parameters computed for this region usually leads to curves that markedly diverge from the experimental data beyond the limits of the dilute domain.
- The semi-dilute region corresponds to ionic strengths comprised between 0.7 – 1 mol/L and 7 – 10 mol/L. The set of parameters is a compromise between the previous two yielding good agreement in the semi-dilute region and acceptable fitting beyond.

It is to be noted that the general set was computed for all electrolytes. The other sets were computed only if needed or if relevant.

The procedure to determine the parameters consisted of 7 steps and is summarized in the picture below.

Lower Bounds	Initialization	Upper Bounds
▪ w = 1 (sometimes 0)	▪ w = 2.5	▪ w = 8 (sometimes 9)
▪ λ_α, λ_β = ionic radii σ_α, σ_β	▪ λ_α, λ_β from literature	▪ λ_α, λ_β = 6 (sometimes 5)

Solve for w, λ_α, λ_β
Plot of the corresponding solution and experimental data

Change the initial value of w to find other possible solutions

Modify the bounds to force correct convergence in the most relevant solution

Plot of the final solution and experimental data
Compilation of the values of the three parameters

Below is a long series of graphs that illustrate the accuracy of the various fittings. The values determined for the three parameters are given in Appendix D, Table 10.4

V.1 Fluorides
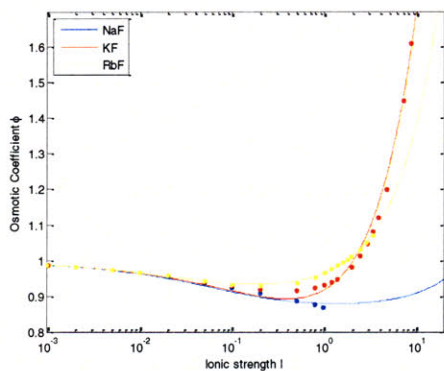
Figure 28: General fit of alkali fluorides

Figure 29: General fit of alkali fluorides – partial view
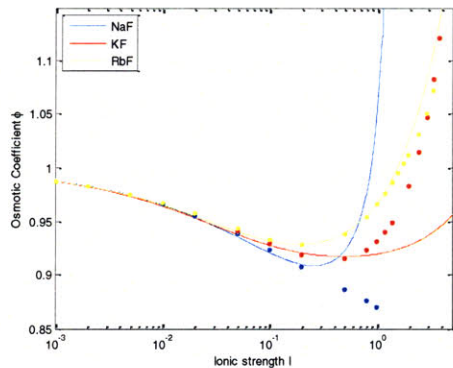
Figure 30: Dilute fit of alkali fluorides
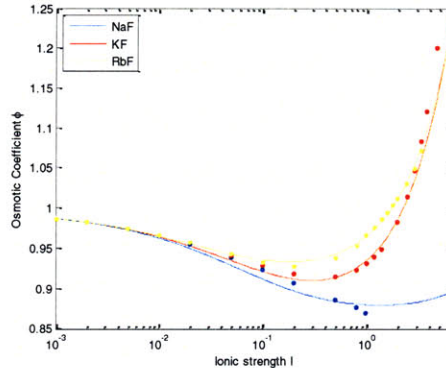
Figure 31: Semi-dilute fit of alkali fluorides

Rubidium fluoride has a very good general fit. The dilute fit is excellent and valid over the semi-dilute region too.

The experimental data on sodium fluoride is limited to the semi-dilute region because the solubility limit is reached at ionic strengths less than 1 mol/L. The dilute fit is good and extends to all available data points. The general fit is mediocre probably because the correlation length and the hydrated radii undergo significant changes in the vicinity of the solubility limit.

Potassium fluoride needs the three different sets of parameters since their values change significantly. Each fit is accurate in its region.

Curiously the order of the curves is inversed with respect to the other series.

There are no experimental data for lithium fluoride and cesium fluoride.

V.2 Chlorides
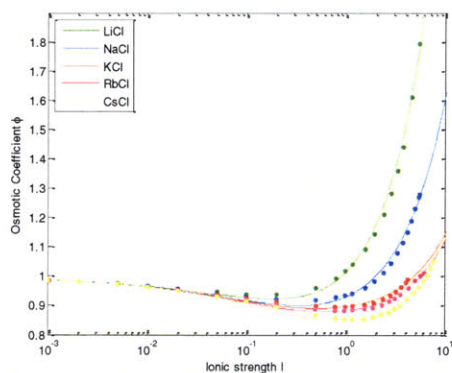
Figure 32: General fit of alkali chlorides
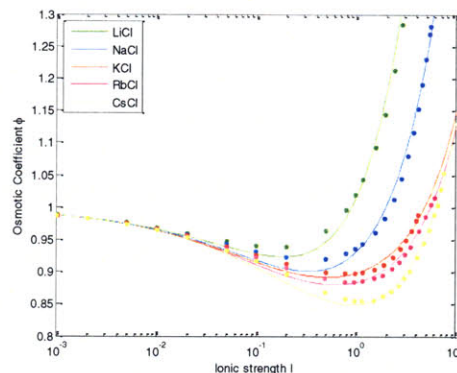
Figure 33: General fit of alkali chlorides – partial view
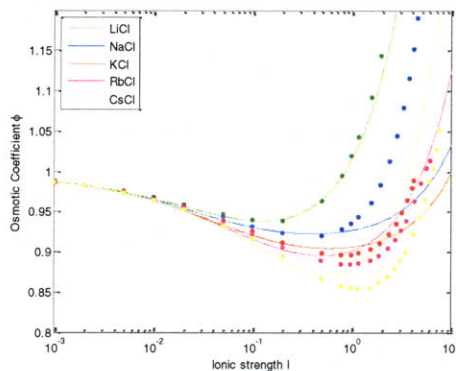
Figure 34: Dilute fit of alkali chlorides
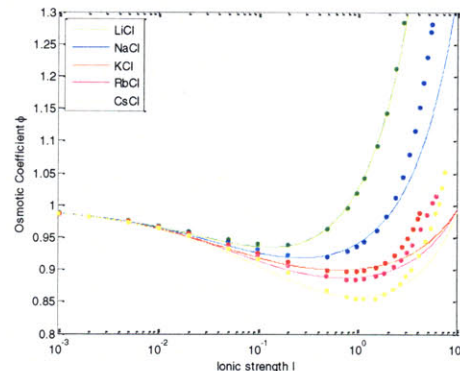
Figure 35: Semi-dilute fit of alkali chlorides

The series of alkali chlorides is well behaved. The three sets of parameters make the curves reproduce the experimental quite well in each region.

Figure 36: General fit of alkaline metal chlorides

Figure 37: General fit of alkaline metal chlorides – partial view
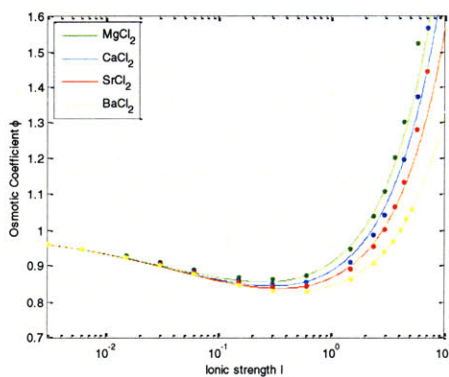
Figure 38: Dilute fit of alkaline metal chlorides

Figure 39: Dilute fit of alkaline metal chlorides – partial view

Figure 40: Semi-dilute fit of alkaline metal chlorides
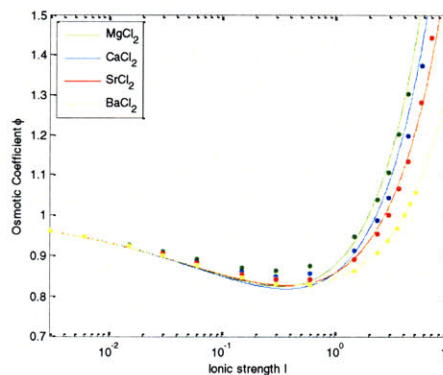
Figure 41: Semi-dilute fit of alkaline metal chlorides – partial view

The series of alkali metal chlorides again exhibits three distinct regions and the experimental data is well reproduced in each region.
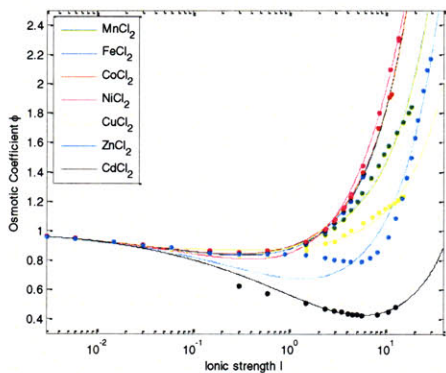
Figure 42: General fit of transition metal chlorides
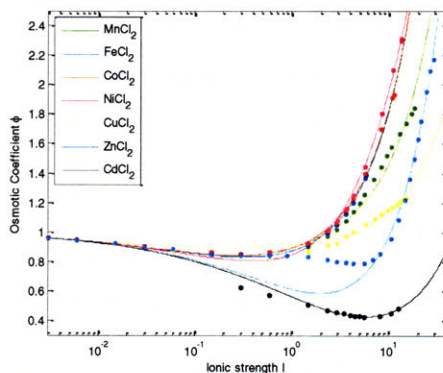
Figure 43: General fit of transition metal chlorides except concentrated fit for MnCl₂, CuCl₂ and ZnCl₂
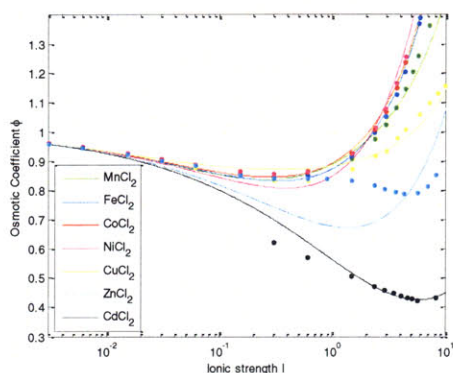
Figure 44: General fit of trans. metal chlorides – first partial view
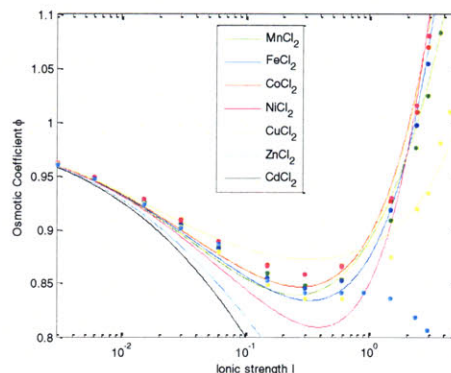
Figure 45: General fit of trans. metal chlorides – sec. partial view
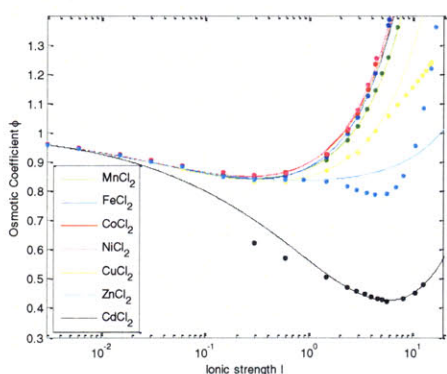
Figure 46: Dilute fit of transition metal chlorides
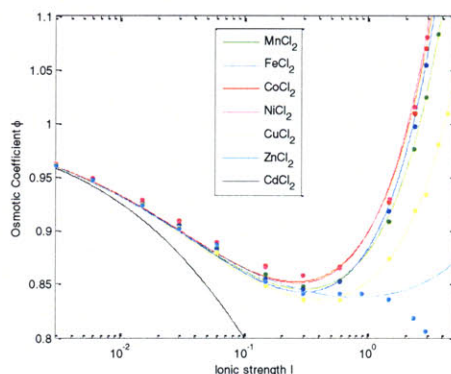
Figure 47: Dilute fit of transition metal chlorides – partial view

The transition metal chlorides series again exhibits mainly two distinct regions. For three electrolytes, ferrous chloride, cobalt chloride and nickel chloride, the osmotic coefficient is well reproduced, albeit less well than in the two previous series.

For cadmium chloride experimental data was available only in the semi-dilute and concentrated regions and solely the general fit was made; the agreement is very good at ionic strengths greater than 1 mol/L.

For manganous chloride and copper chloride the dilute region is normal and the experimental data is well reproduced. However in the concentrated region the osmotic coefficient appears to be linear in the logarithm of the ionic strength instead of simply the ionic strength; this pattern can be reproduced only over a small range hence an imperfect fit. Nevertheless the curve and the experimental values are close.

Last the osmotic coefficient of zinc chloride is unusual and has four regions. It can be reproduced well in the dilute and concentrated regions and not at all in the semi-dilute region and the very concentrated region close to the solubility limit. In the semi-dilute region, there is an obvious chemical transition that cannot be described by modeling the ions with charged hard spheres. When close to saturation, other phenomena, such as ion pairing, may occur and make the osmotic coefficient deviate from the theoretical curve.
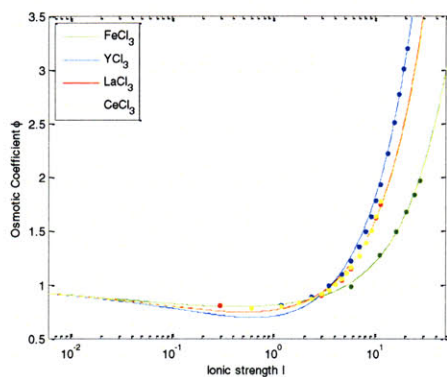
Figure 48: General fit of metal trichlorides
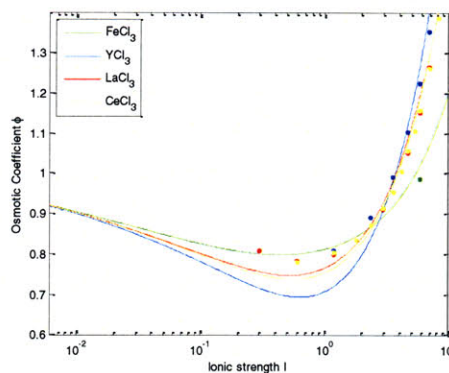
Figure 49: General fit of metal trichlorides – partial view
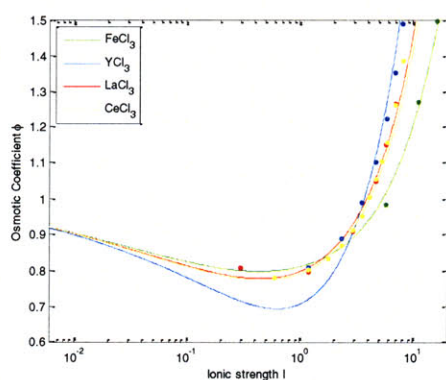
Figure 50: Semi-dilute fit of lanthanum and cerium chloride
General fit of iron and yttrium chloride

Experimental data for metal trichlorides is available only in the semi-dilute and concentrated regions. The general fit is in good agreement with experimental data.

V.3   Bromides
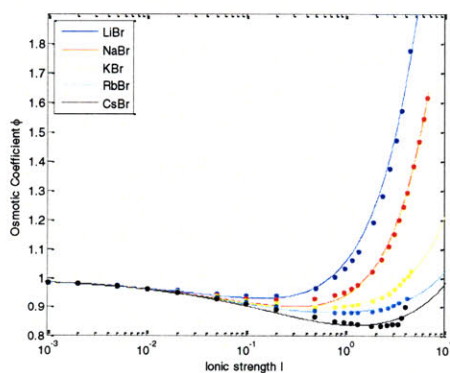
Figure 51: General fit of alkali bromides
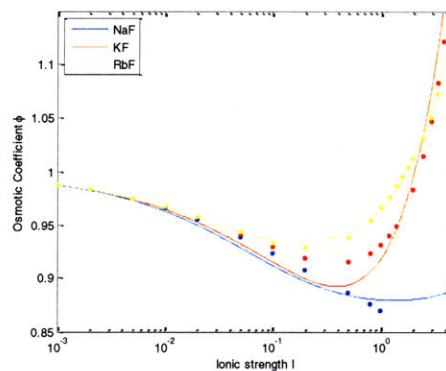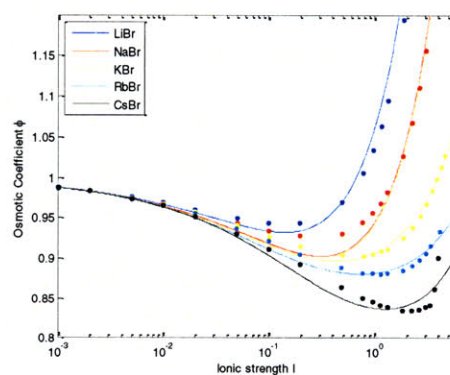

Figure 52: General fit of alkali bromides – partial view
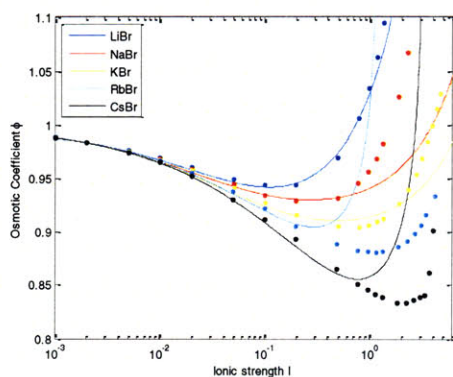
Figure 53: Dilute fit of alkali bromides
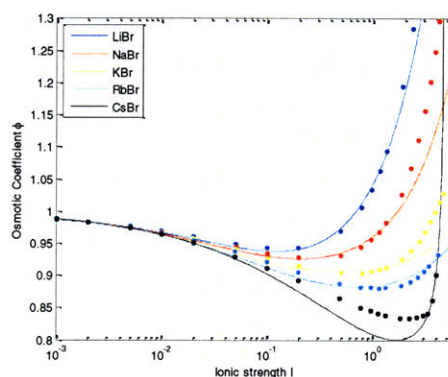
Figure 54: Semi-dilute fit of alkali bromides

The experimental data of the four lighter alkali bromides – lithium bromide, sodium bromide, potassium bromide and rubidium bromide – exhibit the normal behavior and experimental data is well reproduced using three sets of parameters. For cesium bromide, the pattern is unusual but is acceptably reproduced by the general fit; the dilute fit is good; the semi-dilute is replaced with a concentrated fit to capture the experimental data close to saturation. There is a brutal change in the behavior of cesium bromide as an electrolyte at ionic strength close to 4 mol/L, therefore reproducing the whole set of data with a single fit cannot be done properly.
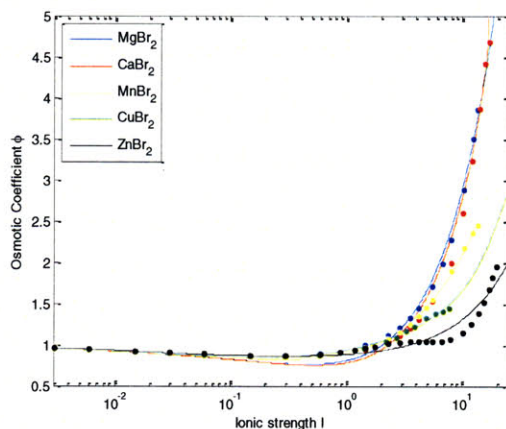
Figure 55: General fit of metal bromides
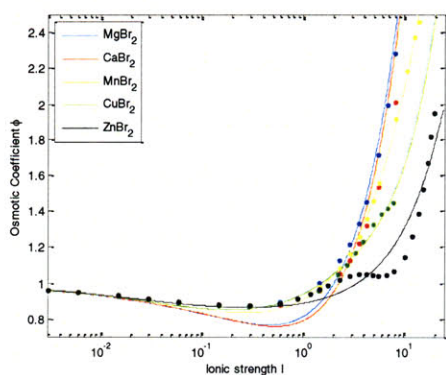
Figure 56: General fit of metal bromides – first partial view
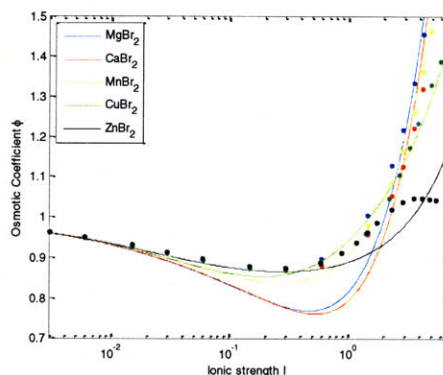
Figure 57: General fit of metal bromides – second partial view
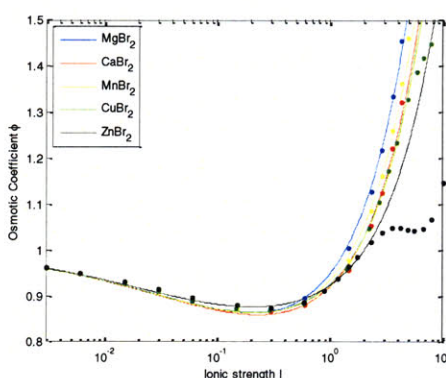
Figure 58: Dilute fit of metal bromides
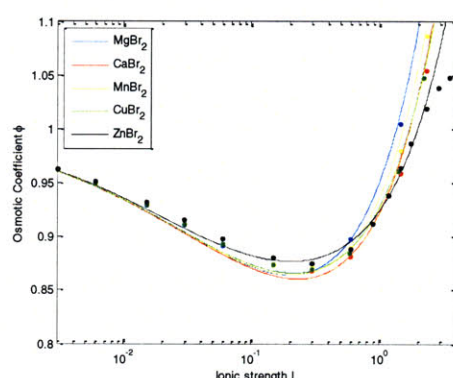
Figure 59: Dilute fit of metal bromides – partial view
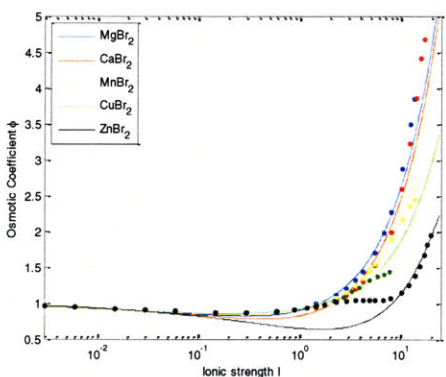
Figure 60: Semi-dilute fit of metal bromides and concentrated fit of zinc bromide
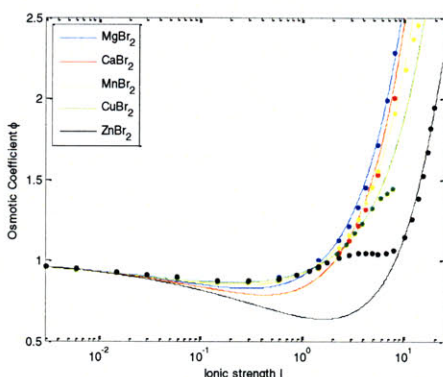
Figure 61: Semi-dilute fit of metal bromides and concentrated fit of zinc bromide – partial view

The experimental data and the corresponding fitted curves of magnesium bromide and calcium bromide have the normal pattern and are in good agreement using the usual three sets of parameters.

Manganous bromide and copper bromide have the normal pattern too, except close to the solubility limit. Their dilute fits are very good and extend in the semi-dilute region. The general fit includes all experimental points whereas the semi-dilute fit excludes the experimental points close to saturation and yields an excellent fit over the semi-dilute and concentrated regions.

90

The experimental values of zinc bromide are divided in four distinct regions. In the dilute and concentrated regions they can be accurately reproduced. The transition in the semi-dilute region and the slight decrease in the very concentrated region are beyond the reach of the model. The general fit is a compromise between the solutions in the four regions.

V.4   Iodides
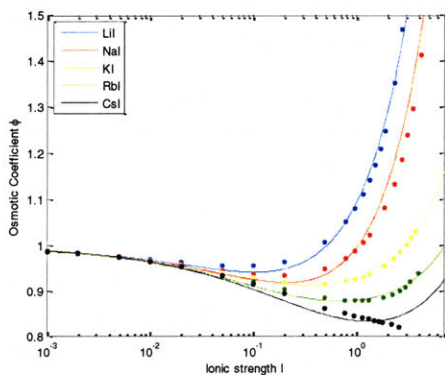
Figure 62: General fit of alkali iodides
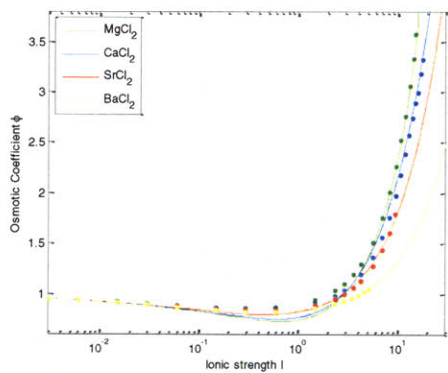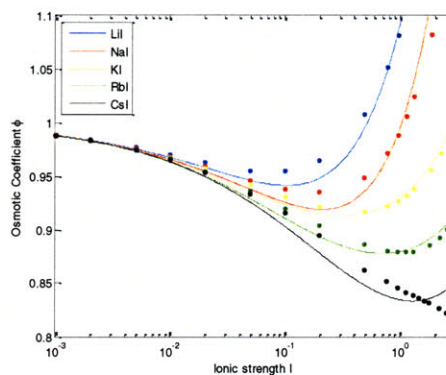

Figure 63: General fit of alkali iodides – partial view
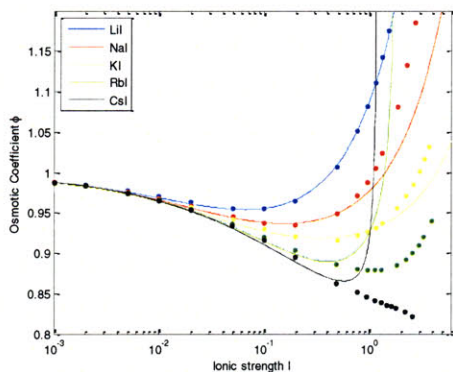
Figure 64: Dilute fit of alkali iodides
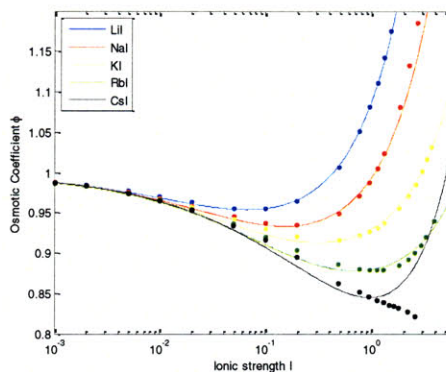
Figure 65: Semi-dilute fit of alkali iodides

The experimental data of most alkali iodides is quite normal and can be reproduced accurately with only two sets of parameters: the general fit and the dilute fit. Sodium iodide requires three sets of parameters. Cesium iodide has a good dilute fit and a mediocre semi-dilute fit. At ionic strengths above 1 mol/L, the osmotic coefficient is linear in the logarithm of the ionic strength and this cannot be reproduced by the model; hence a bad general fit.
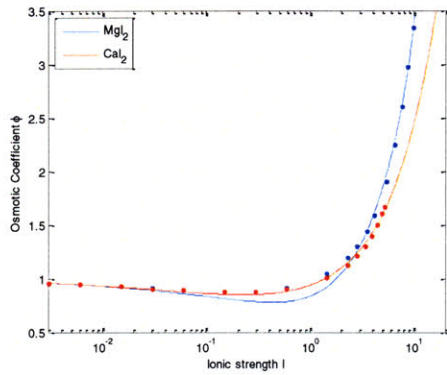
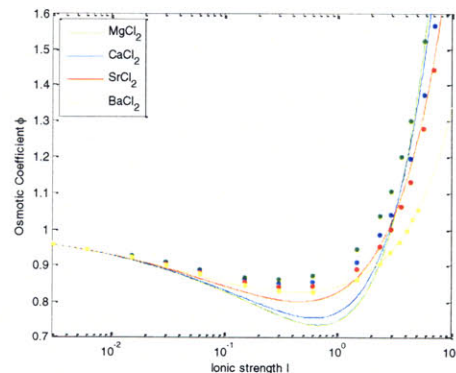**Figure 66: General fit of alkaline metal iodides**
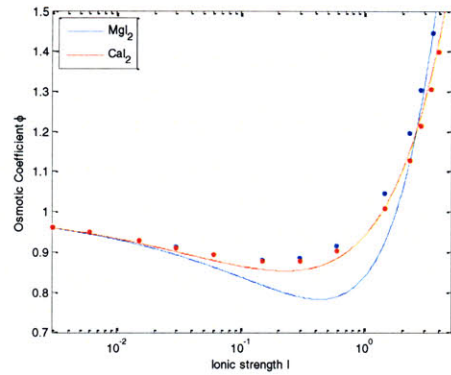
Figure 67: General fit of alkaline metal iodides – partial view
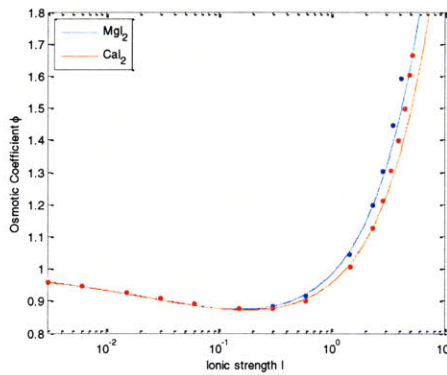
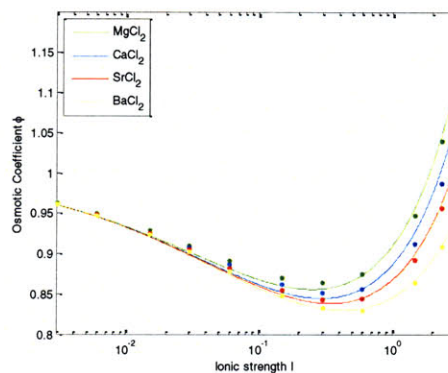**Figure 68: Dilute fit of alkaline metal iodides**

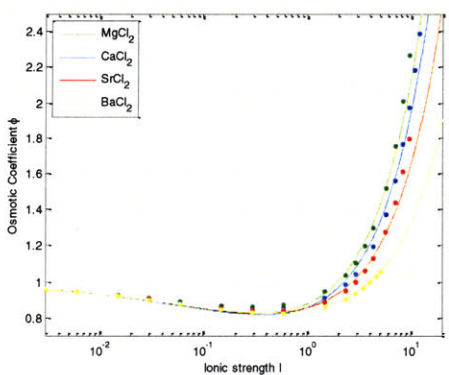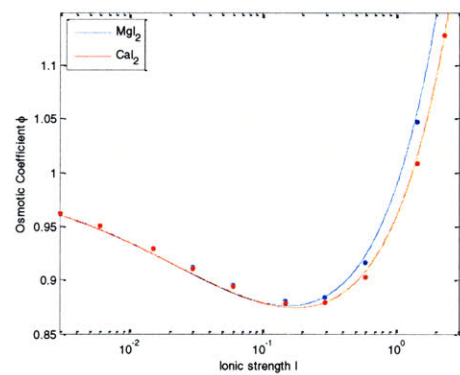**Figure 69: Dilute fit of alkaline metal iodides – partial view**

Alkaline metal iodides exhibit the usual pattern and it can be reproduced with only two sets of parameters.

V.5 Nitrates
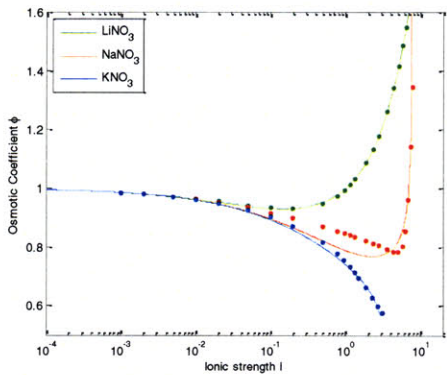
Figure 70: General fit of alkali nitrates
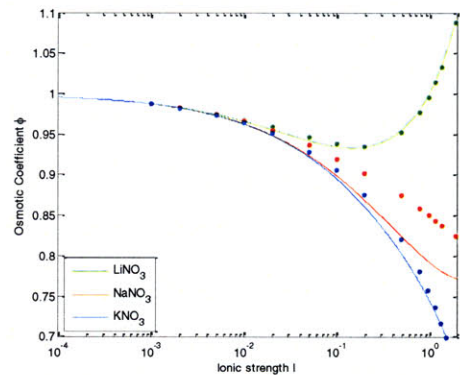
Figure 71: General fit of alkali nitrates – first partial view
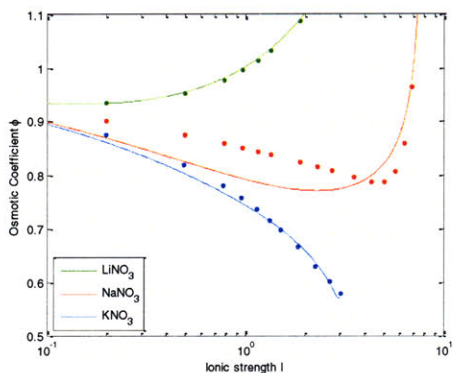
Figure 72: General fit of alkali nitrates – second partial view
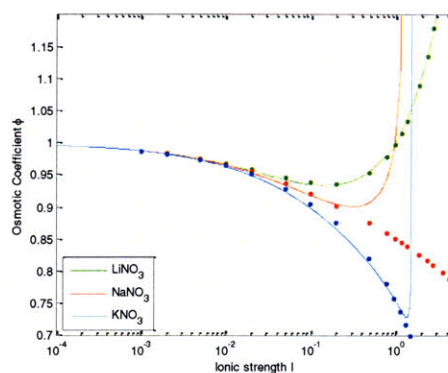
Figure 73: Dilute fit of alkali nitrates

The entire dataset of lithium nitrate is fit with a single set of parameters. Potassium nitrate requires two sets of parameters for precise reproduction. The general fit of sodium nitrate is good close to saturation and bad elsewhere; in the dilute region are experimental values are well reproduced; in the semi-dilute region, the decrease is roughly linear in the logarithm of the ionic strength and this part cannot be meaningfully reproduced.
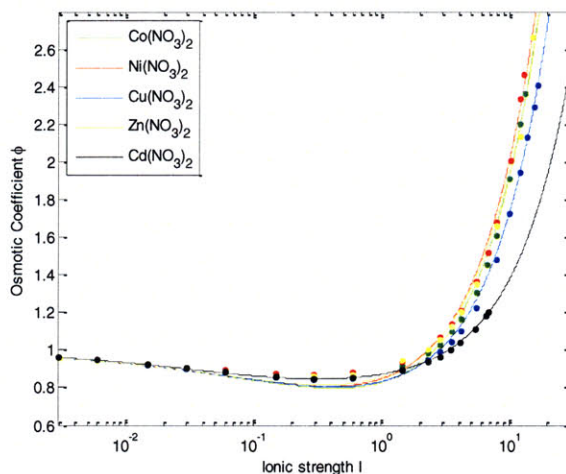
Figure 74: General fit of transition metal nitrates
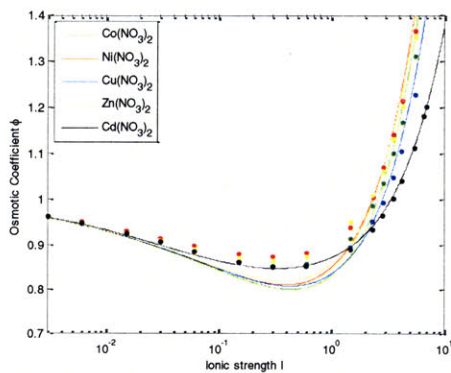
Figure 75: General fit of trans. metal nitrates – first partial view
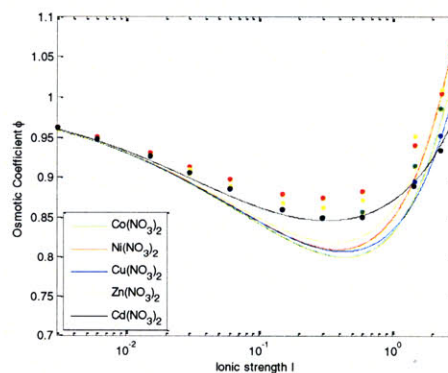
Figure 76: General fit of trans. metal nitrates – second partial view

93
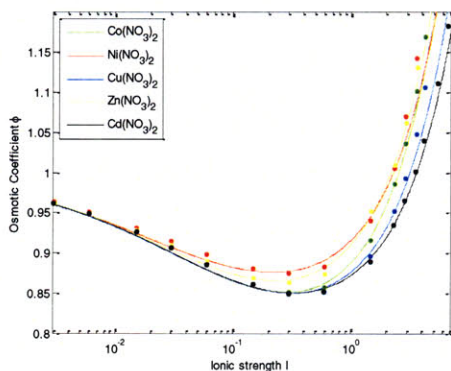
Figure 77: Dilute fit of transition metal nitrates
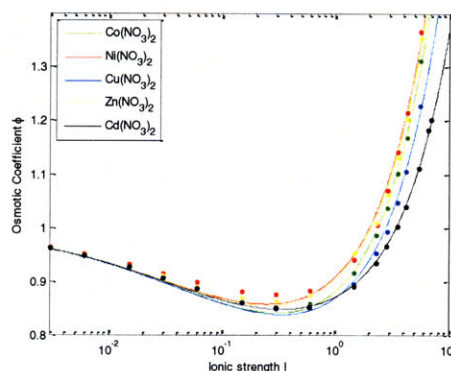
Figure 78: Semi-dilute fit of transition metal nitrates

These electrolytes exhibit the normal pattern and correspondingly experimental data is reproduced well in the three regions using three sets of parameters.

V.6 Perchlorates
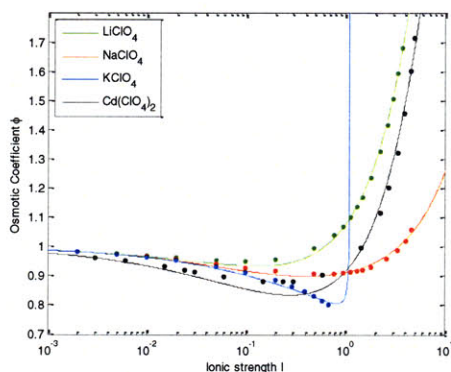
Figure 79: General fit of alkali and cadmium perchlorates
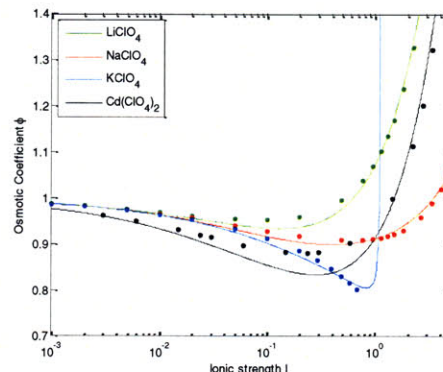
Figure 80: General fit of alkali and cadmium perchl. – partial view
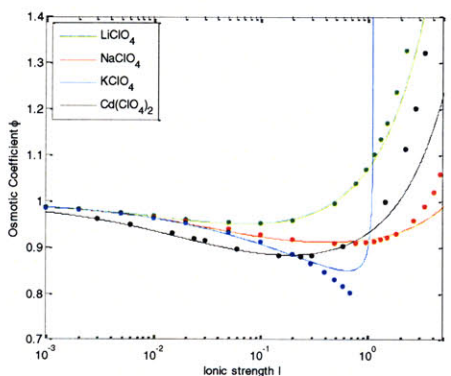
Figure 81: Dilute fit of alkali and cadmium perchlorates
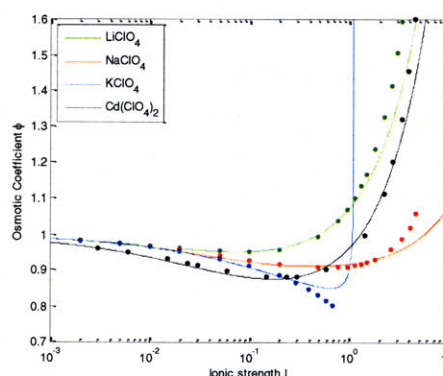
Figure 82: Semi-dilute fit of alkali and cadmium perchlorates

The alkali perchlorates behave normally and experimental points are well reproduced using two sets of parameters. Cadmium perchlorate requires three sets of parameters.

V.7 Acids
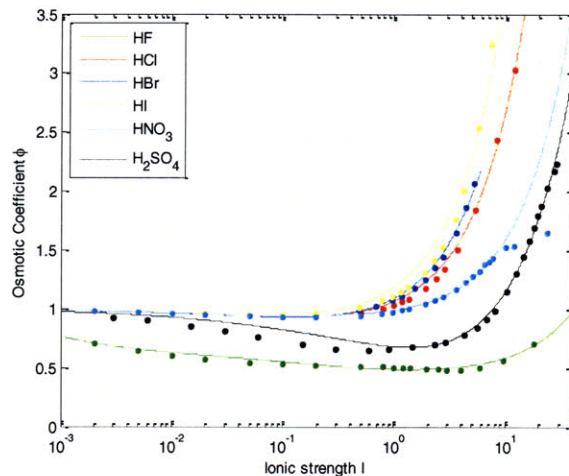
Figure 83: General fit of acids
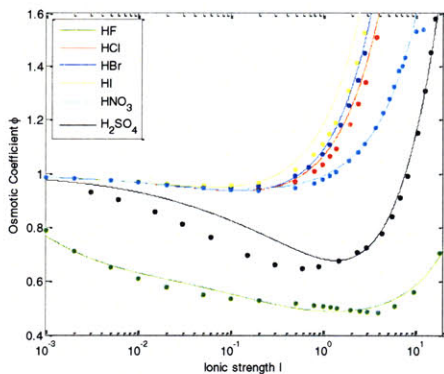
Figure 84: General fit of acids – first partial view
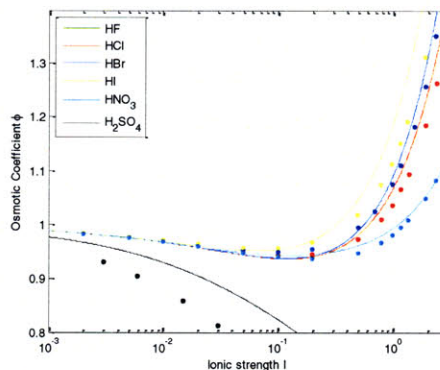
Figure 85: General fit of acids – second partial view
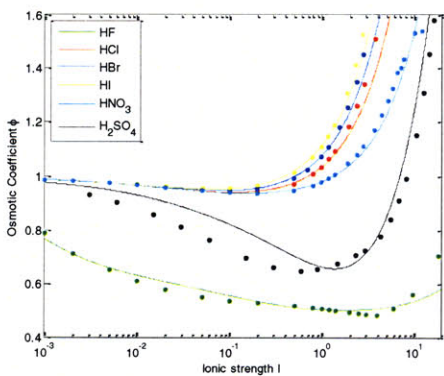
Figure 86: Dilute fit of acids
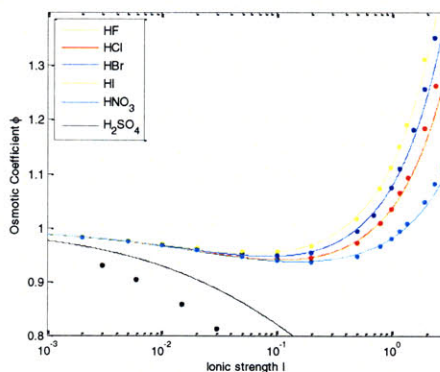
Figure 87: Dilute fit of acids

The osmotic coefficient of the hydrochloric, hydrobromic and hydroiodic acids has the normal behavior and is accurately reproduced using two sets of parameters, one for the dilute region, another for the concentrated region.

The last two experimental values of nitric acid are outside the expected pattern and were ignored because they cannot be explained by the model. Indeed the pK_a of nitric acid is -1.5 so for concentrations above 6 mol/L it cannot be considered a simple 1:1 electrolyte. It becomes either a mixture of an electrolyte and a non-electrolyte. Except for this correction, nitric acid is like the previous ones and requires only two set of parameters to reproduce the remaining experimental data.

The osmotic coefficient of the hydrofluoric acid markedly deviates from the normal pattern even in the dilute region; the values are considerably lower than in other 1:1 electrolytes. Its general fit was made only in the semi-dilute and concentrated regions and was achieved by modifying the mathematical formula of the osmotic coefficient.

$$\phi = \left[0.65 + \frac{0.35}{1 + \rho^0 / 0.0006 \ mol/L} \right] \phi_{usual}$$

The agreement is good. The extraordinary lowering of the osmotic coefficient is caused by the fact that hydrofluoric acid is a weak acid with $pK_a = 3.15$ and by the presence of the bifluoride ion, FHF⁻, which links two fluorines through a very strong hydrogen bond; thus hydrofluoric acid is not a regular 1:1 electrolyte.

Sulfuric acid exhibits a more complicated behavior. Its pK_a's are 1.9 and -3.0. This means that sulfuric acid is a diacid and simple electrolyte only for ionic strengths below 0.005 mol/L. Between 0.005 mol/L and 0.5 mol/L it is a mixture of a monoacid and of a diacid. Between 0.1 mol/L and 40 mol/L it is a monoacid. Beyond 40 mol/L it is a mixture of a monoacid and of a non-acidic compound. Thus the last six experimental points were ignored because outside the modeling possibilities. The concentrated fit was performed twice, the sulfuric acid being considered a 1:1 or a 2:1 electrolyte; the curves were undistinguishable in the concentrated region but deviated markedly in the dilute region; the agreement with experimental data was good in both cases. The general fit uses a 2:1 electrolyte because it is the best one; its accuracy is acceptable. The low fit uses a 2:1 electrolyte and again is acceptable.

V.8 Bases
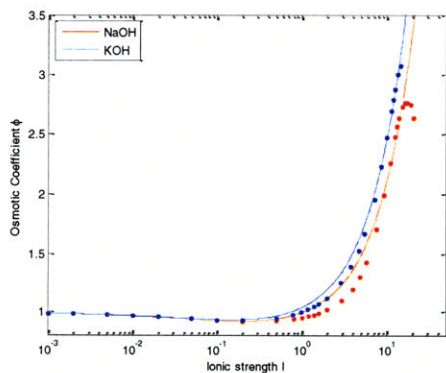
Figure 88: General fit of bases

96
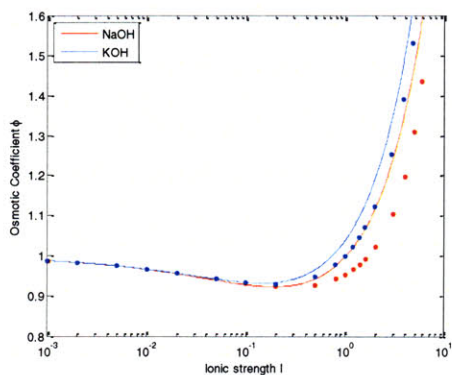
Figure 89: General fit of bases – first partial view
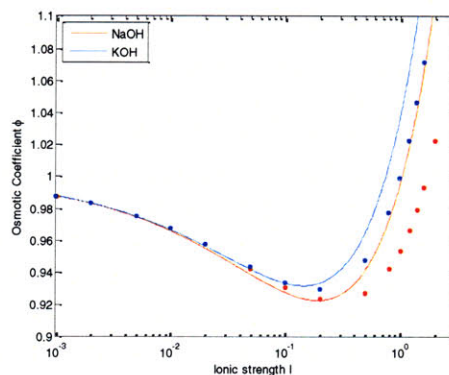
Figure 90: General fit of bases – second partial view
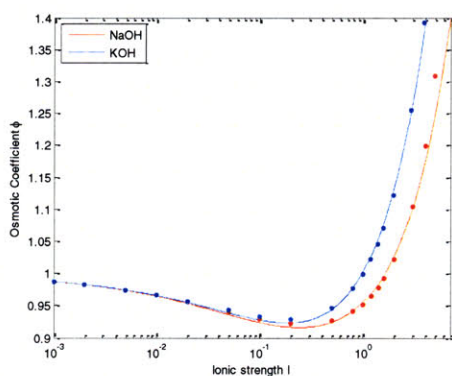
Figure 91: Dilute fit of bases
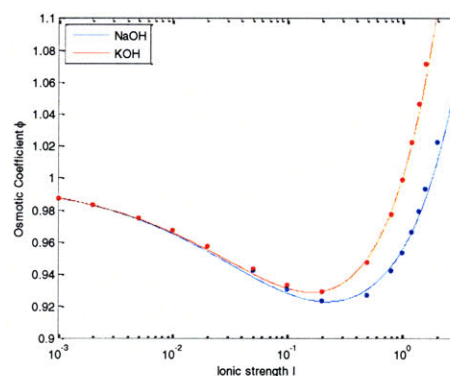
Figure 92: Dilute fit of bases – partial view

Except the experimental values of the most concentrated solutions, sodium and potassium hydroxide behave like two normal 1:1 electrolytes. Two sets of parameters are needed to accurately reproduce experimental data. The last four data points of sodium hydroxide are outside the normal pattern because close to saturation the compound ceases to behave purely as an electrolyte.

V.9   Sulfates
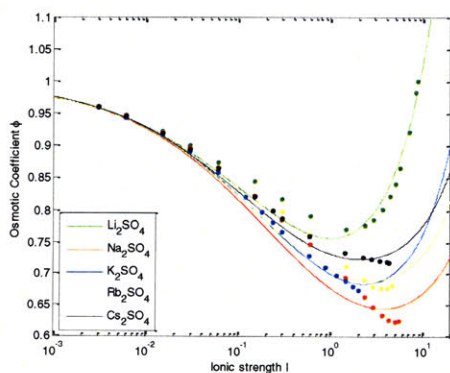
Figure 93: General fit of alkali sulfates
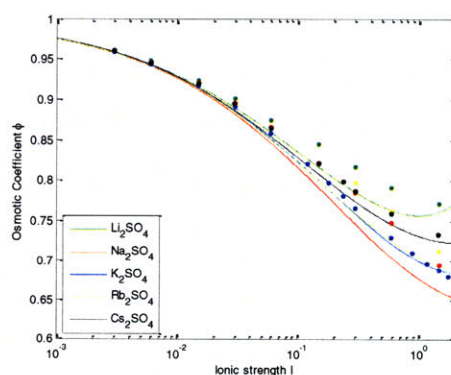
Figure 94: General fit of alkali sulfates – partial view
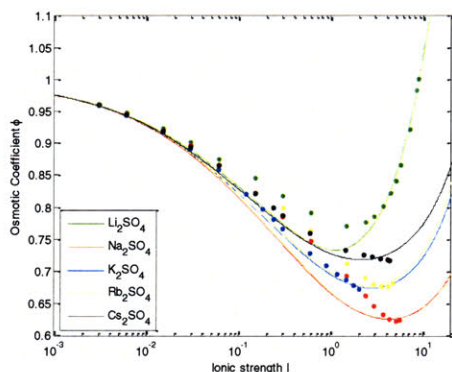
Figure 95: Concentrated fit of alkali sulfates
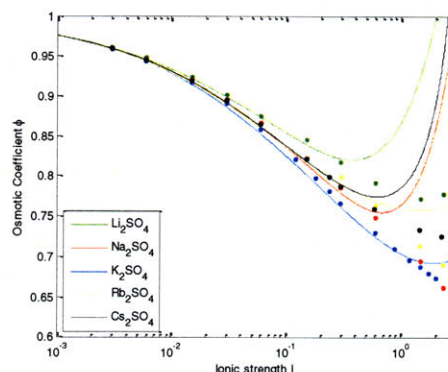
Figure 96: Dilute fit of alkali sulfates

Lithium sulfate behaves differently than the rest of the series. Three fits have been made, general fit, dilute fit and concentrated fit and all of them are good.

The four other alkali sulfates exhibit two regions. In the dilute region, the pattern is normal and is well reproduced. In the region near saturation, the osmotic coefficient is roughly constant; a special concentrated fit is required to attain these points more or less well. The general fit is a compromise between the two distinct behaviors and is in poor agreement with experimental data.
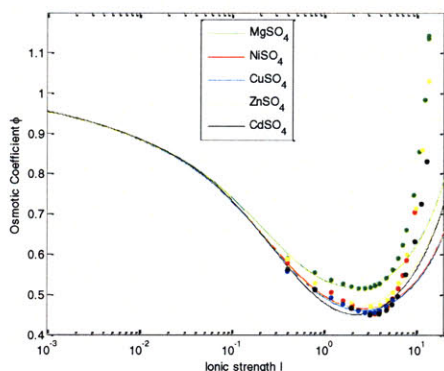
Figure 97: General fit of metal sulfates
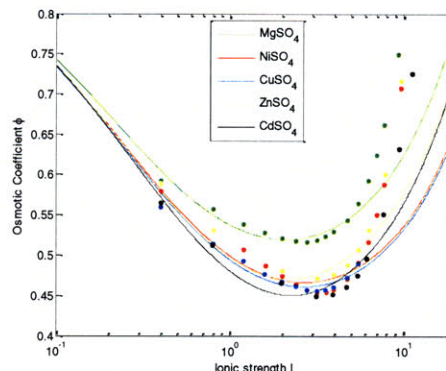
Figure 98: General fit of metal sulfates – partial view
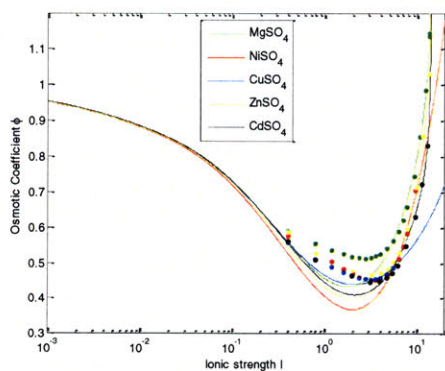
Figure 99: Concentrated fit of metal sulfates
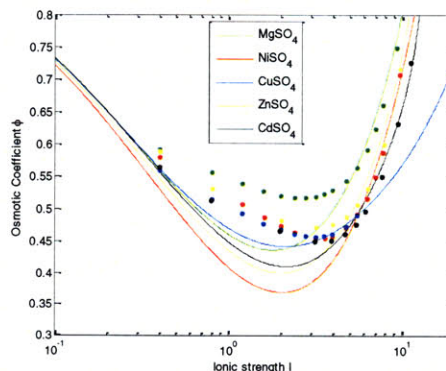
Figure 100: Concentrated fit of metal sulfates – partial view

98
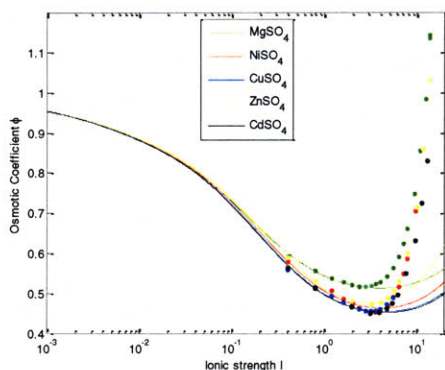
| **Figure 101: Semi-dilute fit of metal sulfates** | **Figure 102: Semi-dilute fit of metal sulfates – partial view** |
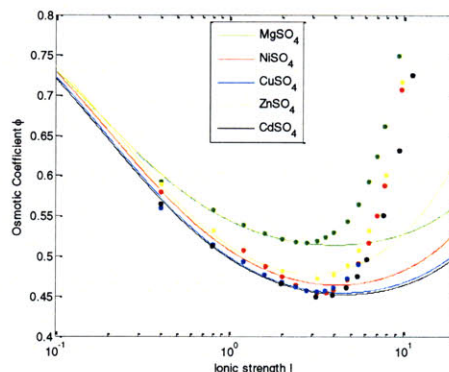
No experimental data is available in the dilute region. Experimental values are reproduced with three different fits. The semi-dilute and concentrated fits are peculiar to each region; both of them are good. The general fit uses the central part of the dataset in order to provide a compromise and is good in the central region. These fits were made with a modified formula for the osmotic coefficient

$$\phi = \left[1.15 - \frac{0.15}{1 + \rho^0 / 0.01 \ mol/L} \right] \phi_{usual}$$

An equally good concentrated fit can be made without modifying the expression of the osmotic coefficient. However both the semi-dilute and the general fits need the modification to be accurate. One possible explanation for the need for such a modification is the phenomenon of ion pairing [10,14]: two divalent ions of opposite charges form a temporary bond by sharing the water molecules in their shells of hydration; they are thus linked through a weak sequence of hydrogen bonds; this is sufficient to induced a marked difference in the osmotic coefficient that cannot be captured by a theory of the electrical interactions.

V.10 Conclusions

V.10.1 Limits of the primitive model and of this development

The model assumes that ions are hard spheres and bear a fixed electrical charge. Ions are always hydrated so the radius that matters is the hydrated radius. However the hydrated radius does not have a unique definition and cannot be measured precisely. In the present work, it is a parameter that is fit to reproduce data and can vary considerably with the concentration and with the nature of the counterion.

Some cases, but not all, exhibit a linear pattern in the logarithm of the ionic strength and the fits can be markedly improved if the hydrated radii, λ, are allowed to be less than the ionic radii, σ. These solutions, though better, were excluded because they are unphysical. The electrolytes concerned are CsBr, CsI, NaNO$_3$, Na$_2$SO$_4$, K$_2$SO$_4$ and Cs$_2$SO$_4$.

In three cases, H$_2$SO$_4$, ZnCl$_2$ and ZnBr$_2$, the concentrated fits can be made both as 2:1 and 1:1 electrolytes. They are both equally good. This confirms that at high concentrations, these electrolytes are partially associated and effectively become 1:1 electrolytes; they are part of group known as strongly complexing compounds.

Some polyatomic ions such the nitrite, sulfate and perchlorate ions and the hydronium ion

are far from being spherical. Yet their behavior is still well captured by the model.

The correlation parameter is an attempt to capture the effect of electrical interactions of order two or higher. It is impossible to determine a priori. The model assumed it constant and peculiar to each electrolyte. However it seems to vary with concentration, albeit not much.

These are the main limits of the model. What causes the ionic radii and the correlation parameter to change is linked to the molecular nature of the solvent – mainly to its polarity and ability to form hydrogen bonds – and to the chemical properties of each ion, resulting from its underlying orbitals. These elements are beyond the scope of the present work.

V.10.2 Other notes

Some sets of experimental data indicated the solubility limit for the electrolyte and the computations stopped at this point, because the model is not adapted to deal with the equilibrium between ions in solution and in crystal form. Other sets did not indicate the solubility limit so the limit was placed arbitrarily between 3 mol/L and 7 mol/L.

The fitting procedure had as lower bounds the ionic radii of ions and as upper bounds 6 Å. The hydrated radii from literature – see Appendix D – were used as initial guesses. The bounds for the correlation parameter were usually 1 and 6, but sometimes could be extended to 0 and 8.

In some cases, allowing charges to take non-integer values yields better fits. These solutions were however ruled out as unphysical.

VI   COMPARISON OF THE MEAN IONIC ACTIVITY COEFFICIENT WITH EXPERIMENTAL DATA

Extensive experimental data for 75 electrolytes was collected from reference [19] and grouped in series by anion. The equation describing the mean ionic activity coefficient is:

$$\ln \gamma_{\pm} = \frac{4\pi}{3}\left(v_\alpha \lambda_\alpha^3 + v_\beta \lambda_\beta^3\right)\rho^0$$

$$-\frac{1}{2}\frac{l_B}{\sigma_\alpha}\frac{z_\alpha^2 v_\alpha}{v_\alpha + v_\beta}\left[\begin{array}{l}\ln\left(1 + \dfrac{e^{-\gamma}\sigma_\alpha}{\lambda_\alpha - \sigma_\alpha} + \dfrac{e^{-\gamma}}{2}\sqrt{\dfrac{\sigma_\alpha}{\lambda_\alpha - \sigma_\alpha}}\right) \\[3mm] -e^{-\kappa(\lambda_\alpha - \sigma_\alpha)}\ln\left(1 + \dfrac{e^{-\gamma}}{1 + \kappa\sigma_\alpha}\dfrac{\sigma_i}{\lambda_\alpha - \sigma_\alpha} + \dfrac{e^{-\gamma}}{2}\dfrac{1}{\sqrt{1 + \kappa\sigma_\alpha}}\sqrt{\dfrac{\sigma_\alpha}{\lambda_\alpha - \sigma_\alpha}}\right)\end{array}\right]$$

$$-\frac{1}{2}\frac{l_B}{\sigma_\beta}\frac{z_\beta^2 v_\beta}{v_\alpha + v_\beta}\left[\begin{array}{l}\ln\left(1 + \dfrac{e^{-\gamma}\sigma_\beta}{\lambda_\beta - \sigma_\beta} + \dfrac{e^{-\gamma}}{2}\sqrt{\dfrac{\sigma_\beta}{\lambda_\beta - \sigma_\beta}}\right) \\[3mm] -e^{-\kappa(\lambda_\beta - \sigma_\beta)}\ln\left(1 + \dfrac{e^{-\gamma}}{1 + \kappa\sigma_\beta}\dfrac{\sigma_\beta}{\lambda_\beta - \sigma_\beta} + \dfrac{e^{-\gamma}}{2}\dfrac{1}{\sqrt{1 + \kappa\sigma_\beta}}\sqrt{\dfrac{\sigma_\beta}{\lambda_\beta - \sigma_\beta}}\right)\end{array}\right]$$

100

ρ^0 is the concentration of the electrolyte; ν_α and ν_β are the multiplicity of the cation and anion; z_α and z_β are their charges; σ_α and σ_β are their ionic radii; λ_α and λ_β are their hydrated radii. K_α, K_β, K and κ are constants given by the formulae above; they are all homogenous to the inverse of a length. γ is the Euler-Mascheroni constant; $\gamma = 0.577215665$.

The equation is fitted to experimental data in method similar to the one used for the osmotic coefficient. Electrolytes are grouped in families by their anion. The results are presented below.

VI.1 Fluorides
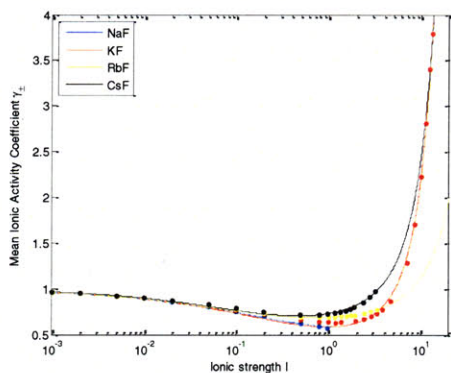
Figure 103: General fit of alkali fluorides
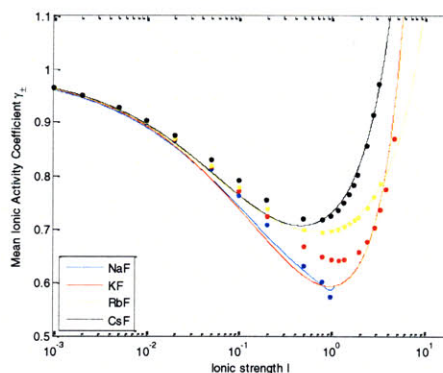
Figure 104: General fit of alkali fluorides – partial view
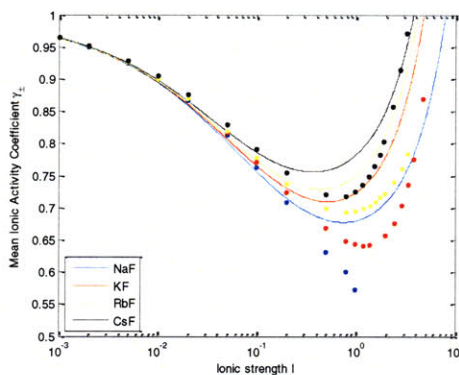
Figure 105: Dilute fit of alkali fluorides
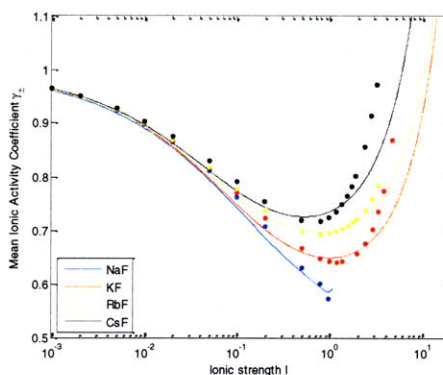
Figure 106: Semi-dilute fit of alkali fluorides

In the series of alkali fluorides the usual order of curves is reversed. Potassium fluoride, rubidium fluoride and cesium fluoride exhibit the usual pattern and the corresponding experimental data is accurately described using three sets of parameters. Only the general fit and the dilute fit are needed for sodium fluoride, because the solubility limit is reached at ionic strengths close to 1 mol/L; both fits are in good agreement with experimental data.

No experimental data is available for lithium fluoride.

VI.2 Chlorides
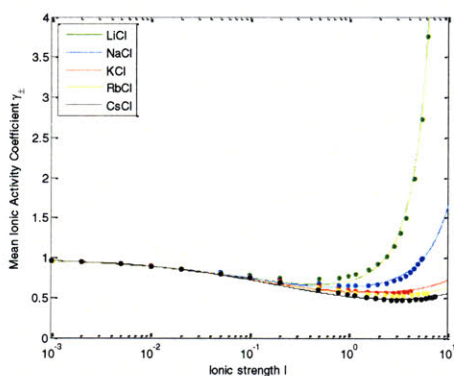
Figure 107: General fit of alkali chlorides
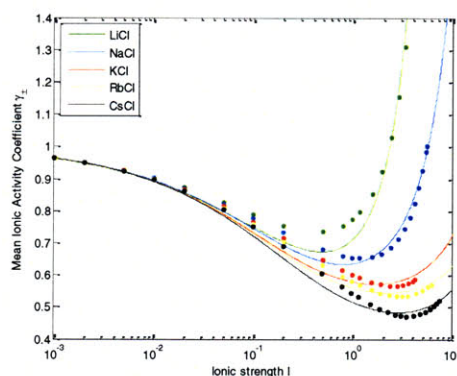
Figure 108: General fit of alkali chlorides – partial view
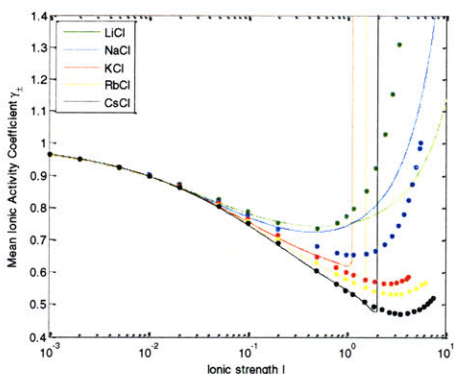
Figure 109: Dilute fit of alkali chlorides
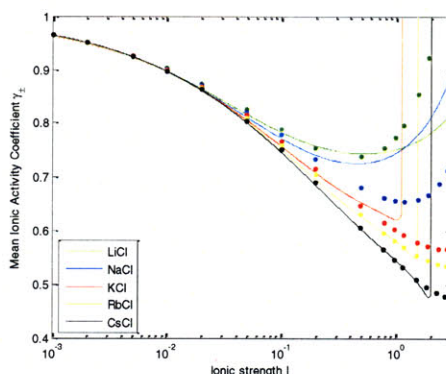
Figure 110: Dilute fit of alkali chlorides – partial view
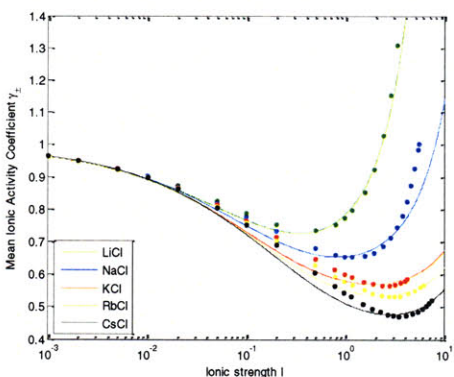
Figure 111: Semi-dilute fit of alkali chlorides
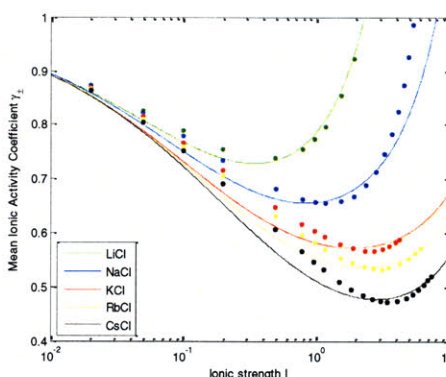
Figure 112: Semi-dilute fit of alkali chlorides – partial view

The series of alkali chlorides is archetypal. Three sets of parameters are needed. The general fit reproduces experimental points very well in the concentrated region and poorly in the semi-dilute and dilute regions; the divergence starts close to the inflexion point of the curve. The dilute fit is accurate in the dilute region and the semi-dilute fit is a compromise that works well in the semi-dilute region.
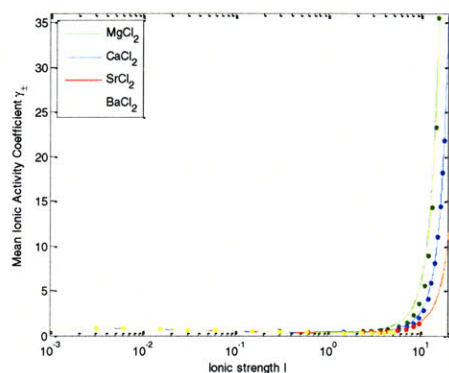
Figure 113: General fit of alkali-metal chlorides
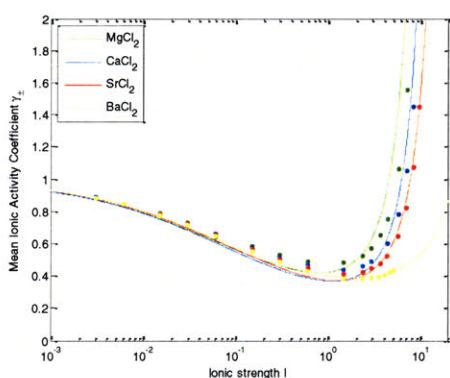
Figure 114: General fit of alkali-metal chlorides – first partial view
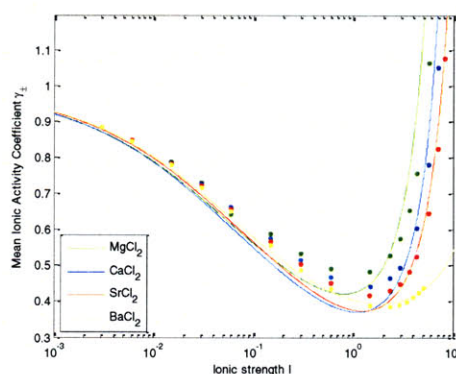
Figure 115: Gen. fit of alkali-metal chlorides –second partial view
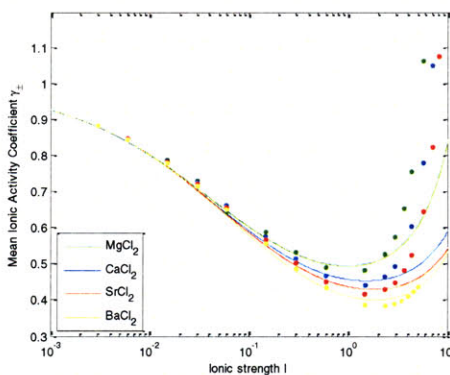
Figure 116: Dilute fit of alkali-metal chlorides
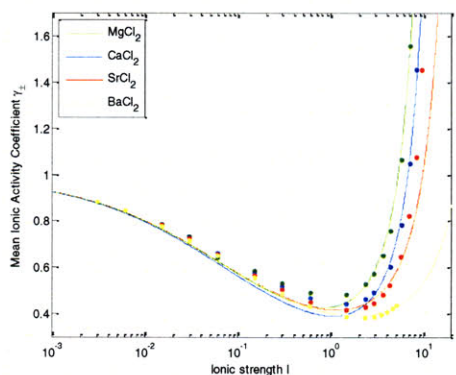
Figure 117: Semi-dilute fit of alkali-metal chlorides

For the series of alkali metal chlorides, experimental data is reproduced well with three sets of parameters, except for barium chloride which requires only two.

103
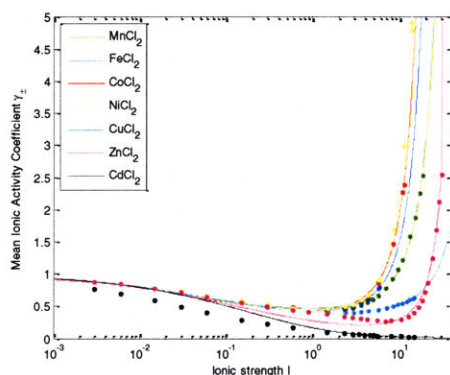
Figure 118: General fit of alkali-metal chlorides
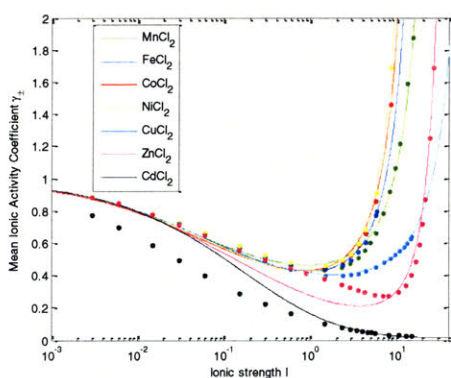
Figure 119: General fit of alkali-metal chlorides – first partial view
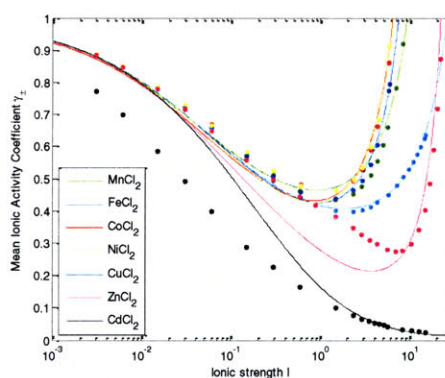
Figure 120: Gen. fit of alkali-metal chlorides – second partial view
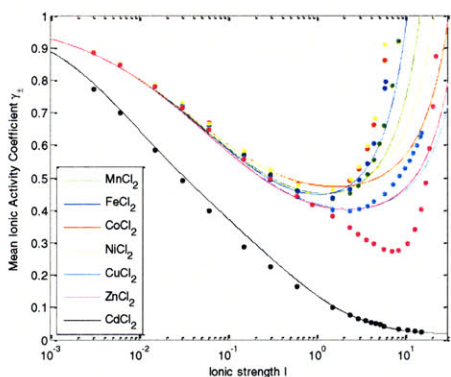
Figure 121: Dilute fit of alkali-metal chlorides
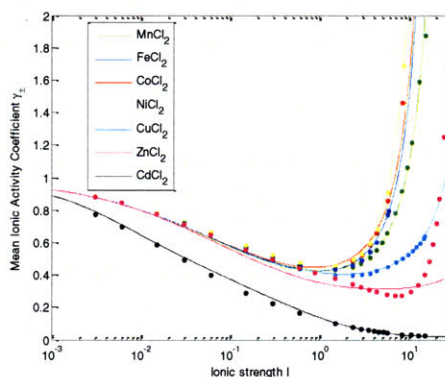
Figure 122: Semi-dilute fit of alkali-metal chlorides

Manganous chloride, cobalt chloride and nickel chloride exhibit the usual pattern and their experimental points are well reproduced using three sets of parameters. This situation is in sharp contrast with the data for the osmotic coefficient where manganous and copper chloride exhibited abnormal behavior akin to that of zinc chloride. Ferrous chloride and copper chloride require only two sets of parameters for accurate reproduction.

Zinc chloride exhibits three distinct regions. In the dilute and concentrated regions, the dilute and general fits track experimental points very well. In the semi-dilute region, the mean ionic activity coefficient diminishes almost linearly and cannot be properly reproduced; hence a mediocre semi-dilute fit and a marked divergence of the general fit from the data points in this

104

region. This behavior mirrors the anomaly observed in the data of the osmotic coefficient. It must originate in the transition from a mixture of Zn^{2+} and Cl^- ions to a mixture of $ZnCl^+$ and Cl^- ions.

Cadmium chloride exhibits a marked divergence from the rest of the curves even in the dilute region. The lower values and the steep decrease cannot be reproduced using the mathematical expression of the mean ionic activity coefficient. This expression was modified for the dilute fit:

$$\gamma_{\pm} = \frac{\gamma_{\pm,usual}}{1+\rho^0/0.002 \ mol/L}$$

The general fit was made without this modification because experimental points in the concentrated region can be reproduced without it. The semi-dilute fit was not made.

The behavior of zinc chloride and of cadmium chloride echoes the phenomena observed for the osmotic coefficient.
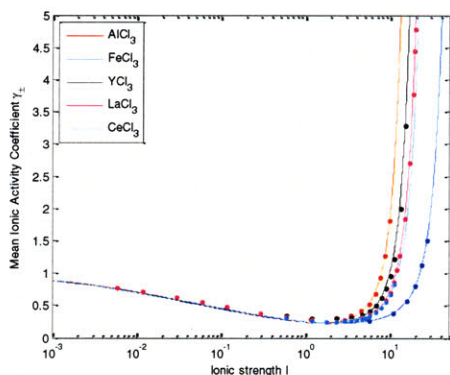
Figure 123: General fit of metal chlorides
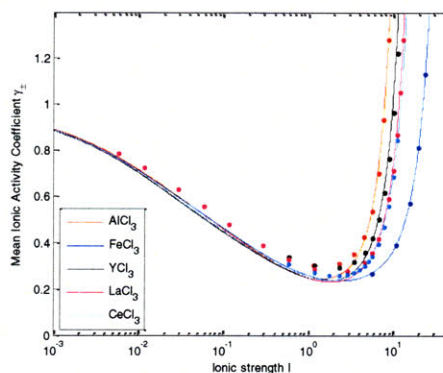
Figure 124: General fit of metal chlorides – partial view
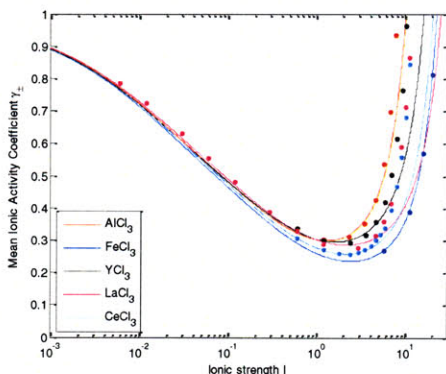
Figure 125: Dilute fit of lanthanum chloride and semi-dilute fit for the other metal chlorides
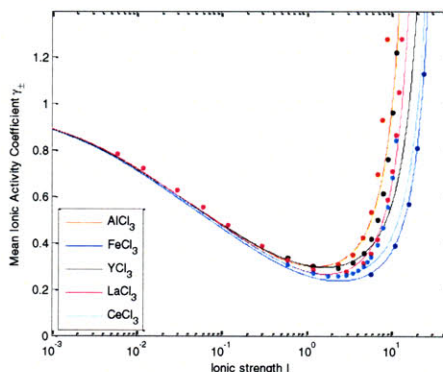
Figure 126: Semi-dilute fit of metal chlorides

Lanthanum chloride requires three sets of parameters to accurately reproduce experimental points. The other metal trichlorides lack data in the dilute region hence only the general and the semi-dilute fits were made; these fits are good.

105
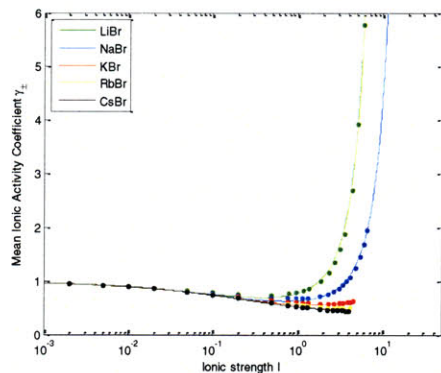
VI.3 Bromides

Figure 127: General fit of alkali bromides
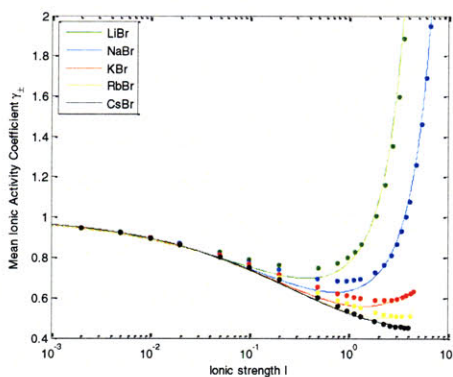
Figure 128: General fit of alkali bromides – first partial view
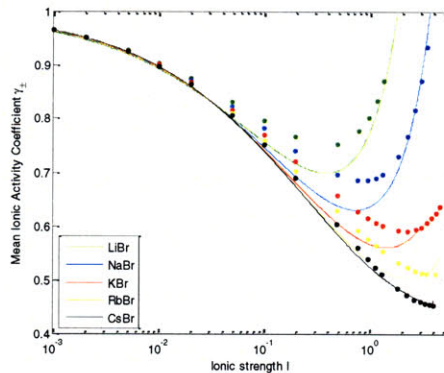
Figure 129: General fit of alkali bromides – second partial view
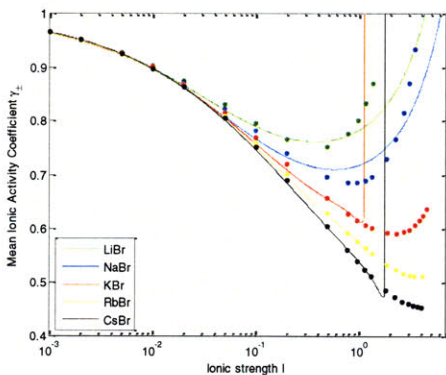
Figure 130: Dilute fit of alkali bromides
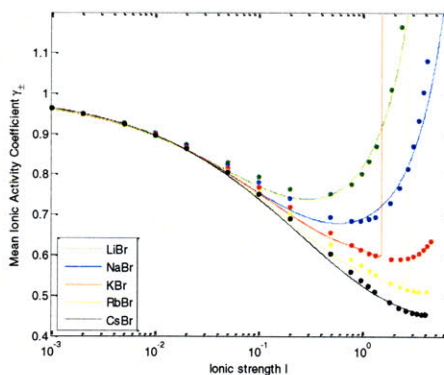
Figure 131: Semi-dilute fit of alkali bromides

The experimental points of all alkali bromides except cesium bromide are reproduced using three sets of parameters; cesium bromide requires only two. The dilute and semi-dilute fits are good. The general fit of potassium bromide is good only in the concentrated region; the general fit of rubidium chloride is mediocre and cannot track the data even qualitatively. These results contrast with the data for the osmotic coefficient for which this series was well behaved.
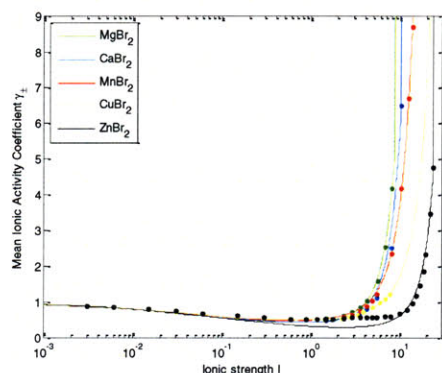
Figure 132: General fit of metal bromides
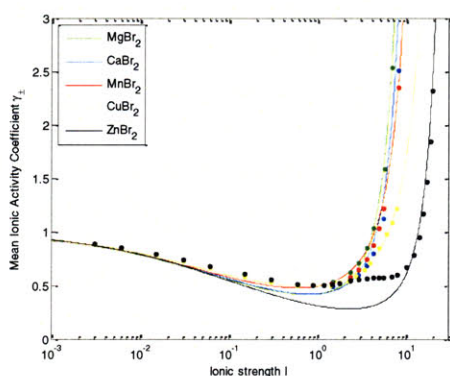
Figure 133: General fit of alkali bromides – first partial view
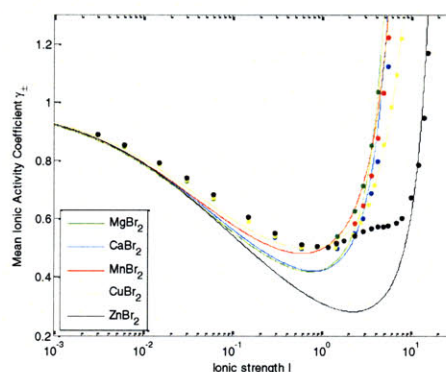
Figure 134: General fit of alkali bromides – second partial view
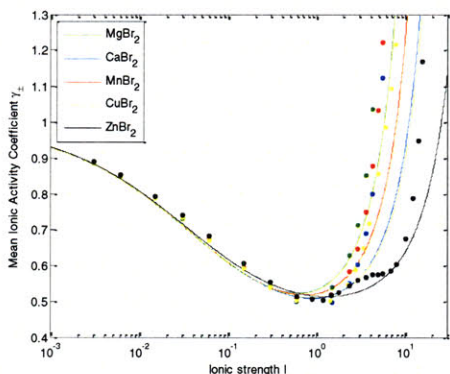
Figure 135: Dilute fit of alkali bromides
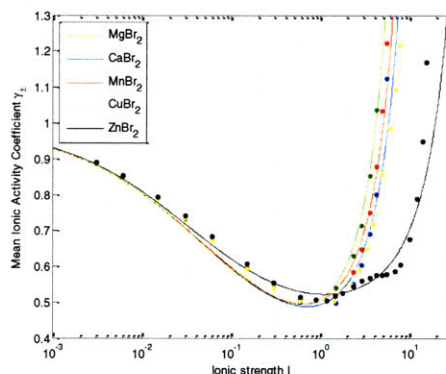
Figure 136: Semi-dilute fit of alkali bromides

Magnesium, calcium, manganous and copper bromides have the usual behavior and the corresponding experimental data is reproduced with three sets of parameters. Like manganous and copper chlorides, manganous and copper bromides appear quite normal for the ionic activity coefficient and abnormal for the osmotic coefficient. The three fits always underestimate experimental values in the dilute region, which reduces the usefulness of the dilute fit; the two other fits are good.

Zinc bromide, like zinc chloride, has an unusual semi-dilute region. The change of behavior is pronounced and the cause is the replacement of Zn^{2+} with $ZnCl^+$ as the main cation. Consequently the dilute and concentrated fits are good but the semi-dilute one is mediocre.

107

VI.4   Iodides
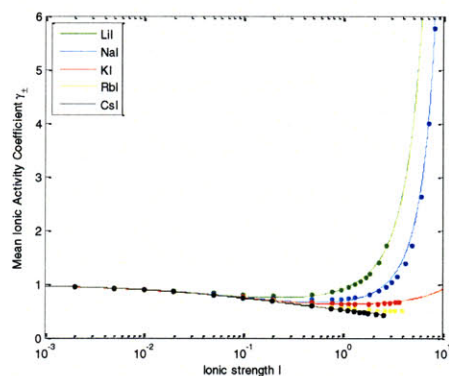
Figure 137: General fit of alkali iodides
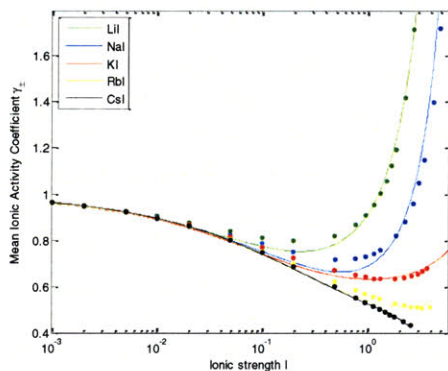
Figure 138: General fit of alkali iodides – first partial view
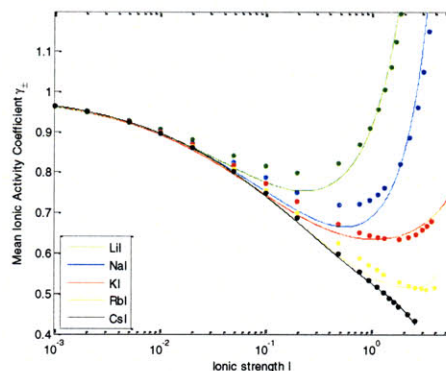
Figure 139: General fit of alkali iodides – second partial view
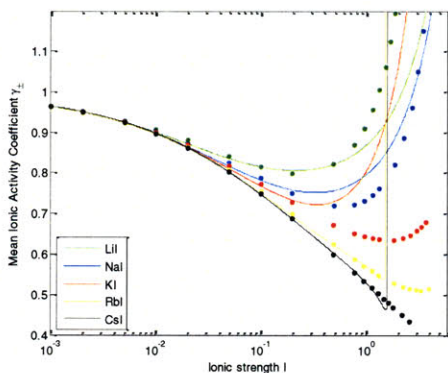
Figure 140: Dilute fit of alkali iodides
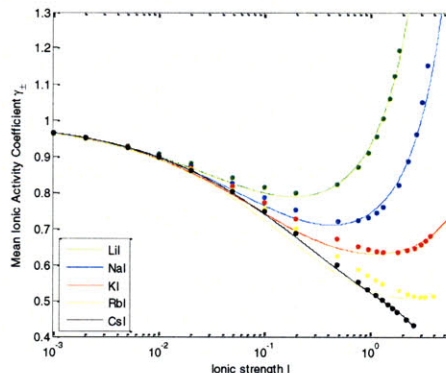
Figure 141: Semi-dilute fit of alkali iodides

The experimental points of all alkali iodides except cesium iodide are reproduced using three sets of parameters; cesium iodide requires only two. All fits are good for lithium, sodium and cesium iodides. The general fits of potassium and rubidium bromide are mediocre. Their semi-dilute fits aims at reproducing experimental data close to saturation. Their dilute fits are good.

For the osmotic coefficient cesium iodide was the most troublesome electrolyte of the series and the others were quite normal.
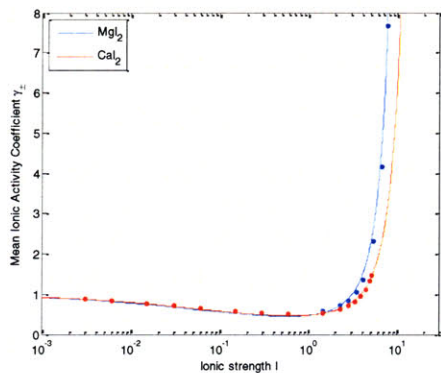
Figure 142: General fit of alkali-metal iodides
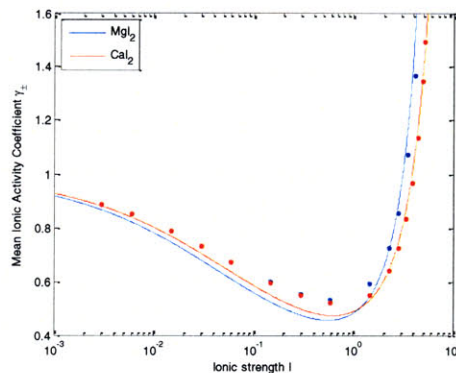
Figure 143: General fit of alkali-metal iodides – partial view
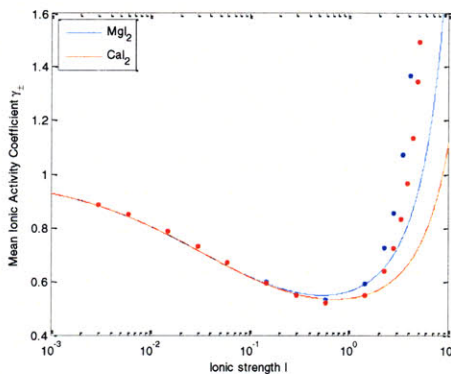
Figure 144: Dilute fit of alkali-metal iodides
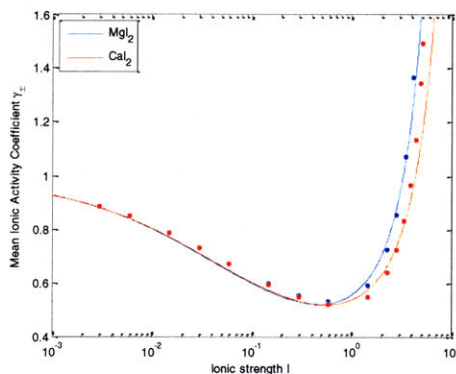
Figure 145: Semi-dilute fit of alkali-metal iodides

The experimental points of the two alkali metal iodides have the usual pattern and are well reproduced using three sets of parameters. There is no significant difference in behavior between the osmotic coefficient and ionic activity coefficient.

VI.5   Nitrates
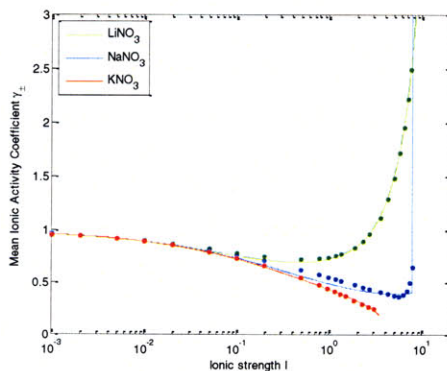
Figure 146: General fit of alkali nitrates

109
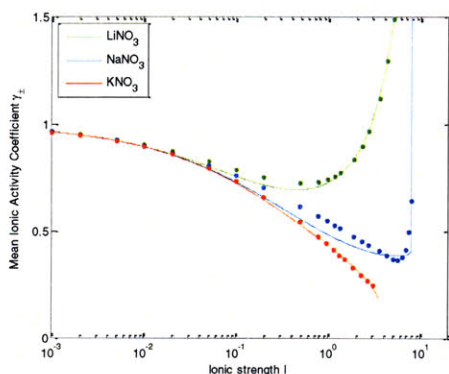
Figure 147: General fit of alkali nitrates – first partial view
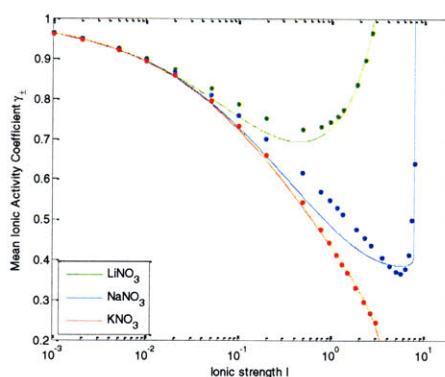
Figure 148: General fit of alkali nitrates – second partial view
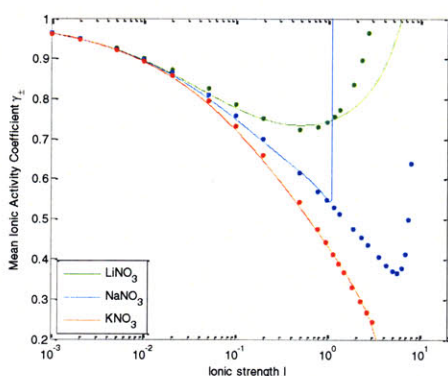
Figure 149: Dilute fit of alkali nitrates
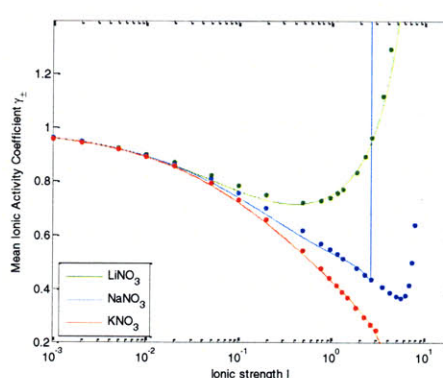
Figure 150: Semi-dilute fit of alkali nitrates

The experimental data of lithium nitrate is well reproduced using three sets of parameters. That of potassium nitrate is very well reproduced using a single set of parameters. The dilute and semi-dilute fits of sodium nitrate are good in their respective regions. The general fit is close to experimental points only near the inflexion point and diverges to infinity as the solution reaches saturation. In this series the behavior of the mean ionic activity coefficient perfectly mirrors that of the osmotic coefficient.
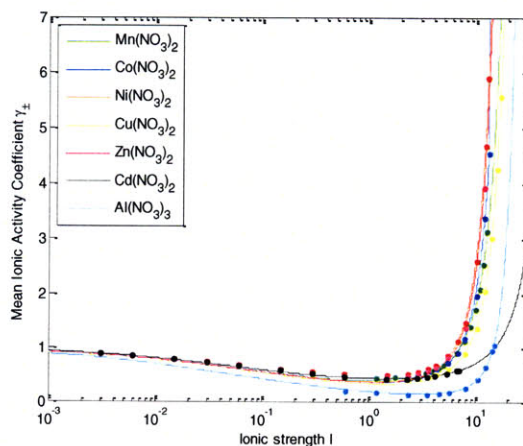
Figure 151: General fit of metal nitrates

110
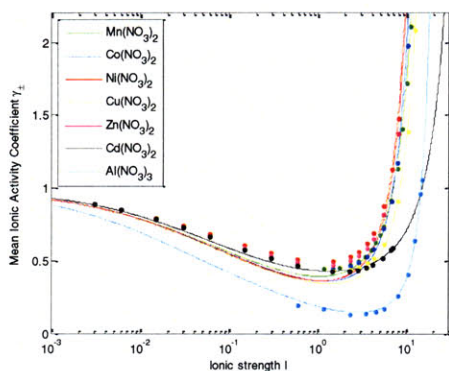
Figure 152: General fit of metal nitrates – first partial view
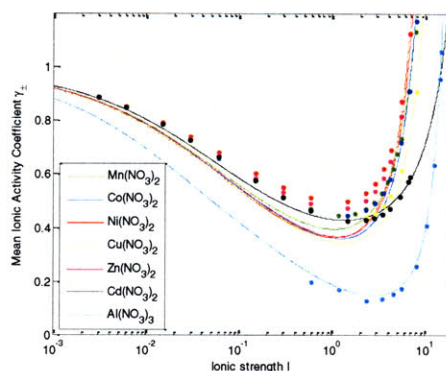
Figure 153: General fit of metal nitrates – second partial view
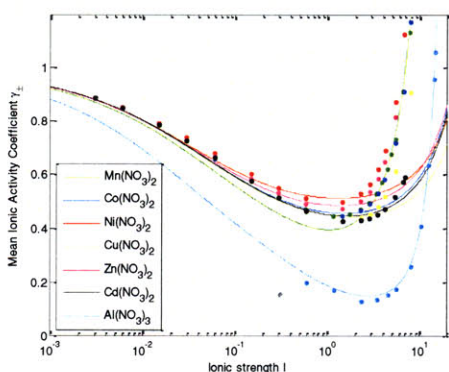
Figure 154: Dilute fit of metal nitrates
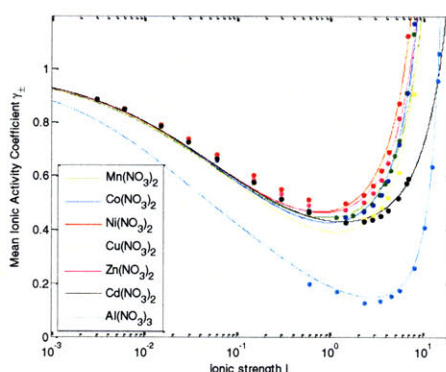
Figure 155: Semi-dilute fit of metal nitrates

Metal di-nitrates exhibit the normal pattern and correspondingly experimental data is reproduced well in the three regions using three sets of parameters. For aluminum nitrate experimental data is available only in the concentrated region and only the general fit is necessary.

VI.6 Perchlorates
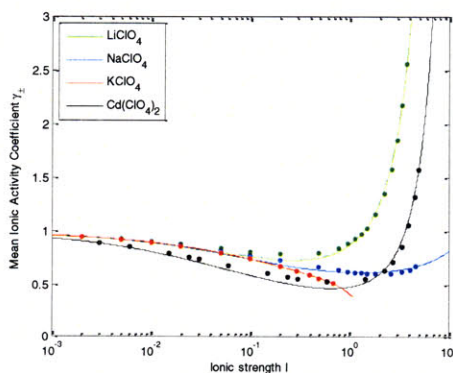
Figure 156: General fit of alkali and cadmium perchlorates
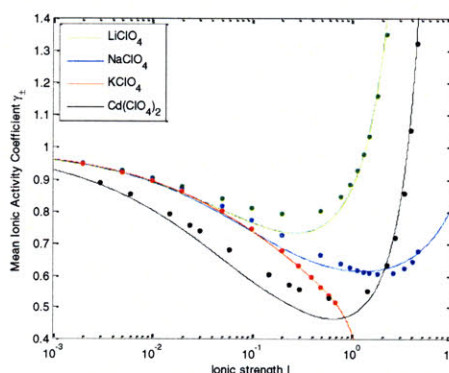
Figure 157: Gen. fit of alkali and cadmium perchl. – partial view

111
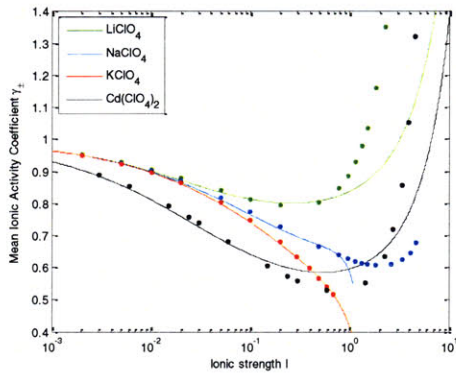
Figure 158: Dilute fit of alkali and cadmium perchlorates
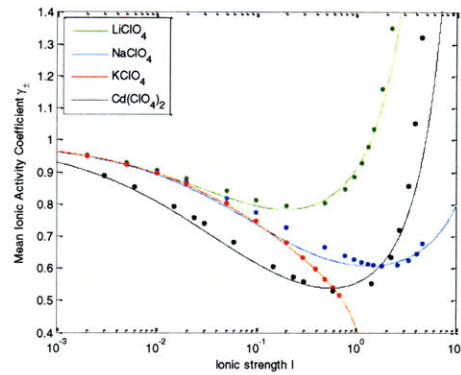
Figure 159: Semi-dilute fit of alkali and cadmium perchlorates

The experimental data of potassium perchlorate is extremely well reproduced with a single set of parameters. For the three other perchlorates, three sets of parameters are needed.

VI.7   Acids
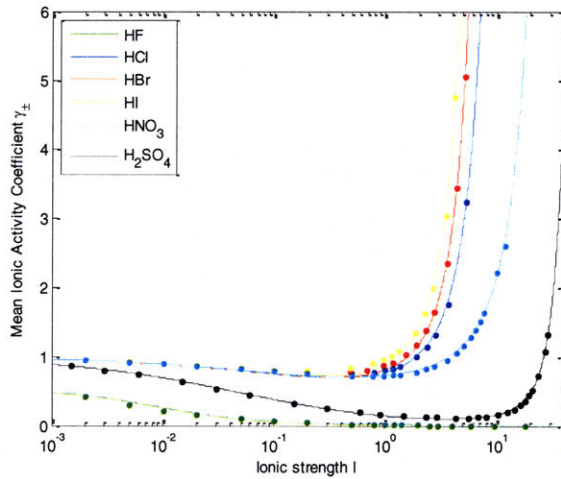
Figure 160: General fit of acids
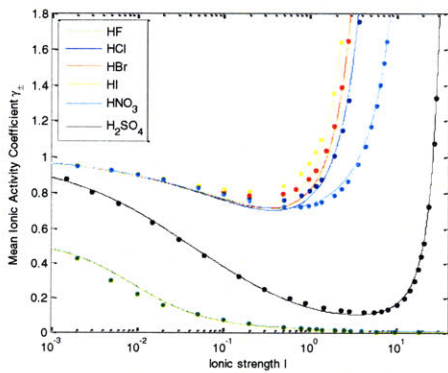
Figure 161: General fit of acids – first partial view
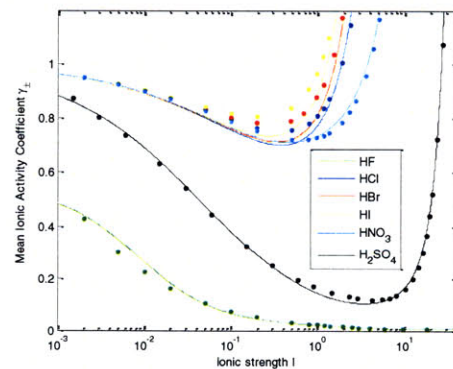
Figure 162: General fit of acids – second partial view

112
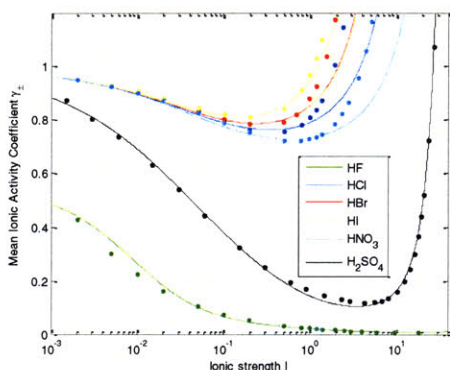
Figure 163: Dilute fit of acids
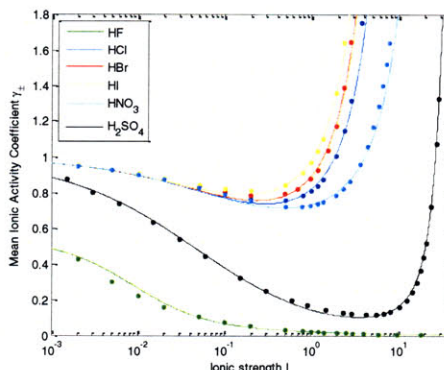
Figure 164: Semi-dilute fit of acids

Hydrochloric, hydrobromic, hydroiodic and nitric acids appear to be usual electrolytes and their behavior is well reproduced using three sets of parameters. Sulfuric acid is extremely well reproduced using a single set of parameters; the only divergence is small and occurs in the semi-dilute region. The fit has a peculiarity as the size of the cation is taken to be 0.04 Å, which means that the proton is taken to be independent not part of a hydronium ion; for the other acids, the cation is always the hydronium ion and its size is taken to be that of a water molecule 1.15 Å.

Hydrofluoric acid is a weak acid of $pK_a = 3.15$, and has an extremely unusual behavior that cannot be reproduced with the normal expression of the mean ionic activity coefficient; it is not a simple electrolyte as the hydronium ion H_3O^+ and fluoride ion F^- coexist with a solvated HF and the bifluoride ion FHF^-. Thus the mathematical formula was modified:

$$\gamma_\pm = \left[0.05 + \frac{0.50}{1 + \rho^0 / 0.01 \ mol/L} \right] \gamma_{\pm,usual}$$

Only one fit was made and it is reasonably accurate. This is the only compound for which the fitted mean ionic activity coefficient does not converge to 1 in the limit of infinite dilution.

VI.8   Bases
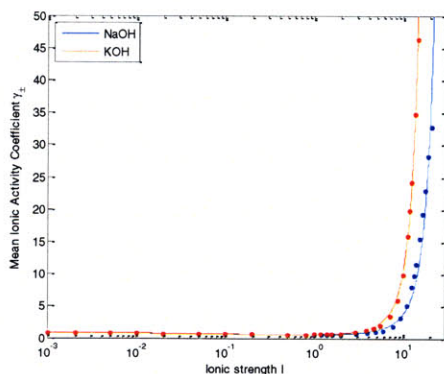
Figure 165: General fit of bases

113
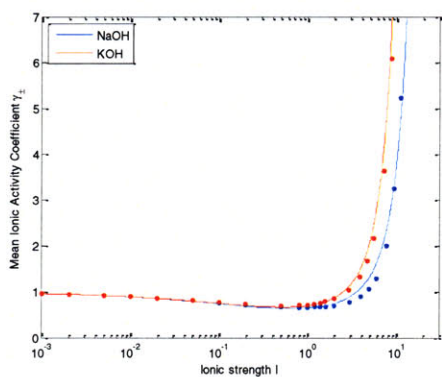
Figure 166: General fit of bases – first partial view
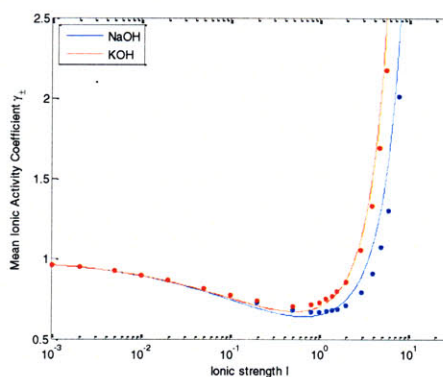
Figure 167: General fit of bases – second partial view
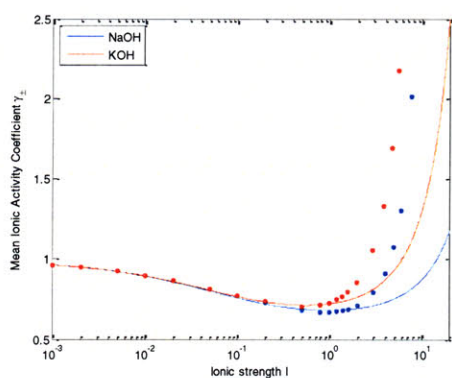
Figure 168: Dilute fit of bases
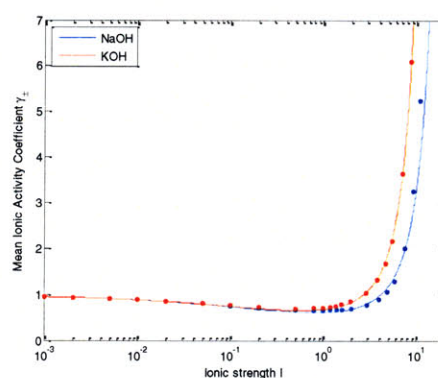
Figure 169: Semi-dilute fit of bases

The two bases exhibit the usual pattern and experimental data is reproduced well using three sets of parameters. The behavior of the mean ionic activity coefficient and of the osmotic coefficient is identical.

VI.9 Sulfates
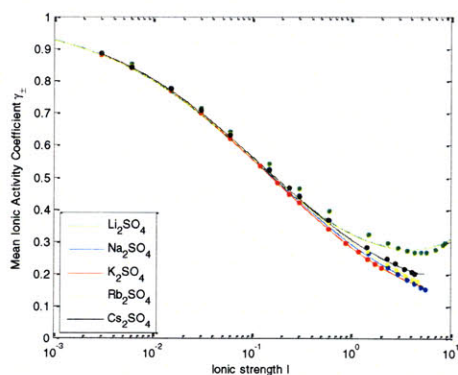
Figure 170: General fit of alkali sulfates
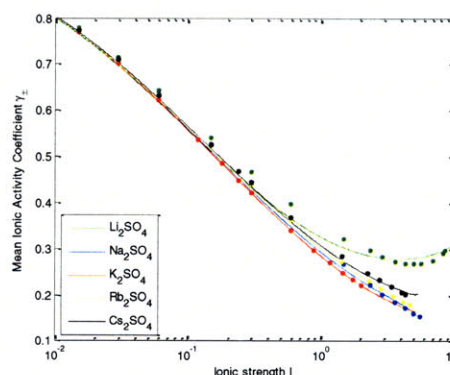
Figure 171: General fit of alkali sulfates – partial view

114
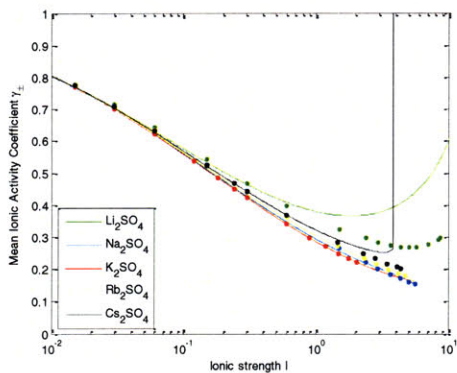
Figure 172: Dilute fit of alkali sulfates
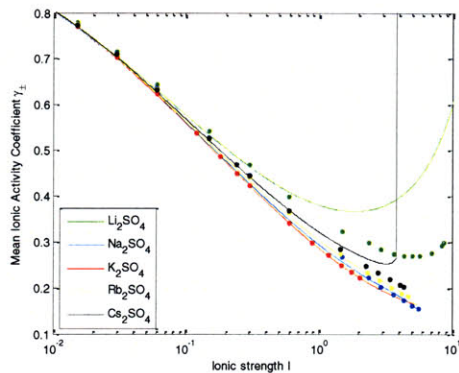
Figure 173: Dilute fit of alkali sulfates – partial view

Experimental points of sodium, potassium and rubidium sulfate are very well reproduced using a single set of parameters. For lithium and cesium sulfate, two sets of parameters are needed. The difference between the mean ionic activity coefficient and the osmotic coefficient is considerable; the data of the latter requires three fits and is reproduced poorly.
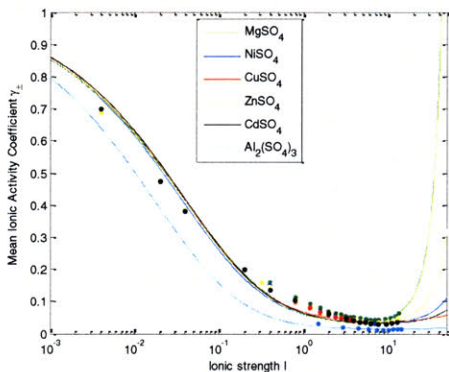
Figure 174: Concentrated fit of metal sulfates
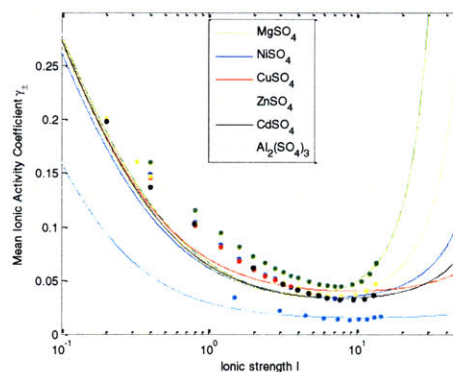
Figure 175: Concentrated fit of metal sulfates – partial view
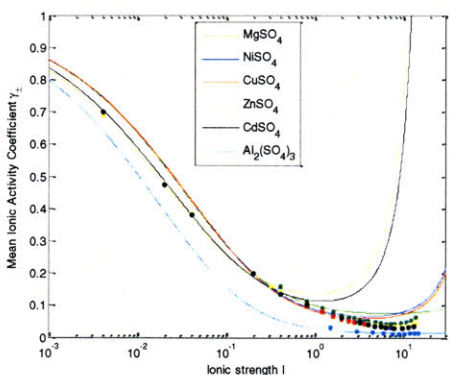
Figure 176: Dilute fit of metal sulfates
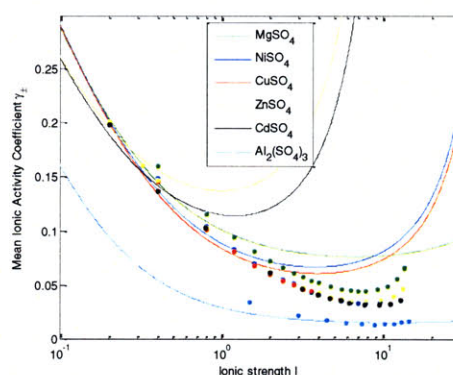
Figure 177: Dilute fit of metal sulfates – partial view
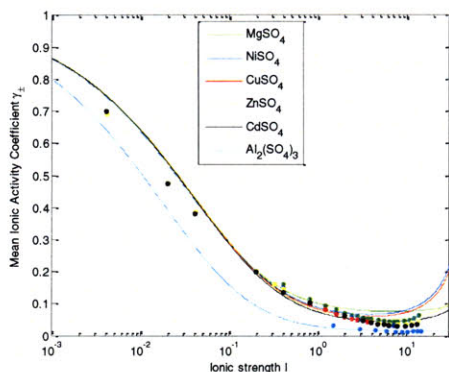
Figure 178: Semi-dilute fit of metal sulfates
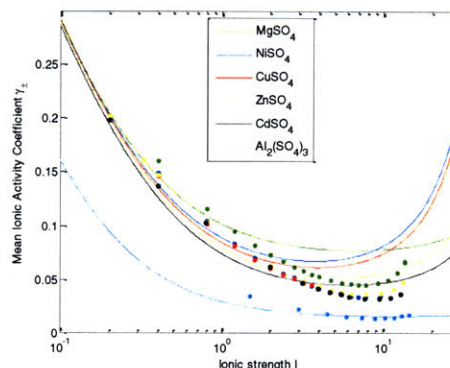
Figure 179: Semi-dilute fit of metal sulfates – partial view

No general fit was made for this series because it strays from the experimental points. The concentrated fits are accurate for all electrolytes. The semi-dilute ones are mediocre. Zinc and cadmium sulfate have dilute fits because experimental data is available, albeit scarcely; their dilute fits are good. In contrast to the osmotic coefficient there is no need to modify the expression of the mean activity coefficient to reproduce data in the dilute and semi-dilute region.

Aluminum sulfate only has the concentrated fit and it is good at ionic strengths higher than 3 mol/L.

VI.10 Notes

The general equation for the mean ionic activity coefficient is good at describing the experimental data of most binary electrolytes; a general fit, a dilute fit and a semi-dilute fit are usually necessary. The general fit generally captures the qualitative behavior of the electrolyte; it is very accurate in the concentrated region; it underestimates the numerical values in the semi-dilute region before converging to the normal Debye-Hückel limiting law. The same phenomenon is observed for the osmotic coefficient but it is somewhat more pronounced for the mean ionic activity coefficient.

Three parameters are fitted in the equations of both the osmotic coefficient and the mean ionic activity coefficient: the correlation parameter, w; the hydrated radii of the anion and of the cation, σ_α and σ_β. Ideally the numerical values of these parameters yielded by the fittings over the osmotic coefficient and over the mean ionic activity coefficient should be the same; they are markedly different. Two explanations are advanced for the discrepancy. First the two coefficients are normally linked by a modified form of the Gibbs-Duhem identity:

$$\ln \gamma_\pm = \phi_s - 1 + \int_0^m \frac{\phi_s - 1}{m'} \, dm'$$

However because of several approximations in their derivations, the final formulas do not satisfy the relationship, which introduces numerical differences in the two sets parameters. Second the two hydrated radii are heavily correlated, which complicates the fitting procedure; often the sum of the radii mattered more than their separate values, which resulted in heavy dependence on the initial condition. Consequently the values of the hydrated radii derived from these fittings have little or no physical significance.

The fact that the formulae of the osmotic coefficient and the mean ionic activity coefficient do not satisfy the Gibbs-Duhem identity explains why some experimental series have good fittings for one coefficient and poor fittings with the other.

The ionic radii were not adjusted by the fitting procedure. They are considered to be a physical characteristic of the ion, independent of the other ions present in solution, and their values were taken from the literature – values given in Appendix D. There is one exception, sulfuric acid, for which the hydronium ion was replaced with a free proton in the fitting over the mean ionic activity coefficient.

Chapter 7   Comparison of the correlated hard spheres model with other models for binary electrolytes

This chapter aims at comparing the accuracy of four models for ionic solutions:
- Debye-Hückel limiting law
- Meissner model
- Pitzer model
- Correlated hard spheres model

I   DEBYE-HUCKEL LIMITING LAW

We consider a binary electrolyte $A_{v\alpha}B_{v\beta}$ dissolved in water at T = 298 K. The original Debye-Hückel model provides the limiting law at low concentrations. Its formulation is described below [13,16]:

$$\ln \gamma_\pm = -A|z_\alpha z_\beta|\sqrt{I}$$

$$A = (l_B)^{\frac{3}{2}}\sqrt{2000\pi N_A d_w} \qquad l_B = \text{Bjerrum length} = \frac{e^2}{4\pi\varepsilon_0\varepsilon_r k_B T} \qquad I = \frac{1}{2}(v_\alpha z_\alpha^2 + v_\beta z_\beta^2)m$$

N_A = Avogadro's number = $6.02 \cdot 10^{23}$ mol^{-1} l_B = 7.13 Å at room temperature
d_w = water density (kg/L) = 0.997 kg/L at room temperature
m = molality of the solution (moles of solute/kg water)

At room temperature A = 1.17 and has units of kg$^{1/2}$/mol$^{1/2}$. Note that the ionic strength is based on the molality, not on molarity.

II   MEISSNER MODEL

It is based on the principle of corresponding states and has only one parameter q [13,16].

$$\ln \gamma_\pm = |z_\alpha z_\beta|\ln\Gamma$$

$$\ln\Gamma = -\frac{A\sqrt{I}}{1+(1+0.055\cdot q\cdot e^{-0.023I^3})\sqrt{I}} + \ln\left[1+(0.75-0.065\cdot q)\left(\left(1+\frac{I}{10}\right)^q -1\right)\right]$$

III   PITZER MODEL

It is the most successful semi-empirical extension of the Debye-Hückel approach [13,16].

$$\ln \gamma_\pm = -|z_\alpha z_\beta|f^\gamma + B_\pm^\gamma \cdot m + C_\pm^\gamma \cdot m^2$$

$$f^\gamma = A'\left(\frac{\sqrt{I}}{1+b\sqrt{I}} + \frac{2}{b}\ln(1+b\sqrt{I})\right) \text{ with A' = 0.3915 and b = 1.2}$$

$$B_\pm^\gamma = 2\beta_0 + \frac{2\beta_1}{\alpha^2 I}\left[1 - \left(1 + \alpha\sqrt{I} - \frac{\alpha^2}{2}I\right)e^{-\alpha\sqrt{I}}\right] \text{ with } \alpha = 2.0$$

$$C_\pm^\gamma = \frac{3}{2}C_\pm^\phi$$

In the case of 2:2 electrolytes the expression of $B_\pm^\gamma$ is modified:

$$B_\pm^\gamma = 2\beta_0 + \frac{2\beta_1}{\alpha_1^2 I}\left[1 - \left(1 + \alpha_1\sqrt{I} - \frac{\alpha_1^2}{2}I\right)e^{-\alpha_1\sqrt{I}}\right] + \frac{2\beta_2}{\alpha_2^2 I}\left[1 - \left(1 + \alpha_2\sqrt{I} - \frac{\alpha_2^2}{2}I\right)e^{-\alpha_2\sqrt{I}}\right]$$

with $\alpha_1 = 1.4$ and $\alpha_2 = 12$.
The parameters β_0, β_1, β_2, $C_\pm^\phi$ are adjusted for each electrolyte to fit experimental data.

IV   CORRELATED HARD SPHERES MODEL

The expression of the mean ionic activity coefficient as a function of concentration is

$$\ln\gamma_\pm = \frac{4\pi}{3}\left(\nu_\alpha\lambda_\alpha^3 + \nu_\beta\lambda_\beta^3\right)\rho^0$$

$$-\frac{1}{2}\frac{l_B}{\sigma_\alpha}\frac{z_\alpha^2\nu_\alpha}{\nu_\alpha + \nu_\beta}\left[\begin{array}{l}\ln\left(1 + \frac{e^{-\gamma}\sigma_\alpha}{\lambda_\alpha - \sigma_\alpha} + \frac{e^{-\gamma}}{2}\sqrt{\frac{\sigma_\alpha}{\lambda_\alpha - \sigma_\alpha}}\right)\\[2mm] -e^{-\kappa(\lambda_\alpha - \sigma_\alpha)}\ln\left(1 + \frac{e^{-\gamma}}{1 + \kappa\sigma_\alpha}\frac{\sigma_i}{\lambda_\alpha - \sigma_\alpha} + \frac{e^{-\gamma}}{2}\frac{1}{\sqrt{1 + \kappa\sigma_\alpha}}\sqrt{\frac{\sigma_\alpha}{\lambda_\alpha - \sigma_\alpha}}\right)\end{array}\right]$$

$$-\frac{1}{2}\frac{l_B}{\sigma_\beta}\frac{z_\beta^2\nu_\beta}{\nu_\alpha + \nu_\beta}\left[\begin{array}{l}\ln\left(1 + \frac{e^{-\gamma}\sigma_\beta}{\lambda_\beta - \sigma_\beta} + \frac{e^{-\gamma}}{2}\sqrt{\frac{\sigma_\beta}{\lambda_\beta - \sigma_\beta}}\right)\\[2mm] -e^{-\kappa(\lambda_\beta - \sigma_\beta)}\ln\left(1 + \frac{e^{-\gamma}}{1 + \kappa\sigma_\beta}\frac{\sigma_\beta}{\lambda_\beta - \sigma_\beta} + \frac{e^{-\gamma}}{2}\frac{1}{\sqrt{1 + \kappa\sigma_\beta}}\sqrt{\frac{\sigma_\beta}{\lambda_\beta - \sigma_\beta}}\right)\end{array}\right]$$

ρ^0 is the number density of the electrolyte in units of number of ions per Å^3; σ_α and σ_β are the ionic radii; λ_α and λ_β are their hydrated radii. K_α, K_β, K and κ are constants given by the formulae below and they are all homogenous to the inverse of a length. γ is the Euler-Mascheroni constant; $\gamma = 0.577215665$.

$$\frac{4\pi l_B}{\kappa^2} = \frac{1}{2K^2}\left(\frac{1}{z_\alpha^2}\frac{K_\alpha^2}{\rho_\alpha^0} + \frac{1}{z_\beta^2}\frac{K_\beta^2}{\rho_\beta^0}\right) + \frac{1}{2}\frac{1}{K^2}\left(\frac{1}{z_\alpha} + \frac{1}{z_\beta}\right)\frac{8K_\alpha^2\sigma_\alpha^3/z_\alpha + 8K_\beta^2\sigma_\beta^3/z_\beta}{1 - 8\sigma_\alpha^3\rho_\alpha^0 - 8\sigma_\beta^3\rho_\beta^0}$$

$$+ 2.3w^2 l_B^3 + \frac{w l_B^3}{4}\left[\frac{10.58}{2K^2}(z_\alpha + z_\beta)(z_\alpha K_\alpha^2 + z_\beta K_\beta^2) - 17\right]$$

$$K_\alpha^2 = \cfrac{4\pi l_B z_\alpha^2 \nu_\alpha \rho^0}{1 + \cfrac{8\sigma_\alpha^3 \left(\nu_\alpha + \nu_\beta\right)\rho^0}{1 - 8\left(\nu_\alpha \sigma_\alpha^3 + \nu_\beta \sigma_\beta^3\right)\rho^0} - 2.645 w l_B^3 z_\alpha^3 z_\beta \left(\nu_\alpha + \nu_\beta\right)\rho^0}$$

$$K_\beta^2 = \cfrac{4\pi l_B z_\beta^2 \nu_\beta \rho^0}{1 + \cfrac{8\sigma_\beta^3 \left(\nu_\alpha + \nu_\beta\right)\rho^0}{1 - 8\left(\nu_\alpha \sigma_\alpha^3 + \nu_\beta \sigma_\beta^3\right)\rho^0} - 2.645 w l_B^3 z_\beta^3 z_\alpha \left(\nu_\alpha + \nu_\beta\right)\rho^0}$$

$$K^2 = K_\alpha^2 + K_\beta^2$$

The parameters that are adjusted for each electrolyte are the correlation parameter w and the hydrated radii λ_α and λ_β.

V   OTHER MODELS

A few other semi-empirical extensions of the Debye-Hückel law exist, such as the Guggenheim or Bromley models. But they are not as successful as the Pitzer model and have not been included in the present study [16].

The Chen model mixes a local composition model akin to the non-random two liquids model with a modified version of the Debye-Hückel limiting law, derived by Pitzer. Its formulae are more complicated because they involve both the ionic strength and the molar fractions of the electrolyte [13,16]. However it is not significantly better than the Meissner or the Pitzer models and has not been included.

VI   ILLUSTRATION OF THE RESPECTIVE ACCURACIES

The figures always show the experimental data of a binary electrolyte and the curves corresponding to the Debye-Hückel limiting law, the Meissner model, the Pitzer model and one of the fits of the correlated hard spheres model. The experimental data is from [19,20]. The parameters for the Meissner and Pitzer models are from [16] and given in Appendix D.

VI.1   Chlorides
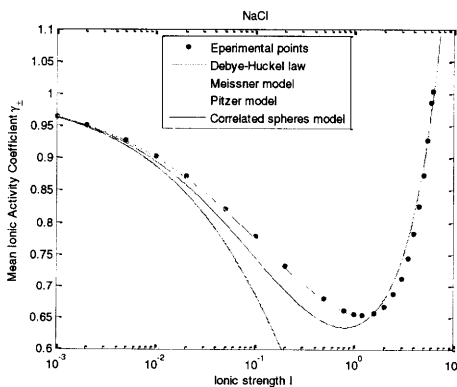
Figure 180: General fit of sodium chloride
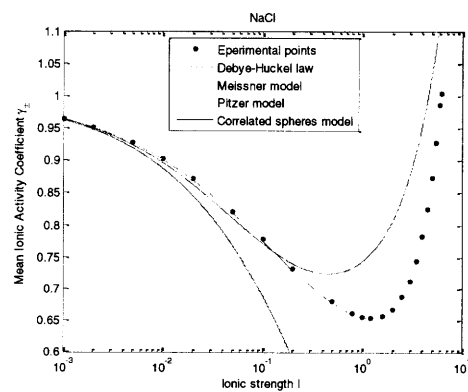
Figure 181: Dilute fit of sodium chloride

120
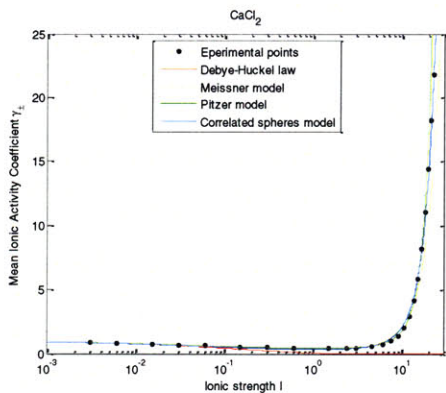
Figure 182: General fit of calcium chloride
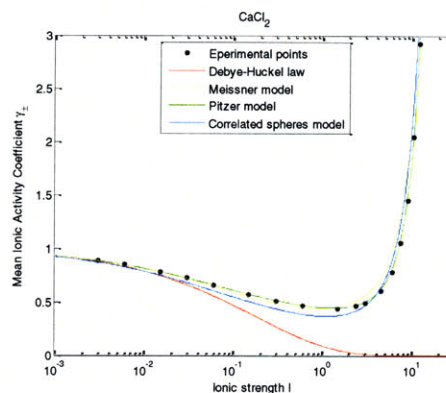
Figure 183: General fit of calcium chloride – partial view
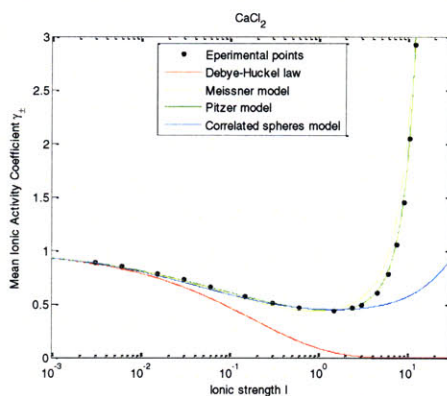
Figure 184: Dilute fit of calcium chloride
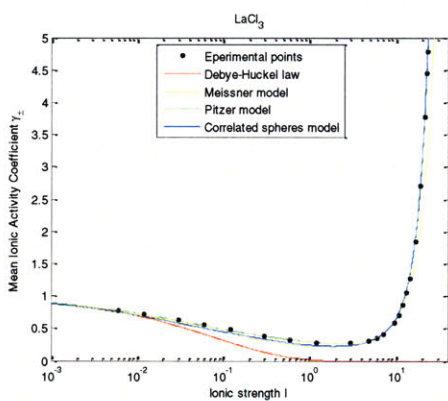
Figure 185: General fit of lanthanum chloride
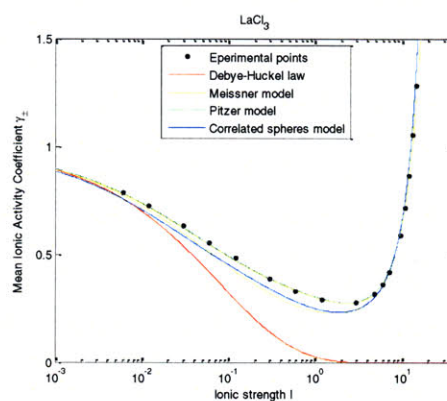
Figure 186: General fit of lanthanum chloride – partial view

121
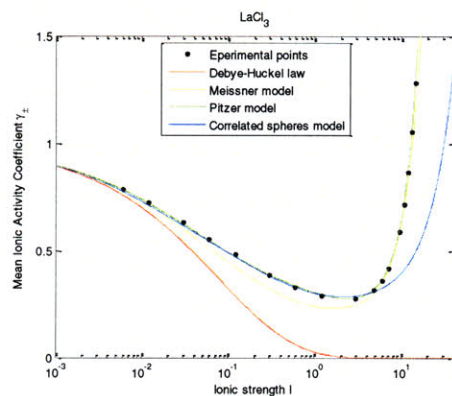
Figure 187: Dilute fit of lanthanum chloride

VI.2 Bromides
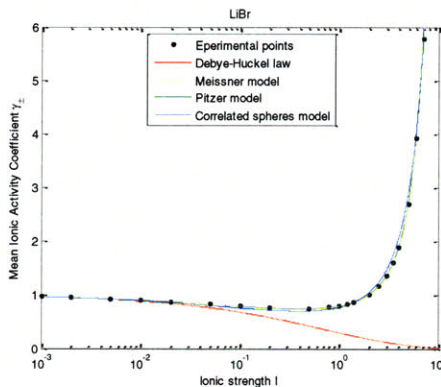
Figure 188: General fit of lithium bromide
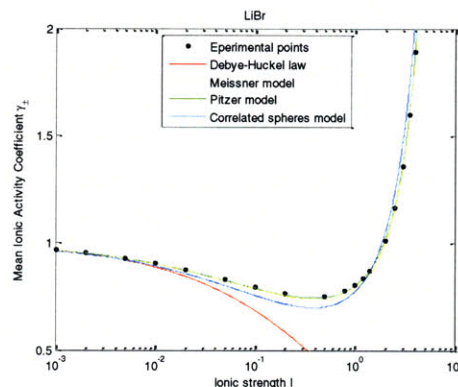
Figure 189: General fit of lithium bromide – partial view
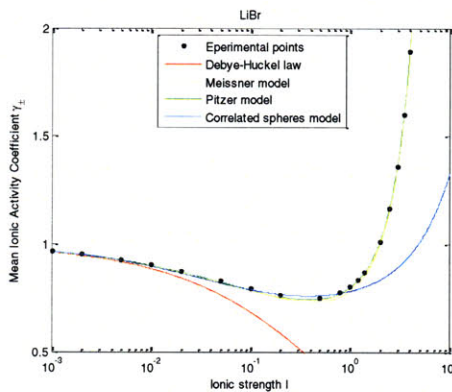
Figure 190: Dilute fit of lithium bromide
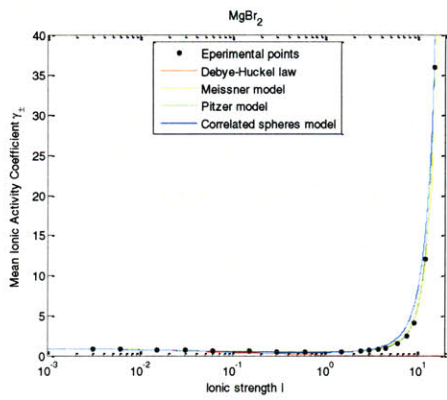
Figure 191: General fit of magnesium bromide
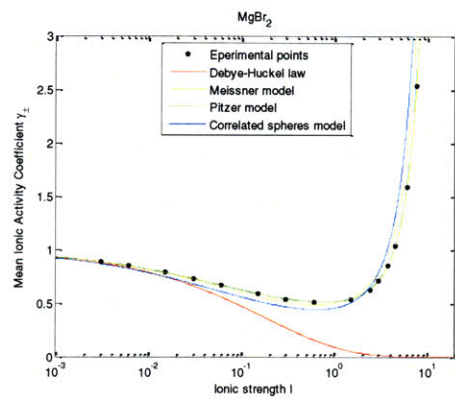
Figure 192: General fit of magnesium bromide – partial view
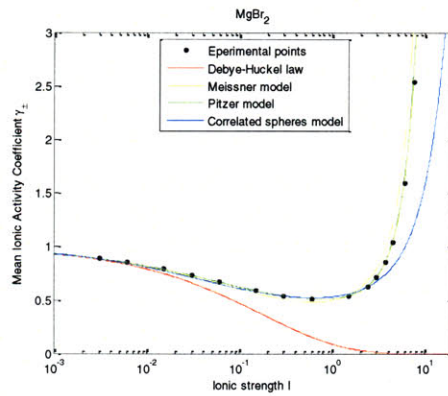
Figure 193: Dilute fit of magnesium bromide

VI.3 Other univalent electrolytes
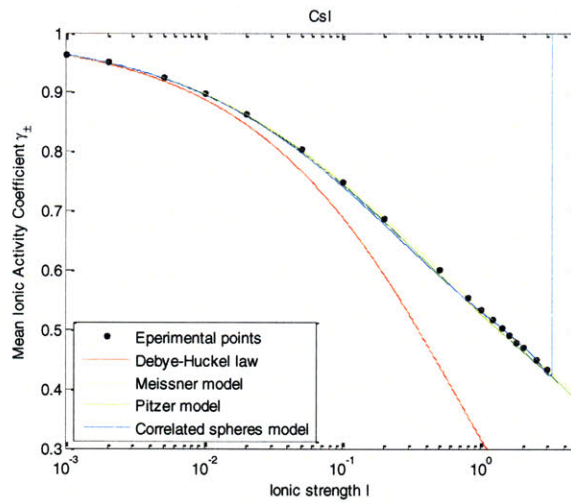
Figure 194: General fit of cesium iodide
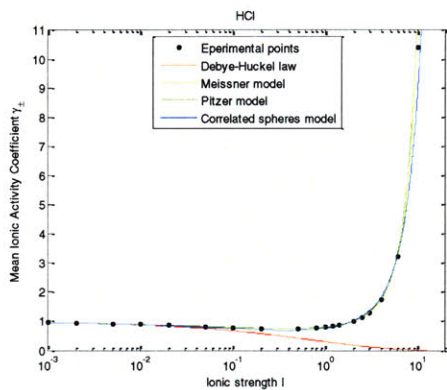
Figure 195: General fit of hydrochloric acid
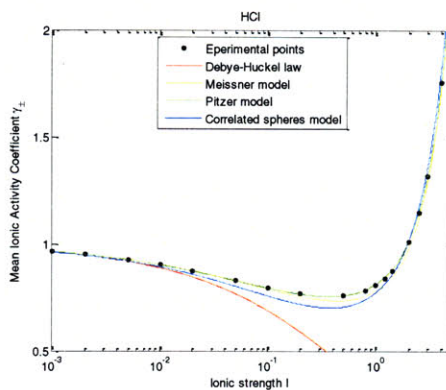
Figure 196: General fit of hydrochloric acid – partial view
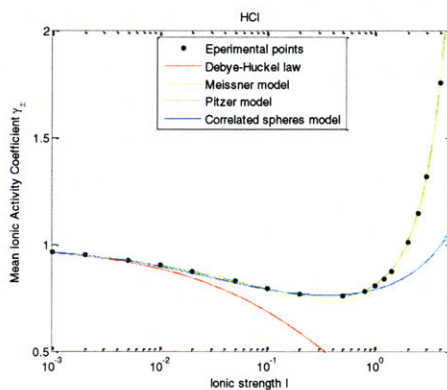
Figure 197: Dilute fit of hydrochloric acid
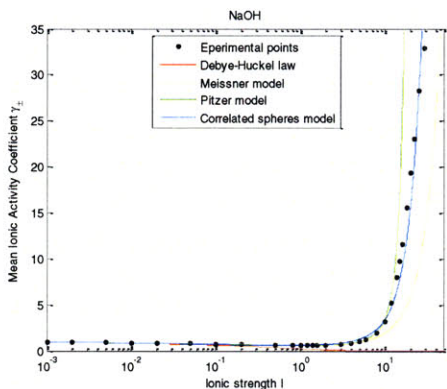
Figure 198: General fit of sodium hydroxide
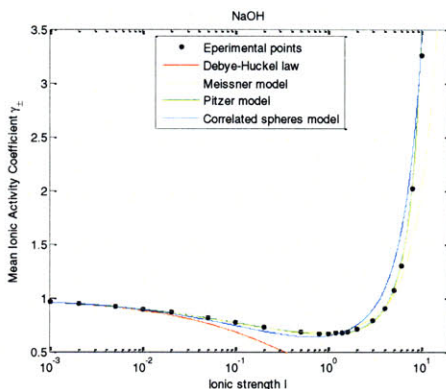
Figure 199: General fit of sodium hydroxide – partial view

124
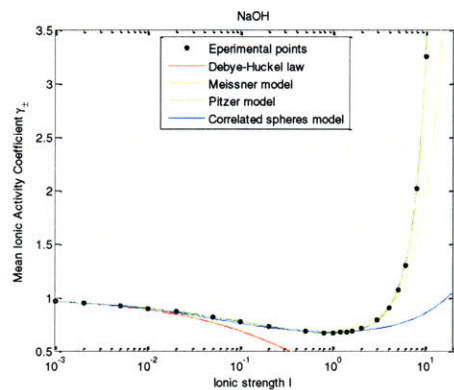
Figure 200: Dilute fit of sodium hydroxide

VI.4 Nitrates
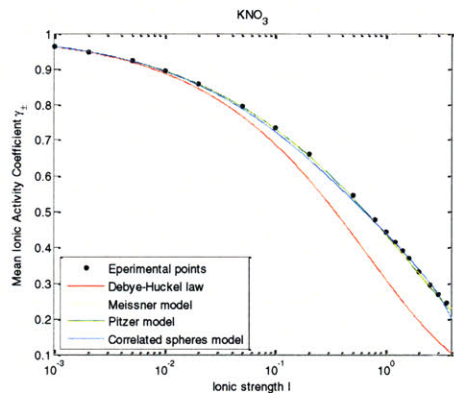
Figure 201: General fit potassium nitrate
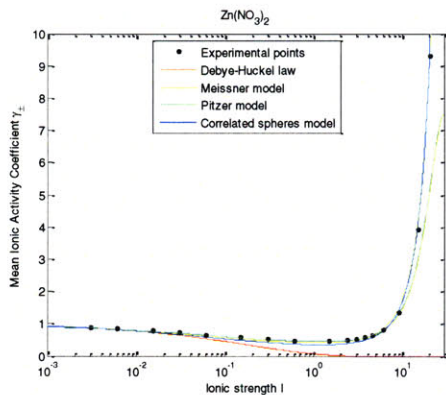
Figure 202: General fit of zinc nitrate
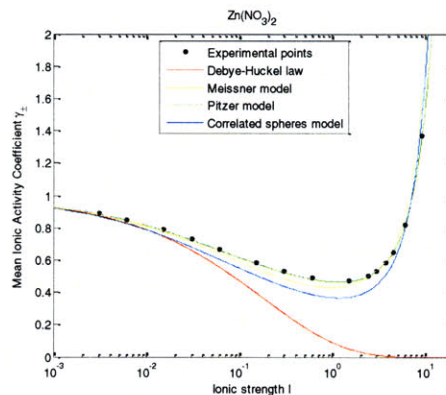
Figure 203: General fit of zinc nitrate – partial view

125
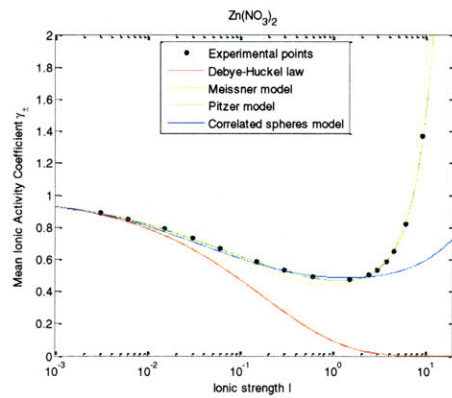
Figure 204: Dilute fit of zinc nitrate

VI.5 Sulfates
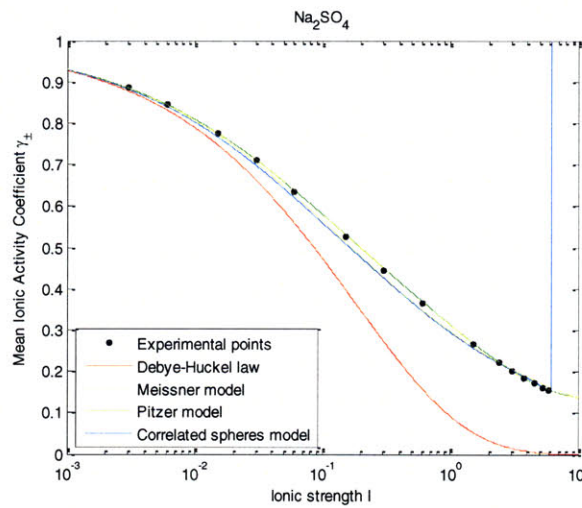
Figure 205: General fit of sodium sulfate
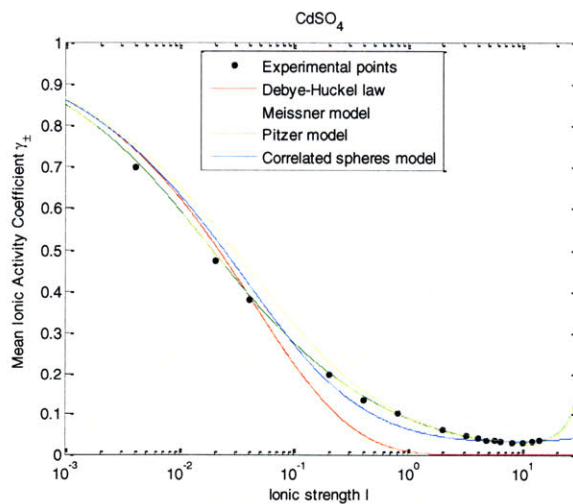
Figure 206: General fit of cadmium sulfate

VII   COMPARISON INCLUDING EXPERIMENTAL ERRORS

The experimental data was compiled by several authors from a multitude of papers reporting experiments over five decades [19]. However experimental uncertainty and possible errors are never mentioned. For some common electrolytes like sodium chloride or hydrochloric acid, so many experiments were made that experimental errors have effectively been eliminated. For less common electrolytes like cadmium sulfate or cesium iodide the reported data implicitly contains some experimental uncertainty. In order to ascertain the effect of experimental errors on the relevance of the various models, several plots were made for a few electrolytes: cadmium sulfate, cesium iodide, sodium hydroxide, magnesium bromide and lanthanum chloride. The errors are taken to be the greater of 5 % or 10 % of the value of the mean ionic activity coefficient γ and 0.01; indeed for the lower values of γ the relative error becomes too small therefore a lower bound at 0.01 is imposed.
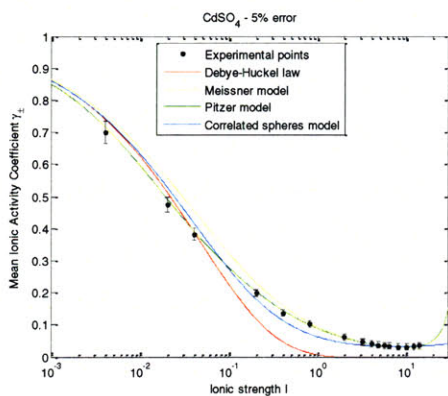
Figure 207: General fit of cadmium sulfate with 5 % relative error
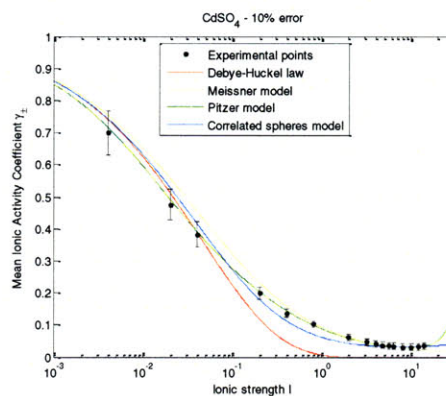
Figure 208: Gen. fit of cadmium sulfate with 10 % relative error
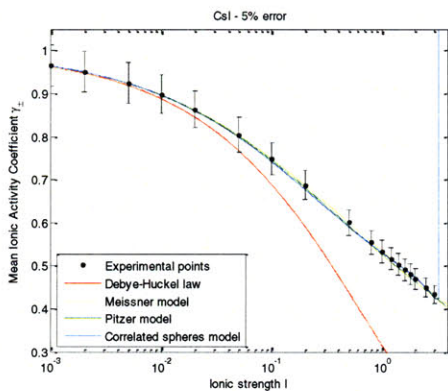
Figure 209: General fit of cesium chloride with 5 % relative error
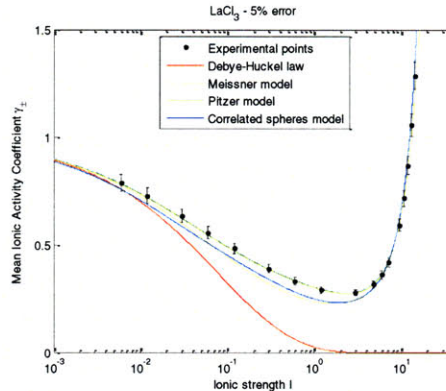
Figure 210: Gen. fit of lanthanum chloride with 5 % relative error
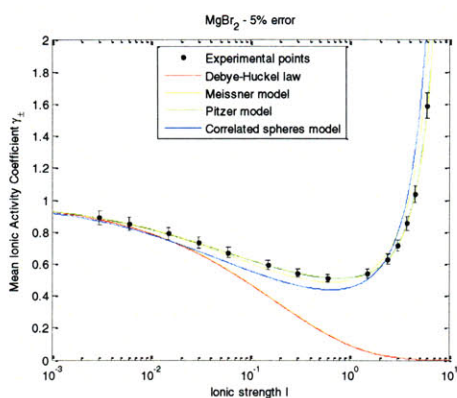
Figure 211: Gen. fit of magnesium bromide with 5 % rel. error
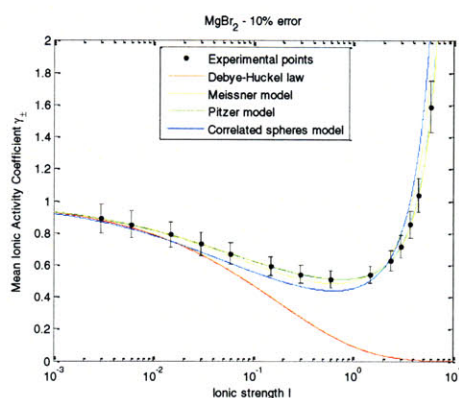
Figure 212: Gen. fit of magnesium bromide with 10 % rel. error
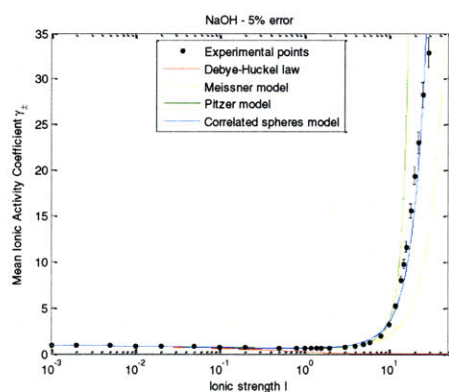
Figure 213: Gen. fit of sodium hydroxide with 5 % relative error
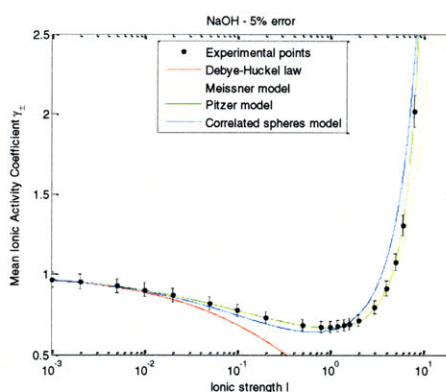
Figure 214: Gen. fit of sodium hyd. with 5 % rel. error – part. view

VIII   CONCLUSION

The Debye-Hückel law is valid in the limit of infinite dilution and all models converge to it. The Pitzer model is by far the best: in the dilute and semi-dilute regions experimental data is reproduced with very high accuracy; for the vast majority of electrolytes, the Pitzer model is equally accurate in the concentrated region too. On the plots displaying error bars, the Pitzer model is always well within the margins and extremely close to the experimental points.

The Meissner model is the second best because it is usually quite accurate in the dilute and semi-dilute regions albeit not as accurate as the Pitzer model; for most electrolytes the Meissner model is still acceptable in the concentrated region but it strays noticeably from experimental data. On the plots displaying error bars it is usually within the error margin in the dilute and semi-dilute regions and slips out only in the concentrated region when it strays from the experimental points. The performance of the Meissner model is remarkable since it has only one parameter.

The correlated hard spheres model with the general fit is approximately as good as the Meissner model but it has three parameters instead of one. In the concentrated region it is usually more accurate than the Meissner model and sometimes even the Pitzer model. It markedly underestimates the mean ionic activity coefficient in the semi-dilute and dilute regions; the graphs displaying error bars confirm that the difference between the calculated curve and experimental points is large and cannot be reduced to experimental uncertainty. For three of the

electrolytes shown above, the three models perform equally well over the whole range of concentration and are effectively undistinguishable.

The dilute fit of the correlated hard spheres model is usually as good as the Meissner model and very close to the Pitzer model in the dilute region but completely strays from the experimental points and other models in the semi-dilute region.

The correlated hard spheres model is fairly accurate but fails to surpass the two most common models: the Meissner model with only one parameter and the Pitzer model with 3 or 4 parameters. The main reason for this shortcoming is the fact that it is based on three parameters, the correlation length and the hydrated radii of the ions, the values of which are not independent of concentration.

Chapter 8 Equilibrium of a solution containing three or more ionic species

I GENERAL SOLUTION

I.1 System of differential equations and potential

The solution contains n species of small ions fully dissolved in water. The bulk concentrations are denoted ρ_α^0, the charges z_α, the ionic radii σ_α, $\alpha \in [\![1,n]\!]$. The solution is electroneutral overall:

$$\sum_{\alpha=1}^{n} z_\alpha \rho_\alpha = 0$$

The set of general equations governing equilibrium is: for each $\alpha \in [\![1,n]\!]$

$$J_\alpha = 0$$

$$\frac{z_\alpha e}{k_B T} \nabla V + \frac{\nabla \rho_\alpha}{\rho_\alpha} + \frac{\sum_{\beta=1}^{n} 8\sigma_\beta^3 \nabla \rho_\beta}{1 - \sum_{\beta=1}^{n} 8\sigma_\beta^3 \rho_\beta} + 2.3 w^2 l_B^3 z_\alpha \sum_{\beta=1}^{n} z_\beta \nabla \rho_\beta - \frac{w l_B^3}{4} \left[\begin{array}{c} -10.58 z_\alpha^2 \sum_{\beta=1}^{n} z_\beta^2 \nabla \rho_\beta \\ +17 z_\alpha \sum_{\beta=1}^{n} z_\beta \nabla \rho_\beta \end{array} \right] = 0$$

The electrical field is determined from the relation

$$\nabla \cdot E = \frac{e}{\varepsilon_0 \varepsilon_r} \sum_{\beta=1}^{n} z_\beta \rho_\beta$$

We examine a hard sphere of radius R and charge Z. In the vicinity of the sphere the charge distribution has on average spherical symmetry and depends only on the radial coordinate r. We use the theorem of Gauss to calculate the electrical field:

$$\nabla \cdot E = \frac{e}{\varepsilon_0 \varepsilon_r} \sum_{\beta=1}^{n} z_\beta \rho_\beta$$

$$4\pi r^2 E(r) = \frac{e}{\varepsilon_0 \varepsilon_r} \left(Z + \int_R^r 4\pi r'^2 \sum_{\beta=1}^{n} z_\beta \rho_\beta(r') dr' \right)$$

$$E(r) = \frac{e}{4\pi \varepsilon_0 \varepsilon_r r^2} \left(Z + \int_R^r 4\pi r'^2 \sum_{\beta=1}^{n} z_\beta \rho_\beta(r') dr' \right)$$

$$\frac{eE(r)}{k_B T} = \frac{e^2}{4\pi \varepsilon_0 \varepsilon_r k_B T r^2} \left(Z + \int_R^r 4\pi r'^2 \sum_{\beta=1}^{n} z_\beta \rho_\beta(r') dr' \right)$$

$$\frac{eE\left(r\right)}{k_BT} = \frac{Zl_B}{r^2} + \frac{4\pi l_B}{r^2}\int\limits_R^r r'^2\sum_{\beta=1}^n z_\beta\rho_\beta\left(r'\right)dr'$$

We introduce the Bjerrum length $l_B = \dfrac{e^2}{4\pi\varepsilon_0\varepsilon_r k_BT}$. We substitute the expression of the electrical field in the equation $J_\alpha = 0$ and write gradients as derivatives with respect to r.

$$-\frac{z_\alpha Zl_B}{r^2} + \frac{\rho'_\alpha}{\rho_\alpha} + \frac{\sum\limits_{\beta=1}^n 8\sigma_\beta^3\rho'_\beta}{1 - \sum\limits_{\beta=1}^n 8\sigma_\beta^3\rho_\beta} - \frac{4\pi z_\alpha l_B}{r^2}\int\limits_R^r r'^2\sum_{\beta=1}^n z_\beta\rho_\beta\left(r'\right)dr'$$
$$+2.3w^2l_B^3 z_\alpha\sum_{\beta=1}^n z_\beta\rho'_\beta - \frac{wl_B^3}{4}\left[-10.58z_\alpha^2\sum_{\beta=1}^n z_\beta^2\rho'_\beta + 17z_\alpha\sum_{\beta=1}^n z_\beta\rho'_\beta\right] = 0$$

We divide by z_α and separate terms containing z_α from the others.

$$-\frac{Zl_B}{r^2} + \frac{1}{z_\alpha}\left[\frac{\rho'_\alpha}{\rho_\alpha} + \frac{\sum\limits_{\beta=1}^n 8\sigma_\beta^3\rho'_\beta}{1 - \sum\limits_{\beta=1}^n 8\sigma_\beta^3\rho_\beta}\right] - \frac{4\pi l_B}{r^2}\int\limits_R^r r'^2\sum_{\beta=1}^n z_\beta\rho_\beta\left(r'\right)dr'$$
$$+2.3w^2l_B^3\sum_{\beta=1}^n z_\beta\rho'_\beta - \frac{wl_B^3}{4}\left[-10.58z_\alpha\sum_{\beta=1}^n z_\beta^2\rho'_\beta + 17\sum_{\beta=1}^n z_\beta\rho'_\beta\right] = 0$$

$$\frac{1}{z_\alpha}\left[\frac{\rho'_\alpha}{\rho_\alpha} + \frac{\sum\limits_{\beta=1}^n 8\sigma_\beta^3\rho'_\beta}{1 - \sum\limits_{\beta=1}^n 8\sigma_\beta^3\rho_\beta}\right] + \frac{10.58}{4}z_\alpha wl_B^3\sum_{\beta=1}^n z_\beta^2\rho'_\beta = \begin{array}{l}\dfrac{Zl_B}{r^2} + \dfrac{4\pi l_B}{r^2}\int\limits_R^r r'^2\sum\limits_{\beta=1}^n z_\beta\rho_\beta\left(r'\right)dr' \\[2mm] -2.3w^2l_B^3\sum\limits_{\beta=1}^n z_\beta\rho'_\beta + \dfrac{17}{4}wl_B^3\sum\limits_{\beta=1}^n z_\beta\rho'_\beta\end{array}$$

The term on the right hand of the equation does not depend on the ionic species. It is an invariant of the system of equations and plays the role of a potential. To pursue calculations we assume that either the charge Z is small or that the radius of the sphere is small so the electrical fields are small so the local variations from the bulk concentrations are small. We write for each ionic species in solution

$$\rho_\alpha = \rho_\alpha^0 + \rho_\alpha^\varepsilon \text{ with } \left|\frac{\rho_\alpha^\varepsilon}{\rho_\alpha^0}\right| \ll 1$$

We have $\rho'_\alpha = \rho_\alpha'^\varepsilon$ and $\displaystyle\sum_{\beta=1}^n z_\beta\rho_\beta = \underbrace{\sum_{\beta=1}^n z_\beta\rho_\beta^0}_{\substack{=0 \\ \text{electroneutrality}}} + \sum_{\beta=1}^n z_\beta\rho_\beta^\varepsilon = \sum_{\beta=1}^n z_\beta\rho_\beta^\varepsilon$. Thus we get the equality

131

$$\frac{1}{z_\alpha}\left[\rho_\alpha'^\varepsilon + \frac{\sum\limits_{\beta=1}^{n}8\sigma_\beta^3\rho_\beta'^\varepsilon}{\rho_\alpha^0 \ \ 1-\sum\limits_{\beta=1}^{n}8\sigma_\beta^3\rho_\beta^0}\right] + \frac{10.58}{4}z_\alpha w l_B^3\sum\limits_{\beta=1}^{n}z_\beta^2\rho_\beta'^\varepsilon = \begin{array}{l}\dfrac{Zl_B}{r^2}+\dfrac{4\pi l_B}{r^2}\int\limits_{R}^{r}r'^2\sum\limits_{\beta=1}^{n}z_\beta\rho_\beta^\varepsilon\left(r'\right)dr' \\[2em] -2.3w^2l_B^3\sum\limits_{\beta=1}^{n}z_\beta\rho_\beta'^\varepsilon + \dfrac{17}{4}wl_B^3\sum\limits_{\beta=1}^{n}z_\beta\rho_\beta'^\varepsilon\end{array}$$

Then for any two species of ions, α and β, we can write

$$\frac{1}{z_\alpha}\left[\frac{\rho_\alpha'^\varepsilon}{\rho_\alpha^0}+\frac{\sum\limits_{s=1}^{n}8\sigma_s^3\rho_s'^\varepsilon}{1-\sum\limits_{s=1}^{n}8\sigma_s^3\rho_s^0}\right] = \frac{1}{z_\beta}\left[\frac{\rho_\beta'^\varepsilon}{\rho_\beta^0}+\frac{\sum\limits_{s=1}^{n}8\sigma_s^3\rho_s'^\varepsilon}{1-\sum\limits_{s=1}^{n}8\sigma_s^3\rho_s^0}\right]$$
$$+\frac{10.58}{4}z_\alpha w l_B^3\sum\limits_{s=1}^{n}z_s^2\rho_s'^\varepsilon \qquad\qquad +\frac{10.58}{4}z_\beta w l_B^3\sum\limits_{s=1}^{n}z_s^2\rho_s'^\varepsilon$$

This is a simple linear equality. We integrate it and obtain

$$\frac{1}{z_\alpha}\left[\frac{\rho_\alpha^\varepsilon}{\rho_\alpha^0}+\frac{\sum\limits_{s=1}^{n}8\sigma_s^3\rho_s^\varepsilon}{1-\sum\limits_{s=1}^{n}8\sigma_s^3\rho_s^0}\right] = \frac{1}{z_\beta}\left[\frac{\rho_\beta^\varepsilon}{\rho_\beta^0}+\frac{\sum\limits_{s=1}^{n}8\sigma_s^3\rho_s^\varepsilon}{1-\sum\limits_{s=1}^{n}8\sigma_s^3\rho_s^0}\right]$$
$$+\frac{10.58}{4}z_\alpha w l_B^3\sum\limits_{s=1}^{n}z_s^2\rho_s^\varepsilon \qquad\qquad +\frac{10.58}{4}z_\beta w l_B^3\sum\limits_{s=1}^{n}z_s^2\rho_s^\varepsilon$$

This is a linear system of n − 1 equations with n unknowns, ρ_1^ε ... ρ_n^ε. We want to express all of them with respect to a single function, the potential Ω.

$$\Omega = \frac{1}{z_\alpha}\left[\frac{\rho_\alpha^\varepsilon}{\rho_\alpha^0}+\frac{\sum\limits_{s=1}^{n}8\sigma_s^3\rho_s^\varepsilon}{1-\sum\limits_{s=1}^{n}8\sigma_s^3\rho_s^0}\right] + \frac{10.58}{4}z_\alpha w l_B^3\sum\limits_{s=1}^{n}z_s^2\rho_s^\varepsilon$$

While in principle it is possible to explicitly write the relation between any ρ_i^ε and Ω, the expressions are extremely heavy. The most meaningful way to approach the problem is first to reduce the number of variables, second to solve the system by introducing two auxiliary functions.

I.2   Reduction in the number of variables

Let us denote the number of different charges in solution by c and order the species so as to group the ones with similar charge:

$$\underbrace{\rho_1,\ldots,\rho_{n_1}}_{\text{charge } z_1},\underbrace{\rho_{n_1+1},\ldots,\rho_{n_1+n_2}}_{\text{charge } z_2},\ldots,\underbrace{\rho_{n_1+\ldots+n_{c-1}+1},\ldots,\rho_{n_1+\ldots+n_{c-1}+n_c}}_{\text{charge } z_c}$$

Note that if $z_\alpha = z_\beta$, the relationship between α and β is very simple

$$\frac{\rho_\alpha^\varepsilon}{\rho_\alpha^0} = \frac{\rho_\beta^\varepsilon}{\rho_\beta^0}$$

The reduction consists of replacing all the species that have the same charge by a non-dimensional number charge density:

$$\tilde{\rho}_i = \frac{\rho_{n_0+\cdots+n_{i-1}+1}^\varepsilon}{\rho_{n_0+\cdots+n_{i-1}+1}^0} = \cdots = \frac{\rho_{n_0+\cdots+n_{i-1}+n_i}^\varepsilon}{\rho_{n_0+\cdots+n_{i-1}+n_i}^0} \quad \text{corresponding to charge } z_i, \ i \in [\![1,c]\!]$$

The system of $n - 1$ equations becomes a system of $c - 1$ equations with c unknowns.

$$\frac{1}{z_\alpha}\left[\tilde{\rho}_\alpha + \sum_{s=1}^c u_s \tilde{\rho}_s\right] + z_\alpha \sum_{s=1}^c v_s \tilde{\rho}_s = \frac{1}{z_\beta}\left[\tilde{\rho}_\beta + \sum_{s=1}^c u_s \tilde{\rho}_s\right] + z_\beta \sum_{s=1}^c v_s \tilde{\rho}_s$$

The constants u_i and v_i are defined as follows:

$$u_i = \frac{\displaystyle\sum_{s=n_0+\cdots+n_{i-1}+1}^{n_0+\cdots+n_{i-1}+n_i} 8\sigma_s^3 \rho_s^0}{1 - \displaystyle\sum_{s=1}^n 8\sigma_s^3 \rho_s^0} \qquad\qquad v_i = \frac{10.58}{4} w l_B^3 \sum_{s=n_0+\cdots+n_{i-1}+1}^{n_0+\cdots+n_{i-1}+n_i} z_s^2 \rho_s^0$$

I.3   Potential and reduced variables

The system is made of a set of equations of the form

$$\Omega = \frac{1}{z_i}\left[\tilde{\rho}_i + \sum_{s=1}^c u_s \tilde{\rho}_s\right] + z_i \sum_{s=1}^c v_s \tilde{\rho}_s \qquad \text{where } i = 1 \ldots c$$

We introduce two additional functions of the non-dimensional number densities.

$$u = \sum_{s=1}^c u_s \tilde{\rho}_s \qquad v = \sum_{s=1}^c v_s \tilde{\rho}_s$$

Thus the set of equations can be written in a very simple form.

$$\Omega = \frac{1}{z_i}\left[\tilde{\rho}_i + u\right] + z_i v \qquad \text{where } i = 1 \ldots c$$

We want to express u, v and Ω as functions of the non-dimensional number densities and charges. We begin by eliminating u and v in order to determine an expression for Ω. We take any three distinct charges and denote them α, β, γ.

$$\begin{cases} \Omega = \dfrac{1}{z_\alpha}\left[\tilde{\rho}_\alpha + u\right] + z_\alpha v \\[2mm] \Omega = \dfrac{1}{z_\beta}\left[\tilde{\rho}_\beta + u\right] + z_\beta v \\[2mm] \Omega = \dfrac{1}{z_\gamma}\left[\tilde{\rho}_\gamma + u\right] + z_\gamma v \end{cases}$$

$$\begin{cases} \dfrac{\Omega}{z_\alpha} = \dfrac{1}{z_\alpha^2}\big[\tilde{\rho}_\alpha + u\big] + v \\[2mm] \dfrac{\Omega}{z_\beta} = \dfrac{1}{z_\beta^2}\big[\tilde{\rho}_\beta + u\big] + v \quad \text{then} \\[2mm] \dfrac{\Omega}{z_\gamma} = \dfrac{1}{z_\gamma^2}\big[\tilde{\rho}_\gamma + u\big] + v \end{cases} \qquad \begin{cases} \dfrac{\Omega}{z_\alpha} - \dfrac{\Omega}{z_\beta} = \dfrac{1}{z_\alpha^2}\tilde{\rho}_\alpha - \dfrac{1}{z_\beta^2}\tilde{\rho}_\beta + \left(\dfrac{1}{z_\alpha^2} - \dfrac{1}{z_\beta^2}\right)u \\[2mm] \dfrac{\Omega}{z_\alpha} - \dfrac{\Omega}{z_\gamma} = \dfrac{1}{z_\alpha^2}\tilde{\rho}_\alpha - \dfrac{1}{z_\gamma^2}\tilde{\rho}_\gamma + \left(\dfrac{1}{z_\alpha^2} - \dfrac{1}{z_\gamma^2}\right)u \\[2mm] \dfrac{\Omega}{z_\beta} - \dfrac{\Omega}{z_\gamma} = \dfrac{1}{z_\beta^2}\tilde{\rho}_\beta - \dfrac{1}{z_\gamma^2}\tilde{\rho}_\gamma + \left(\dfrac{1}{z_\beta^2} - \dfrac{1}{z_\gamma^2}\right)u \end{cases}$$

$$\begin{cases} \dfrac{z_\beta - z_\alpha}{z_\alpha z_\beta}\Omega = \dfrac{1}{z_\alpha^2}\tilde{\rho}_\alpha - \dfrac{1}{z_\beta^2}\tilde{\rho}_\beta + \dfrac{z_\beta^2 - z_\alpha^2}{z_\alpha^2 z_\beta^2}u \\[3mm] \dfrac{z_\gamma - z_\alpha}{z_\alpha z_\gamma}\Omega = \dfrac{1}{z_\alpha^2}\tilde{\rho}_\alpha - \dfrac{1}{z_\gamma^2}\tilde{\rho}_\gamma + \dfrac{z_\gamma^2 - z_\alpha^2}{z_\alpha^2 z_\gamma^2}u \\[3mm] \dfrac{z_\gamma - z_\beta}{z_\beta z_\gamma}\Omega = \dfrac{1}{z_\beta^2}\tilde{\rho}_\beta - \dfrac{1}{z_\gamma^2}\tilde{\rho}_\gamma + \dfrac{z_\gamma^2 - z_\beta^2}{z_\beta^2 z_\gamma^2}u \end{cases}$$

$$\begin{cases} \dfrac{z_\alpha z_\beta}{z_\beta + z_\alpha}\Omega = \dfrac{z_\alpha^2 z_\beta^2}{z_\beta^2 - z_\alpha^2}\left(\dfrac{1}{z_\alpha^2}\tilde{\rho}_\alpha - \dfrac{1}{z_\beta^2}\tilde{\rho}_\beta\right) + u \\[3mm] \dfrac{z_\alpha z_\gamma}{z_\gamma + z_\alpha}\Omega = \dfrac{z_\alpha^2 z_\gamma^2}{z_\gamma^2 - z_\alpha^2}\left(\dfrac{1}{z_\alpha^2}\tilde{\rho}_\alpha - \dfrac{1}{z_\gamma^2}\tilde{\rho}_\gamma\right) + u \\[3mm] \dfrac{z_\beta z_\gamma}{z_\gamma - z_\beta}\Omega = \dfrac{z_\beta^2 z_\gamma^2}{z_\gamma^2 - z_\beta^2}\left(\dfrac{1}{z_\beta^2}\tilde{\rho}_\beta - \dfrac{1}{z_\gamma^2}\tilde{\rho}_\gamma\right) + u \end{cases}$$

$$\begin{cases} \left(\dfrac{z_\alpha z_\beta}{z_\beta + z_\alpha} - \dfrac{z_\alpha z_\gamma}{z_\gamma + z_\alpha}\right)\Omega = \dfrac{z_\alpha^2 z_\beta^2}{z_\beta^2 - z_\alpha^2}\left(\dfrac{1}{z_\alpha^2}\tilde{\rho}_\alpha - \dfrac{1}{z_\beta^2}\tilde{\rho}_\beta\right) - \dfrac{z_\alpha^2 z_\gamma^2}{z_\gamma^2 - z_\alpha^2}\left(\dfrac{1}{z_\alpha^2}\tilde{\rho}_\alpha - \dfrac{1}{z_\gamma^2}\tilde{\rho}_\gamma\right) \\[3mm] \left(\dfrac{z_\alpha z_\beta}{z_\beta + z_\alpha} - \dfrac{z_\beta z_\gamma}{z_\gamma - z_\beta}\right)\Omega = \dfrac{z_\alpha^2 z_\beta^2}{z_\beta^2 - z_\alpha^2}\left(\dfrac{1}{z_\alpha^2}\tilde{\rho}_\alpha - \dfrac{1}{z_\beta^2}\tilde{\rho}_\beta\right) - \dfrac{z_\beta^2 z_\gamma^2}{z_\gamma^2 - z_\beta^2}\left(\dfrac{1}{z_\beta^2}\tilde{\rho}_\beta - \dfrac{1}{z_\gamma^2}\tilde{\rho}_\gamma\right) \\[3mm] \left(\dfrac{z_\alpha z_\gamma}{z_\gamma + z_\alpha} - \dfrac{z_\beta z_\gamma}{z_\gamma - z_\beta}\right)\Omega = \dfrac{z_\alpha^2 z_\gamma^2}{z_\gamma^2 - z_\alpha^2}\left(\dfrac{1}{z_\alpha^2}\tilde{\rho}_\alpha - \dfrac{1}{z_\gamma^2}\tilde{\rho}_\gamma\right) - \dfrac{z_\beta^2 z_\gamma^2}{z_\gamma^2 - z_\beta^2}\left(\dfrac{1}{z_\beta^2}\tilde{\rho}_\beta - \dfrac{1}{z_\gamma^2}\tilde{\rho}_\gamma\right) \end{cases}$$

The three equations turn out to be identical. Solving for Ω we obtain an expression symmetrical in α, β, γ.

$$\Omega = -\dfrac{z_\beta + z_\gamma}{\left(z_\alpha - z_\beta\right)\left(z_\alpha - z_\gamma\right)}\tilde{\rho}_\alpha - \dfrac{z_\alpha + z_\gamma}{\left(z_\beta - z_\alpha\right)\left(z_\beta - z_\gamma\right)}\tilde{\rho}_\beta - \dfrac{z_\alpha + z_\beta}{\left(z_\gamma - z_\alpha\right)\left(z_\gamma - z_\beta\right)}\tilde{\rho}_\gamma$$

In order to find corresponding expression for u we merely take the first equation in the system of equations involving u and Ω and substitute the expression of Ω.

$$\dfrac{\Omega}{z_\alpha} - \dfrac{\Omega}{z_\beta} = \dfrac{1}{z_\alpha^2}\tilde{\rho}_\alpha - \dfrac{1}{z_\beta^2}\tilde{\rho}_\beta + \left(\dfrac{1}{z_\alpha^2} - \dfrac{1}{z_\beta^2}\right)u$$

134

$$u = \frac{z_\alpha z_\beta}{z_\beta + z_\alpha}\Omega + \frac{z_\alpha^2 z_\beta^2}{z_\alpha^2 - z_\beta^2}\left(\frac{1}{z_\alpha^2}\tilde{\rho}_\alpha - \frac{1}{z_\beta^2}\tilde{\rho}_\beta\right)$$

$$\boxed{u = -\frac{z_\beta z_\gamma \tilde{\rho}_\alpha}{\left(z_\alpha - z_\beta\right)\left(z_\alpha - z_\gamma\right)} - \frac{z_\alpha z_\gamma \tilde{\rho}_\beta}{\left(z_\beta - z_\alpha\right)\left(z_\beta - z_\gamma\right)} - \frac{z_\alpha z_\beta \tilde{\rho}_\gamma}{\left(z_\gamma - z_\alpha\right)\left(z_\gamma - z_\beta\right)}}$$

The expression of u is symmetrical in α, β, γ. Using the other equations in the system would yield and identical formula. Next in order to find v we use the first equation in the system containing v and substitute the expressions of Ω and u.

$$\frac{\Omega}{z_\alpha} = \frac{1}{z_\alpha^2}\tilde{\rho}_\alpha + \frac{1}{z_\alpha^2}u + v$$

$$v = \frac{\Omega}{z_\alpha} - \frac{1}{z_\alpha^2}\tilde{\rho}_\alpha - \frac{1}{z_\alpha^2}u$$

$$\boxed{v = -\frac{\tilde{\rho}_\alpha}{\left(z_\alpha - z_\beta\right)\left(z_\alpha - z_\gamma\right)} - \frac{\tilde{\rho}_\beta}{\left(z_\beta - z_\alpha\right)\left(z_\beta - z_\gamma\right)} - \frac{\tilde{\rho}_\gamma}{\left(z_\gamma - z_\alpha\right)\left(z_\gamma - z_\beta\right)}}$$

The expression of v is again symmetrical in α, β, γ.

The main conclusion from these calculations is that the potential Ω and the two auxiliary functions u and v can be expressed using any three non-dimensional number densities corresponding to distinct charges. Reciprocally we want to express each non-dimensional number density as a function of u, v and Ω only. We take the three expressions determined in the previous pages and write them as a system of equations.

$$\begin{cases} -\dfrac{1}{\left(z_\alpha - z_\beta\right)\left(z_\alpha - z_\gamma\right)}\tilde{\rho}_\alpha - \dfrac{1}{\left(z_\beta - z_\alpha\right)\left(z_\beta - z_\gamma\right)}\tilde{\rho}_\beta - \dfrac{1}{\left(z_\gamma - z_\alpha\right)\left(z_\gamma - z_\beta\right)}\tilde{\rho}_\gamma = v \\[3mm] -\dfrac{z_\beta + z_\gamma}{\left(z_\alpha - z_\beta\right)\left(z_\alpha - z_\gamma\right)}\tilde{\rho}_\alpha - \dfrac{z_\alpha + z_\gamma}{\left(z_\beta - z_\alpha\right)\left(z_\beta - z_\gamma\right)}\tilde{\rho}_\beta - \dfrac{z_\alpha + z_\beta}{\left(z_\gamma - z_\alpha\right)\left(z_\gamma - z_\beta\right)}\tilde{\rho}_\gamma = \Omega \\[3mm] -\dfrac{z_\beta z_\gamma}{\left(z_\alpha - z_\beta\right)\left(z_\alpha - z_\gamma\right)}\tilde{\rho}_\alpha - \dfrac{z_\alpha z_\gamma}{\left(z_\beta - z_\alpha\right)\left(z_\beta - z_\gamma\right)}\tilde{\rho}_\beta - \dfrac{z_\alpha z_\beta}{\left(z_\gamma - z_\alpha\right)\left(z_\gamma - z_\beta\right)}\tilde{\rho}_\gamma = u \end{cases}$$

We seek to solve the new system of equations by the method of Gauss.

$$\begin{cases} -\dfrac{1}{\left(z_\alpha - z_\beta\right)\left(z_\alpha - z_\gamma\right)}\tilde{\rho}_\alpha - \dfrac{1}{\left(z_\beta - z_\alpha\right)\left(z_\beta - z_\gamma\right)}\tilde{\rho}_\beta - \dfrac{1}{\left(z_\gamma - z_\alpha\right)\left(z_\gamma - z_\beta\right)}\tilde{\rho}_\gamma = v \\[3mm] \dfrac{1}{z_\beta - z_\gamma}\tilde{\rho}_\beta + \dfrac{1}{z_\gamma - z_\beta}\tilde{\rho}_\gamma = \Omega - \left(z_\beta + z_\gamma\right)v \\[3mm] \dfrac{z_\gamma}{z_\beta - z_\gamma}\tilde{\rho}_\beta + \dfrac{z_\beta}{z_\gamma - z_\beta}\tilde{\rho}_\gamma = u - z_\beta z_\gamma v \end{cases}$$

135

$$\begin{cases} -\dfrac{1}{\left(z_\alpha - z_\beta\right)\left(z_\alpha - z_\gamma\right)}\tilde\rho_\alpha - \dfrac{1}{\left(z_\beta - z_\alpha\right)\left(z_\beta - z_\gamma\right)}\tilde\rho_\beta - \dfrac{1}{\left(z_\gamma - z_\alpha\right)\left(z_\gamma - z_\beta\right)}\tilde\rho_\gamma = v \\[3mm] \dfrac{1}{z_\beta - z_\gamma}\tilde\rho_\beta + \dfrac{1}{z_\gamma - z_\beta}\tilde\rho_\gamma = \Omega - \left(z_\beta + z_\gamma\right)v \\[3mm] \dfrac{z_\beta - z_\gamma}{z_\gamma - z_\beta}\tilde\rho_\gamma = u - z_\beta z_\gamma v - z_\gamma\Omega + z_\gamma\left(z_\beta + z_\gamma\right)v \end{cases}$$

Therefore

$$\begin{aligned} \tilde\rho_\alpha &= z_\alpha\Omega - u - z_\alpha^2 v \\ \tilde\rho_\beta &= z_\beta\Omega - u - z_\beta^2 v \\ \tilde\rho_\gamma &= z_\gamma\Omega - u - z_\gamma^2 v \end{aligned}$$

These formulae are valid for any group of three non-dimensional number densities hence any non-dimensional number density is related to u, v and Ω by such a relationship.

$$\tilde\rho_i = z_i\Omega - u - z_i^2 v$$

Because of the very simple form of these relationships we can make use of them together with the definitions of u and v to express u and v as functions of Ω only.

$$u = \sum_{s=1}^{c} u_s\tilde\rho_s = \left(\sum_{s=1}^{c} z_s u_s\right)\Omega - \left(\sum_{s=1}^{c} u_s\right)u - \left(\sum_{s=1}^{c} z_s^2 u_s\right)v$$

$$\left(\sum_{s=1}^{c} z_s u_s\right)\Omega - \left(1 + \sum_{s=1}^{c} u_s\right)u - \left(\sum_{s=1}^{c} z_s^2 u_s\right)v = 0$$

$$v = \sum_{s=1}^{c} v_s\tilde\rho_s = \left(\sum_{s=1}^{c} z_s v_s\right)\Omega - \left(\sum_{s=1}^{c} v_s\right)u - \left(\sum_{s=1}^{c} z_s^2 v_s\right)v$$

$$\left(\sum_{s=1}^{c} z_s v_s\right)\Omega - \left(\sum_{s=1}^{c} v_s\right)u - \left(1 + \sum_{s=1}^{c} z_s^2 v_s\right)v = 0$$

Therefore

$$\frac{\sum\limits_{s=1}^{c} z_s u_s}{\sum\limits_{s=1}^{c} z_s^2 u_s}\Omega - \frac{1 + \sum\limits_{s=1}^{c} u_s}{\sum\limits_{s=1}^{c} z_s^2 u_s}u - v = 0 \quad \text{and} \quad \frac{\sum\limits_{s=1}^{c} z_s v_s}{1 + \sum\limits_{s=1}^{c} z_s^2 v_s}\Omega - \frac{\sum\limits_{s=1}^{c} v_s}{1 + \sum\limits_{s=1}^{c} z_s^2 v_s}u - v = 0$$

$$\left(\frac{\sum\limits_{s=1}^{c} z_s u_s}{\sum\limits_{s=1}^{c} z_s^2 u_s} - \frac{\sum\limits_{s=1}^{c} z_s v_s}{1 + \sum\limits_{s=1}^{c} z_s^2 v_s}\right)\Omega - \left(\frac{1 + \sum\limits_{s=1}^{c} u_s}{\sum\limits_{s=1}^{c} z_s^2 u_s} - \frac{\sum\limits_{s=1}^{c} v_s}{1 + \sum\limits_{s=1}^{c} z_s^2 v_s}\right)u = 0$$

136

$$\left[\left(1+\sum_{s=1}^{c} z_s^2 v_s\right)\sum_{s=1}^{c} z_s u_s - \sum_{s=1}^{c} z_s^2 u_s \sum_{s=1}^{c} z_s v_s\right]\Omega = \left[\left(1+\sum_{s=1}^{c} u_s\right)\left(1+\sum_{s=1}^{c} z_s^2 v_s\right) - \sum_{s=1}^{c} z_s^2 u_s \sum_{s=1}^{c} v_s\right]u$$

$$\left[\sum_{s=1}^{c} z_s u_s + \sum_{s=1}^{c}\sum_{t=1}^{c} z_s z_t^2\left(u_s v_t - u_t v_s\right)\right]\Omega = \left[1+\sum_{s=1}^{c} u_s + \sum_{s=1}^{c} z_s^2 v_s + \sum_{s=1}^{c}\sum_{t=1}^{c} z_s^2\left(u_t v_s - u_s v_t\right)\right]u$$

$$u = \Omega \times \frac{\displaystyle\sum_{s=1}^{c} z_s u_s + \sum_{s=1}^{c}\sum_{t=1}^{c} z_s z_t^2\left(u_s v_t - u_t v_s\right)}{\displaystyle 1 + \sum_{s=1}^{c} u_s + \sum_{s=1}^{c} z_s^2 v_s + \sum_{s=1}^{c}\sum_{t=1}^{c} z_s^2\left(u_t v_s - u_s v_t\right)}$$

We use a similar calculation to find the relationship between v and Ω.

$$\frac{\displaystyle\sum_{s=1}^{c} z_s u_s}{\displaystyle 1+\sum_{s=1}^{c} u_s}\Omega - u - \frac{\displaystyle\sum_{s=1}^{c} z_s^2 u_s}{\displaystyle 1+\sum_{s=1}^{c} u_s}v = 0 \quad \text{and} \quad \frac{\displaystyle\sum_{s=1}^{c} z_s v_s}{\displaystyle\sum_{s=1}^{c} v_s}\Omega - u - \frac{\displaystyle 1+\sum_{s=1}^{c} z_s^2 v_s}{\displaystyle\sum_{s=1}^{c} v_s}v = 0$$

$$\left(\frac{\displaystyle\sum_{s=1}^{c} z_s v_s}{\displaystyle\sum_{s=1}^{c} v_s} - \frac{\displaystyle\sum_{s=1}^{c} z_s u_s}{\displaystyle 1+\sum_{s=1}^{c} u_s}\right)\Omega - \left(\frac{\displaystyle 1+\sum_{s=1}^{c} z_s^2 v_s}{\displaystyle\sum_{s=1}^{c} v_s} - \frac{\displaystyle\sum_{s=1}^{c} z_s^2 u_s}{\displaystyle 1+\sum_{s=1}^{c} u_s}\right)v = 0$$

$$\left[\sum_{s=1}^{c} z_s v_s\left(1+\sum_{s=1}^{c} u_s\right) - \sum_{s=1}^{c} z_s u_s \sum_{s=1}^{c} v_s\right]\Omega = \left[\left(1+\sum_{s=1}^{c} u_s\right)\left(1+\sum_{s=1}^{c} z_s^2 v_s\right) - \sum_{s=1}^{c} z_s^2 u_s \sum_{s=1}^{c} v_s\right]v$$

$$\left[\sum_{s=1}^{c} z_s v_s + \sum_{s=1}^{c}\sum_{t=1}^{c} z_s\left(u_t v_s - u_s v_t\right)\right]\Omega = \left[1+\sum_{s=1}^{c} u_s + \sum_{s=1}^{c} z_s^2 v_s + \sum_{s=1}^{c}\sum_{t=1}^{c} z_s^2\left(u_t v_s - u_s v_t\right)\right]v$$

$$v = \Omega \times \frac{\displaystyle\sum_{s=1}^{c} z_s v_s + \sum_{s=1}^{c}\sum_{t=1}^{c} z_s\left(u_t v_s - u_s v_t\right)}{\displaystyle 1 + \sum_{s=1}^{c} u_s + \sum_{s=1}^{c} z_s^2 v_s + \sum_{s=1}^{c}\sum_{t=1}^{c} z_s^2\left(u_t v_s - u_s v_t\right)}$$

Thus we can express any non-dimensional number density as a function of the potential Ω only.

$$\tilde{\rho}_i = z_i \Omega - u - z_i^2 v \qquad \tilde{\rho}_i = K_i \Omega$$

$$K_i = \frac{\displaystyle z_i + \sum_{s=1}^{c}\left(z_i - z_s\right)\left[u_s - z_i z_s v_s\right] + \sum_{s=1}^{c}\sum_{t=1}^{c} z_s\left(z_i z_s + z_t^2 - z_i^2\right)\left(u_t v_s - u_s v_t\right)}{\displaystyle 1 + \sum_{s=1}^{c} u_s + \sum_{s=1}^{c} z_s^2 v_s + \sum_{s=1}^{c}\sum_{t=1}^{c} z_s^2\left(u_t v_s - u_s v_t\right)}$$

The last step is to substitute the definitions of u_s and v_s in order to recover the number densities and the physical parameters.

$$\tilde{\rho}_i = \frac{\rho_{n_0+\ldots+n_{i-1}+1}^{\varepsilon}}{\rho_{n_0+\ldots+n_{i-1}+1}^{0}} = \cdots = \frac{\rho_{n_0+\ldots+n_{i-1}+n_i}^{\varepsilon}}{\rho_{n_0+\ldots+n_{i-1}+n_i}^{0}} \quad \text{corresponding to charge } z_i, \ i \in [\![1,c]\!]$$

$$u_i = \frac{\displaystyle\sum_{s=n_0+\ldots+n_{i-1}}^{n_0+\ldots+n_{i-1}+n_i} 8\sigma_s^3 \rho_s^0}{1 - \displaystyle\sum_{s=1}^{} 8\sigma_s^3 \rho_s^0} \qquad\qquad v_i = \frac{10.58}{4} w l_B^3 \displaystyle\sum_{s=n_0+\ldots+n_{i-1}+1}^{n_0+\ldots+n_{i-1}+n_i} z_s^2 \rho_s^0$$

The main conclusion is that the number densities are proportional to the potential Ω.

$$\rho_\alpha^\varepsilon = \rho_\alpha^0 \cdot K_\alpha \cdot \Omega \quad \text{with} \quad K_\alpha = K_\alpha\left(w, \left(z_i\right)_{i=1\ldots c}, \left(\sigma_s\right)_{s=1\ldots n}, \left(\rho_s^0\right)_{s=1\ldots n}\right)$$

I.4 Corresponding calculations for exactly three ionic species in solution

The initial set of equations is

$$\begin{cases} \Omega = \dfrac{1}{z_\alpha}\left[\tilde{\rho}_\alpha + u_\alpha\tilde{\rho}_\alpha + u_\beta\tilde{\rho}_\beta + u_\gamma\tilde{\rho}_\gamma\right] + z_\alpha\left[v_\alpha\tilde{\rho}_\alpha + v_\beta\tilde{\rho}_\beta + v_\gamma\tilde{\rho}_\gamma\right] \\[2mm] \Omega = \dfrac{1}{z_\beta}\left[\tilde{\rho}_\beta + u_\alpha\tilde{\rho}_\alpha + u_\beta\tilde{\rho}_\beta + u_\gamma\tilde{\rho}_\gamma\right] + z_\beta\left[v_\alpha\tilde{\rho}_\alpha + v_\beta\tilde{\rho}_\beta + v_\gamma\tilde{\rho}_\gamma\right] \\[2mm] \Omega = \dfrac{1}{z_\gamma}\left[\tilde{\rho}_\gamma + u_\alpha\tilde{\rho}_\alpha + u_\beta\tilde{\rho}_\beta + u_\gamma\tilde{\rho}_\gamma\right] + z_\gamma\left[v_\alpha\tilde{\rho}_\alpha + v_\beta\tilde{\rho}_\beta + v_\gamma\tilde{\rho}_\gamma\right] \end{cases}$$

We rewrite the set of equations using the functions u and v defined below.

$$\begin{cases} \Omega = \dfrac{1}{z_\alpha}\left[\tilde{\rho}_\alpha + u\right] + z_\alpha v \\[2mm] \Omega = \dfrac{1}{z_\beta}\left[\tilde{\rho}_\beta + u\right] + z_\beta v \\[2mm] \Omega = \dfrac{1}{z_\gamma}\left[\tilde{\rho}_\gamma + u\right] + z_\gamma v \end{cases} \qquad \begin{cases} u = u_\alpha\tilde{\rho}_\alpha + u_\beta\tilde{\rho}_\beta + u_\gamma\tilde{\rho}_\gamma \\[2mm] v = v_\alpha\tilde{\rho}_\alpha + v_\beta\tilde{\rho}_\beta + v_\gamma\tilde{\rho}_\gamma \end{cases}$$

Now we proceed to express Ω, u and v as functions of the three non-dimensional number densities and three charges. We start by eliminating u and v from the system to obtain Ω.

138

$$\left\{\begin{array}{l} \dfrac{\Omega}{z_\alpha} = \dfrac{1}{z_\alpha^2}\big[\tilde{\rho}_\alpha + u\big] + v \\[3mm] \dfrac{\Omega}{z_\beta} = \dfrac{1}{z_\beta^2}\big[\tilde{\rho}_\beta + u\big] + v \\[3mm] \dfrac{\Omega}{z_\gamma} = \dfrac{1}{z_\gamma^2}\big[\tilde{\rho}_\gamma + u\big] + v \end{array}\right. \quad \text{then} \quad \left\{\begin{array}{l} \dfrac{\Omega}{z_\alpha} - \dfrac{\Omega}{z_\beta} = \dfrac{1}{z_\alpha^2}\tilde{\rho}_\alpha - \dfrac{1}{z_\beta^2}\tilde{\rho}_\beta + \left(\dfrac{1}{z_\alpha^2} - \dfrac{1}{z_\beta^2}\right)u \\[3mm] \dfrac{\Omega}{z_\alpha} - \dfrac{\Omega}{z_\gamma} = \dfrac{1}{z_\alpha^2}\tilde{\rho}_\alpha - \dfrac{1}{z_\gamma^2}\tilde{\rho}_\gamma + \left(\dfrac{1}{z_\alpha^2} - \dfrac{1}{z_\gamma^2}\right)u \\[3mm] \dfrac{\Omega}{z_\beta} - \dfrac{\Omega}{z_\gamma} = \dfrac{1}{z_\beta^2}\tilde{\rho}_\beta - \dfrac{1}{z_\gamma^2}\tilde{\rho}_\gamma + \left(\dfrac{1}{z_\beta^2} - \dfrac{1}{z_\gamma^2}\right)u \end{array}\right.$$

$$\left\{\begin{array}{l} \dfrac{z_\beta - z_\alpha}{z_\alpha z_\beta}\Omega = \dfrac{1}{z_\alpha^2}\tilde{\rho}_\alpha - \dfrac{1}{z_\beta^2}\tilde{\rho}_\beta + \dfrac{z_\beta^2 - z_\alpha^2}{z_\alpha^2 z_\beta^2}u \\[4mm] \dfrac{z_\gamma - z_\alpha}{z_\alpha z_\gamma}\Omega = \dfrac{1}{z_\alpha^2}\tilde{\rho}_\alpha - \dfrac{1}{z_\gamma^2}\tilde{\rho}_\gamma + \dfrac{z_\gamma^2 - z_\alpha^2}{z_\alpha^2 z_\gamma^2}u \\[4mm] \dfrac{z_\gamma - z_\beta}{z_\beta z_\gamma}\Omega = \dfrac{1}{z_\beta^2}\tilde{\rho}_\beta - \dfrac{1}{z_\gamma^2}\tilde{\rho}_\gamma + \dfrac{z_\gamma^2 - z_\beta^2}{z_\beta^2 z_\gamma^2}u \end{array}\right.$$

$$\left\{\begin{array}{l} \dfrac{z_\alpha z_\beta}{z_\beta + z_\alpha}\Omega = \dfrac{z_\alpha^2 z_\beta^2}{z_\beta^2 - z_\alpha^2}\left(\dfrac{1}{z_\alpha^2}\tilde{\rho}_\alpha - \dfrac{1}{z_\beta^2}\tilde{\rho}_\beta\right) + u \\[4mm] \dfrac{z_\alpha z_\gamma}{z_\gamma + z_\alpha}\Omega = \dfrac{z_\alpha^2 z_\gamma^2}{z_\gamma^2 - z_\alpha^2}\left(\dfrac{1}{z_\alpha^2}\tilde{\rho}_\alpha - \dfrac{1}{z_\gamma^2}\tilde{\rho}_\gamma\right) + u \\[4mm] \dfrac{z_\beta z_\gamma}{z_\gamma - z_\beta}\Omega = \dfrac{z_\beta^2 z_\gamma^2}{z_\gamma^2 - z_\beta^2}\left(\dfrac{1}{z_\beta^2}\tilde{\rho}_\beta - \dfrac{1}{z_\gamma^2}\tilde{\rho}_\gamma\right) + u \end{array}\right.$$

$$\left\{\begin{array}{l} \left(\dfrac{z_\alpha z_\beta}{z_\beta + z_\alpha} - \dfrac{z_\alpha z_\gamma}{z_\gamma + z_\alpha}\right)\Omega = \dfrac{z_\alpha^2 z_\beta^2}{z_\beta^2 - z_\alpha^2}\left(\dfrac{1}{z_\alpha^2}\tilde{\rho}_\alpha - \dfrac{1}{z_\beta^2}\tilde{\rho}_\beta\right) - \dfrac{z_\alpha^2 z_\gamma^2}{z_\gamma^2 - z_\alpha^2}\left(\dfrac{1}{z_\alpha^2}\tilde{\rho}_\alpha - \dfrac{1}{z_\gamma^2}\tilde{\rho}_\gamma\right) \\[4mm] \left(\dfrac{z_\alpha z_\beta}{z_\beta + z_\alpha} - \dfrac{z_\beta z_\gamma}{z_\gamma - z_\beta}\right)\Omega = \dfrac{z_\alpha^2 z_\beta^2}{z_\beta^2 - z_\alpha^2}\left(\dfrac{1}{z_\alpha^2}\tilde{\rho}_\alpha - \dfrac{1}{z_\beta^2}\tilde{\rho}_\beta\right) - \dfrac{z_\beta^2 z_\gamma^2}{z_\gamma^2 - z_\beta^2}\left(\dfrac{1}{z_\beta^2}\tilde{\rho}_\beta - \dfrac{1}{z_\gamma^2}\tilde{\rho}_\gamma\right) \\[4mm] \left(\dfrac{z_\alpha z_\gamma}{z_\gamma + z_\alpha} - \dfrac{z_\beta z_\gamma}{z_\gamma - z_\beta}\right)\Omega = \dfrac{z_\alpha^2 z_\gamma^2}{z_\gamma^2 - z_\alpha^2}\left(\dfrac{1}{z_\alpha^2}\tilde{\rho}_\alpha - \dfrac{1}{z_\gamma^2}\tilde{\rho}_\gamma\right) - \dfrac{z_\beta^2 z_\gamma^2}{z_\gamma^2 - z_\beta^2}\left(\dfrac{1}{z_\beta^2}\tilde{\rho}_\beta - \dfrac{1}{z_\gamma^2}\tilde{\rho}_\gamma\right) \end{array}\right.$$

The three equations turn out to be identical. Solving for Ω we obtain an expression symmetrical in α, β, γ.

$$\boxed{\Omega = -\dfrac{z_\beta + z_\gamma}{\left(z_\alpha - z_\beta\right)\left(z_\alpha - z_\gamma\right)}\tilde{\rho}_\alpha - \dfrac{z_\alpha + z_\gamma}{\left(z_\beta - z_\alpha\right)\left(z_\beta - z_\gamma\right)}\tilde{\rho}_\beta - \dfrac{z_\alpha + z_\beta}{\left(z_\gamma - z_\alpha\right)\left(z_\gamma - z_\beta\right)}\tilde{\rho}_\gamma}$$

We return to the system of equations containing u and use the first equation to compute an expression for u by substituting the expression of Ω found above.

139

$$\frac{\Omega}{z_\alpha} - \frac{\Omega}{z_\beta} = \frac{1}{z_\alpha^2}\tilde{\rho}_\alpha - \frac{1}{z_\beta^2}\tilde{\rho}_\beta + \left(\frac{1}{z_\alpha^2} - \frac{1}{z_\beta^2}\right)u$$

$$u = \frac{z_\alpha z_\beta}{z_\beta + z_\alpha}\Omega + \frac{z_\alpha^2 z_\beta^2}{z_\alpha^2 - z_\beta^2}\left(\frac{1}{z_\alpha^2}\tilde{\rho}_\alpha - \frac{1}{z_\beta^2}\tilde{\rho}_\beta\right)$$

$$u = -\frac{z_\beta z_\gamma \tilde{\rho}_\alpha}{\left(z_\alpha - z_\beta\right)\left(z_\alpha - z_\gamma\right)} - \frac{z_\alpha z_\gamma \tilde{\rho}_\beta}{\left(z_\beta - z_\alpha\right)\left(z_\beta - z_\gamma\right)} - \frac{z_\alpha z_\beta \tilde{\rho}_\gamma}{\left(z_\gamma - z_\alpha\right)\left(z_\gamma - z_\beta\right)}$$

The expression of u is symmetrical in α, β, γ. Using the other equations in the system would yield and identical formula.

In order to find v we use the first equation in the system containing v and substitute the expressions of Ω and u.

$$\frac{\Omega}{z_\alpha} = \frac{1}{z_\alpha^2}\tilde{\rho}_\alpha + \frac{1}{z_\alpha^2}u + v$$

$$v = \frac{\Omega}{z_\alpha} - \frac{1}{z_\alpha^2}\tilde{\rho}_\alpha - \frac{1}{z_\alpha^2}u$$

$$v = -\frac{\tilde{\rho}_\alpha}{\left(z_\alpha - z_\beta\right)\left(z_\alpha - z_\gamma\right)} - \frac{\tilde{\rho}_\beta}{\left(z_\beta - z_\alpha\right)\left(z_\beta - z_\gamma\right)} - \frac{\tilde{\rho}_\gamma}{\left(z_\gamma - z_\alpha\right)\left(z_\gamma - z_\beta\right)}$$

As expected the expression of v is symmetrical in α, β, γ.

We want to express each non-dimensional number density as a function of u, v and Ω only. We take the three expressions determined in the previous pages and write them as a system of equations.

$$\begin{cases} -\dfrac{1}{\left(z_\alpha - z_\beta\right)\left(z_\alpha - z_\gamma\right)}\tilde{\rho}_\alpha - \dfrac{1}{\left(z_\beta - z_\alpha\right)\left(z_\beta - z_\gamma\right)}\tilde{\rho}_\beta - \dfrac{1}{\left(z_\gamma - z_\alpha\right)\left(z_\gamma - z_\beta\right)}\tilde{\rho}_\gamma = v \\[4mm] -\dfrac{z_\beta + z_\gamma}{\left(z_\alpha - z_\beta\right)\left(z_\alpha - z_\gamma\right)}\tilde{\rho}_\alpha - \dfrac{z_\alpha + z_\gamma}{\left(z_\beta - z_\alpha\right)\left(z_\beta - z_\gamma\right)}\tilde{\rho}_\beta - \dfrac{z_\alpha + z_\beta}{\left(z_\gamma - z_\alpha\right)\left(z_\gamma - z_\beta\right)}\tilde{\rho}_\gamma = \Omega \\[4mm] -\dfrac{z_\beta z_\gamma}{\left(z_\alpha - z_\beta\right)\left(z_\alpha - z_\gamma\right)}\tilde{\rho}_\alpha - \dfrac{z_\alpha z_\gamma}{\left(z_\beta - z_\alpha\right)\left(z_\beta - z_\gamma\right)}\tilde{\rho}_\beta - \dfrac{z_\alpha z_\beta}{\left(z_\gamma - z_\alpha\right)\left(z_\gamma - z_\beta\right)}\tilde{\rho}_\gamma = u \end{cases}$$

We seek to solve the new system of equations by the method of Gauss.

$$\begin{cases} -\dfrac{1}{\left(z_\alpha - z_\beta\right)\left(z_\alpha - z_\gamma\right)}\tilde{\rho}_\alpha - \dfrac{1}{\left(z_\beta - z_\alpha\right)\left(z_\beta - z_\gamma\right)}\tilde{\rho}_\beta - \dfrac{1}{\left(z_\gamma - z_\alpha\right)\left(z_\gamma - z_\beta\right)}\tilde{\rho}_\gamma = v \\[4mm] \dfrac{1}{z_\beta - z_\gamma}\tilde{\rho}_\beta + \dfrac{1}{z_\gamma - z_\beta}\tilde{\rho}_\gamma = \Omega - \left(z_\beta + z_\gamma\right)v \\[4mm] \dfrac{z_\gamma}{z_\beta - z_\gamma}\tilde{\rho}_\beta + \dfrac{z_\beta}{z_\gamma - z_\beta}\tilde{\rho}_\gamma = u - z_\beta z_\gamma v \end{cases}$$

140

$$\left\{ \begin{array}{l} -\dfrac{1}{\left(z_\alpha - z_\beta\right)\left(z_\alpha - z_\gamma\right)}\tilde{\rho}_\alpha - \dfrac{1}{\left(z_\beta - z_\alpha\right)\left(z_\beta - z_\gamma\right)}\tilde{\rho}_\beta - \dfrac{1}{\left(z_\gamma - z_\alpha\right)\left(z_\gamma - z_\beta\right)}\tilde{\rho}_\gamma = v \\[3mm] \dfrac{1}{z_\beta - z_\gamma}\tilde{\rho}_\beta + \dfrac{1}{z_\gamma - z_\beta}\tilde{\rho}_\gamma = \Omega - \left(z_\beta + z_\gamma\right)v \\[3mm] \dfrac{z_\beta - z_\gamma}{z_\gamma - z_\beta}\tilde{\rho}_\gamma = u - z_\beta z_\gamma v - z_\gamma\Omega + z_\gamma\left(z_\beta + z_\gamma\right)v \end{array} \right.$$

Therefore

$$\begin{aligned} \tilde{\rho}_\alpha &= z_\alpha\Omega - u - z_\alpha^2 v \\ \tilde{\rho}_\beta &= z_\beta\Omega - u - z_\beta^2 v \\ \tilde{\rho}_\gamma &= z_\gamma\Omega - u - z_\gamma^2 v \end{aligned}$$

We can use these three formulae together with the definitions of u and v to express the number densities as functions of Ω only. We proceed by successive substitutions. We start by determining v as a function of Ω only.

$$u = u_\alpha\tilde{\rho}_\alpha + u_\beta\tilde{\rho}_\beta + u_\gamma\tilde{\rho}_\gamma$$

$$u = \left(z_\alpha u_\alpha + z_\beta u_\beta + z_\gamma u_\gamma\right)\Omega - \left(u_\alpha + u_\beta + u_\gamma\right)u - \left(z_\alpha^2 u_\alpha + z_\beta^2 u_\beta + z_\gamma^2 u_\gamma\right)v$$

$$\left(1 + u_\alpha + u_\beta + u_\gamma\right)u = \left(z_\alpha u_\alpha + z_\beta u_\beta + z_\gamma u_\gamma\right)\Omega - \left(z_\alpha^2 u_\alpha + z_\beta^2 u_\beta + z_\gamma^2 u_\gamma\right)v$$

$$u = \frac{\left(z_\alpha u_\alpha + z_\beta u_\beta + z_\gamma u_\gamma\right)\Omega - \left(z_\alpha^2 u_\alpha + z_\beta^2 u_\beta + z_\gamma^2 u_\gamma\right)v}{1 + u_\alpha + u_\beta + u_\gamma}$$

$$v = v_\alpha\tilde{\rho}_\alpha + v_\beta\tilde{\rho}_\beta + v_\gamma\tilde{\rho}_\gamma$$

$$v = \left(z_\alpha v_\alpha + z_\beta v_\beta + z_\gamma v_\gamma\right)\Omega - \left(v_\alpha + v_\beta + v_\gamma\right)u - \left(z_\alpha^2 v_\alpha + z_\beta^2 v_\beta + z_\gamma^2 v_\gamma\right)v$$

$$v = \begin{aligned}[t] &\left(z_\alpha v_\alpha + z_\beta v_\beta + z_\gamma v_\gamma\right)\Omega - \left(z_\alpha^2 v_\alpha + z_\beta^2 v_\beta + z_\gamma^2 v_\gamma\right)v \\ &-\frac{v_\alpha + v_\beta + v_\gamma}{1 + u_\alpha + u_\beta + u_\gamma}\left[\left(z_\alpha u_\alpha + z_\beta u_\beta + z_\gamma u_\gamma\right)\Omega - \left(z_\alpha^2 u_\alpha + z_\beta^2 u_\beta + z_\gamma^2 u_\gamma\right)v\right] \end{aligned}$$

$$v = \frac{\left[\begin{array}{l} z_\alpha\left(v_\alpha\left(u_\beta + u_\gamma\right) - \left(v_\beta + v_\gamma\right)u_\alpha\right) \quad +z_\alpha v_\alpha + z_\beta v_\beta + z_\gamma v_\gamma + \\ z_\beta\left(v_\beta\left(u_\alpha + u_\gamma\right) - \left(v_\alpha + v_\gamma\right)u_\beta\right) \quad +z_\gamma\left(v_\gamma\left(u_\alpha + u_\beta\right) - \left(v_\alpha + v_\beta\right)u_\gamma\right) \end{array}\right]\Omega}{1 + u_\alpha + u_\beta + u_\gamma}$$
$$- \frac{\left[\begin{array}{l} z_\alpha^2\left(v_\alpha\left(u_\beta + u_\gamma\right) - \left(v_\beta + v_\gamma\right)u_\alpha\right) + z_\alpha^2 v_\alpha + z_\beta^2 v_\beta + z_\gamma^2 v_\gamma + \\ z_\beta^2\left(v_\beta\left(u_\alpha + u_\gamma\right) - \left(v_\alpha + v_\gamma\right)u_\beta\right) + z_\gamma^2\left(v_\gamma\left(u_\alpha + u_\beta\right) - \left(v_\alpha + v_\beta\right)u_\gamma\right) \end{array}\right]v}{1 + u_\alpha + u_\beta + u_\gamma}$$

$$v \;=\; \Omega \times \cfrac{\begin{array}{l} z_\alpha v_\alpha + z_\alpha\Big(v_\alpha\big(u_\beta + u_\gamma\big) - \big(v_\beta + v_\gamma\big)u_\alpha\Big) + \\[4pt] z_\beta v_\beta + z_\beta\Big(v_\beta\big(u_\alpha + u_\gamma\big) - \big(v_\alpha + v_\gamma\big)u_\beta\Big) + \\[4pt] z_\gamma v_\gamma + z_\gamma\Big(v_\gamma\big(u_\alpha + u_\beta\big) - \big(v_\alpha + v_\beta\big)u_\gamma\Big) \end{array}}{1 + \begin{array}{l} u_\alpha + z_\alpha^2 v_\alpha + z_\alpha^2\Big(v_\alpha\big(u_\beta + u_\gamma\big) - \big(v_\beta + v_\gamma\big)u_\alpha\Big) + \\[4pt] u_\beta + z_\beta^2 v_\beta + z_\beta^2\Big(v_\beta\big(u_\alpha + u_\gamma\big) - \big(v_\alpha + v_\gamma\big)u_\beta\Big) + \\[4pt] u_\gamma + z_\gamma^2 v_\gamma + z_\gamma^2\Big(v_\gamma\big(u_\alpha + u_\beta\big) - \big(v_\alpha + v_\beta\big)u_\gamma\Big) \end{array}}$$

We repeat the same method to determine u as a function of Ω only.

$$v = v_\alpha \tilde\rho_\alpha + v_\beta \tilde\rho_\beta + v_\gamma \tilde\rho_\gamma$$

$$v = \Big(z_\alpha v_\alpha + z_\beta v_\beta + z_\gamma v_\gamma\Big)\Omega - \Big(v_\alpha + v_\beta + v_\gamma\Big)u - \Big(z_\alpha^2 v_\alpha + z_\beta^2 v_\beta + z_\gamma^2 v_\gamma\Big)v$$

$$\Big(1 + z_\alpha^2 v_\alpha + z_\beta^2 v_\beta + z_\gamma^2 v_\gamma\Big)v = \Big(z_\alpha v_\alpha + z_\beta v_\beta + z_\gamma v_\gamma\Big)\Omega - \Big(v_\alpha + v_\beta + v_\gamma\Big)u$$

$$v = \frac{\Big(z_\alpha v_\alpha + z_\beta v_\beta + z_\gamma v_\gamma\Big)\Omega - \Big(v_\alpha + v_\beta + v_\gamma\Big)u}{1 + z_\alpha^2 v_\alpha + z_\beta^2 v_\beta + z_\gamma^2 v_\gamma}$$

$$u = u_\alpha \tilde\rho_\alpha + u_\beta \tilde\rho_\beta + u_\gamma \tilde\rho_\gamma$$

$$u = \Big(z_\alpha u_\alpha + z_\beta u_\beta + z_\gamma u_\gamma\Big)\Omega - \Big(u_\alpha + u_\beta + u_\gamma\Big)u - \Big(z_\alpha^2 u_\alpha + z_\beta^2 u_\beta + z_\gamma^2 u_\gamma\Big)v$$

$$u = \begin{array}{l}\Big(z_\alpha u_\alpha + z_\beta u_\beta + z_\gamma u_\gamma\Big)\Omega - \Big(u_\alpha + u_\beta + u_\gamma\Big)u \\[6pt] -\Big(z_\alpha^2 u_\alpha + z_\beta^2 u_\beta + z_\gamma^2 u_\gamma\Big)\dfrac{\Big(z_\alpha v_\alpha + z_\beta v_\beta + z_\gamma v_\gamma\Big)\Omega - \Big(v_\alpha + v_\beta + v_\gamma\Big)u}{1 + z_\alpha^2 v_\alpha + z_\beta^2 v_\beta + z_\gamma^2 v_\gamma}\end{array}$$

$$u = \cfrac{\begin{array}{l} z_\alpha u_\alpha + z_\alpha u_\alpha\Big(z_\beta\big(z_\beta - z_\alpha\big)v_\beta + z_\gamma\big(z_\gamma - z_\alpha\big)v_\gamma\Big) + \\[4pt] z_\beta u_\beta + z_\beta u_\beta\Big(z_\alpha\big(z_\alpha - z_\beta\big)v_\alpha + z_\gamma\big(z_\gamma - z_\beta\big)v_\gamma\Big) + \\[4pt] z_\gamma u_\gamma + z_\gamma u_\gamma\Big(z_\alpha\big(z_\alpha - z_\gamma\big)v_\alpha + z_\beta\big(z_\beta - z_\gamma\big)v_\beta\Big) \end{array}}{1 + z_\alpha^2 v_\alpha + z_\beta^2 v_\beta + z_\gamma^2 v_\gamma}\,\Omega$$
$$\quad - \cfrac{\begin{array}{l} u_\alpha + z_\alpha^2\Big(\big(u_\beta + u_\gamma\big)v_\alpha - u_\alpha\big(v_\beta + v_\gamma\big)\Big) + \\[4pt] u_\beta + z_\beta^2\Big(\big(u_\beta + u_\gamma\big)v_\beta - u_\beta\big(v_\beta + v_\gamma\big)\Big) + \\[4pt] u_\gamma + z_\gamma^2\Big(\big(u_\alpha + u_\beta\big)v_\gamma - u_\gamma\big(v_\alpha + v_\beta\big)\Big) \end{array}}{1 + z_\alpha^2 v_\alpha + z_\beta^2 v_\beta + z_\gamma^2 v_\gamma}\,u$$

$$u = \Omega \times \frac{\begin{aligned} &z_\alpha u_\alpha + z_\alpha u_\alpha \left(z_\beta \left(z_\beta - z_\alpha \right) v_\beta + z_\gamma \left(z_\gamma - z_\alpha \right) v_\gamma \right) + \\ &z_\beta u_\beta + z_\beta u_\beta \left(z_\alpha \left(z_\alpha - z_\beta \right) v_\alpha + z_\gamma \left(z_\gamma - z_\beta \right) v_\gamma \right) + \\ &z_\gamma u_\gamma + z_\gamma u_\gamma \left(z_\alpha \left(z_\alpha - z_\gamma \right) v_\alpha + z_\beta \left(z_\beta - z_\gamma \right) v_\beta \right) \end{aligned}}{1 + \begin{aligned} &u_\alpha + z_\alpha^2 v_\alpha + z_\alpha^2 \left(\left(u_\beta + u_\gamma \right) v_\alpha - u_\alpha \left(v_\beta + v_\gamma \right) \right) + \\ &u_\beta + z_\beta^2 v_\beta + z_\beta^2 \left(\left(u_\alpha + u_\gamma \right) v_\beta - u_\beta \left(v_\alpha + v_\gamma \right) \right) + \\ &u_\gamma + z_\gamma^2 v_\gamma + z_\gamma^2 \left(\left(u_\alpha + u_\beta \right) v_\gamma - u_\gamma \left(v_\alpha + v_\beta \right) \right) \end{aligned}}$$

At last we can express the number densities as functions of only the potential Ω.

$$\begin{cases} \tilde{\rho}_\alpha = z_\alpha \Omega - u - z_\alpha^2 v \\ \tilde{\rho}_\beta = z_\beta \Omega - u - z_\beta^2 v \\ \tilde{\rho}_\gamma = z_\gamma \Omega - u - z_\gamma^2 v \end{cases} \qquad \begin{cases} \tilde{\rho}_\alpha = K_\alpha \Omega \\ \tilde{\rho}_\beta = K_\beta \Omega \\ \tilde{\rho}_\gamma = K_\gamma \Omega \end{cases}$$

$$K_\alpha = \frac{\begin{aligned} z_\alpha \quad &+ \left(z_\alpha - z_\beta \right) u_\beta + z_\alpha z_\beta \left(z_\beta - z_\alpha \right) v_\beta \\ &+ \left(z_\alpha - z_\gamma \right) u_\gamma + z_\alpha z_\gamma \left(z_\gamma - z_\alpha \right) v_\gamma \\ &- \left(z_\alpha - z_\beta \right) \left(z_\beta - z_\gamma \right) \left(z_\gamma - z_\alpha \right) \left(u_\beta v_\gamma - u_\gamma v_\beta \right) \end{aligned}}{1 + \begin{aligned} &u_\alpha + z_\alpha^2 v_\alpha + z_\alpha^2 \left(\left(u_\beta + u_\gamma \right) v_\alpha - u_\alpha \left(v_\beta + v_\gamma \right) \right) + \\ &u_\beta + z_\beta^2 v_\beta + z_\beta^2 \left(\left(u_\alpha + u_\gamma \right) v_\beta - u_\beta \left(v_\alpha + v_\gamma \right) \right) + \\ &u_\gamma + z_\gamma^2 v_\gamma + z_\gamma^2 \left(\left(u_\alpha + u_\beta \right) v_\gamma - u_\gamma \left(v_\alpha + v_\beta \right) \right) \end{aligned}}$$

$$K_\beta = \frac{\begin{aligned} z_\beta \quad &+ \left(z_\beta - z_\alpha \right) u_\alpha + z_\alpha z_\beta \left(z_\alpha - z_\beta \right) v_\alpha \\ &+ \left(z_\beta - z_\gamma \right) u_\gamma + z_\beta z_\gamma \left(z_\gamma - z_\beta \right) v_\gamma \\ &- \left(z_\alpha - z_\beta \right) \left(z_\beta - z_\gamma \right) \left(z_\gamma - z_\alpha \right) \left(u_\gamma v_\alpha - u_\alpha v_\gamma \right) \end{aligned}}{1 + \begin{aligned} &u_\alpha + z_\alpha^2 v_\alpha + z_\alpha^2 \left(\left(u_\beta + u_\gamma \right) v_\alpha - u_\alpha \left(v_\beta + v_\gamma \right) \right) + \\ &u_\beta + z_\beta^2 v_\beta + z_\beta^2 \left(\left(u_\alpha + u_\gamma \right) v_\beta - u_\beta \left(v_\alpha + v_\gamma \right) \right) + \\ &u_\gamma + z_\gamma^2 v_\gamma + z_\gamma^2 \left(\left(u_\alpha + u_\beta \right) v_\gamma - u_\gamma \left(v_\alpha + v_\beta \right) \right) \end{aligned}}$$

$$K_\gamma = \frac{\begin{aligned} z_\gamma \quad &+ \left(z_\gamma - z_\alpha \right) u_\alpha + z_\gamma z_\alpha \left(z_\alpha - z_\gamma \right) v_\alpha \\ &+ \left(z_\gamma - z_\beta \right) u_\beta + z_\gamma z_\beta \left(z_\beta - z_\gamma \right) v_\beta \\ &- \left(z_\alpha - z_\beta \right) \left(z_\beta - z_\gamma \right) \left(z_\gamma - z_\alpha \right) \left(u_\alpha v_\beta - u_\beta v_\alpha \right) \end{aligned}}{1 + \begin{aligned} &u_\alpha + z_\alpha^2 v_\alpha + z_\alpha^2 \left(\left(u_\beta + u_\gamma \right) v_\alpha - u_\alpha \left(v_\beta + v_\gamma \right) \right) + \\ &u_\beta + z_\beta^2 v_\beta + z_\beta^2 \left(\left(u_\alpha + u_\gamma \right) v_\beta - u_\beta \left(v_\alpha + v_\gamma \right) \right) + \\ &u_\gamma + z_\gamma^2 v_\gamma + z_\gamma^2 \left(\left(u_\alpha + u_\beta \right) v_\gamma - u_\gamma \left(v_\alpha + v_\beta \right) \right) \end{aligned}}$$

Reminder that the definitions of u_i and v_i are: for $i = \alpha, \beta, \gamma$

$$u_i = \frac{8\sigma_i^3 \rho_i^0}{1 - \displaystyle\sum_{s \in \{\alpha,\beta,\gamma\}} 8\sigma_s^3 \rho_s^0}$$

$$v_i = \frac{10.58}{4} w l_B^3 \cdot z_i^2 \rho_i^0$$

I.5   Solution to the final differential equation

The n differential equations determining $\rho_1^\varepsilon, \ldots, \rho_n^\varepsilon$ are of the form:

$$\frac{1}{z_\alpha}\left[\frac{\rho_\alpha'^\varepsilon}{\rho_\alpha^0} + \frac{\displaystyle\sum_{\beta=1}^{n} 8\sigma_\beta^3 \rho_\beta'^\varepsilon}{1 - \displaystyle\sum_{\beta=1}^{n} 8\sigma_\beta^3 \rho_\beta^0}\right] + \frac{10.58}{4} z_\alpha w l_B^3 \sum_{\beta=1}^{n} z_\beta^2 \rho_\beta'^\varepsilon = \begin{aligned} &\frac{Z l_B}{r^2} + \frac{4\pi l_B}{r^2} \int_R^r r'^2 \sum_{\beta=1}^{n} z_\beta \rho_\beta^\varepsilon (r') dr' \\ &- 2.3 w^2 l_B^3 \sum_{\beta=1}^{n} z_\beta \rho_\beta'^\varepsilon + \frac{17}{4} w l_B^3 \sum_{\beta=1}^{n} z_\beta \rho_\beta'^\varepsilon \end{aligned}$$

The potential Ω is defined as

$$\Omega = \frac{1}{z_\alpha}\left[\frac{\rho_\alpha^\varepsilon}{\rho_\alpha^0} + \frac{\displaystyle\sum_{s=1}^{n} 8\sigma_s^3 \rho_s^\varepsilon}{1 - \displaystyle\sum_{s=1}^{n} 8\sigma_s^3 \rho_s^0}\right] + \frac{10.58}{4} z_\alpha w l_B^3 \sum_{s=1}^{n} z_s^2 \rho_s^\varepsilon$$

Thus the set of differential equations can be reduced to a single differential equation.

$$\Omega' = \frac{Z l_B}{r^2} + \frac{4\pi l_B}{r^2} \int_R^r r'^2 \sum_{\beta=1}^{n} z_\beta \rho_\beta^\varepsilon (r') dr' - 2.3 w^2 l_B^3 \sum_{\beta=1}^{n} z_\beta \rho_\beta'^\varepsilon + \frac{17}{4} w l_B^3 \sum_{\beta=1}^{n} z_\beta \rho_\beta'^\varepsilon$$

To pursue the calculations we need the relationship between the net charge density $\rho_\pm$ and the potential Ω.

$$\rho_\pm = \sum_{s=1}^{n} z_s \rho_s^\varepsilon = \left(\sum_{s=1}^{n} z_s K_s \rho_s^0\right)\Omega$$

Thus

$$\frac{\rho_\pm'}{\displaystyle\sum_{s=1}^{n} z_s K_s \rho_s^0} = \frac{Z l_B}{r^2} + \frac{4\pi l_B}{r^2} \int_R^r r'^2 \rho_\pm (r') dr' - 2.3 w^2 l_B^3 \rho_\pm' + \frac{17}{4} w l_B^3 \rho_\pm'$$

$$\frac{Z l_B}{r^2} + \frac{4\pi l_B}{r^2} \int_R^r r'^2 \rho_\pm (r') dr' - 2.3 w^2 l_B^3 \rho_\pm' + \frac{17}{4} w l_B^3 \rho_\pm' - \frac{\rho_\pm'}{\displaystyle\sum_{s=1}^{n} z_s K_s \rho_s^0} = 0$$

We introduce a new constant κ; it homogenous to the inverse of a length.

$$\frac{4\pi l_B}{\kappa^2} = \frac{1}{\displaystyle\sum_{s=1}^{n} z_s K_s \rho_s^0} + 2.3 w^2 l_B^3 - \frac{17}{4} w l_B^3$$

The differential equation becomes

144

$$\frac{Zl_B}{r^2} + \frac{4\pi l_B}{r^2} \int\limits_R^r r'^2 \rho_\pm\left(r'\right) dr' - \frac{4\pi l_B}{\kappa^2} \rho_\pm' = 0$$

We substitute the variable u = 1/r in the differential equation.

$$Zl_B u^2 - 4\pi l_B u^2 \int\limits_{1/R}^u \rho_\pm\left(u'\right)\frac{du'}{u'^4} + \frac{4\pi l_B}{\kappa^2} u^2 \frac{d\rho_\pm}{du} = 0$$

$$Zl_B - 4\pi l_B \int\limits_{1/R}^u \rho_\pm\left(u'\right)\frac{du'}{u'^4} + \frac{4\pi l_B}{\kappa^2} \frac{d\rho_\pm}{du} = 0$$

We differentiate once and obtain a second order differential equation.

$$-\frac{4\pi l_B}{u^4} \rho_\pm + \frac{4\pi l_B}{\kappa^2} \frac{d^2\rho_\pm}{du^2} = 0$$

$$\frac{1}{\kappa^2} \frac{d^2\rho_\pm}{du^2} - \frac{1}{u^4} \rho_\pm = 0$$

We reintroduce the variable r = 1/u.

$$\frac{r^2}{\kappa^2} \frac{d}{dr}\left(r^2 \frac{d\rho_\pm}{dr}\right) - r^4 \rho_\pm = 0$$

$$\frac{1}{\kappa^2 r^2} \frac{d}{dr}\left(r^2 \frac{d\rho_\pm}{dr}\right) - \rho_\pm = 0$$

The solution to the differential equation is $\rho_\pm\left(r\right) = A\dfrac{e^{-\kappa r}}{r} + B\dfrac{e^{\kappa r}}{r}$. The boundary conditions

are $\dfrac{d\rho_\pm}{dr}\left(R\right) = \dfrac{\kappa^2 Z}{4\pi R^2}$ and $\rho_\pm\left(r\right)\xrightarrow[r\to+\infty]{}0$. Thus B = 0 and $A = -Z\dfrac{e^{\kappa R}}{4\pi}\dfrac{\kappa^2}{1+\kappa R}$.

Therefore

$$\rho_\pm\left(r\right) = \frac{-Z\kappa^2}{4\pi\left(1+\kappa R\right)} \frac{e^{\kappa\left(R-r\right)}}{r}$$

$$\rho_\pm\left(r\right) = -\frac{Z}{4\pi} \frac{\kappa^2 e^{\kappa R}}{1+\kappa R} \frac{e^{-\kappa r}}{r}$$

The final solution corresponding to high order electrolytes is identical to the solution resulting from the binary electrolytes. The definition of the constant κ is different and absorbs all the physical characteristics of ions, i.e. charges, radii and correlation length. The constant κ is an extended version of the Debye-Hückel parameter.

The number densities are: for α = 1,…, n

$$\rho_\alpha\left(r\right) = \rho_\alpha^0 + \rho_\alpha^\varepsilon\left(r\right) = \rho_\alpha^0 + \frac{K_\alpha \rho_\alpha^0}{\sum\limits_{s=1}^n z_s \rho_s^0 K_s} \rho_\pm\left(r\right)$$

145

$$\rho_\alpha\left(r\right) = \rho_\alpha^0 - \frac{Z}{4\pi} \frac{K_\alpha \rho_\alpha^0}{\sum\limits_{s=1}^{n} z_s \rho_s^0 K_s} \frac{\kappa^2 e^{\kappa R}}{1+\kappa R} \frac{e^{-\kappa r}}{r}$$

The potential Ω is inferred from the expression of the net density $\rho\pm$.

$$\Omega = \rho_\pm \left[\sum_{s=1}^{n} z_s K_s \rho_s^0\right]^{-1} = -\frac{Z}{4\pi}\left[\sum_{s=1}^{n} z_s K_s \rho_s^0\right]^{-1} \frac{\kappa^2 e^{\kappa R}}{1+\kappa R} \frac{e^{-\kappa r}}{r}$$

II   SUMMARY

The initial system consisted of n differential equations with n unknowns, $\rho_1{}^0, \ldots, \rho_n{}^0$.

$$-\frac{Zl_B}{r^2} + \frac{1}{z_\alpha}\left[\frac{\rho_\alpha'}{\rho_\alpha} + \frac{\sum\limits_{s=1}^{n} 8\sigma_s^3 \rho_s'}{1 - \sum\limits_{s=1}^{n} 8\sigma_s^3 \rho_s}\right] - \frac{4\pi l_B}{r^2} \int_R^r r'^2 \sum_{s=1}^{n} z_s \rho_s\left(r'\right) dr'$$
$$+2.3w^2 l_B^3 \sum_{s=1}^{n} z_s \rho_s' - \frac{wl_B^3}{4}\left[-10.58 z_\alpha \sum_{s=1}^{n} z_s^2 \rho_s' + 17\sum_{s=1}^{n} z_s \rho_s'\right] = 0$$

Once the system linearized the potential Ω and the net density $\rho_\pm$ are defined as

$$\Omega = \frac{1}{z_\alpha}\left[\frac{\rho_\alpha^\varepsilon}{\rho_\alpha^0} + \frac{\sum\limits_{s=1}^{n} 8\sigma_s^3 \rho_s^\varepsilon}{1 - \sum\limits_{s=1}^{n} 8\sigma_s^3 \rho_s^0}\right] + \frac{10.58}{4} z_\alpha wl_B^3 \sum_{s=1}^{n} z_s^2 \rho_s^\varepsilon$$

$$\rho_\pm = \sum_{s=1}^{n} z_s \rho_s^\varepsilon$$

The system of n differential equations is reduced to one differential equation.

$$\Omega' = \frac{Zl_B}{r^2} + \frac{4\pi l_B}{r^2} \int_R^r r'^2 \rho_\pm\left(r'\right) dr' - 2.3w^2 l_B^3 \rho_\pm' + \frac{17}{4} wl_B^3 \rho_\pm'$$

The relationship between $\rho_\alpha{}^0$ and Ω is given by

$$\rho_i = \rho_i^0 + \rho_i^\varepsilon \quad \text{and} \quad \rho_i^\varepsilon = \rho_i^0 \cdot K_i \cdot \Omega$$

$$K_i = \frac{z_i + \sum\limits_{s=1}^{c}\left(z_i - z_s\right)\left[u_s - z_i z_s v_s\right] + \sum\limits_{s=1}^{c}\sum\limits_{t=1}^{c} z_s\left(z_i z_s + z_t^2 - z_i^2\right)\left(u_t v_s - u_s v_t\right)}{1 + \sum\limits_{s=1}^{c} u_s + \sum\limits_{s=1}^{c} z_s^2 v_s + \sum\limits_{s=1}^{c}\sum\limits_{t=1}^{c} z_s^2\left(u_t v_s - u_s v_t\right)}$$

146

$$u_i = \frac{\displaystyle\sum_{s=n_0+...+n_{i-1}}^{n_0+...+n_{i-1}+n_i} 8\sigma_s^3 \rho_s^0}{1 - \displaystyle\sum_{s=1}^{n} 8\sigma_s^3 \rho_s^0} \qquad\qquad v_i = \frac{10.58}{4} w l_B^3 \sum_{s=n_0+...+n_{i-1}+1}^{n_0+...+n_{i-1}+n_i} z_s^2 \rho_s^0$$

Next the relationship between the net density and the potential is

$$\rho_\pm = \sum_{s=1}^{n} z_s \rho_s^\varepsilon = \left(\sum_{s=1}^{n} z_s K_s \rho_s^0 \right) \Omega$$

Last the solution to the differential equation is

$$\rho_\pm(r) = -\frac{Z}{4\pi} \frac{\kappa^2 e^{\kappa R}}{1+\kappa R} \frac{e^{-\kappa r}}{r} \qquad\qquad \rho_\alpha(r) = \rho_\alpha^0 - \frac{Z}{4\pi} \frac{K_\alpha \rho_\alpha^0}{\displaystyle\sum_{s=1}^{n} z_s \rho_s^0 K_s} \frac{\kappa^2 e^{\kappa R}}{1+\kappa R} \frac{e^{-\kappa r}}{r}$$

III   OSMOTIC COEFFICIENT

We again seek to compute the rational osmotic coefficient given by the scale of McMillan and Mayer. The rational osmotic coefficient is denoted by ϕ. It is defined from the osmotic pressure Π.

$$\phi = \frac{\Pi}{\left(\displaystyle\sum_{i=1}^{n} \rho_i^0 \right) k_B T}$$

From the integral theory of liquids we have the following formula:

$$\phi = 1 - \frac{2\pi}{3 \left(\displaystyle\sum_{s=1}^{n} \rho_s^0 \right) k_B T} \sum_{i=1}^{n} \sum_{j=1}^{n} \rho_i^0 \rho_j^0 \int_0^{+\infty} \frac{\partial u_{ij}}{\partial r} g_{ij}(r) r^3 dr$$

The summation over the two indices has n^2 combinations. The two functions to be integrated are:

- u_{ij} = potential of the interaction between a central ion of species i and the surrounding ions of species j

$$\frac{u_{ij}}{k_B T} = \begin{vmatrix} +\infty \; for \; r < \lambda_i \\ z_i z_j \dfrac{l_B}{r} \; for \; r \geq \lambda_i \end{vmatrix}$$

- g_{ij} = correlation function between a central ion of species i and the surrounding ions of species j

$$g_{ij} = \begin{vmatrix} 0 \; for \; r < \lambda_i \\ 1 - \dfrac{z_i}{4\pi} \dfrac{K_j}{\displaystyle\sum_{s=1}^{n} z_s \rho_s^0 K_s} \dfrac{\kappa^2 e^{\kappa \sigma_i}}{1+\kappa \sigma_i} \dfrac{e^{-\kappa r}}{r} \; for \; r \geq \lambda_i \end{vmatrix}$$

147

λ_i is the distance of closest approach to ion i. $g_{ij} = 0$ for $r < \lambda_i$ because two ions cannot be closer than λ_i.

In the calculations below we introduce the step function of Heaviside Hv(.) and the delta function of Dirac δ(.).

$$\phi = 1 - \frac{2\pi}{3\left(\sum\limits_{s=1}^{n} \rho_s^0\right) k_B T} \sum_{i=1}^{n}\sum_{j=1}^{n} \rho_i^0 \rho_j^0 \int_0^{+\infty} \frac{\partial u_{ij}}{\partial r} g_{ij}(r) r^3 dr$$

$$\phi = 1 - \frac{2\pi}{3\sum\limits_{s=1}^{n} \rho_s^0} \sum_{i=1}^{n}\sum_{j=1}^{n} \rho_i^0 \rho_j^0 \int_0^{+\infty} -\frac{\partial}{\partial r}\left[e^{\frac{u_{ij}}{k_B T}} \right] e^{\frac{u_{ij}}{k_B T}} g_{ij}(r) r^3 dr$$

$$\phi = 1 - \frac{2\pi}{3\sum\limits_{s=1}^{n} \rho_s^0} \sum_{i=1}^{n}\sum_{j=1}^{n} \rho_i^0 \rho_j^0 \int_0^{+\infty} -\frac{\partial}{\partial r}\left[Hv(r - \lambda_i) e^{-z_i z_j \frac{l_B}{r}} \right] e^{\frac{u_{ij}}{k_B T}} g_{ij}(r) r^3 dr$$

$$\phi = 1 + \frac{2\pi}{3\sum\limits_{s=1}^{n} \rho_s^0} \sum_{i=1}^{n}\sum_{j=1}^{n} \rho_i^0 \rho_j^0 \int_0^{+\infty} \left[z_i z_j \frac{l_B}{r^2} Hv(r - \lambda_i) e^{-z_i z_j \frac{l_B}{r}} + \delta(r - \lambda_i) e^{-z_i z_j \frac{l_B}{r}} \right] e^{\frac{u_{ij}}{k_B T}} g_{ij}(r) r^3 dr$$

$$\phi = 1 + \frac{2\pi}{3\sum\limits_{s=1}^{n} \rho_s^0} \sum_{i=1}^{n}\sum_{j=1}^{n} \rho_i^0 \rho_j^0 \left[\begin{array}{l} \int\limits_{\lambda_i}^{+\infty} z_i z_j \frac{l_B}{r^2} e^{-z_i z_j \frac{l_B}{r}} \times e^{z_i z_j \frac{l_B}{r}} g_{ij}(r) r^3 dr + \\[2ex] \int\limits_0^{+\infty} \delta(r - \lambda_i) e^{-z_i z_j \frac{l_B}{r}} \times e^{\frac{u_{ij}}{k_B T}} g_{ij}(r) r^3 dr \end{array} \right]$$

$$\phi = 1 + \frac{2\pi}{3\sum\limits_{s=1}^{n} \rho_s^0} \sum_{i=1}^{n}\sum_{j=1}^{n} \rho_i^0 \rho_j^0 \left[z_i z_j l_B \int\limits_{\lambda_i}^{+\infty} g_{ij}(r) r dr + g_{ij}(\lambda_i) \lambda_i^3 \right]$$

The two pieces are calculated separately.

- $$g_{ij}(\lambda_i)\lambda_i^3 = \lambda_i^3 \left(1 - \frac{z_i}{4\pi} \frac{K_j}{\sum\limits_{s=1}^{n} z_s \rho_s^0 K_s} \frac{\kappa^2 e^{\kappa \sigma_i}}{1 + \kappa \sigma_i} \frac{e^{-\kappa \lambda_i}}{\lambda_i} \right) = \lambda_i^3 - \frac{z_i}{4\pi} \frac{K_j}{\sum\limits_{s=1}^{n} z_s \rho_s^0 K_s} \frac{\kappa^2 \lambda_i^2}{1 + \kappa \sigma_i} e^{-\kappa(\lambda_i - \sigma_i)}$$

- $$\int\limits_{\lambda_i}^{+\infty} g_{ij}(r) r dr = \int\limits_{\lambda_i}^{+\infty} \left(1 - \frac{z_i}{4\pi} \frac{K_j}{\sum\limits_{s=1}^{n} z_s \rho_s^0 K_s} \frac{\kappa^2 e^{\kappa \sigma_i}}{1 + \kappa \sigma_i} \frac{e^{-\kappa r}}{r} \right) r dr$$

$$\int\limits_{\lambda_i}^{+\infty} g_{ij}(r) r dr = \lim_{\varsigma \to +\infty} \int\limits_{\lambda_i}^{\varsigma} r dr - \frac{z_i}{4\pi} \frac{K_j}{\sum\limits_{s=1}^{n} z_s \rho_s^0 K_s} \frac{\kappa^2 e^{\kappa \sigma_i}}{1 + \kappa \sigma_i} \int\limits_{\lambda_i}^{+\infty} e^{-\kappa r} dr$$

148

$$\int_{\lambda_i}^{+\infty} g_{ij}(r)r\,dr = Lim - \frac{z_i}{4\pi} \frac{K_j}{\sum_{s=1}^{n} z_s \rho_s^0 K_s} \frac{\kappa^2 e^{\kappa\sigma_i}}{1+\kappa\sigma_i} \frac{e^{-\kappa\lambda_i}}{\kappa} = Lim - \frac{z_i}{4\pi} \frac{K_j}{\sum_{s=1}^{n} z_s \rho_s^0 K_s} \frac{\kappa e^{\kappa(\sigma_i-\lambda_i)}}{1+\kappa\sigma_i}$$

Thus

$$\phi = 1 + \frac{2\pi}{3\sum_{s=1}^{n}\rho_s^0} \sum_{i=1}^{n} \lambda_i^3 \rho_i^0 \times \sum_{j=1}^{n} \rho_j^0 - \frac{2\pi}{3\sum_{s=1}^{n}\rho_s^0} \left(\sum_{i=1}^{n} \frac{z_i \rho_i^0}{4\pi} \frac{\kappa^2 \lambda_i^2}{1+\kappa\sigma_i} e^{-\kappa(\lambda_i-\sigma_i)} \right) \frac{\sum_{j=1}^{n} K_j \rho_j^0}{\sum_{s=1}^{n} z_s K_s \rho_s^0}$$

$$+ \frac{2\pi l_B Lim}{3\sum_{s=1}^{n}\rho_s^0} \left(\sum_{i=1}^{n} z_i \rho_i^0 \right)^2 - \frac{2\pi \kappa l_B}{3\sum_{s=1}^{n}\rho_s^0} \frac{1}{\sum_{s=1}^{n} z_s \rho_s^0 K_s} \left(\sum_{i=1}^{n} \frac{z_i^2 \rho_i^0}{4\pi} \frac{e^{\kappa(\sigma_i-\lambda_i)}}{1+\kappa\sigma_i} \right) \left(\sum_{j=1}^{n} z_j K_j \rho_j^0 \right)$$

The solution is electroneutral, i.e. $\sum_{i=1}^{n} z_i \rho_i^0 = 0$, which eliminates the term with an infinite value. The expression of the osmotic coefficient can be simplified to

$$\boxed{\phi = 1 + \frac{2\pi}{3}\sum_{i=1}^{n} \lambda_i^3 \rho_i^0 - \frac{\kappa l_B}{6\sum_{i=1}^{n}\rho_i^0} \left(\sum_{i=1}^{n} z_i^2 \rho_i^0 \frac{e^{-\kappa(\lambda_i-\sigma_i)}}{1+\kappa\sigma_i} \right) - \frac{\kappa^2}{6\sum_{i=1}^{n}\rho_i^0} \frac{\sum_{i=1}^{n} K_i \rho_i^0}{\sum_{i=1}^{n} z_i K_i \rho_i^0} \left(\sum_{i=1}^{n} \frac{z_i \lambda_i^2 \rho_i^0}{1+\kappa\sigma_i} e^{-\kappa(\lambda_i-\sigma_i)} \right)}$$

IV   MEAN IONIC ACTIVITY COEFFICIENT

The mean ionic activity coefficient can be calculated using the integral theory of liquids from the following expression:

$$k_B T \ln \gamma_\pm = \frac{1}{\sum_{s=1}^{n}\rho_s^0} \sum_{i=1}^{n} \sum_{j=1}^{n} \rho_i^0 \rho_j^0 \int_{\zeta=0}^{1} \int_{\xi=0}^{1} \int_{r=0}^{+\infty} u_{ij}(r) g_{ij}(r;\xi,\zeta) 4\pi r^2\, dr\, d\xi\, d\zeta$$

There are n^2 combinations 'ij'. The two functions to be integrated are the same as for the osmotic coefficient:

- u_{ij} = potential of the interaction between a central ion of species i and the surrounding ions of species j

$$\frac{u_{ij}}{k_B T} = \begin{vmatrix} +\infty \; for \; r < \lambda_i \\ z_i z_j \dfrac{l_B}{r} \; for \; r \geq \lambda_i \end{vmatrix}$$

149

- g_{ij} = correlation function between a central ion of species i and the surrounding ions of species j

$$g_{ij} = \left| \begin{array}{l} 0 \text{ for } r < \lambda_i \\ \\ 1 - \dfrac{\zeta \cdot z_i}{4\pi} \dfrac{K_j}{\displaystyle\sum_{s=1}^{n} z_s \rho_s^0 K_s} \dfrac{\kappa^2 e^{\xi \cdot \kappa \sigma_i}}{1 + \xi \cdot \kappa \sigma_i} \dfrac{e^{-\kappa r}}{r} \text{ for } r \geq \xi \cdot \lambda_i \end{array} \right.$$

The two parameters, ξ and ζ, are used to describe the progressive introduction of the central ion in the solution; ξ describes the introduction of a hard sphere of radius σ_i and ζ describes the charging from 0 to z_i.

λ_i is again the distance of closest approach to an ion of species i. We have $g_{ij} = 0$ for $r < \lambda_i$ because two ions cannot be closer than allowed by the distance of closest approach. Thus the product $u_{ij} \cdot g_{ij}$ is undefined for $r < \lambda_i$; we assign the value 4 to the product $u_{ij} \cdot g_{ij}$ in order to recover the usual term representing the excluded volume of a hard sphere.

$$I_{ij} = \int_{\zeta=0}^{1} \int_{\xi=0}^{1} \int_{r=0}^{+\infty} u_{ij}(r) g_{ij}(r;\xi,\zeta) 4\pi r^2 dr d\xi d\zeta$$

$$I_{ij} = \int_{\zeta=0}^{1} \int_{\xi=0}^{1} \int_{r=0}^{\xi \cdot \lambda_i} 16\pi r^2 dr d\xi d\zeta + \int_{\zeta=0}^{1} \int_{\xi=0}^{1} \int_{r=\xi \cdot \lambda_i}^{+\infty} \frac{z_i z_j l_B}{r} \left(1 - \frac{\zeta \cdot z_i}{4\pi} \frac{K_j}{\displaystyle\sum_{s=1}^{n} z_s \rho_s^0 K_s} \frac{\kappa^2 e^{\xi \cdot \kappa \sigma_i}}{1 + \xi \cdot \kappa \sigma_i} \frac{e^{-\kappa r}}{r} \right) 4\pi r^2 dr d\xi d\zeta$$

$$I_{ij} = \int_{\zeta=0}^{1} \int_{\xi=0}^{1} \frac{16\pi}{3} \lambda_i^3 \xi^3 d\xi d\zeta + 4\pi l_B z_i z_j \int_{\zeta=0}^{1} \int_{\xi=0}^{1} \int_{r=\xi \cdot \lambda_i}^{+\infty} \left(r - \frac{\zeta \cdot z_i}{4\pi} \frac{K_j}{\displaystyle\sum_{s=1}^{n} z_s \rho_s^0 K_s} \frac{\kappa^2 e^{\xi \cdot \kappa \sigma_i}}{1 + \xi \cdot \kappa \sigma_i} e^{-\kappa r} \right) dr d\xi d\zeta$$

$$I_{ij} = \int_{\zeta=0}^{1} \frac{4\pi}{3} \lambda_i^3 d\zeta + 4\pi l_B z_i z_j \int_{r=\xi \cdot \lambda_i}^{+\infty} r dr - 4\pi l_B z_i z_j \int_{\zeta=0}^{1} \int_{\xi=0}^{1} \int_{r=\xi \cdot \lambda_i}^{+\infty} \frac{\zeta \cdot z_i}{4\pi} \frac{K_j}{\displaystyle\sum_{s=1}^{n} z_s \rho_s^0 K_s} \frac{\kappa^2 e^{\xi \cdot \kappa \sigma_i}}{1 + \xi \cdot \kappa \sigma_i} e^{-\kappa r} dr d\xi d\zeta$$

$$I_{ij} = \frac{4\pi}{3} \lambda_i^3 + 4\pi l_B z_i z_j \int_{r=\xi \cdot \lambda_i}^{+\infty} r dr - \frac{l_B z_i^2 z_j K_j}{\displaystyle\sum_{s=1}^{n} z_s \rho_s^0 K_s} \int_{\zeta=0}^{1} \int_{\xi=0}^{1} \zeta \frac{\kappa e^{\xi \cdot \kappa \sigma_i}}{1 + \xi \cdot \kappa \sigma_i} e^{-\xi \cdot \kappa \lambda_i} d\xi d\zeta$$

$$I_{ij} = \frac{4\pi}{3} \lambda_i^3 + 4\pi l_B z_i z_j \int_{r=\xi \cdot \lambda_i}^{+\infty} r dr - \frac{l_B z_i^2 z_j K_j}{\displaystyle\sum_{s=1}^{n} z_s \rho_s^0 K_s} \int_{\xi=0}^{1} \frac{1}{2} \frac{\kappa e^{\xi \cdot \kappa (\sigma_i - \lambda_i)}}{1 + \xi \cdot \kappa \sigma_i} d\xi$$

$$I_{ij} = \frac{4\pi}{3} \lambda_i^3 + 4\pi l_B z_i z_j \int_{r=\xi \cdot \lambda_i}^{+\infty} r dr - \frac{l_B z_i^2 z_j K_j}{\displaystyle\sum_{s=1}^{n} z_s \rho_s^0 K_s} \frac{e^{\frac{\lambda_i}{\sigma_i}-1}}{2\sigma_i} \left[Ei\left(\frac{\lambda_i}{\sigma_i} - 1\right) - Ei\left((1 + \kappa\sigma_i)\left(\frac{\lambda_i}{\sigma_i} - 1\right)\right) \right]$$

150

Thus we find the mean ionic activity coefficient

$$\ln \gamma_\pm = \frac{1}{\sum\limits_{s=1}^{n} \rho_s^0} \sum_{i=1}^{n} \sum_{j=1}^{n} \rho_i^0 \rho_j^0 I_{ij}$$

$$\ln \gamma_\pm = \frac{4\pi}{3} \sum_{i=1}^{n} \lambda_i^3 \rho_i^0 - \frac{l_B}{\sum\limits_{s=1}^{n} \rho_s^0} \sum_{i=1}^{n} z_i^2 \rho_i^0 \frac{e^{\frac{\lambda_i}{\sigma_i}-1}}{2\sigma_i} \left[Ei\left(\frac{\lambda_i}{\sigma_i}-1\right) - Ei\left((1+\kappa\sigma_i)\left(\frac{\lambda_i}{\sigma_i}-1\right)\right) \right]$$

$Ei(.)$ is the exponential integral and is defined as $Ei(x) = \int\limits_{x}^{+\infty} \frac{e^{-t}}{t} dt$.

The second term is eliminated because the solution is electroneutral i.e. $\sum\limits_{i=1}^{n} z_i \rho_i^0 = 0$. The

expression of $\gamma_\pm$ can be simplified using an approximation for the exponential integral.

$$Ei(x) = e^{-x} \ln\left[1 + e^{-\gamma}\left(\frac{1}{x} + \frac{1}{2\sqrt{x}} \right) \right]$$

In this expression $\gamma = 0.577215665$ is the Euler-Mascheroni constant.

$$e^{\frac{\lambda_i}{\sigma_i}-1} Ei\left(\frac{\lambda_i}{\sigma_i}-1\right) = \ln\left[1 + e^{-\gamma}\left(\frac{\sigma_i}{\lambda_i - \sigma_i} + \frac{1}{2}\sqrt{\frac{\sigma_i}{\lambda_i - \sigma_i}} \right) \right]$$

$$e^{\frac{\lambda_i}{\sigma_i}-1} Ei\left((1+\kappa\sigma_i)\left(\frac{\lambda_i}{\sigma_i}-1\right)\right) = e^{-\kappa(\lambda_i-\sigma_i)} \ln\left[1 + e^{-\gamma}\left(\frac{\sigma_i}{(1+\kappa\sigma_i)(\lambda_i - \sigma_i)} + \frac{1}{2}\sqrt{\frac{\sigma_i}{(1+\kappa\sigma_i)(\lambda_i - \sigma_i)}} \right) \right]$$

The final formula for the mean ionic activity coefficient of an aqueous solution containing small ions is

$$\ln \gamma_\pm = \frac{4\pi}{3} \sum_{i=1}^{n} \lambda_i^3 \rho_i^0 - \frac{1}{2} \frac{l_B}{\sum\limits_{s=1}^{n} \rho_s^0} \sum_{i=1}^{n} \frac{z_i^2 \rho_i^0}{\sigma_i} \ln\left[1 + e^{-\gamma}\left(\frac{\sigma_i}{\lambda_i - \sigma_i} + \frac{1}{2}\sqrt{\frac{\sigma_i}{\lambda_i - \sigma_i}} \right) \right]$$

$$+ \frac{1}{2} \frac{l_B}{\sum\limits_{s=1}^{n} \rho_s^0} \sum_{i=1}^{n} \frac{z_i^2 \rho_i^0}{\sigma_i} e^{-\kappa(\lambda_i-\sigma_i)} \ln\left[1 + e^{-\gamma}\left(\frac{\sigma_i}{(1+\kappa\sigma_i)(\lambda_i - \sigma_i)} + \frac{1}{2}\sqrt{\frac{\sigma_i}{(1+\kappa\sigma_i)(\lambda_i - \sigma_i)}} \right) \right]$$

V   COMPARISON WITH EXPERIMENTAL DATA

The new theory of ionic solutions provides general expressions for the net charge density, the potential, the osmotic coefficient and the mean ionic activity coefficient for any solution containing small ions. The theory has been shown to be accurate for solutions of binary electrolytes and it is now tested against experimental data on solutions containing more than two species of small ions. However experimental data on the osmotic coefficient, the mean ionic activity coefficient and the relative permittivity for mixtures of electrolytes is much less abundant than for binary electrolytes and there is no major compilation of data that has been

151

reviewed and criticized. Therefore the comparison of the theory with experimental data has focused on three areas:

- direct comparison for the osmotic coefficient and the mean ionic activity coefficient of seawater
- comparison of solubility limits of one binary electrolyte in a solution of another; for instance solubility limit of NaCl in a solution of KCl
- improved prediction of the osmotic coefficient and mean ionic activity coefficient of binary electrolytes that do not completely dissociate; for example $ZnCl_2$ dissociates in Zn^{2+}, Cl^-, $(ZnCl)^+$ and other minor ions of the form $(ZnCl_n)^{2-n}$

V.1 Seawater

Seawater has been studied by oceanographers for decades so a large amount of experimental data is available for both the osmotic coefficient and the mean ionic activity coefficient [115,116,117]. Here it is modeled as an aqueous solution with 8 major ions: Na^+, K^+, Mg^{2+}, Ca^{2+}, Cl^-, Br^-, HCO_3^- and SO_4^{2-}. The reference seawater has salinity S = 35 ‰ and its composition is given below [117].

Table 4: Composition of reference seawater

Ion	Concentration (mol/kg water)
Na^+	0.83733
K^+	0.01822
Mg^{2+}	0.09429
Ca^{2+}	0.01836
Cl^-	0.97521
Br^-	0.00150
HCO_3^-	0.00332
SO_4^{2-}	0.05042

Other ions are present but their concentrations are less than 1 mmol/kg water and are neglected. For seawater the relationships between the salinity S (‰) and the molality and ionic strength in mol/kg are [117]:

$$m = \frac{16.0030 \cdot S}{1000 - 1.00488 \cdot S}$$

$$I = \frac{19.9201 \cdot S}{1000 - 1.00488 \cdot S}$$

The concentrations of ions in mol/kg are taken to change linearly with the salinity. Experimental data is available for salinities ranging from 5 ‰ to 120 ‰ for the osmotic coefficient and from 5 ‰ to 40 ‰ for the activity coefficient. The density of reference seawater at salinity S = 35 ‰ and 25°C is 1.026; because more data on the density of seawater mixtures could not be found, the density is taken to be simply an affine function of salinity

$$d = 0.997 + 1.026 \frac{S}{35}$$

152

No data on the relative permittivity of seawater was found so the permittivity of seawater was taken to be the permittivity of a solution of sodium chloride with the same ionic strength. The experimental data for the osmotic coefficient and for the mean ionic activity are successfully reproduced using the formulae derived above.
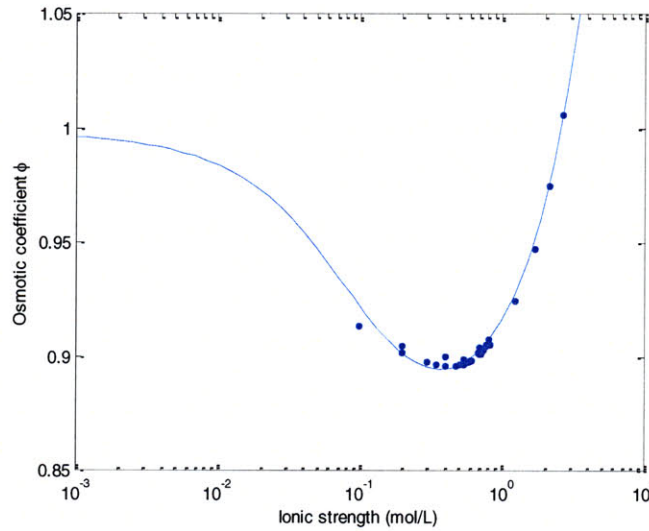
Figure 215: Osmotic coefficient of seawater at 25ºC
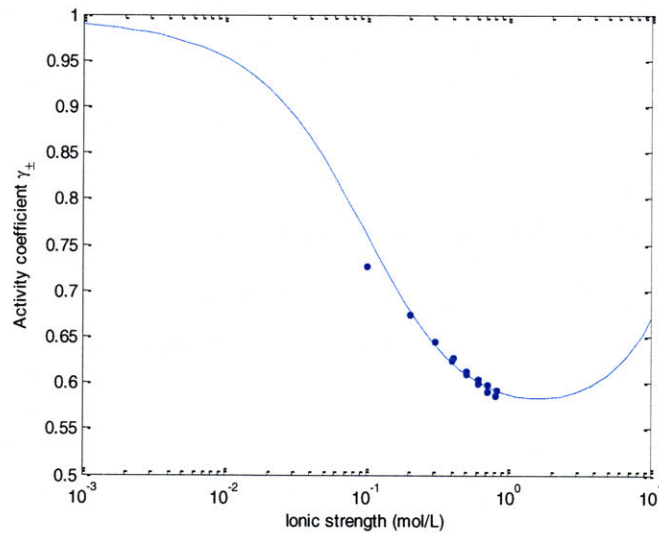
Figure 216: Mean ionic activity coefficient of seawater at 25ºC

Note that seawater can be considered as an electrolyte with charge z = 1.2457 [116] and the corresponding Debye-Hückel law in dilute solutions is, with A = 1.171 $(L/mol)^{1/2}$:

$$\ln \gamma_{\pm} = -1.2457 A \sqrt{I} \qquad \phi = 1 - 1.2457 \frac{A}{3} \sqrt{I}$$

This first comparison with experimental data suggests that ionic solutions containing more than two ionic species behave essentially the same as binary electrolytes and that the

formulae for the osmotic coefficient and the mean ionic activity coefficient are similarly accurate.

V.2 Solubility limits

The main criticism against the comparison with experimental data on seawater is that it tests the formulae on a single dimension for a solution with 8 ions. Unfortunately there is very little data on the ionic activity coefficient or osmotic coefficient of mixtures of electrolytes XY and AB with the concentrations of XY and AB varying independently. So another way for testing the accuracy of the formulae for the mean ionic activity coefficient is to determine the solubility limit of electrolyte XY in a solution containing electrolyte AB at a given concentration [16].

In a nutshell computing the solubility limit of XY in AB is tantamount to solving a complicated non-linear equation with a single unknown m_{XY} for a given m_{AB}.

The situation consists of AB and XY being dissolved and yielding ions A, B, X, Y.

$$m_A = \nu_A m_{AB} \qquad m_B = \nu_B m_{AB} \qquad m_X = \nu_X m_{XY} \qquad m_Y = \nu_Y m_{XY}$$

For an aqueous solution containing ions A, B, X, Y, the precipitate $X_xY_y{\cdot}(H_2O)_h$ forms through the reaction

$$xX + yY + hH_2O \rightleftarrows X_xY_y \cdot \left(H_2O\right)_h$$
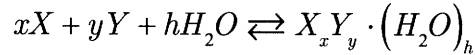
Therefore the solubility product K is

$$K = \left(\gamma_X m_X\right)^x \left(\gamma_Y m_Y\right)^y a_{H_2O}^h$$

γ_X and γ_Y are the individual ionic activity coefficients. m_X and m_Y are the molalities of each ion. h is the hydration number; h = 0 for anhydrous precipitates. The solubility product can be rewritten as

$$\ln K = x\ln\gamma_X + y\ln\gamma_Y + x\ln m_X + y\ln m_Y + h\ln a_{H_2O}$$

The value of the solubility product is calculated from the Gibbs free energy of reaction, which in turn is calculated from the standard Gibbs free energies of formation.

$$RT\ln K = -\Delta G_{RXN}^0 = xG_X^0 + yG_Y^0 + hG_{H_2O}^0 - G_{X_xY_y\cdot(H_2O)_h}^0$$

The activity of water is calculated from the practical osmotic coefficient, which in turn is related to the rational osmotic coefficient.

$$\ln a_{H_2O} = -\frac{M_{water}\sum\limits_{ions} m_i}{1000}\phi_{practical} \qquad \phi_{practical} = \left(1 - \sum\limits_{solutes} C_s \bar{V}_s\right)\phi_{rational}$$

M_{water} = 18.015 g/mol is the molar mass of water; m_i is the molality of ionic species "i"; C_s is the molarity of solute s; $\bar{V}_s$ is the partial molar volume of solute s.

Furthermore the partial molar volumes can be computed from the density of the solution which is given in the literature as a function of the molarity, $d = f(C_1,...,C_n)$. M_i's are the molar masses of the solutes or ions and n_i's the number of moles present in volume Vol.

$$d = \frac{1}{\rho_w}\left[C_s M_s + C_{water}M_{water} + \sum\limits_{i\neq s} C_i M_i\right]$$

154

$$d = \frac{1}{\rho_w Vol}\left[n_s M_s + n_{water} M_{water} + \sum_{i \neq s} n_i M_i\right]$$

$$\frac{\partial d}{\partial n_s} = \frac{M_s}{\rho_w Vol} - \frac{1}{\rho_w}\frac{1}{Vol^2}\frac{\partial Vol}{\partial n_s}\left[n_s M_s + n_{water} M_{water} + \sum_{i \neq s} n_i M_i\right]$$

$$\frac{\partial d}{\partial n_s} = \frac{M_s}{\rho_w Vol} - \frac{\bar{V}_s}{Vol}d$$

In parallel

$$\frac{\partial d}{\partial n_s} = \frac{\partial d}{\partial C_s}\frac{\partial C_s}{\partial n_s} = \frac{\partial d}{\partial C_s}\frac{\partial}{\partial n_s}\left(\frac{n_s}{Vol}\right) = \frac{\partial d}{\partial C_s}\left(\frac{1}{Vol} - \frac{n_s \bar{V}_s}{Vol^2}\right) = \frac{\partial d}{\partial C_s}\left(\frac{1}{Vol} - \frac{\bar{V}_s}{Vol}C_s\right)$$

Thus

$$\frac{\partial d}{\partial C_s}\left(\frac{1}{Vol} - \frac{\bar{V}_s}{Vol}C_s\right) = \frac{M_s}{\rho_w Vol} - \frac{\bar{V}_s}{Vol}d$$

$$\frac{\partial d}{\partial C_s}\left(1 - \bar{V}_s C_s\right) = \frac{M_s}{\rho_w} - \bar{V}_s d$$

$$\bar{V}_s\left(d - C_s\frac{\partial d}{\partial C_s}\right) = \frac{M_s}{\rho_w} - \frac{\partial d}{\partial C_s}$$

$$\bar{V}_s = \frac{\dfrac{M_s}{\rho_w} - \dfrac{\partial d}{\partial C_s}}{d - C_s\dfrac{\partial d}{\partial C_s}}$$

Furthermore

$$1 - C_s \bar{V}_s = 1 - \frac{\dfrac{C_s M_s}{\rho_w} - C_s\dfrac{\partial d}{\partial C_s}}{d - C_s\dfrac{\partial d}{\partial C_s}} = \frac{d - \dfrac{C_s M_s}{\rho_w}}{d - C_s\dfrac{\partial d}{\partial C_s}}$$

Finally

$$\phi_{practical} = \frac{d - \dfrac{C_s M_s}{\rho_w}}{d - C_s\dfrac{\partial d}{\partial C_s}}\phi_{rational}$$

Another piece of the puzzle is the relationship between the molalities and molarities of ions.

$$c_i = \frac{1000 \cdot d \cdot m_i}{1000 + \sum_{j=1}^{n} m_j M_j}$$

155

The calculations involving the ionic activity coefficients and the osmotic coefficient are performed in molarities and the calculations involving the solubility constant are performed using molalities.

The last difficulty is to calculate the density and permittivity of solutions containing AB and XY from the available data on the density of solutions containing only AB and only XY. A simple and reasonable method is used. For the density determine $\hat{C}_{AB}$ and $\hat{C}_{XY}$ the concentrations of pure AB and pure XY such that the total number of moles in the pure solutions is equal to the total number of moles in the mixture. Then

$$d_{r,mix} = \frac{C_{AB}d_{r,AB}\left(\hat{C}_{AB}\right) + C_{XY}d_{r,XY}\left(\hat{C}_{XY}\right)}{C_{AB} + C_{XY}}$$

For the permittivity determine $\hat{C}_{AB}$ and $\hat{C}_{XY}$, the concentrations of pure AB and pure XY such that the ionic strength on molar fraction basis of the pure solutions is equal to the ionic strength on a molar fraction of the mixture. Then

$$\varepsilon_{r,mix} = \frac{C_{AB}\varepsilon_{r,AB}\left(\hat{C}_{AB}\right) + C_{XY}\varepsilon_{r,XY}\left(\hat{C}_{XY}\right)}{C_{AB} + C_{XY}}$$

The data on the Gibbs free energies of formation is taken from references [16,21]. The data on the solubility limits is taken from reference [16]. The data on the densities is taken from reference [20].

The numerical computations were done as described in the diagram below.
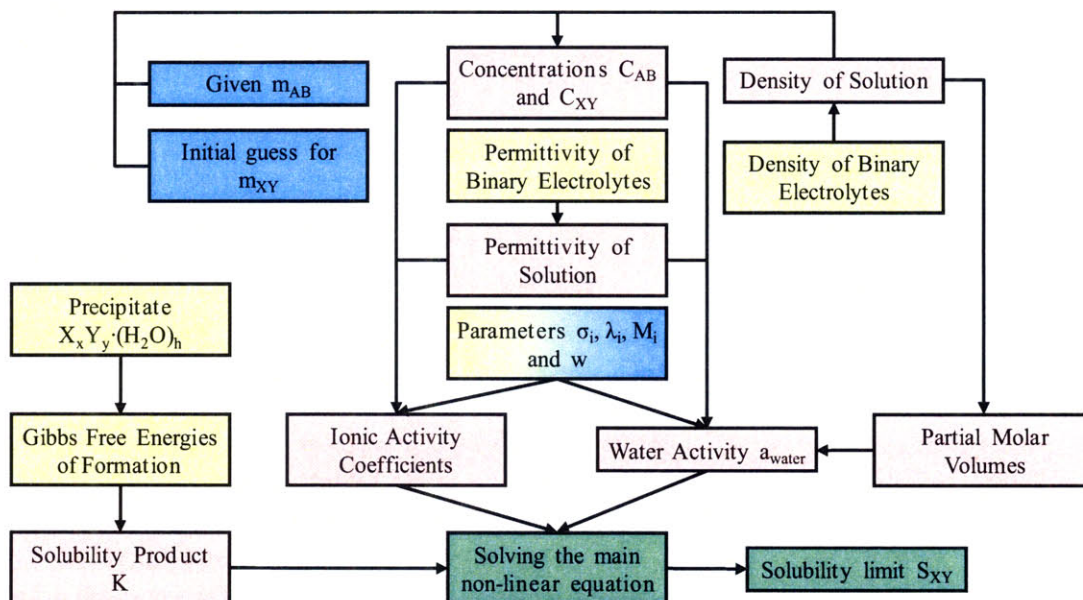
Figure 217: Computation of the solubility limit of binary electrolyte XY in a solution of binary electrolyte AB at a given concentration – yellow = data from literature, blue = variable parameters, purple = main intermediaries in calculations, green = main calculation and output

156

V.2.1 Solubility of sodium chloride and potassium chloride in hydrochloric acid

The first two systems for which calculations were performed are simple. They are ternary mixtures of monovalent ions; only one precipitate may form; the precipitate is anhydrous [16]. The correlation parameter w and the three hydrated radii were adjusted to fit experimental data. The results are shown below.
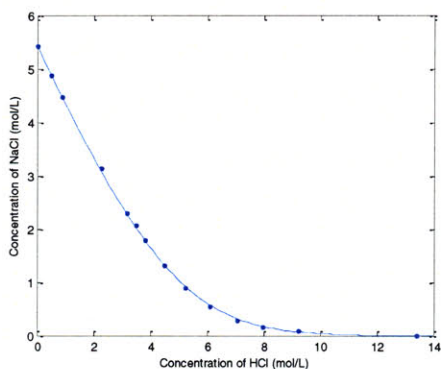
Figure 218: Solubility limit of NaCl in HCl-H₂O – normal scale
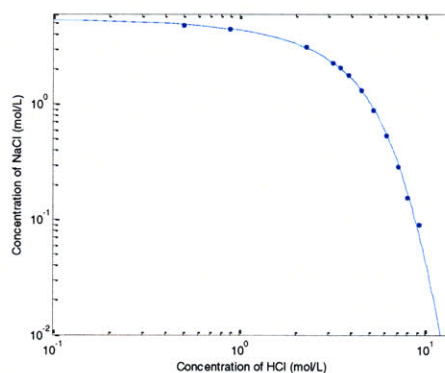
Figure 219: Solubility limit of NaCl in HCl-H₂O – logarithmic scale
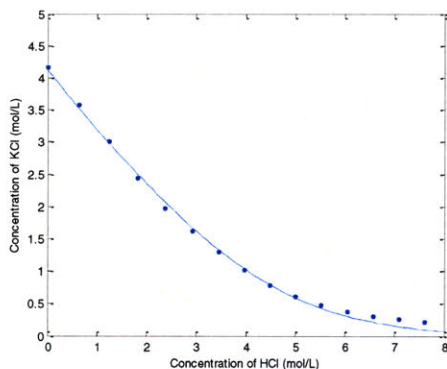
Figure 220: Solubility limit of KCl in HCl-H₂O – normal scale
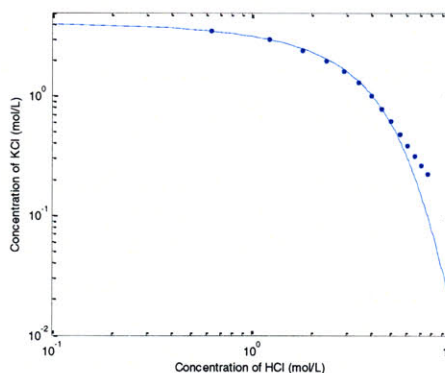
Figure 221: Solubility limit of KCl in HCl-H₂O – logarithmic scale

Hence the equations appear to be able to reproduce experimental data quite well in these simple cases.

V.2.2 Solubility in aqueous mixtures of sodium and potassium chloride

The third system studied added more complexity. It is again a ternary mixture of monovalent ions but two precipitates may form, NaCl or KCl; both precipitates are anhydrous [16]. Again the correlation parameter w and the three hydrated radii were adjusted to fit experimental data.
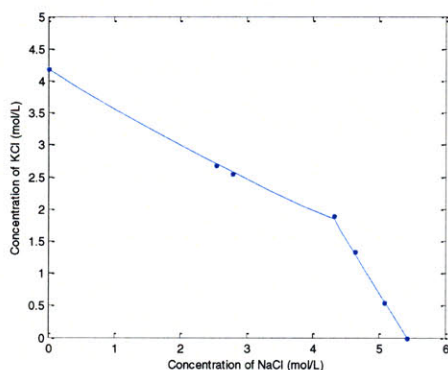
Figure 222: Solubility limits of KCl and NaCl in aqueous mixtures of KCl and NaCl– normal scale
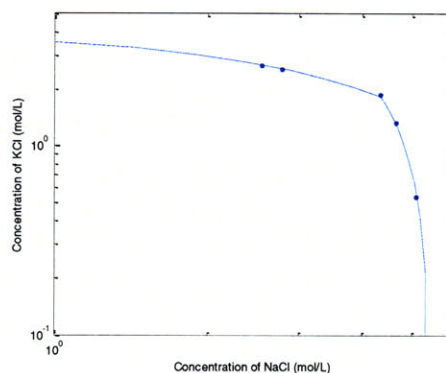
Figure 223: Solubility limits of KCl and NaCl in aqueous mixtures of KCl and NaCl – logarithmic scale

The equations appear to reproduce experimental data well. However two sets of parameters are needed. Each set contains four adjustable parameters and is fitted over four points therefore in this case experimental data is reproduced through mere exact fitting. Nevertheless the potassium-sodium-chlorine system does not exhibit eccentric behavior so additional experimental points should fall close to the predicted line. Thus this system confirms the accuracy of the formulae for the ionic activity coefficients and of the underlying theory even though experimental data is insufficient.

V.2.3 Solubility in aqueous mixtures of potassium and calcium chloride

The fourth example is a ternary mixture of a divalent cation and two monovalent ions. Two precipitates may form; one is anhydrous, KCl, the other contains six molecules of water, $CaCl_2 \cdot (H_2O)_6$ [16]. Experimental data was fit with two sets of four parameters. One set of parameters covers the range $C_{KCl} < 0.1$ mol/L and the other set the range $C_{KCl} > 0.1$ mol/L. The first range is almost insignificant.
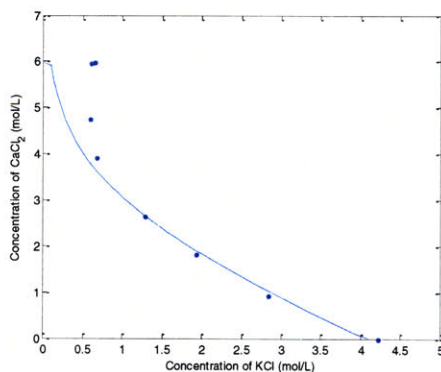
Figure 224: Solubility limits of $CaCl_2 \cdot (H_2O)_6$ and KCl in aqueous mixtures of $CaCl_2$ and KCl – normal scale
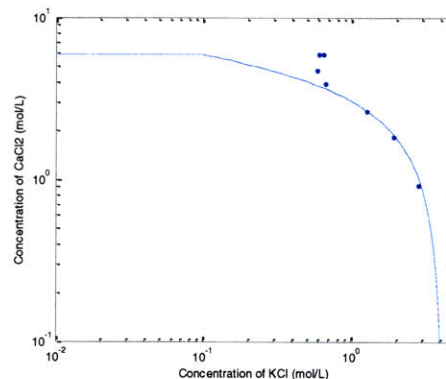
Figure 225: Solubility limits of $CaCl_2 \cdot (H_2O)_6$ and KCl in aqueous mixtures of $CaCl_2$ and KCl – log. scale

Calculations were much more difficult than previously because the system was much more sensitive to the initial conditions both for the molality and for the parameters. Experimental

data is reproduced well only when $C_{KCl} > 1$ mol/L; experimental data cannot be reproduced at all when $CaCl_2 \cdot (H_2O)_6$ precipitates.

V.2.4 Other systems

Calculations were performed for two more systems with complicated behavior [16]:

- mixtures of sodium hydroxide and sodium sulfate with two possible precipitates, Na_2SO_4 and $Na_2SO_4 \cdot (H_2O)_{10}$
- mixtures of magnesium sulfate and calcium sulfate with one possible precipitate, $CaSO_4 \cdot (H_2O)_2$

In both cases calculations were unsuccessful resulting in either aberrant results or numerical noise. Experimental data is shown below.
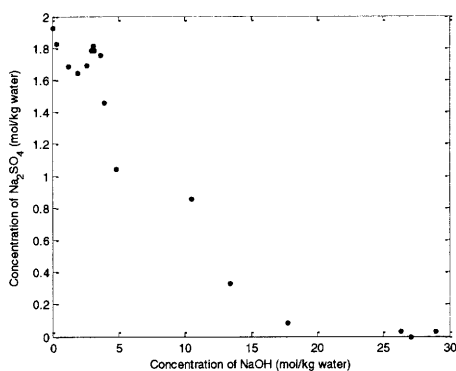
Figure 226: Solubility limits of Na_2SO_4 and $Na_2SO_4 \cdot (H_2O)_{10}$ in aqueous mixtures of NaOH and Na_2SO_4 – normal scale
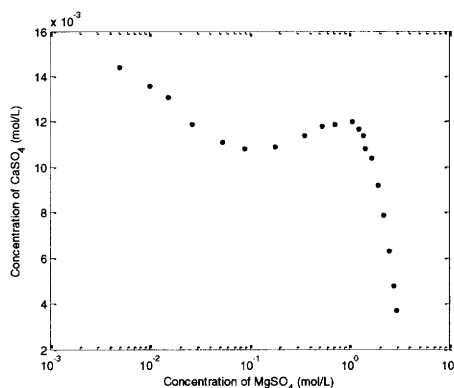
Figure 227: Solubility limit of $CaSO_4$ in aqueous mixtures of $CaSO_4$ and $MgSO_4$ – logarithmic scale

V.2.5 Conclusion

The four successful examples show that the formulae for the ionic activity coefficients and the underlying theory can be used to predict the solubility limit for a binary electrolyte in a solution containing a given concentration of another binary electrolyte. The calculations however require a considerable amount of physical data on the mixtures that is sometimes reliable, sometimes not or that is often merely not available and must be estimated. The estimation process nolens volens introduces errors in the calculations. Therefore computing solubility limits is inevitably fraught with errors independent of the theory of electrolyte solutions. For solutions involving monovalent ions and anhydrous precipitates, the errors appear to be small; for solutions involving multivalent ions and hydrated precipitates the errors have derailed numerical calculations.

In a nutshell the comparison with experimental data provides a further confirmation of the effectiveness of the theory of equilibrium of ionic solutions, though a somewhat weak one.

V.3 Partially associated binary electrolytes

Certain binary electrolytes do not completely dissociate in water so more than two ions are present in solution. Most transition metal halides are in this situation and their osmotic coefficient and mean ionic activity coefficient exhibit anomalous behavior that cannot be reproduced by treating them as mere binary electrolytes. A short study has been made on zinc chloride and zinc bromide; the main ions usually present in solution are Zn^{2+}, X^-, ZnX^+ where X represents the halide Cl or Br; other ions are present at high concentrations such as ZnX_3^- and ZnX_4^{2-} and their effect can be seen on the leveling of the osmotic coefficient close to saturation [16]. Nevertheless in order to keep numerical calculations tractable the solution zinc halide is described as a mixture of only the three main ions Zn^{2+}, X^-, ZnX^+.

At a given molality m_{ZnX2}, the concentrations of the three ions are determined by a system of three equations, one for the conservation of zinc, one for the conservation of the halide and one for the equilibrium

$$Zn^{2+} + X^- \rightleftarrows ZnX^+$$
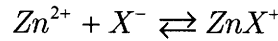
The system is

$$\begin{cases} m_{Zn^{2+}} + m_{ZnX^+} = m_{ZnX_2} \\ m_{X^-} + m_{ZnX^+} = 2m_{ZnX_2} \\ \gamma_{ZnX^+} m_{ZnX^+} = K\left(\gamma_{Zn^{2+}} m_{Zn^{2+}}\right)\left(\gamma_{X^-} m_{X^-}\right) \end{cases}$$

The equilibrium constant K is calculated using the Gibbs free energies of formation of the ions given in reference [16,21].

$$RT \ln K = -\Delta G_{RXN}^0 = -\left(G_{ZnX^+}^0 - G_{Zn^{2+}}^0 - G_{X^-}^0\right)$$

Table 5: Gibbs free energies of formation of ions

Ions	Gibbs free energy of formation (kJ/mol)
Zn^{2+}	– 147.1
Cl^-	– 131.2
Br^-	– 104.0
$ZnCl^+$	– 275.3
$ZnBr^+$	– 247.7

The Gibbs free energies of formation are given with the aqueous reference state of a hypothetical ideal solution at unit molality.

The correlation parameter w and the hydrated radii of the ions were determined by fitting empirical data. Numerical calculations are described in the diagram below. The results of these calculations are shown in the graphs below. The values of the parameters are in Appendix D.
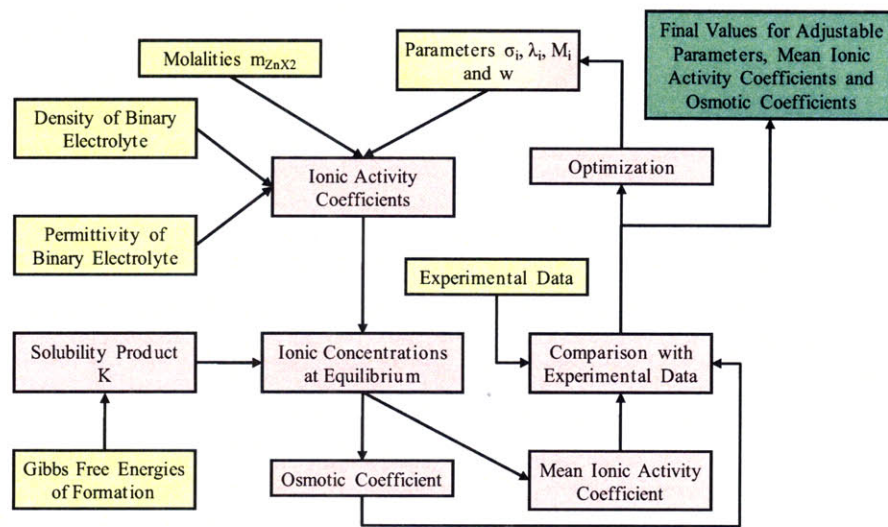
Figure 228: Computation of the correlation parameter and hydrated radii for electrolyte ZnX₂ – yellow = data from literature, purple = main calculations, green = output

V.3.1 Zinc chloride
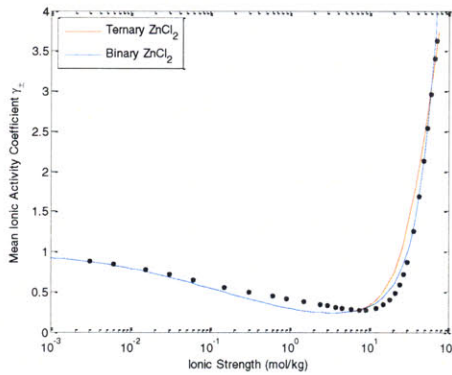
Figure 229: Mean ionic activity coefficient of zinc chloride
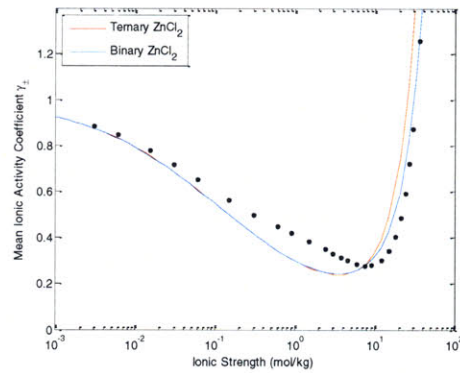
Figure 230: Mean ionic activity coefficient of zinc chloride – partial view
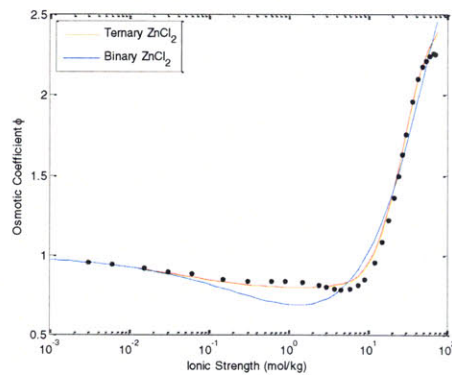
Figure 231: Osmotic coefficient of zinc chloride
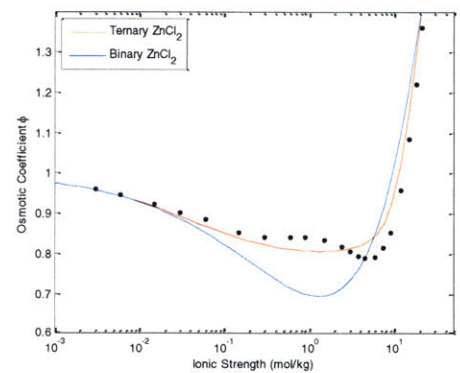
Figure 232: Osmotic coefficient of zinc chloride – partial view

V.3.2 Zinc bromide
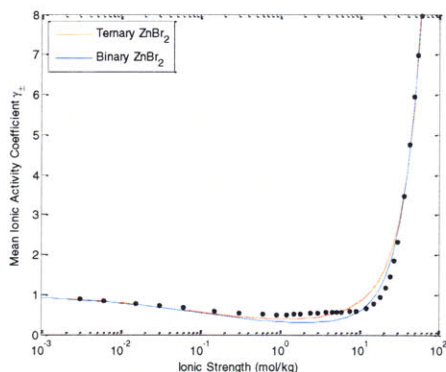
Figure 233: Mean ionic activity coefficient of zinc bromide
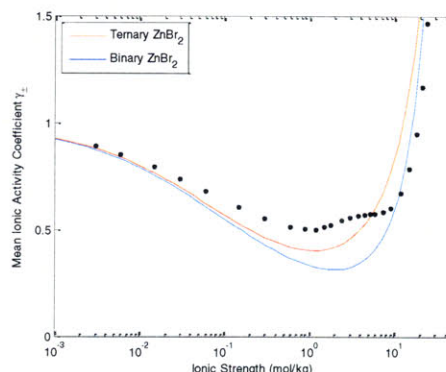
Figure 234: Mean ionic activity coefficient of zinc bromide – partial view
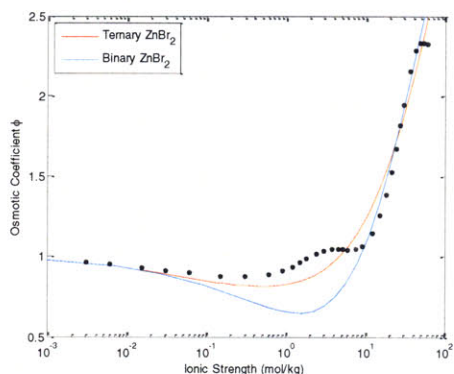
Figure 235: Osmotic coefficient of zinc bromide
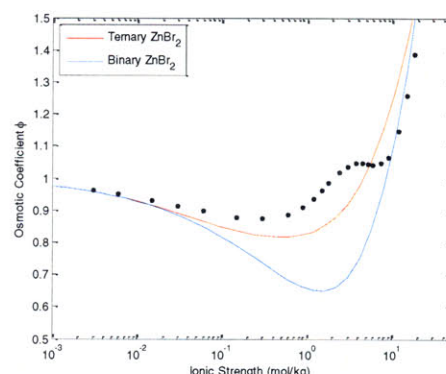
Figure 236: Osmotic coefficient of zinc bromide – partial view

V.3.3 Notes

The computations were not straightforward because the calculations for both the concentrations of ions and the values of the adjustable parameters are sensitive to the initial guess in the semi-dilute and concentrated portions of the curve. Moreover poorly defined bounds for the four adjustable parameters usually results in fanciful values for the ionic activity coefficients, erroneous concentrations for the ions and in failed optimization. Consequently only the general fits were made. Last in order to achieve good fits the values of the two equilibrium constants had to be modified: for zinc chloride it is divided by 10, for zinc bromide multiplied by 4; such modifications should not be shocking since $ZnCl^+$ and $ZnBr^+$ are unstable ions and their Gibbs free energies of formation are poorly measured.

For the mean ionic activity coefficient of both zinc chloride and zinc bromide there is little or no improvement in the fitting. For the osmotic coefficient of zinc chloride, the improvement is considerable; for the osmotic coefficient of zinc bromide, the improvement is important. Nevertheless the qualitative behavior is not captured well, because with a single set of parameters it is impossible to obtain a second local decrease of the osmotic coefficient; indeed even with a large difference in ionic radii the transition between Zn^{2+} and ZnX^+ as dominant ion

162

is not brutal enough to create more than a long flattening. Thus this is another proof that the correlation parameter and the hydrated radii are not independent of the concentration.

V.4   Conclusion

The theory of ionic solutions and the general formulae for the mean ionic activity coefficient and for the osmotic coefficient have successfully undergone the comparison with experimental data. When direct experimental data is available as for seawater or incompletely dissociated binary electrolytes, the behavior observed is the same as for binary electrolytes. The comparison between computed and experimental solubility limits of one binary electrolyte into another is difficult because of the complexity of numerical calculations; when these could be completed, the outcome is satisfying.

Thus the theory of binary electrolytes has been proved to be good for solutions containing any number of small ions. It is complete and consistent and represents a considerable improvement over the Debye-Hückel theory. It usually reproduces experimental data on the osmotic coefficient and the mean ionic activity coefficient quite well with three fits but it does not surpass the semi-empirical formulae of Pitzer and Meissner. The main disadvantage of the model is the dependence of the correlation parameter and of the hydrated radii on the concentration. A second disadvantage is the need for numerous auxiliary data from the literature such as the relative permittivity and the density of solutions.

Chapter 9   Linear waves in ionic solutions

I   GENERAL EQUATIONS FOR LINEAR PLANE WAVES IN BINARY ELECTROLYTES

We consider an aqueous solution containing two ionic species with bulk densities $(\rho_\alpha{}^0, \rho_\beta{}^0)$, with charges (z_α, z_β), with ionic radii $(\sigma_\alpha, \sigma_\beta)$ and with masses (m_α, m_β). The solution is electroneutral i.e. $z_\alpha \cdot \rho_\alpha{}^0 + z_\beta \cdot \rho_\beta{}^0 = 0$. The medium is static.
The momentum equations are

$$m_\alpha \rho_\alpha \left(\frac{\partial v_\alpha}{\partial t} + \left(v_\alpha \cdot \nabla \right) v_\alpha \right) = -\nabla \Pi + z_\alpha \rho_\alpha eE \qquad m_\beta \rho_\beta \left(\frac{\partial v_\beta}{\partial t} + \left(v_\beta \cdot \nabla \right) v_\beta \right) = -\nabla \Pi + z_\beta \rho_\beta eE$$

Π is the osmotic pressure and E is the electric field. They are governed by the equations

$$\Pi = \phi \left(\rho_\alpha + \rho_\beta \right) k_B T \qquad \nabla \cdot E = \frac{e}{\varepsilon_0 \varepsilon_r} \left(z_\alpha \rho_\alpha + z_\beta \rho_\beta \right)$$

ϕ is the osmotic coefficient. It depends on the local mesoscopic concentrations ρ_α and ρ_β.
The equations for the conservation of species α and β are

$$\frac{\partial \rho_\alpha}{\partial t} + \nabla \cdot \left(\rho_\alpha v_\alpha + J_\alpha \right) = 0 \qquad \frac{\partial \rho_\beta}{\partial t} + \nabla \cdot \left(\rho_\beta v_\beta + J_\beta \right) = 0$$

J_i is the component of the flux reflecting diffusion, electric interactions and excluded volume restrictions.

We assume that the waves propagate at speeds that make diffusion, electric interactions and excluded volume restrictions negligible when compared to the velocity of the wave. Thus the equations for the conservation of species simply become

$$\frac{\partial \rho_\alpha}{\partial t} + \nabla \cdot \left(\rho_\alpha v_\alpha \right) = 0 \qquad \frac{\partial \rho_\beta}{\partial t} + \nabla \cdot \left(\rho_\beta v_\beta \right) = 0$$

We pursue the calculations by assuming that the amplitude of ionic waves is small and do not significantly alter the local concentrations. Thus we write

$$\rho_i = \rho_i^0 + \rho_i^\varepsilon \quad \text{with} \quad \left| \frac{\rho_i^\varepsilon}{\rho_i^0} \right| \ll 1$$

$$\phi = \phi^0 \left(\rho_\alpha^0, \rho_\beta^0 \right) + \rho_\alpha^\varepsilon \frac{\partial \phi}{\partial \rho_\alpha} \left(\rho_\alpha^0, \rho_\beta^0 \right) + \rho_\beta^\varepsilon \frac{\partial \phi}{\partial \rho_\beta} \left(\rho_\alpha^0, \rho_\beta^0 \right)$$

We rewrite the expression of the osmotic coefficient as

$$\phi = \phi^0 + \phi_\alpha' \rho_\alpha^\varepsilon + \phi_\beta' \rho_\beta^\varepsilon$$

Moreover the velocity of the wave is also assumed to be small. Using these assumptions we linearize all equations.

$\nabla \cdot E = \dfrac{e}{\varepsilon_0 \varepsilon_r} \left(z_\alpha \rho_\alpha^\varepsilon + z_\beta \rho_\beta^\varepsilon \right)$ hence E is also a small quantity

$$m_\alpha \rho_\alpha^0 \frac{\partial v_\alpha}{\partial t} = -\phi^0 k_B T \nabla \left(\rho_\alpha^\varepsilon + \rho_\beta^\varepsilon \right) - \left(\rho_\alpha^0 + \rho_\beta^0 \right) k_B T \left(\phi_\alpha' \cdot \nabla \rho_\alpha^\varepsilon + \phi_\beta' \cdot \nabla \rho_\beta^\varepsilon \right) + z_\alpha \rho_\alpha^0 e E$$

$$m_\beta \rho_\beta^0 \frac{\partial v_\beta}{\partial t} = -\phi^0 k_B T \nabla \left(\rho_\alpha^\varepsilon + \rho_\beta^\varepsilon \right) - \left(\rho_\alpha^0 + \rho_\beta^0 \right) k_B T \left(\phi_\alpha' \cdot \nabla \rho_\alpha^\varepsilon + \phi_\beta' \cdot \nabla \rho_\beta^\varepsilon \right) + z_\beta \rho_\beta^0 e E$$

$$\frac{\partial \rho_\alpha^\varepsilon}{\partial t} + \rho_\alpha^0 \nabla \cdot v_\alpha = 0 \qquad \text{and} \qquad \frac{\partial \rho_\beta^\varepsilon}{\partial t} + \rho_\beta^0 \nabla \cdot v_\beta = 0$$

Last we restrict the study to plane waves and switch to complex notation.

$$\frac{\partial}{\partial t} = i\omega \qquad \nabla = -ik$$

We have a system of five equations and five unknowns, v_α, v_β, ρ_α^ε, ρ_β^ε and E.

$$i\omega \rho_\alpha^\varepsilon - ik\rho_\alpha^0 v_\alpha = 0$$

$$i\omega \rho_\beta^\varepsilon - ik\rho_\beta^0 v_\beta = 0$$

$$i\omega m_\alpha \rho_\alpha^0 v_\alpha - ik\phi^0 k_B T \left(\rho_\alpha^\varepsilon + \rho_\beta^\varepsilon \right) - ik \left(\rho_\alpha^0 + \rho_\beta^0 \right) k_B T \left(\phi_\alpha' \rho_\alpha^\varepsilon + \phi_\beta' \rho_\beta^\varepsilon \right) - z_\alpha \rho_\alpha^0 e E = 0$$

$$i\omega m_\beta \rho_\beta^0 v_\beta - ik\phi^0 k_B T \left(\rho_\alpha^\varepsilon + \rho_\beta^\varepsilon \right) - ik \left(\rho_\alpha^0 + \rho_\beta^0 \right) k_B T \left(\phi_\alpha' \rho_\alpha^\varepsilon + \phi_\beta' \rho_\beta^\varepsilon \right) - z_\beta \rho_\beta^0 e E = 0$$

$$\frac{e}{\varepsilon_0 \varepsilon_r} \left(z_\alpha \rho_\alpha^\varepsilon + z_\beta \rho_\beta^\varepsilon \right) + ikE = 0$$

We simplify the system by substituting ρ_α^ε to v_α and ρ_β^ε to v_β and keeping only three equations.

$$\rho_\alpha^0 v_\alpha = \frac{\omega}{k} \rho_\alpha^\varepsilon$$

$$\rho_\beta^0 v_\beta = \frac{\omega}{k} \rho_\beta^\varepsilon$$

$$im_\alpha \frac{\omega^2}{k} \rho_\alpha^\varepsilon - ik\phi^0 k_B T \left(\rho_\alpha^\varepsilon + \rho_\beta^\varepsilon \right) - ik \left(\rho_\alpha^0 + \rho_\beta^0 \right) k_B T \left(\phi_\alpha' \rho_\alpha^\varepsilon + \phi_\beta' \rho_\beta^\varepsilon \right) - z_\alpha \rho_\alpha^0 e E = 0$$

$$im_\beta \frac{\omega^2}{k} \rho_\beta^\varepsilon - ik\phi^0 k_B T \left(\rho_\alpha^\varepsilon + \rho_\beta^\varepsilon \right) - ik \left(\rho_\alpha^0 + \rho_\beta^0 \right) k_B T \left(\phi_\alpha' \rho_\alpha^\varepsilon + \phi_\beta' \rho_\beta^\varepsilon \right) - z_\beta \rho_\beta^0 e E = 0$$

$$\frac{e}{\varepsilon_0 \varepsilon_r} \left(z_\alpha \rho_\alpha^\varepsilon + z_\beta \rho_\beta^\varepsilon \right) + ikE = 0$$

We substitute ρ_α^ε and ρ_β^ε to E and keep only two equations.

$$E = -\frac{1}{ik} \frac{e}{\varepsilon_0 \varepsilon_r} \left(z_\alpha \rho_\alpha^\varepsilon + z_\beta \rho_\beta^\varepsilon \right)$$

$$m_\alpha \omega^2 \rho_\alpha^\varepsilon - k^2 \phi^0 k_B T \left(\rho_\alpha^\varepsilon + \rho_\beta^\varepsilon \right) - k^2 \left(\rho_\alpha^0 + \rho_\beta^0 \right) k_B T \left(\phi_\alpha' \rho_\alpha^\varepsilon + \phi_\beta' \rho_\beta^\varepsilon \right) - \frac{z_\alpha \rho_\alpha^0 e^2}{\varepsilon_0 \varepsilon_r} \left(z_\alpha \rho_\alpha^\varepsilon + z_\beta \rho_\beta^\varepsilon \right) = 0$$

$$m_\beta \omega^2 \rho_\beta^\varepsilon - k^2 \phi^0 k_B T \left(\rho_\alpha^\varepsilon + \rho_\beta^\varepsilon \right) - k^2 \left(\rho_\alpha^0 + \rho_\beta^0 \right) k_B T \left(\phi_\alpha' \rho_\alpha^\varepsilon + \phi_\beta' \rho_\beta^\varepsilon \right) - \frac{z_\beta \rho_\beta^0 e^2}{\varepsilon_0 \varepsilon_r} \left(z_\alpha \rho_\alpha^\varepsilon + z_\beta \rho_\beta^\varepsilon \right) = 0$$

$$\left[\left(m_\alpha \omega^2 - \frac{z_\alpha^2 \rho_\alpha^0 e^2}{\varepsilon_0 \varepsilon_r} - k^2 k_B T\left(\phi^0 + \phi_\alpha'\left(\rho_\alpha^0 + \rho_\beta^0\right)\right)\right)\rho_\alpha^\varepsilon - \left(\frac{z_\alpha z_\beta \rho_\alpha^0 e^2}{\varepsilon_0 \varepsilon_r} + k^2 k_B T\left(\phi^0 + \phi_\beta'\left(\rho_\alpha^0 + \rho_\beta^0\right)\right)\right)\rho_\beta^\varepsilon \right] = 0$$

$$\left[\left(\frac{z_\alpha z_\beta \rho_\beta^0 e^2}{\varepsilon_0 \varepsilon_r} + k^2 k_B T\left(\phi^0 + \phi_\alpha'\left(\rho_\alpha^0 + \rho_\beta^0\right)\right)\right)\rho_\alpha^\varepsilon - \left(m_\beta \omega^2 - \frac{z_\beta^2 \rho_\beta^0 e^2}{\varepsilon_0 \varepsilon_r} - k^2 k_B T\left(\phi^0 + \phi_\beta'\left(\rho_\alpha^0 + \rho_\beta^0\right)\right)\right)\rho_\beta^\varepsilon \right] = 0$$

The equation has a non-zero solution if and only if the determinant is zero.

$$Det = \begin{vmatrix} m_\alpha \omega^2 - \dfrac{z_\alpha^2 \rho_\alpha^0 e^2}{\varepsilon_0 \varepsilon_r} - k^2 k_B T\left(\phi^0 + \phi_\alpha'\left(\rho_\alpha^0 + \rho_\beta^0\right)\right) & -\dfrac{z_\alpha z_\beta \rho_\alpha^0 e^2}{\varepsilon_0 \varepsilon_r} - k^2 k_B T\left(\phi^0 + \phi_\beta'\left(\rho_\alpha^0 + \rho_\beta^0\right)\right) \\[2em] -\dfrac{z_\alpha z_\beta \rho_\beta^0 e^2}{\varepsilon_0 \varepsilon_r} - k^2 k_B T\left(\phi^0 + \phi_\alpha'\left(\rho_\alpha^0 + \rho_\beta^0\right)\right) & m_\beta \omega^2 - \dfrac{z_\beta^2 \rho_\beta^0 e^2}{\varepsilon_0 \varepsilon_r} - k^2 k_B T\left(\phi^0 + \phi_\beta'\left(\rho_\alpha^0 + \rho_\beta^0\right)\right) \end{vmatrix}$$

$$Det = \left[m_\alpha \omega^2 - \frac{z_\alpha^2 \rho_\alpha^0 e^2}{\varepsilon_0 \varepsilon_r} - k^2 k_B T\left(\phi^0 + \phi_\alpha'\left(\rho_\alpha^0 + \rho_\beta^0\right)\right)\right]\left[m_\beta \omega^2 - \frac{z_\beta^2 \rho_\beta^0 e^2}{\varepsilon_0 \varepsilon_r} - k^2 k_B T\left(\phi^0 + \phi_\beta'\left(\rho_\alpha^0 + \rho_\beta^0\right)\right)\right]$$
$$- \left[\frac{z_\alpha z_\beta \rho_\beta^0 e^2}{\varepsilon_0 \varepsilon_r} + k^2 k_B T\left(\phi^0 + \phi_\alpha'\left(\rho_\alpha^0 + \rho_\beta^0\right)\right)\right]\left[\frac{z_\alpha z_\beta \rho_\alpha^0 e^2}{\varepsilon_0 \varepsilon_r} + k^2 k_B T\left(\phi^0 + \phi_\beta'\left(\rho_\alpha^0 + \rho_\beta^0\right)\right)\right]$$

$$Det = \left[\begin{aligned} & m_\alpha m_\beta \omega^4 - \frac{e^2}{\varepsilon_0 \varepsilon_r}\left(m_\alpha z_\beta^2 \rho_\beta^0 + m_\beta z_\alpha^2 \rho_\alpha^0\right)\omega^2 \\ & -\left[m_\alpha\left(\phi^0 + \phi_\beta'\left(\rho_\alpha^0 + \rho_\beta^0\right)\right) + m_\beta\left(\phi^0 + \phi_\alpha'\left(\rho_\alpha^0 + \rho_\beta^0\right)\right)\right]k_B T k^2 \omega^2 \\ & +k^2 k_B T \frac{e^2}{\varepsilon_0 \varepsilon_r}\left[z_\alpha^2 \rho_\alpha^0\left(\phi^0 + \phi_\beta'\left(\rho_\alpha^0 + \rho_\beta^0\right)\right) + z_\beta^2 \rho_\beta^0\left(\phi^0 + \phi_\alpha'\left(\rho_\alpha^0 + \rho_\beta^0\right)\right)\right] + \frac{z_\alpha^2 \rho_\alpha^0 e^2}{\varepsilon_0 \varepsilon_r}\frac{z_\beta^2 \rho_\beta^0 e^2}{\varepsilon_0 \varepsilon_r} \\ & +\left(k^2 k_B T\right)^2\left(\phi^0 + \phi_\alpha'\left(\rho_\alpha^0 + \rho_\beta^0\right)\right)\left(\phi^0 + \phi_\beta'\left(\rho_\alpha^0 + \rho_\beta^0\right)\right) \end{aligned}\right]$$
$$- \left[\begin{aligned} & \frac{z_\alpha z_\beta \rho_\alpha^0 e^2}{\varepsilon_0 \varepsilon_r}\frac{z_\alpha z_\beta \rho_\beta^0 e^2}{\varepsilon_0 \varepsilon_r} + k^2 k_B T \frac{z_\alpha z_\beta e^2}{\varepsilon_0 \varepsilon_r}\left[\rho_\alpha^0\left(\phi^0 + \phi_\alpha'\left(\rho_\alpha^0 + \rho_\beta^0\right)\right) + \rho_\beta^0\left(\phi^0 + \phi_\beta'\left(\rho_\alpha^0 + \rho_\beta^0\right)\right)\right] \\ & +\left(k^2 k_B T\right)^2\left(\phi^0 + \phi_\alpha'\left(\rho_\alpha^0 + \rho_\beta^0\right)\right)\left(\phi^0 + \phi_\beta'\left(\rho_\alpha^0 + \rho_\beta^0\right)\right) \end{aligned}\right]$$

$$Det = \begin{vmatrix} m_\alpha m_\beta \omega^4 - \dfrac{e^2}{\varepsilon_0 \varepsilon_r}\left(m_\alpha z_\beta^2 \rho_\beta^0 + m_\beta z_\alpha^2 \rho_\alpha^0\right)\omega^2 - \phi^0 k_B T k^2 \omega^2\left(m_\alpha + m_\beta\right) \\[1em] -k^2 \omega^2 k_B T\left(\rho_\alpha^0 + \rho_\beta^0\right)\left(m_\alpha \phi_\beta' + m_\beta \phi_\alpha'\right) + k^2 \phi^0 k_B T\left(z_\alpha - z_\beta\right)\dfrac{e^2}{\varepsilon_0 \varepsilon_r}\left(z_\alpha \rho_\alpha^0 - z_\beta \rho_\beta^0\right) \\[1em] +k^2 k_B T \dfrac{e^2}{\varepsilon_0 \varepsilon_r}\left(\rho_\alpha^0 + \rho_\beta^0\right)\left(z_\alpha \phi_\beta' - z_\beta \phi_\alpha'\right)\left(z_\alpha \rho_\alpha^0 - z_\beta \rho_\beta^0\right) \end{vmatrix}$$

The determinant is divided by $k_B T$ and we introduce the Bjerrum length.

166

$$\frac{Det}{k_B T} = \begin{vmatrix} \dfrac{m_\alpha m_\beta}{k_B T}\omega^4 + 4\pi l_B\left(m_\alpha z_\beta^2 \rho_\beta^0 + m_\beta z_\alpha^2 \rho_\alpha^0\right)\omega^2 - k^2\omega^2\phi^0\left(m_\alpha + m_\beta\right) \\ -k^2\omega^2\left(\rho_\alpha^0 + \rho_\beta^0\right)\left(m_\alpha\phi_\beta' + m_\beta\phi_\alpha'\right) + 4\pi l_B k_B T k^2 \phi^0\left(z_\alpha - z_\beta\right)\left(z_\alpha\rho_\alpha^0 - z_\beta\rho_\beta^0\right) \\ +4\pi l_B k_B T k^2 \left(\rho_\alpha^0 + \rho_\beta^0\right)\left(z_\alpha\phi_\beta' - z_\beta\phi_\alpha'\right)\left(z_\alpha\rho_\alpha^0 - z_\beta\rho_\beta^0\right) \end{vmatrix}$$

The dispersion relation is given by Det = 0. It is a second degree polynomial in ω^2.

$$\frac{m_\alpha m_\beta}{k_B T}\omega^4 + \begin{bmatrix} 4\pi l_B\left(m_\alpha z_\beta^2 \rho_\beta^0 + m_\beta z_\alpha^2 \rho_\alpha^0\right) - \\ \phi^0\left(m_\alpha + m_\beta\right)k^2 - \\ \left(\rho_\alpha^0 + \rho_\beta^0\right)\left(m_\alpha\phi_\beta' + m_\beta\phi_\alpha'\right)k^2 \end{bmatrix}\omega^2 + 4\pi l_B k_B T\left(z_\alpha\rho_\alpha^0 - z_\beta\rho_\beta^0\right)\begin{bmatrix} \phi^0\left(z_\alpha - z_\beta\right) + \\ \left(\rho_\alpha^0 + \rho_\beta^0\right)\left(z_\alpha\phi_\beta' - z_\beta\phi_\alpha'\right) \end{bmatrix}k^2 = 0$$

$$\Delta = \begin{bmatrix} 4\pi l_B\left(m_\alpha z_\beta^2 \rho_\beta^0 + m_\beta z_\alpha^2 \rho_\alpha^0\right) - \\ \phi^0\left(m_\alpha + m_\beta\right)k^2 - \\ \left(\rho_\alpha^0 + \rho_\beta^0\right)\left(m_\alpha\phi_\beta' + m_\beta\phi_\alpha'\right)k^2 \end{bmatrix}^2 - 16\pi l_B m_\alpha m_\beta k^2\left(z_\alpha\rho_\alpha^0 - z_\beta\rho_\beta^0\right)\begin{bmatrix} \phi^0\left(z_\alpha - z_\beta\right) + \\ \left(\rho_\alpha^0 + \rho_\beta^0\right)\left(z_\alpha\phi_\beta' - z_\beta\phi_\alpha'\right) \end{bmatrix}$$

The equation usually has two solutions. Because the third term is positive, the two solutions have the same sign. If they are positive, two types of waves can travel in the solution; if they are negative, no linear waves can travel. If the wavenumber k is small, the equation reduces to

$$\frac{m_\alpha m_\beta}{k_B T}\omega^4 + 4\pi l_B\left(m_\alpha z_\beta^2 \rho_\beta^0 + m_\beta z_\alpha^2 \rho_\alpha^0\right)\omega^2 = 0$$

The solutions to the equations are not positive so an ionic solution cannot conduct waves with small wavenumber or equivalently large wavelengths. On the contrary if the wavenumber is large, the discriminant Δ is positive and the equation has two solutions; moreover the second term in the equation is negative so the sum of the two solutions is positive hence both solutions are positive. Thus the ionic solution can conduct two types of waves if the wavenumber is large or equivalently their wavelength small.

The solutions to the equation can be written as

$$\omega^2 = \frac{\left[\phi^0\left(m_\alpha + m_\beta\right) + \left(\rho_\alpha^0 + \rho_\beta^0\right)\left(m_\alpha\phi_\beta' + m_\beta\phi_\alpha'\right)\right]k^2 - 4\pi l_B\left(m_\alpha z_\beta^2 \rho_\beta^0 + m_\beta z_\alpha^2 \rho_\alpha^0\right) \pm \sqrt{\Delta}}{2\dfrac{m_\alpha m_\beta}{k_B T}}$$

$$\omega^2 = \frac{k_B T}{2m_\alpha m_\beta}\begin{bmatrix} \left[\phi^0\left(m_\alpha + m_\beta\right) + \left(\rho_\alpha^0 + \rho_\beta^0\right)\left(m_\alpha\phi_\beta' + m_\beta\phi_\alpha'\right)\right]k^2 - 4\pi l_B\left(m_\alpha z_\beta^2 \rho_\beta^0 + m_\beta z_\alpha^2 \rho_\alpha^0\right) \pm \\ \begin{bmatrix} \left\{\left[\phi^0\left(m_\alpha + m_\beta\right) + \left(\rho_\alpha^0 + \rho_\beta^0\right)\left(m_\alpha\phi_\beta' + m_\beta\phi_\alpha'\right)\right]k^2 - 4\pi l_B\left(m_\alpha z_\beta^2 \rho_\beta^0 + m_\beta z_\alpha^2 \rho_\alpha^0\right)\right\}^2 \\ -16\pi l_B m_\alpha m_\beta k^2\left(z_\alpha\rho_\alpha^0 - z_\beta\rho_\beta^0\right)\left[\phi^0\left(z_\alpha - z_\beta\right) + \left(\rho_\alpha^0 + \rho_\beta^0\right)\left(z_\alpha\phi_\beta' - z_\beta\phi_\alpha'\right)\right] \end{bmatrix}^{\frac{1}{2}} \end{bmatrix}$$

$$\omega = \sqrt{\frac{k_B T}{2m_\alpha m_\beta}} \left[\begin{array}{l} \left[\phi^0 \left(m_\alpha + m_\beta \right) + \left(\rho_\alpha^0 + \rho_\beta^0 \right) \left(m_\alpha \phi_\beta' + m_\beta \phi_\alpha' \right) \right] k^2 - 4\pi l_B \left(m_\alpha z_\beta^2 \rho_\beta^0 + m_\beta z_\alpha^2 \rho_\alpha^0 \right) \pm \\ \left[\left\{ \left[\phi^0 \left(m_\alpha + m_\beta \right) + \left(\rho_\alpha^0 + \rho_\beta^0 \right) \left(m_\alpha \phi_\beta' + m_\beta \phi_\alpha' \right) \right] k^2 - 4\pi l_B \left(m_\alpha z_\beta^2 \rho_\beta^0 + m_\beta z_\alpha^2 \rho_\alpha^0 \right) \right\}^2 \\ \left[-16\pi l_B m_\alpha m_\beta k^2 \left(z_\alpha \rho_\alpha^0 - z_\beta \rho_\beta^0 \right) \left[\phi^0 \left(z_\alpha - z_\beta \right) + \left(\rho_\alpha^0 + \rho_\beta^0 \right) \left(z_\alpha \phi_\beta' - z_\beta \phi_\alpha' \right) \right] \right] \end{array} \right]^{\frac{1}{2}}$$

II   PHASE AND GROUP VELOCITIES

The phase velocity is $v_\varphi = \dfrac{\omega}{k}$ and the group velocity is $v_g = \dfrac{d\omega}{dk}$. To calculate the two velocities we rewrite the expression of ω in a simpler form.

$$\omega = \sqrt{\frac{k_B T}{2m_\alpha m_\beta}} \sqrt{ak^2 - b \pm \sqrt{\left(ak^2 - b\right)^2 - ck^2}}$$

$$v_\varphi = \frac{\omega}{k} = \sqrt{\frac{k_B T}{2m_\alpha m_\beta}} \sqrt{a - \frac{b}{k^2} \pm \sqrt{\left(a - \frac{b}{k^2}\right)^2 - \frac{c}{k^2}}}$$

$$\frac{d\omega}{dk} = \sqrt{\frac{k_B T}{8m_\alpha m_\beta}} \frac{2ak \pm \dfrac{4ak\left(ak^2 - b\right) - 2ck}{2\sqrt{\left(ak^2 - b\right)^2 - ck^2}}}{\sqrt{ak^2 - b \pm \sqrt{\left(ak^2 - b\right)^2 - ck^2}}}$$

$$v_g = \frac{d\omega}{dk} = \sqrt{\frac{k_B T}{2m_\alpha m_\beta}} \frac{k}{\sqrt{ak^2 - b \pm \sqrt{\left(ak^2 - b\right)^2 - ck^2}}} \left(a \pm \frac{a\left(ak^2 - b\right) - \dfrac{c}{2}}{\sqrt{\left(ak^2 - b\right)^2 - ck^2}} \right)$$

Instead of the wavenumber k, we can use the wavelength λ as a variable.

$$k = \frac{2\pi}{\lambda}$$

At high wavenumers or low wavelengths, the ionic solution can conduct two types of waves. The limit dispersion relations and velocities are:

- Faster waves

$$\omega = k\sqrt{\frac{ak_B T}{m_\alpha m_\beta}} = k\sqrt{\phi^0 k_B T \left(\frac{1}{m_\alpha} + \frac{1}{m_\beta}\right) + \left(\rho_\alpha^0 + \rho_\beta^0\right) k_B T \left(\frac{\phi_\alpha'}{m_\alpha} + \frac{\phi_\beta'}{m_\beta}\right)}$$

$$v_{\varphi,\text{lim}} = v_{g,\text{lim}} = \sqrt{\frac{ak_B T}{m_\alpha m_\beta}} = \sqrt{\phi^0 k_B T \left(\frac{1}{m_\alpha} + \frac{1}{m_\beta} \right) + \left(\rho_\alpha^0 + \rho_\beta^0 \right) k_B T \left(\frac{\phi_\alpha'}{m_\alpha} + \frac{\phi_\beta'}{m_\beta} \right)}$$

- Slower waves

$$\omega = \sqrt{\frac{k_B T}{2 m_\alpha m_\beta}} \sqrt{\frac{c}{2a}} \quad \text{independent of k}$$

$$v_{\varphi,\text{lim}} = \frac{1}{k} \sqrt{\frac{k_B T}{2 m_\alpha m_\beta}} \sqrt{\frac{c}{2a}} \qquad v_{g,\text{lim}} \simeq 0$$

The slower waves are effectively stationary and do not propagate.

Chapter 10   Conclusion

I   SUMMARY

The present work was motivated by the desire to understand the physical mechanism underlying the propagation of nervous influx in neurons as well as the modulation and summation of electrical signals during their progression in dendrites. The survey of existing literature showed that most studies model dendrites and axons as passive or active cables transporting simple electrical signals modulated through resistances, capacitors or inductors and undergoing linear summation. These models simply ignore the physical basis of these electrical signals. Two exceptions have been found but because their scope was limited, they did not bring significant improvements.

Nervous influx is an alteration of the electrical potential that exists across the plasmic membrane of any cell. It is carried by ionic currents flowing both across the membrane and in the neuron under the membrane. The study ambitioned to build a model for the propagation of nervous influx based on ionic currents and surveyed the literature on electrolytes and polyelectrolytes to discover the methods for describing the equilibrium and ionic currents in aqueous solutions containing polyelectrolytes mimicking the inner medium of a cell. Numerous approaches were found and can be classified in five categories:

- Purely numerical methods or heavily reliant on numerical methods; examples are direct molecular simulations, the integral theory of liquids and the hypernetted chain theory
- Complex intractable mathematics; the best examples are the theories using density functionals
- Approaches tied to a specific situation and impossible to extend; examples are the Manning condensation, the ionic Wigner crystal and the condensation on charged lattices
- A fully consistent theory by Debye and Hückel with interesting extensions but valid only in dilute solutions
- A set of semi-empirical formulae that describe equilibria very well but cannot be used to describe dynamical phenomena; examples are the Meissner model, the Pitzer model and the Chen model.

After reviewing these methods the elaboration of a new consistent theory extending the one by Debye and Hückel appeared to be necessary in order to correctly model the nervous influx. The Debye-Hückel theory is insufficient on two points: it considers ions as infinitesimally small and ignores their correlations. Therefore the present study developed a new theory of small ions that treats ions as hard spheres and includes their correlations. The theory is consistent and can be reduced to the Debye-Hückel theory when the radius of ions and the correlation length are taken to be zero.

The theory assigns to each ion an ionic radius corresponding to the extent of its electronic cloud and a hydrated radius corresponding to the extent of its shell of hydration. The ionic radius has a fixed value taken from the literature whereas the hydrated radius depends on the surrounding solution and is determined from experimental data. The solution as a whole has a

correlation length determining the volume around each ion in which correlations have a significant effect. The correlation length is determined from experimental data.

The correlation length and the hydrated radii were determined for 75 binary electrolytes by calculating the osmotic coefficient and the mean ionic activity coefficient and by fitting the wealth of experimental data available. Usually three fits were made for each electrolyte. The general fit is always close to experimental points but underestimates the values in the semi-dilute region. The dilute fit and the semi-dilute fit approximate experimental points very well in their respective regions but markedly stray from them in the concentrated region. Last some electrolytes required only two or even one fit. The main explanation for the need for three fits is that the correlation length and the hydrated radii actually change with the concentration of ions whereas the model assumes them to be constant. The rate of change being small, the whole set of experimental points can be approximated very well with three fits.

The next step was to compare these three fits with the semi-empirical models of Meissner and Pitzer for the mean ionic activity coefficient. All three are good approximations. The Pitzer model is the most precise far almost all electrolytes; the Meissner model and the present model are equivalent in their accuracy.

After binary electrolytes a short study was performed on multicomponent electrolytes.

The last part of the present study examines the propagation of linear plane waves. In bulk solutions the propagation is generally conservative; the phase and group velocities are on the order of hundreds of meters per second. However no experimental data has been found in order to make a comparison. These velocities are much higher than the ones observed for the propagation of nervous influx.

II   CONCLUSION

The present work has developed a new theory of aqueous solutions with small ions that takes into account the finite size of ions and their correlations. For binary electrolytes it reproduces experimental data well. One of the two main objectives has been fulfilled. The theory is then applied to describe the propagation of linear waves in bulk solutions and has found group velocities on the order of hundreds of meters per second. Nevertheless the equations developed thus far cannot be applied to describe the environment under the plasmic membrane of neurons because they assume that local concentrations are small perturbations from the bulk concentrations, which is not the case. Thus the other objective of the thesis is only partially fulfilled; ionic waves are a plausible mechanism for the propagation of nervous influx and the most probable one, but the demonstration is incomplete.

III   FUTURE RESEARCH

The present study naturally leads to five other investigations. They consist of enhancing the fundamental equations of the theory and of applying them to all relevant fields.

i.   The expressions of the partition function and of the thermodynamic functions of a solution with small ions are made of terms with direct physical meaning multiplied by numerical constants.

$$\rho_{\pm} = \sum_{i=1}^{n} z_i \rho_i \qquad I = \frac{1}{2} \sum_{i=1}^{n} z_i^2 \rho_i \qquad \psi = \sum_{i=1}^{n} 8 \sigma_i^3 \rho_i$$

171

$$J_\alpha = -D_\alpha \rho_\alpha \left[\frac{\nabla \rho_\alpha}{\rho_\alpha} + \frac{z_\alpha e}{k_B T} \nabla V + \frac{\nabla \psi}{1-\psi} + 2.3 w^2 l_B^3 \nabla \rho_\pm - w l_B^3 \left[\frac{17}{4} \nabla \rho_\pm - (2.3)^2 \nabla I \right] \right]$$

These constants – 8, 2.3, 17/4 – result from the choice of the initial geometrical setting. Their impact should be investigated. A large scale optimization should be performed on the 75 electrolytes used to determine which values of these constants are the best.

ii. The osmotic pressure plays a considerable role for cells. Small changes result in their instant destruction. However in biology and biological engineering the osmotic pressure is calculated using the van't Hoff formula. This calculation is really crude so the method for computing the osmotic coefficient developed in the present work should be used to derive a new formula for the osmotic pressure in cells and biological media.

iii. The study of binary and multicomponent electrolytes was based on solving the linearized version of the no flux equation $J_\alpha = 0$ in spherical geometry. The linearized equation should also be solved in planar geometry to study the electrical double layer at weakly charged surfaces; and in cylindrical geometry to study weakly charged linear polyelectrolytes.

iv. One last study of solutions at equilibrium is based on solving the no flux equation $J_\alpha = 0$ in the general case, without linearizing it. The solution in planar geometry enables the study of electrical double layers close to highly charged surfaces. The solution in cylindrical and spherical geometries enable the study of highly charged linear and spheroidal polyelectrolytes. In all three cases it should show the phenomenon of overcharging and charge oscillations. If an external electrical field is applied the cloud of counterions should polarize.

v.   The last interesting point that could be studied using the theory developed in this work is the propagation of non-linear waves in ionic solutions. Nervous influx should fall into this category.

172

Appendix A Complete Hodgkin – Huxley model

$$C_m \frac{\partial V}{\partial t} - \frac{\partial^2 V}{\partial z^2} = g_{Na}m^3 h\left(V - E_{Na}\right) + g_K n^4 \left(V - E_K\right) + g_L \left(V - E_L\right) + I$$

Membrane properties [3,5,22]

$C_m = 1 \ \mu F/cm^2$ (capacity per unit surface of the membrane)

$g_{Na} = 100 \ mS/cm^2$ (conductivity per unit surface of voltage – gated sodium channels)
$E_{Na} = 50 \ mV$ (inversion potential of voltage – gated sodium channels)

$g_K = 80 \ mS/cm^2$ (conductivity per unit surface of voltage – gated potassium channels)
$E_K = -100 \ mV$ (inversion potential of voltage – gated potassium channels)

$g_L = 0.1 \ mS/cm^2$ (conductivity per unit surface of potassium channels open in resting state)
$E_L = -67 \ mV$ (inversion potential of potassium channels open in resting state)

m is the probability of a gate of a voltage – gated sodium channel to be activated
h is the probability of an open voltage – gated sodium channel to remain activated
n is the probability of a gate of a voltage – gated potassium channel to be activated

The 3 gates of a voltage – gated sodium channel have to be activated for the channel to be open and the 4 gates of a voltage – gated potassium channel have to be activated for the channel to be open.

Equations relating the ion channel parameters to the membrane potential:

$$\frac{dm}{dt} = \alpha_m\left(V\right)\left(1-m\right) - \beta_m\left(V\right)m \qquad \alpha_m\left(V\right) = \frac{0.32 \cdot \left(V + 54\right)}{1 - e^{-\frac{V+54}{4}}},$$

$$\beta_m\left(V\right) = -\frac{0.28 \cdot \left(V + 27\right)}{1 - e^{\frac{V+27}{5}}}$$

$$\frac{dh}{dt} = \alpha_h\left(V\right)\left(1-h\right) - \beta_h\left(V\right)h \qquad \alpha_h\left(V\right) = 0.128 \cdot e^{-\frac{V+50}{18}}, \quad \beta_h\left(V\right) = \frac{4}{1 + e^{-\frac{V+27}{5}}}$$

$$\frac{dn}{dt} = \alpha_n\left(V\right)\left(1-n\right) - \beta_n\left(V\right)n \qquad \alpha_n\left(V\right) = \frac{0.032 \cdot \left(V + 52\right)}{1 - e^{-\frac{V+52}{5}}}, \quad \beta_n\left(V\right) = 0.5 \cdot e^{-\frac{V+57}{40}}$$

The parameters α and β were determined empirically by Hodgkin and Huxley.

Appendix B   Manning condensation theory

The condensation theory was first developed by Manning [86] in the 1960's and 1970's and confirmed experimentally [87]. However it had several mathematical weaknesses that have been subsequently addressed. We present the condensation theory in its neater formulation by B. Zimm and M. Le Bret [88,89,65]. When no additional ionic compounds are introduced in the solution, an analytical solution has been discovered and this case will be detailed; numerical simulations have shown that when ionic salts are added the results remain essentially the same as in the case with no salt.

B.1   General theory

Definition: in a solution containing long poly-ions, counterions are condensed on the poly-ions if at infinite dilution they remain within a finite distance of the poly-ion

Poisson – Boltzmann equation $$\vec{\nabla}^2 V = -\frac{\rho_{macroscopic}}{\varepsilon\varepsilon_0} - \frac{F}{\varepsilon\varepsilon_0}\sum_{ions} z_i C_i^0 e^{-\frac{z_i eV}{kT}}$$

where V electrical potential   k Boltzmann constant
       C_i^0 concentration in absence of electric field   R ideal gas constant
       C_i actual concentration   F Faraday
       J_i flux of "i" ε_0 vacuum permittivity
       z_i charge of "i" ε relative permittivity
       T absolute temperature

The equation is solved for an infinitely long cylinder of radius R with surface charge -σ immersed in a solution containing ions with opposite charge z:

$$\vec{\nabla}^2 V = -\frac{F}{\varepsilon\varepsilon_0} z C^0 e^{-\frac{zeV}{kT}}$$

$$\frac{1}{r}\frac{d}{dr}\left(r\frac{dV}{dr}\right) = -\frac{F}{\varepsilon\varepsilon_0} z C^0 e^{-\frac{zeV}{kT}}$$

we substitute $u = \ln r$ in the differential equation

$$\frac{1}{e^u}\frac{d}{du}\left(e^u\frac{dV}{du}\frac{du}{dr}\right)\frac{du}{dr}=-\frac{zFC^0}{\varepsilon\varepsilon_0}zC^0 e^{-\frac{zeV}{kT}}$$

$$\frac{1}{e^u}\frac{d}{du}\left(e^u\frac{dV}{du}e^{-u}\right)e^{-u}=-\frac{zFC^0}{\varepsilon\varepsilon_0}e^{-\frac{zeV}{kT}}$$

$$\frac{d^2V}{du^2}=-\frac{zFC^0}{\varepsilon\varepsilon_0}e^{-\frac{zeV}{kT}+2u}$$

$$\frac{d^2V}{du^2}\left(-\frac{ze}{kT}\frac{dV}{du}+2\right)=-\frac{zFC^0}{\varepsilon\varepsilon_0}\left(-\frac{ze}{kT}\frac{dV}{du}+2\right)e^{-\frac{zeV}{kT}+2u}$$

$$2\left[\frac{dV}{du}(u)-\frac{dV}{du}(\ln R)\right]-\frac{ze}{2kT}\left[\left(\frac{dV}{du}\right)^2(u)-\left(\frac{dV}{du}\right)^2(\ln R)\right]=-\frac{zFC^0}{\varepsilon\varepsilon_0}\left(e^{-\frac{zeV(u)}{kT}+2u}-e^{-\frac{zeV(\ln R)}{kT}+2\ln R}\right)$$

from the theorem of Gauss $\quad -2\pi R\dfrac{dV}{dr}(R)=-\dfrac{2\pi R\sigma}{\varepsilon\varepsilon_0}\quad\Rightarrow\quad -\dfrac{dV}{du}(\ln R)=-\dfrac{\sigma R}{\varepsilon\varepsilon_0}$

$$2\left[\frac{dV}{du}-\frac{\sigma R}{\varepsilon\varepsilon_0}\right]-\frac{ze}{2kT}\left[\left(\frac{dV}{du}\right)^2-\left(\frac{\sigma R}{\varepsilon\varepsilon_0}\right)^2\right]=-\frac{zFC^0}{\varepsilon\varepsilon_0}\left(e^{-\frac{zeV}{kT}+2u}-e^{-\frac{zeV(\ln R)}{kT}+2\ln R}\right)$$

$$\frac{ze}{2kT}\left[\left(\frac{dV}{du}\right)^2-2\frac{2kT}{ze}\frac{dV}{du}\right]+2\frac{\sigma R}{\varepsilon\varepsilon_0}-\frac{ze}{2kT}\left(\frac{\sigma R}{\varepsilon\varepsilon_0}\right)^2=\frac{zFC^0}{\varepsilon\varepsilon_0}\left(e^{-\frac{zeV(u)}{kT}+2u}-e^{-\frac{zeV(\ln R)}{kT}+2\ln R}\right)$$

$$\frac{ze}{2kT}\left[\frac{dV}{du}-\frac{2kT}{ze}\right]^2-\frac{2kT}{ze}+2\frac{\sigma R}{\varepsilon\varepsilon_0}-\frac{ze}{2kT}\left(\frac{\sigma R}{\varepsilon\varepsilon_0}\right)^2=\frac{zFC^0}{\varepsilon\varepsilon_0}\left(e^{-\frac{zeV(u)}{kT}+2u}-e^{-\frac{zeV(\ln R)}{kT}+2\ln R}\right)$$

in order to handle the equation more easily we write $y(u)=-\dfrac{ze}{kT}V(u)$

$$\frac{kT}{2ze}\left[\frac{dy}{du}+2\right]^2-\frac{2kT}{ze}+2\frac{\sigma R}{\varepsilon\varepsilon_0}-\frac{ze}{2kT}\left(\frac{\sigma R}{\varepsilon\varepsilon_0}\right)^2=\frac{zFC^0}{\varepsilon\varepsilon_0}\left(e^{y+2u}-e^{y(\ln R)+2\ln R}\right)$$

then we introduce the Bjerrum length $l_B=\dfrac{e^2}{4\pi\varepsilon\varepsilon_0 kT}$ and $K=\dfrac{2z^2eFC^0}{\varepsilon\varepsilon_0 kT}=8\pi l_B N_A C^0$

$$\left[\frac{dy}{du}+2\right]^2-4+4\frac{\sigma R}{\varepsilon\varepsilon_0}\frac{ze}{kT}-\left(\frac{\sigma R}{\varepsilon\varepsilon_0}\frac{ze}{kT}\right)^2=K\left(e^{y+2u}-e^{y(\ln R)+2\ln R}\right)$$

we group all the constants into $A=Ke^{y(\ln R)+2\ln R}-4+4\dfrac{\sigma R}{\varepsilon\varepsilon_0}\dfrac{ze}{kT}-\left(\dfrac{\sigma R}{\varepsilon\varepsilon_0}\dfrac{ze}{kT}\right)^2$

$$\left[\frac{dy}{du}+2\right]^2+A=Ke^{y+2u}$$

175

we substitute $g = e^{-\frac{1}{2}y-u} \iff e^{y+2u} = \frac{1}{g^2}$ $\qquad g' = \left(-\frac{1}{2}\frac{dy}{du} - 1\right)e^{-\frac{1}{2}y-u} = -\frac{1}{2}\left(\frac{dy}{du} + 2\right)g$

$$\left[-\frac{2g'}{g}\right]^2 + A = \frac{K}{g^2}$$

$$4g'^2 + Ag^2 = K$$

$$8g'g'' + 2Agg' = 0$$

$$g'' + \frac{A}{4}g = 0$$

therefore $g(u) = \alpha\cos\left(\frac{\sqrt{A}}{2}u + \varphi\right)$; reversing the substitutions yields

$$e^{-\frac{1}{2}y+u} = \alpha\cos\left(\frac{\sqrt{A}}{2}u + \varphi\right)$$

$$e^{-\frac{1}{2}y} = \alpha e^u\cos\left(\frac{\sqrt{A}}{2}u + \varphi\right)$$

$$e^y = \frac{1}{\alpha^2 e^{2u}\cos^2\left(\frac{\sqrt{A}}{2}u + \varphi\right)}$$

$$-\frac{zeV}{kT} = -\ln\left[\alpha^2 e^{2u}\cos^2\left(\frac{\sqrt{A}}{2}u + \varphi\right)\right]$$

$$V = \frac{2kT}{ze}\ln\left[\alpha e^u\cos\left(\frac{\sqrt{A}}{2}u + \varphi\right)\right]$$

$$V(r) = \frac{2kT}{ze}\ln\left[\alpha r\cos\left(\frac{\sqrt{A}}{2}\ln r + \varphi\right)\right]$$

we rewrite the constants A, φ in another form $\boxed{V(r) = \frac{2kT}{ze}\ln\left[\alpha r\cos\left(\gamma\ln\frac{r}{R_M}\right)\right]}$.

Relationships between the constants:

$$V(r) = \frac{2kT}{ze} \ln\left[\alpha r \cos\left(\gamma \ln \frac{r}{R_M} \right) \right]$$

$$\frac{dV}{dr} = \frac{2kT}{ze} \frac{\alpha \cos\left(\gamma \ln \frac{r}{R_M} \right) - \alpha r \sin\left(\gamma \ln \frac{r}{R_M} \right) \gamma \frac{1}{r}}{\alpha r \cos\left(\gamma \ln \frac{r}{R_M} \right)}$$

$$\frac{dV}{dr} = \frac{2kT}{ze} \frac{\cos\left(\gamma \ln \frac{r}{R_M} \right) - \gamma \sin\left(\gamma \ln \frac{r}{R_M} \right)}{r \cos\left(\gamma \ln \frac{r}{R_M} \right)}$$

$$r\frac{dV}{dr} = \frac{2kT}{ze}\left[1 - \gamma \tan\left(\gamma \ln \frac{r}{R_M} \right) \right]$$

$$\frac{d}{dr}\left(r\frac{dV}{dr} \right) = -\frac{2kT}{ze} \gamma \frac{\gamma \frac{1}{r}}{\cos^2\left(\gamma \ln \frac{r}{R_M} \right)}$$

$$\frac{1}{r}\frac{d}{dr}\left(r\frac{dV}{dr} \right) = -\frac{2kT}{ze} \frac{\gamma^2}{r^2 \cos^2\left(\gamma \ln \frac{r}{R_M} \right)}$$

hence from the Poisson – Boltzmann equation $\dfrac{1}{r}\dfrac{d}{dr}\left(r\dfrac{dV}{dr} \right) = -\dfrac{F}{\varepsilon \varepsilon_0} zC^0 e^{-\frac{zeV}{kT}}$

$$\frac{2kT}{ze}\gamma^2 = \frac{F}{\varepsilon \varepsilon_0} zC^0 \frac{1}{\gamma^2}$$

$$a^2\gamma^2 = \frac{z^2 eFC^0}{2\varepsilon \varepsilon_0 kT} = 2\pi l_B z^2 N_A C^0$$

the Debye – Huckel parameter is defined by $\kappa^2 = 4\pi l_B z^2 N_A C^0$ so we have $a^2\gamma^2 = \dfrac{\kappa^2}{2}$

boundary condition when r = R (surface of the charged cylinder):

$$-2\pi R \frac{dV}{dr}(R) = -\frac{2\pi R\sigma}{\varepsilon\varepsilon_0}$$

$$-R\frac{dV}{dr}(R) = -\frac{2kT}{ze}\left[1-\gamma\tan\left(\gamma\ln\frac{R}{R_M}\right)\right] = -\frac{R\sigma}{\varepsilon\varepsilon_0}$$

$$1-\gamma\tan\left(\gamma\ln\frac{R}{R_M}\right) = \frac{ze}{2kT}\frac{R\sigma}{\varepsilon\varepsilon_0}$$

$$\gamma\tan\left(\gamma\ln\frac{R}{R_M}\right) = 1-\frac{ze}{2kT}\frac{R\sigma}{\varepsilon\varepsilon_0} = 1-\frac{zl_B 2\pi R\sigma}{e}$$

since $2\pi R\sigma$ is the lineic charge of the polymer we can write it as e/b; then

$$\gamma\tan\left(\gamma\ln\frac{R}{R_M}\right) = 1-\frac{zl_B}{b}$$

we define the Manning parameter $\xi = \frac{l_B}{b} = \frac{e}{2kT}\frac{R\sigma}{\varepsilon\varepsilon_0}$ and write the boundary condition

$$\boxed{\gamma\tan\left(\gamma\ln\frac{R}{R_M}\right) = 1-z\xi}$$

for the potential to be fully determined another boundary condition is needed; the most common one is to impose E = 0 when r = P:

$$E(P) = -\frac{dV}{dr}(P) = -\frac{2kT}{zeP}\left[1-\gamma\tan\left(\gamma\ln\frac{P}{R_M}\right)\right] = 0$$

$$\boxed{\gamma\tan\left(\gamma\ln\frac{P}{R_M}\right) = 1}$$

Note that we can rewrite the last two conditions in order to separate a and RM:

$$\begin{cases}\gamma\tan\left(\gamma\ln\frac{R}{R_M}\right) = 1-z\xi \\ \gamma\tan\left(\gamma\ln\frac{P}{R_M}\right) = 1\end{cases} \Leftrightarrow \begin{cases}\gamma\ln\frac{R}{R_M} = \arctan\left(\frac{1-z\xi}{\gamma}\right) \\ \gamma\ln\frac{P}{R_M} = \arctan\left(\frac{1}{\gamma}\right)\end{cases}$$

therefore $\boxed{\gamma\ln\frac{P}{R} = \arctan\left(\frac{1}{\gamma}\right)-\arctan\left(\frac{1-z\xi}{\gamma}\right)}$ and $\boxed{R_M = Pe^{-\frac{1}{\gamma}\arctan\left(\frac{1}{\gamma}\right)}}$.

Two constraints on the value of γ follow for $\xi > 1$:

$$\gamma\ln\frac{P}{R} \le \frac{\pi}{2}+\frac{\pi}{2} \quad \text{so} \quad \frac{\pi}{\ln\frac{P}{R}} \ge \gamma$$

$$\gamma \ln \frac{P}{R} \geq \frac{\pi}{2} - \gamma + \frac{\pi}{2} - \frac{\gamma}{z\xi - 1} \quad \text{so} \quad \gamma \ln \frac{P}{R} \geq \pi - \frac{\gamma z\xi}{z\xi - 1} \quad \text{then} \quad \gamma \geq \frac{\pi}{\ln \frac{P}{R} + \frac{z\xi}{z\xi - 1}}$$

B.2   Summary of the problem and of the solution

The Poisson – Boltzmann equation is solved for a cylinder with radius R and surface charge -σ and with the additional constraint that the electric field is null at r = P.

$$\frac{1}{r} \frac{d}{dr}\left(r \frac{dV}{dr} \right) = -\frac{F}{\varepsilon\varepsilon_0} zC^0 e^{-\frac{zeV}{kT}}$$

we have the Bjerrum length $l_B = \dfrac{e^2}{4\pi\varepsilon\varepsilon_0 kT}$, the inverse Debye – Huckel length

$\kappa^2 = 4\pi l_B z^2 N_A C^0$, the lineic charge of the cylinder $\dfrac{e}{b} = 2\pi R\sigma$ and the Manning

parameter $\xi = \dfrac{l_B}{b} = \dfrac{e}{2kT} \dfrac{R\sigma}{\varepsilon\varepsilon_0}$

The solution can be expressed as $\quad V(r) = \dfrac{2kT}{ze} \ln\left[\dfrac{\kappa r}{\gamma\sqrt{2}} \cos\left(\gamma \ln \dfrac{r}{R_M} \right) \right]$

with $\quad \gamma \ln \dfrac{P}{R} = \arctan\left(\dfrac{1}{\gamma} \right) - \arctan\left(\dfrac{1 - z\xi}{\gamma} \right) \qquad R_M = P \exp\left(-\dfrac{1}{\gamma} \arctan\left(\dfrac{1}{\gamma} \right) \right)$

and $\quad \dfrac{\pi}{\ln \dfrac{P}{R} + \dfrac{z\xi}{z\xi - 1}} \leq \gamma \leq \dfrac{\pi}{\ln \dfrac{P}{R}} \quad$ for $\xi > 1$

B.3   Condensation of counterions

The constant R_M is called the Manning radius. The number of ions comprised between R and r > R (per unit length of z-axis) is:

$$n_{CI}(r) = N_A C^0 \int_R^r e^{-\frac{zeV}{kT}} 2\pi\rho d\rho$$

$$n_{CI}(r) = N_A C^0 \int_R^r \frac{2\pi\rho}{\dfrac{\kappa^2\rho^2}{2\gamma^2} \cos^2\left(\gamma \ln \dfrac{\rho}{R_M} \right)} d\rho = 4\pi N_A C^0 \frac{\gamma^2}{\kappa^2} \int_R^r \frac{1}{\rho \cos^2\left(\gamma \ln \dfrac{\rho}{R_M} \right)} d\rho$$

$$n_{CI}(r) = \frac{\gamma^2}{l_B} \left[\frac{1}{\gamma} \tan\left(\gamma \ln \dfrac{\rho}{R_M} \right) \right]_R^r = \frac{1}{l_B} \left[\gamma \tan\left(\gamma \ln \dfrac{r}{R_M} \right) - \gamma \tan\left(\gamma \ln \dfrac{R}{R_M} \right) \right]$$

$$n_{CI}(r) = \frac{1}{l_B} \left[\gamma \tan\left(\gamma \ln \dfrac{r}{R_M} \right) - 1 + z\xi \right]$$

179

alternative formula by replacing R_M $\quad n_{CI}(r) = \dfrac{1}{l_B}\left[\gamma\tan\left(\gamma\ln\dfrac{r}{R}+\arctan\dfrac{1-z\xi}{\gamma}\right)-1+z\xi\right]$

$n_{CI}(P) = \dfrac{z\xi}{l_B} = \dfrac{z}{b}$ which means that the region comprised between R and P contains the counterions that compensate for the charge of the rod; beyond P is the bulk of the solution where the electric field generated by the rod is effectively null

At high dilutions, $C^0 \to 0$ so $\kappa^2 \to 0$ but κ^2/γ^2 must remain finite so $\gamma \to 0$.

$R_M = Re^{-\frac{1}{\gamma}\arctan\frac{1-z\xi}{\gamma}}$ and $P = R_M e^{\frac{1}{\gamma}\arctan\frac{1}{\gamma}} = Re^{\frac{1}{\gamma}\left(\arctan\frac{1}{\gamma}-\arctan\frac{1-z\xi}{\gamma}\right)}$

- If $\xi < \dfrac{1}{z}$, $\arctan x = \dfrac{\pi}{2}-\dfrac{1}{x}+o\left(\dfrac{1}{x}\right)$ when x approaches + infinity therefore

$P = Re^{\frac{1}{\gamma}\left(\frac{\pi}{2}-\gamma-\frac{\pi}{2}+\frac{\gamma}{1-z\xi}+o(\gamma)\right)} = Re^{-1+\frac{1}{1-z\xi}+o(1)} = Re^{\frac{z\xi}{1-z\xi}+o(1)}$ so $\lim_{C^0\to 0} R_M = 0$ and

$\lim_{C^0\to 0} P = Re^{\frac{z\xi}{1-z\xi}}$

$n_{CI}(r) = \dfrac{1}{l_B}\left[\gamma\tan\left(\gamma\ln\dfrac{r}{R}+\arctan\dfrac{1-z\xi}{\gamma}\right)-1+z\xi\right]$

$n_{CI}(r) = \dfrac{1}{l_B}\left[\gamma\tan\left(\gamma\ln\dfrac{r}{R}+\dfrac{\pi}{2}-\dfrac{\gamma}{1-z\xi}+o(\gamma)\right)-1+z\xi\right]$

$n_{CI}(r) = \dfrac{1}{l_B}\left[\gamma\left(-\dfrac{1}{\gamma\ln\dfrac{r}{R}-\dfrac{\gamma}{1-z\xi}}+o\left(\dfrac{1}{\gamma}\right)\right)-1+z\xi\right] = \dfrac{1}{l_B}\left[-\dfrac{1}{\ln\dfrac{r}{R}-\dfrac{1}{1-z\xi}}+o(1)-1+z\xi\right]$

$n_{CI}(r) = \dfrac{1}{l_B}\left[\dfrac{(1-z\xi)\ln\dfrac{r}{R}}{-\ln\dfrac{r}{R}+\dfrac{1}{1-z\xi}}+o(1)\right]$

therefore $\lim_{C^0\to 0} n_{CI}(r) = \dfrac{1}{l_B}\dfrac{(1-z\xi)\ln\dfrac{r}{R}}{\dfrac{1}{1-z\xi}-\ln\dfrac{r}{R}}$, $\lim_{C^0\to 0} n_{CI}(R) = 0$

- If $\xi > \dfrac{1}{z}$, $\arctan x = -\dfrac{\pi}{2}+\dfrac{1}{x}+o\left(\dfrac{1}{x}\right)$ when x approaches $-$ infinity therefore

$P = Re^{\frac{1}{\gamma}\left(\frac{\pi}{2}-\gamma+\frac{\pi}{2}-\frac{\gamma}{1-z\xi}+o(\gamma)\right)} = Re^{\frac{1}{\gamma}\left(\pi-\frac{2a-\gamma z\xi}{1-z\xi}+o(\gamma)\right)}$ so $\lim_{C^0\to 0} R_M = +\infty$ and $\lim_{C^0\to 0} P = +\infty$

180

$$n_{CI}(r) = \frac{1}{l_B}\left[\gamma\tan\left(\gamma\ln\frac{r}{R} + \arctan\frac{1-z\xi}{\gamma}\right) - 1 + z\xi\right]$$

$$n_{CI}(r) = \frac{1}{l_B}\left[\gamma\tan\left(\gamma\ln\frac{r}{R} - \frac{\pi}{2} + \frac{\gamma}{1-z\xi} + o(\gamma)\right) - 1 + z\xi\right]$$

$$n_{CI}(r) = \frac{1}{l_B}\left[\gamma\left(-\frac{1}{\gamma\ln\frac{r}{R} + \frac{\gamma}{1-z\xi}} + o\left(\frac{1}{\gamma}\right)\right) - 1 + z\xi\right] = \frac{1}{l_B}\left[-\frac{1}{\ln\frac{r}{R} + \frac{1}{1-z\xi}} + o(1) - 1 + z\xi\right]$$

$$n_{CI}(r) = \frac{1}{l_B}\left[\frac{-2 + (-1+z\xi)\ln\frac{r}{R}}{\ln\frac{r}{R} + \frac{1}{1-z\xi}} + o(1)\right]$$

so $\displaystyle\lim_{c^0\to 0} n_{CI}(r) = \frac{1}{l_B}\frac{-2 + (-1+z\xi)\ln\frac{r}{R}}{\ln\frac{r}{R} + \frac{1}{1-z\xi}}$, $\displaystyle\lim_{c^0\to 0} n_{CI}(R) = \frac{2(z\xi-1)}{l_B}$, $\displaystyle\lim_{c^0\to 0} n_{CI}(+\infty) = \frac{z\xi-1}{l_B}$

B.4 Conclusion

All counterions necessary to compensate the charge of the rod are comprised between r = R and r = P. Beyond P is the bulk of the solution and the electric field generated by the rod is null. When the solution is diluted, there is an important difference in the behavior of counterions depending on the value of the Manning parameter ξ. When $\xi < 1/z$, P increases to a finite value, all counterions are condensed and no counterions adhere to the rod. When $\xi > 1/z$, P increases to infinity, only a fraction of counterions are condensed and some counterions adhere to surface of the rod.

Remark

We have $n_{CI}(R_M) = \frac{-1+z\xi}{l_B}$

if $\xi < \frac{1}{z}$, then no counterion is present within the Manning radius

if $\xi > \frac{1}{z}$, then $n_{CI}(R_M) = \frac{-1+z\xi}{l_B}$ counterions are present within the Manning radius

181

Appendix C Screening length in polyelectrolyte solutions

We consider a solution containing polyelectrolytes and monovalent small salt ions. The size of monomers is noted as b, all polyelectrolytes are assumed to have N monovalent monomers, c is the monomer concentration, c_s is the concentration of salt ions. In solution, because of the condensation of counterions, the charge of some monomers is compensated and d is the average distance between two uncompensated charges.

The Bjerrum length, l_B, the Debye length, λ_D, and the Manning parameter are

$$l_B = \frac{e^2}{4\pi\varepsilon\varepsilon_0 kT} \qquad \lambda_D = \left[4\pi l_B\left(\frac{c}{d}+2c_s\right)\right]^{-1/2} \qquad \xi = \frac{l_B}{b}$$

The average distance between two polyelectrolyte molecules is $R_{pol} = (N/c)^{1/3}$. A polyelectrolyte can be modeled as an extended chain of electrostatic blobs of size D, each one containing g_e monomers. Then the contour length L of the chain is [102,109]:

$$L \approx D\frac{N}{g_e} \approx Nb \begin{cases} \left(\xi/d^2\right)^{2/3}\dfrac{\Theta}{\Theta-T} & T \ll \Theta \\[2mm] \left(\xi/d^2\right)^{1/3} & T \sim \Theta \\[2mm] \left(\xi/d^2\right)^{2/7} & T \gg \Theta \end{cases}$$

Another model for polyelectrolytes is a self-avoiding chain of coils of size B, each coil being and extended chain of g_B blobs of size D. The end-to-end length, R, is [102]:

$$R \approx B\left(\frac{N}{g_B}\right)^{3/5} = B^{2/5}L^{3/5}$$

Three concentration values play important roles in the behavior of polyelectrolyte solutions: the interaction limit concentration, c_{int}, defined as the monomer concentration at which the Debye length is equal to the distance between two molecules of polyelectrolyte; the flexibility limit concentration, c_{fl}, defined as the monomer concentration at which the electrostatic screening length is equal to the contour length of the chain; and the overlap concentration, c*, defined as the monomer concentration at which the distance between two molecules of polyelectrolyte is equal to the end-to-end length of a chain [102]. Usually c_{int}, $c_{fl} \ll c*$ and $c_{int} < c_{fl}$.

$$c_{int} = \frac{1}{N^2}\left(\frac{d}{4\pi l_B}\right)^3 \qquad c_{fl} = \frac{N}{L^3} \qquad c^* = \frac{N}{R^3}$$

In the dilute regime, $c + 2dc_s < c_{int}$, the Debye length is longer than the distance between two polyelectrolyte molecules so the polyelectrolyte molecules interact strongly

and the screening length is the Debye length. The screening length is also longer than the contour length of a polyelectrolyte molecule so the polymer chain is extended and R = L.

$$r_{scr} = \lambda_D = \left[4\pi l_B \left(\frac{c}{d} + 2c_s \right) \right]^{-1/2}$$

For higher monomer or salt concentrations, i.e. $c_{int} < c + 2dc_s < c_{fl}$, the screening length is shorter than the distance between two molecules of polyelectrolyte but larger than the contour length of a polyelectrolyte. Polyelectrolyte molecules are still extended but do not contribute to screening as in the previous situation. Hence the screening length is not the Debye length but is evaluated knowing that in the screening volume around a polyelectrolyte enough ions must be included in order to compensate for the charge borne by the polyelectrolyte [102,109]:

$$r_{scr}^3 \left(\frac{c}{d} + 2c_s \right) = \frac{N}{d} \quad \Leftrightarrow \quad r_{scr} = \left(\frac{N}{c + 2dc_s} \right)^{\frac{1}{3}}$$

As a matter of fact the screening length is larger than the Debye length. We still have an extended polymer and R = L.

For $c_{fl} < c + 2dc_s$ and $c < c^*$, a polyelectrolyte molecule is no longer extended and the polymer is formed by self-avoiding coils the size of which is given by the screening length [102,109]. The screening length appears to be larger but proportional to the Debye length:

$$r_{scr}^3 \left(\frac{c}{d} + 2c_s \right) = \frac{r_{scr}}{D} \frac{g_e}{d} = \frac{r_{scr}}{d} \frac{N}{L} \quad \Leftrightarrow \quad r_{scr} = \left(\frac{N}{L} \right)^{\frac{1}{2}} \left(\frac{1}{c + 2dc_s} \right)^{\frac{1}{2}} = \lambda_D \left(\frac{N}{L} \right)^{\frac{1}{2}}$$

The end-to-end length, R, and the overlap concentration, c*, follow immediately:

$$R = \frac{N^{1/5} L^{2/5}}{\left(c + 2dc_s \right)^{3/5}} \qquad c^* = \frac{N^{2/5}}{L^{6/5}} \left(c^* + 2dc_s \right)^{3/5}$$

The former situations are called dilute-rigid regimes, the latter situation is the dilute-flexible regime.

When $c^* < c$, the solution is in the semi-dilute regime and the screening length is replaced with a correlation length r_{cor}. The correlation length is expressed [102] as

$$r_{cor} = R(c) \left[\frac{f(c)}{f(c^*)} \right]^m \quad \text{with} \quad f(c) = \frac{c^{\frac{5}{2}}}{\left(c + 2dc_s \right)^{3/2}}$$

The authors deduced m from the condition that the correlation length is independent of the degree of polymerization N. The final expression is

$$r_{cor} = c^{-3/4} \left(\frac{N}{L} \right)^{1/2} \left(c + 2dc_s \right)^{1/4}$$

SUMMARY OF ELECTRICAL SCREENING IN POLYELECTROLYTES SOLUTIONS
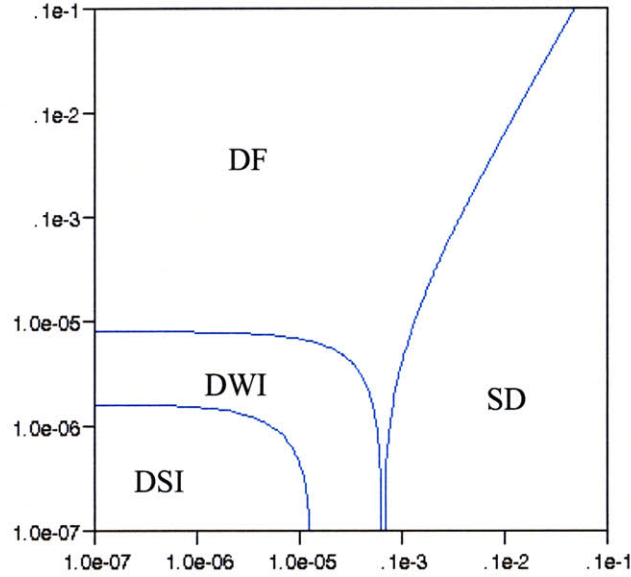
Figure 237: Diagram for aqueous polyelectrolyte solutions. DSI is the dilute regime with strongly interacting stiff polyelectrolytes, DWI with weakly interacting stiff polyelectrolytes, DF with flexible polyelectrolytes and SD is the semi-dilute regime

The electrical screening length is each regime is:

- DSI $\qquad r_{scr} = \lambda_D = \left[4\pi l_B \left(\frac{c}{d} + 2c_s \right) \right]^{-1/2}$

- DWI $\qquad r_{scr}^3 \left(\frac{c}{d} + 2c_s \right) = \frac{N}{d} \quad \Leftrightarrow \quad r_{scr} = \left(\frac{N}{c + 2dc_s} \right)^{\frac{1}{3}}$

- DF $\qquad r_{scr} = \left(\frac{N}{L} \right)^{\frac{1}{2}} \left(\frac{1}{c + 2dc_s} \right)^{\frac{1}{2}} = \lambda_D \left(\frac{N}{L} \right)^{\frac{1}{2}}$

- SD $\qquad r_{cor} = c^{-3/4} \left(\frac{N}{L} \right)^{1/2} \left(c + 2dc_s \right)^{1/4}$

184

Appendix D   Various data and parameters

The first set of tables gathers data on the radii of numerous ions from several sources in the literature.

Table 6: Ionic concentrations in mammals

Ion	Intracellular concentration (mM)	Extracellular concentration (mM)
Na^+	12	145
K^+	139	4
Cl^-	4	116
HCO_3^-	12	29
Mg^{2+}	0.8	1.5
Ca^{2+}	0.0002	1.8
X^-	138	9

Source: H. Lodish, A. Berk, P. Matsudaira, C. A. Kaiser, M. Krieger, M. P. Scott, S. L. Zipursky, J. Darnell; Molecular Cell Biology 5th edition, W.H. Freeman, 2004

Table 7: Mass, ionic radii and hydrated radii of major ions present in mammals

Ion	Mass (g/mol)	Ionic radius (Å)	Hydrated radius (Å)
Na^+	23.0	1.17	3.58
K^+	39.1	1.49	3.31
Mg^{2+}	24.3	0.72	4.28
Ca^{2+}	40.1	1.00	4.12
Cl^-	35.5	1.64	3.32
HCO_3^-*	61.0		5.60
H_3O^+	19.0	1.15	2.80
OH^-	17.0	1.33	3.00
X^-		1.40	

X^- stands for a charge borne by a protein

Source: A.G. Volkov, S. Paula, D.W. Deamer; Two mechanisms of permeation of small neutral molecules and hydrated ions across phospholipid bilayers, Bioelectrochemsitry and Bioenergetics, 42: 153-160, 1997 – except * from M. Ito, P.G. Kostyuk and T. Oshima; Further study on anion permeability of inhibitory post-synaptic membrane of cat motoneurons, Journal of Physiology, 164: 150-156, 1962

Table 8: Mass, ionic radii, hydrated radii and coordination number of inorganic ions

Ion	Mass (g/mol)	Ionic radius (Å)	Hydrated radius (Å)	Coordination
H^+	1.0		1.15	1
H_3O^+	19.0	1.15	2.82	
Li^+	6.9	0.73 – 0.90 – 1.06	3.82	4 – 6 – 8
Na^+	23.0	1.13 – 1.16 – 1.32	3.58	4 – 6 – 8
K^+	39.1	1.51 – 1.52 – 1.65	3.31	4 – 6 – 8
Rb^+	85.5	1.66 – 1.75	3.29	6 – 8
Cs^+	132.9	1.81 – 1.88	3.29	6 – 8
Mg^{2+}	24.3	0.71 – 0.86 – 1.03	4.28	4 – 6 – 8
Ca^{2+}	40.1	1.14 – 1.26	4.12	6 – 8
Sr^{2+}	87.6	1.32 – 1.40	4.12	6 – 8
Ba^{2+}	137.3	1.49 – 1.56	4.04	6 – 8
Mn^{2+}	54.9	0.80 – 0.81 – 1.10	4.38	4 – 6 – 8
Co^{2+}	58.9	0.72 – 0.79 – 1.04	4.23	4 – 6 – 8
Ni^{2+}	58.7	0.63 – 0.83	4.04	4 – 6
Cu^{2+}	63.5	0.71 – 0.87	4.19	4 – 6
Zn^{2+}	65.4	0.74 – 0.88 – 1.04	4.30	4 – 6 – 8
Cd^{2+}	112.4	0.92 – 1.09 – 1.24	4.26	4 – 6 – 8
Fe^{2+}	55.8	0.77 – 0.75 – 1.06	4.28	4 – 6 – 8
Fe^{3+}	55.8	0.63 – 0.69 – 0.92	4.57	4 – 6 – 8
Al^{3+}	27.0	0.53 – 0.675	4.75	4 – 6
Y^{3+}	88.9	1.04 – 1.16	4.55	6 – 8
La^{3+}	138.9	1.17 – 1.30	4.52	6 – 8
Ce^{3+}	140.1	1.15 – 1.28	4.52	6 – 8
F^-	19.0	1.17 – 1.19	3.52	4 – 6
Cl^-	35.5	1.67	3.52	6
Br^-	79.9	1.82	3.30	6
I^-	126.9	2.06	3.31	6
NO_3^-	62.0	2.00 (th.)	3.35	
ClO_4^-	99.5	2.25 (th.)	3.38	
OH^-	17.0	1.52 (th.)	3.00	
HCO_3^-	61.0	2.07 (th.)	5.60	
CO_3^{2-}	60.0	1.89 (th.)	3.94	
SO_4^-	96.1	2.18 (th.)	3.79	

Sources: Molar masses, (crystallographic) ionic radii and coordination numbers from Webelements.com; except (thermochemical) ionic radii of polyatomic ions from H. K. Roobottom, H. D. B. Jenkins, J. Passmore, L. Glasser, J. Chem. Educ. 76(11), 1570 – 1573, 1999; hydrated radii from E. R. Nightingale, J. Phys. Chem. 63(9), 1381 – 1387, 1959

The second set of tables details the parameters used in the calculation of the osmotic coefficient and the mean ionic activity coefficient.

Table 9: Parameters for the Meissner and Pitzer models of binary electrolytes at 25°C

Electrolyte	q	$\beta^{(0)}$	$\beta^{(1)}$	C^Φ
NaCl	2.98	0.0765	0.2664	0.00127
CaCl$_2$	2.40	0.4212	2.1520	− 0.00064
LaCl$_3$	1.41	0.8834	8.4000	− 0.06190
LiBr	7.27	0.1748	0.2547	0.00530
MgBr$_2$	3.50	0.5769	2.3370	0.00589
CsI	− 0.41	0.0244	0.0262	− 0.00365
HCl	6.69	0.1775	0.2945	0.00080
NaOH	3.00	0.0864	0.2530	0.00440
KNO$_3$	− 2.33	− 0.0816	0.0494	0.00660
Zn(NO$_3$)$_2$	2.28	0.4641	2.2550	− 0.02955
Na$_2$SO$_4$	− 0.19	0.0261	1.4840	0.01075
CdSO$_4$	0.016	0.2053	2.6170 − 48.07	0.01140

Source: J. F. Zemaitis Jr., D. M. Clark, M. Rafal, N. C. Scrivner; Handbook of aqueous electrolyte thermodynamics; DIPPR and AIChE Press, 1986

Table 10: Parameters corresponding to the dilute, semi-dilute, concentrated and general fittings of the osmotic coefficient ϕ

Electrolyte	Correlation parameter w			λ_{cation} (Å)			λ_{anion} (Å)		
	Dilute	Semi-Dilute	General	Dilute	Semi-Dilute	General	Dilute	Semi-Dilute	General
LiCl	3.8914	3.3396	1.7797	3.3523	4.4687	5.0180	3.5930	2.3783	2.0808
NaCl	4.9505	3.7199	2.1048	1.7005	2.5500	3.0884	1.6700	2.6535	3.1902
KCl	4.1299	3.9421	3.0933	1.5663	1.5686	2.1629	1.6779	1.7010	2.3481
RbCl	3.3030	3.4856	2.8063	2.2549	1.7643	2.3905	2.0819	1.6700	2.0810
CsCl	2.0005	2.7322	2.0312	2.2259	1.8101	2.3827	3.1976	1.9548	2.4991
MgCl$_2$	3.6772	2.7076	1.7909	3.0065	2.7762	1.7490	4.8784	5.4313	5.8088
CaCl$_2$	3.0943	2.5507	1.8129	3.3589	2.8352	2.1955	4.5587	5.1464	5.3627
SrCl$_2$	3.0528	2.9237	2.4513	3.5309	3.1244	2.6901	4.1370	4.5364	5.0104
BaCl$_2$	3.0936	X	2.9228	3.5356	X	3.7245	3.5103	X	3.4377
	Dilute	Concentrated	General	Dilute	Concentrated	general	Dilute	Concentrated	General
MnCl$_2$	3.2371	1.8504	1.8508	3.4628	4.7583	4.6667	4.2049	2.6362	2.7400
FeCl$_2$	3.1255	X	2.8540	3.2495	X	3.1409	4.5912	X	4.8157
CoCl$_2$	3.0572	X	2.8662	3.7459	X	3.6132	4.4128	X	4.6666
NiCl$_2$	3.4719	X	1.7976	3.0045	X	3.3123	4.7160	X	4.5889
CuCl$_2$	3.2722	7.0016	4.9909	3.2584	3.1821	3.1757	3.4980	2.3958	2.6330
ZnCl$_2$	4.5890	1.8964	2.1057	2.3662	1.0874	1.5619	1.6700	4.3263	4.0292
CdCl$_2$	X	X	2.0214	X	X	0.9200	X	X	2.6344

187

AlCl₃	No data			No data			No data		
FeCl₃	X	X	5.6049	X	X	0.6300	X	X	4.1434
YCl₃	X	X	2.5774	X	X	2.5786	X	X	5.8678
LaCl₃	X	3.2067	2.8484	X	3.9924	3.5403	X	4.6262	5.1696
CeCl₃	X	2.9068	2.7893	X	4.1708	3.3885	X	4.4842	5.2422
NaF	0.9258	X	3.6817	3.5577	X	1.1525	3.4864	X	1.1759
KF	4.7570	3.0667	1.8134	1.5987	2.8760	2.9565	1.5098	2.7421	3.2283
RbF	3.9471	X	4.7000	2.9349	X	2.2945	2.8995	X	2.9780
CsF	No data			No data			No data		
LiBr	3.9984	3.0646	1.7675	3.7854	3.7440	4.1133	3.3972	3.9718	4.0370
NaBr	5.0965	3.9061	1.7780	1.9856	2.6999	3.4376	2.0703	2.9761	3.1956
KBr	4.2189	4.0010	3.1313	1.7666	1.8096	2.2198	1.8200	1.8200	2.5514
RbBr	1.0624	3.2412	3.1698	3.4895	1.9037	1.8988	3.5061	1.8200	1.8798
CsBr *(conc.)*	1.6718	1.7330	2.3363	2.5237	2.2012	1.9838	2.9425	2.4330	2.0352
MgBr₂	3.8332	2.5497	2.0547	2.6635	2.4830	1.1258	5.5204	6.0648	6.6318
CaBr₂	3.7377	2.2290	1.7876	3.0557	1.8845	1.6429	4.9763	6.0537	6.3644
MnBr₂	3.2531	3.0068	1.7767	3.7648	3.2909	4.0377	4.9872	5.3472	4.6466
CuBr₂	3.7874	3.3798	1.7990	3.2182	3.7492	4.6871	4.8259	4.6475	3.3734
ZnBr₂ *(conc.)*	4.2646	1.805	4.0006	3.6681	1.7115	3.7917	4.1166	3.9881	3.0714
LiI	5.0105	X	2.3192	4.1117	X	4.2226	3.8114	X	4.3931
NaI	4.7338	3.8050	1.7903	2.7182	3.3360	4.0979	2.9646	3.2169	3.2724
KI	4.4255	X	3.6788	2.0714	X	2.2202	2.0600	X	2.6932
RbI	1.4519	X	2.9886	3.3326	X	1.8349	3.1173	X	2.2124
CsI	0.9225	1.8084	2.3194	2.9750	2.3909	1.9523	3.0168	2.7637	2.0600
MgI₂	3.0028	X	1.7581	4.1930	X	1.5119	5.4042	X	6.8122
CaI₂	3.6259	X	2.8812	3.8387	X	3.2377	5.0811	X	5.7230
HF	3.1026	X	2.5995	1.1500	X	1.1508	1.3362	X	2.0723
HCl	3.8385	X	2.1682	3.3812	X	3.8742	3.9829	X	4.3979
HBr	3.9097	X	1.7745	3.8340	X	4.1716	4.1821	X	4.3508
HI	4.5499	X	2.3849	4.1229	X	4.7528	4.3825	X	4.9215
HNO₃	4.6774	X	5.1430	3.0649	X	2.9365	2.7502	X	3.0179
H₂SO₄	1.8457	X	1.8564	4.4193	X	3.8475	2.1800	X	2.5719
LiNO₃	X	X	3.5288	X	X	3.6550	X	X	3.1830
NaNO₃	0.9850	X	0.0638	3.3602	X	1.9487	3.4807	X	2.2302
KNO₃	0.4483	X	0.1825	2.4048	X	1.7517	2.0014	X	2.0000
Mn(NO₃)₂	No data			No data			No data		
Co(NO₃)₂	3.3353	2.8909	2.4454	3.4492	3.3572	2.3081	4.1789	4.5504	5.2332
Ni(NO₃)₂	4.8754	3.6069	2.5480	2.6622	3.0378	2.2954	4.1566	4.6872	5.3326
Cu(NO₃)₂	3.6893	3.2264	2.6103	3.0751	2.9131	2.4556	3.8557	4.3393	4.8526
Zn(NO₃)₂	3.4845	3.1678	2.6276	3.9671	3.5951	2.6461	3.9954	4.5258	5.1788

Cd(NO₃)₂	3.3405	3.3627	2.9865	3.9197	3.6899	4.0899	3.1565	3.4695	3.2136
Al(NO₃)₃	No data			No data			No data		
	Dilute	Concen-trated	General	Dilute	Concen-trated	General	Dilute	Concen-trated	General
Li₂SO₄	2.3765	2.0036	2.3772	5.3631	3.0429	2.8613	3.8491	3.3094	3.2866
Na₂SO₄	1.7361	2.4341	2.4716	4.8472	1.1300	1.1300	3.0633	2.2411	2.3353
K₂SO₄	2.0686	2.4214	2.2087	2.2122	1.6070	1.8688	3.0753	2.6217	2.9487
Rb₂SO₄	2.9886	2.3723	2.6145	1.6852	1.6600	1.6600	2.8190	2.7287	2.3740
Cs₂SO₄	1.5799	2.8440	2.9182	3.7241	1.8100	1.8100	3.7149	2.2868	2.2004
	Semi-dilute	Concen-trated	General	Semi-dilute	Concen-trated	General	Semi-dilute	Concen-trated	General
MgSO₄	2.9636	1.8064	2.1757	1.0356	3.3025	2.7420	2.1800	2.4798	3.0401
NiSO₄	2.6027	1.8309	2.1235	1.8289	2.3016	2.5039	2.2462	2.9058	2.9444
CuSO₄	2.6965	1.9452	2.1483	1.3489	2.5314	2.4026	2.1800	2.9454	2.8965
ZnSO₄	2.3535	1.8055	2.0240	2.3908	3.1005	2.6346	2.5910	2.4438	2.9839
CdSO₄	2.7906	1.8068	1.9724	0.9457	3.4593	2.6736	2.2359	2.3334	2.9610
Al₂(SO₄)₃	No data			No data			No data		
LiClO₄	4.9043	X	1.7455	4.0413	X	4.4873	3.6421	X	3.8832
NaClO₄	4.2354	X	3.1414	1.4667	X	2.2327	2.2500	X	2.7044
KClO₄	0.9315	X	0.9236	2.7909	X	2.3799	2.9503	X	2.7580
Cd(ClO₄)₂	4.5221	3.4002	1.7145	3.9576	4.0665	3.6879	3.8878	5.0366	5.2711
NaOH	2.9258	X	2.1525	3.0138	X	3.5843	3.1940	X	3.7329
KOH	2.0491	X	2.1630	3.8090	X	3.9870	3.6455	X	3.9346

Note: The usual fittings for each series are dilute, semi-dilute and general fittings; if certain series have a different set, this set is mentioned in the heading.

Table 11: Parameters corresponding to the dilute, semi-dilute, concentrated and general fittings of the mean ionic activity coefficient $\gamma_\pm$

Electrolyte	Correlation parameter w			λ_{cation} (Å)			λ_{anion} (Å)		
	Dilute	Semi-dilute	General	Dilute	Semi-dilute	General	Dilute	Semi-dilute	General
LiCl	4.0287	3.0127	1.7797	1.7137	3.1172	4.5573	2.4129	3.6960	3.9384
NaCl	3.3930	2.8642	2.4466	2.3402	2.4608	2.5870	2.9809	2.3016	3.1001
KCl	0.9699	2.6895	2.5980	4.2959	1.6510	1.6523	4.5999	1.8083	2.1485
RbCl	1.3972	2.5261	2.5576	3.4588	1.7515	1.7530	4.5666	1.7046	1.6719
CsCl	1.5405	2.2590	2.3038	4.1476	1.8818	1.8819	3.1165	1.8532	1.7135
MgCl₂	3.4544	2.3979	1.7875	1.8089	1.9915	5.6947	3.3057	5.2669	4.7913
CaCl₂	3.2721	2.2104	1.8281	2.2082	2.9923	4.6474	2.5625	4.8830	4.8582
SrCl₂	3.0924	2.5917	2.0472	2.4144	2.8247	3.6087	2.3993	3.9330	4.6301
BaCl₂	2.8368	X	2.7490	2.7190	X	2.8449	2.5147	X	2.6116

189

MnCl$_2$	3.0980	2.7636	2.9888	1.9799	2.0267	3.8979	3.3026	4.0732	3.1972
FeCl$_2$	2.9510	X	2.6176	1.9613	X	1.9886	3.8011	X	4.5029
CoCl$_2$	3.5111	2.7831	2.4744	1.7980	1.9177	4.6885	2.3714	4.4949	3.8945
NiCl$_2$	3.5036	2.4928	2.5539	1.4364	1.5514	1.4521	2.8337	5.0223	4.9979
CuCl$_2$	3.1030	X	2.9981	1.5032	X	1.5327	2.2905	X	2.8156
ZnCl$_2$	3.0296	2.7394	1.8076	1.8236	1.5841	3.6541	2.3375	1.6715	3.4340
CdCl$_2$	1.8923	X	0.0000	1.2400	X	1.6171	1.7483	X	2.1273
AlCl$_3$	X	2.9164	2.2935	X	1.3992	1.4440	X	5.1077	6.3678
FeCl$_3$	X	X	2.6775	X	X	3.3206	X	X	3.9452
YCl$_3$	X	2.7933	1.7726	X	4.1773	5.6098	X	3.7413	5.0724
LaCl$_3$	2.9671	2.5560	1.8420	2.3140	2.4650	5.7667	3.5057	4.6860	4.4887
CeCl$_3$	X	2.5693	1.9351	X	4.1520	6.0162	X	3.4853	4.0597
NaF	3.1081	X	0.9254	2.4264	X	4.3020	2.1502	X	4.4059
KF	3.2624	3.0011	1.9925	2.9820	2.2458	3.1882	2.1435	1.8277	3.3861
RbF	3.4898	3.5102	3.3261	3.0738	2.1962	2.5055	2.0837	1.7580	1.9009
CsF	3.8868	3.6234	2.9762	3.0583	2.6794	3.5587	2.0276	1.8934	2.1756
LiBr	4.1242	3.0526	1.7675	1.7665	3.4624	4.9163	2.9169	3.7418	4.0371
NaBr	3.3971	2.7773	1.8987	2.0923	2.4204	3.7172	2.6292	3.2449	3.6658
KBr	0.9316	1.4049	1.7336	4.9986	4.8258	4.2547	3.8420	3.4502	2.6024
RbBr	1.3160	1.6427	1.7404	4.0939	3.5008	3.2071	4.1107	3.6921	3.3365
CsBr	1.4909	X	1.7155	3.5327	X	3.0181	3.8681	X	3.4507
MgBr$_2$	3.3740	2.8552	1.7712	1.8021	1.8782	6.0665	4.3822	5.2175	5.1264
CaBr$_2$	3.4649	2.9406	1.7574	2.2728	2.3826	5.9896	3.3713	4.5420	4.5503
MnBr$_2$	3.4596	2.9766	2.6453	1.9510	2.0118	5.0365	3.8713	4.7985	4.3046
CuBr$_2$	3.5945	3.2325	3.2042	1.5085	1.5408	1.5220	3.4222	4.3262	4.4194
ZnBr$_2$	3.8159	3.8208	1.7979	1.7724	1.8208	4.7434	2.4620	2.7117	3.4086
LiI	4.8616	3.7741	2.7802	1.8146	1.9713	3.9611	3.4998	4.6355	4.4400
NaI	3.6038	2.9135	1.7903	2.2863	3.1800	4.2277	3.4700	3.1775	3.9596
KI	2.3832	2.9080	2.9043	3.7473	2.0341	2.1201	4.2109	2.0602	2.0625
RbI	1.3990	2.3023	1.7172	4.0385	2.0306	3.3020	3.9659	2.0602	3.4462
CsI	1.4097	X	1.6290	3.5571	X	2.9793	3.9552	X	3.7743
MgI$_2$	3.6373	2.9462	1.7226	1.7986	1.8806	6.6776	4.2992	5.5321	4.9732
CaI$_2$	3.6587	3.0982	2.4638	2.2207	2.3105	2.4974	3.5637	4.8779	5.5994
HF	X	X	1.8604	X	X	1.2304	X	X	1.9966
HCl	4.0994	2.9579	2.1395	2.0191	2.7081	3.7807	2.9829	4.3194	4.4697
HBr	4.2539	2.9547	1.7708	1.9932	3.6601	4.3790	3.7055	4.3676	4.8554
HI	4.5190	3.4691	1.7405	2.0570	4.0168	4.7569	4.3794	4.3108	4.9982
HNO$_3$	3.8936	3.2506	3.1382	1.7114	2.0348	2.5885	2.3450	3.2497	3.1587
H$_2$SO$_4$	X	X	1.9430	X	X	3.1980	X	X	4.3102
LiNO$_3$	3.8185	3.0799	2.6399	1.7065	3.0346	3.4325	2.6497	3.1948	3.3506

	Dilute	Semi-dilute	Concen-trated	Dilute	Semi-dilute	Concen-trated	Dilute	Semi-dilute	Concen-trated
$NaNO_3$	0.9304	0.2088	0.0595	3.9649	2.4520	2.7000	4.4447	4.2438	2.8800
KNO_3	X	X	0.1420	X	X	2.3239	X	X	2.7241
$Mn(NO_3)_2$	X	2.7191	2.1196	X	4.0413	5.2160	X	3.5782	3.7013
$Co(NO_3)_2$	3.3090	2.6110	1.7681	1.7974	1.9320	5.4630	2.6743	4.4976	4.0892
$Ni(NO_3)_2$	3.9064	2.8968	1.8390	1.4077	1.5166	5.0622	2.4310	4.6082	4.6137
$Cu(NO_3)_2$	3.3147	2.4486	1.9012	1.4939	1.6343	5.2149	2.5097	4.5834	3.7813
$Zn(NO_3)_2$	3.5677	2.8998	1.7757	1.7789	1.9041	5.1496	2.5780	4.3391	4.4969
$Cd(NO_3)_2$	3.1962	X	2.8874	2.1347	X	2.2872	2.6041	X	3.3010
$Al(NO_3)_3$	X	X	1.7550	X	X	3.3900	X	X	5.6235
Li_2SO_4	2.3932	X	2.3500	1.8664	X	1.5788	4.3320	X	3.0644
Na_2SO_4	X	X	1.7040	X	X	2.2019	X	X	4.9715
K_2SO_4	X	X	1.7561	X	X	3.3091	X	X	3.7869
Rb_2SO_4	X	X	1.7070	X	X	2.5633	X	X	4.9977
Cs_2SO_4	1.6280	X	1.7037	3.9210	X	3.0200	4.6272	X	4.7681
	Dilute	Semi-dilute	Concen-trated	Dilute	Semi-dilute	Concen-trated	Dilute	Semi-dilute	Concen-trated
$MgSO_4$	X	2.6000	1.8568	X	1.7129	4.4115	X	2.2303	3.9060
$NiSO_4$	X	2.3214	2.1340	X	1.1976	2.8391	X	4.3515	3.0671
$CuSO_4$	X	2.2511	2.3127	X	1.3563	1.2479	X	4.3764	2.5784
$ZnSO_4$	2.5859	2.2531	1.9892	6.1305	1.4157	3.2636	4.7489	3.7107	3.8013
$CdSO_4$	2.4244	2.1995	2.1550	7.0000	1.8262	2.4131	2.4417	3.4341	2.6893
$Al_2(SO_4)_3$	X	X	2.5461	X	X	1.4094	X	X	2.3098
$LiClO_4$	4.9195	3.7818	2.3635	1.7182	3.7455	4.6786	3.0588	3.5923	3.9795
$NaClO_4$	0.9433	2.8205	2.8612	2.6377	1.4696	1.5269	5.8097	2.2511	2.2520
$KClO_4$	X	X	0.9398	X	X	3.6769	X	X	3.6971
$Cd(ClO_4)_2$	4.1333	3.3763	2.2398	2.1552	2.2897	2.4751	3.7564	4.4948	5.9687
$NaOH$	3.4311	1.9559	2.1000	2.0447	3.4965	3.4785	1.5300	3.5445	3.5750
KOH	3.4699	1.8250	1.8434	2.4498	4.1666	3.8831	2.3008	3.9001	4.2878

Note: The usual fittings for each series are dilute, semi-dilute and general fittings; if certain series have a different set, this set is mentioned in the heading.

Table 12: Parameters for the calculation of the solubility limit of one binary electrolyte in an aqueous solution of another binary electrolyte

System	Correlation parameter w	Hydrated radii
NaCl in HCl-H$_2$O	2.5729	$\lambda_{H+} = 3.8206$ $\lambda_{Na+} = 2.1804$ $\lambda_{Cl-} = 3.5016$
KCl in HCl-H$_2$O	3.0570	$\lambda_{H+} = 3.7583$ $\lambda_{K+} = 2.4590$ $\lambda_{Cl-} = 3.7312$
NaCl and KCl in H$_2$O	KCl precipitate – 3.0200	KCl precipitate $\lambda_{Na+} = 2.4401$ $\lambda_{K+} = 2.9302$ $\lambda_{Cl-} = 3.4002$
	NaCl precipitate – 2.6574	NaCl precipitate $\lambda_{Na+} = 1.8940$ $\lambda_{K+} = 2.7172$ $\lambda_{Cl-} = 3.0570$
KCl and CaCl$_2$ in H$_2$O	CaCl$_2$·6H$_2$O precipitate – 4.5	CaCl$_2$·6H$_2$O precipitate* $\lambda_{K+} = 1.8$ $\lambda_{Ca++} = 1.7$ $\lambda_{Cl-} = 1.9$
	KCl precipitate – 4.8059	KCl precipitate $\lambda_{K+} = 1.6944$ $\lambda_{Ca++} = 3.7571$ $\lambda_{Cl-} = 3.4247$

* These parameters could not be numerically adjusted.

Table 13: Composition of reference seawater (S = 35‰)

Ion	Concentration (mol/kg water)
Na$^+$	0.83733
K$^+$	0.01822
Mg^{2+}	0.09429
Ca^{2+}	0.01836
Cl$^-$	0.97521
Br$^-$	0.00150
HCO$_3^-$	0.00332
SO$_4^{2-}$	0.05042

Table 14: Parameters corresponding to the general fitting for seawater

	w	Cations	Anions
Osmotic coefficient	3.4485	$\lambda_{Na} = 2.3887$ $\lambda_K = 3.0479$ $\lambda_{Mg} = 1.7363$ $\lambda_{Ca} = 2.0357$	$\lambda_{Cl} = 3.6115$ $\lambda_{Br} = 3.7462$ $\lambda_{HCO3} = 3.8336$ $\lambda_{SO4} = 3.4855$
Activity coefficient	3.4063	$\lambda_{Na} = 1.3903$ $\lambda_K = 1.8120$ $\lambda_{Mg} = 1.0915$ $\lambda_{Ca} = 1.4114$	$\lambda_{Cl} = 1.9227$ $\lambda_{Br} = 1.9660$ $\lambda_{HCO3} = 2.2381$ $\lambda_{SO4} = 2.3584$

Table 15: A few Gibbs free energies of formation from references [16,21]

Ions	Gibbs free energy of formation (kJ/mol)
Zn^{2+}	$-$ 147.1
Cl^-	$-$ 131.2
Br^-	$-$ 104.0
$ZnCl^+$	$-$ 275.3
$ZnBr^+$	$-$ 247.7

Table 16: Parameters for the general fittings of two partially associated electrolytes

Electrolyte		Osmotic coefficient	Mean ionic activity coefficient
$ZnCl_2$	Binary	w = 2.1143 $\lambda_{Zn} = 1.8702$ $\lambda_{Cl} = 4.0095$	Binary w = 1.9100 $\lambda_{Zn} = 4.0214$ $\lambda_{Cl} = 3.4214$
	Ternary	K = 0.03 w = 4.2865 $\lambda_{Zn} = 1.4987$ $\lambda_{ZnCl} = 4.7911$ $\lambda_{Cl} = 1.6700$	Ternary K = 0.03 w = 1.85 $\lambda_{Zn} = 4.10$ $\lambda_{ZnCl} = 3.95$ $\lambda_{Cl} = 3.55$
$ZnBr_2$	Binary	w = 1.9504 $\lambda_{Zn} = 1.3440$ $\lambda_{Cl} = 4.6604$	Binary w = 2.0113 $\lambda_{Zn} = 4.3953$ $\lambda_{Cl} = 3.6976$
	Ternary	K = 1.0403 w = 4.0914 $\lambda_{Zn} = 1.497$ $\lambda_{ZnCl} = 5.279$ $\lambda_{Cl} = 1.820$	Ternary K = 1.0403 w = 2.6596 $\lambda_{Zn} = 2.4589$ $\lambda_{ZnCl} = 5.0109$ $\lambda_{Cl} = 1.9006$

Bibliography

Books

1. W. K. Purves, D. Sadava, G. H. Orians, H. C. Heller; Life, The Science of Biology, 7th edition; Sinauer Associates Inc. and W. H. Freeman and Company (2003)
2. H. F. Lodish, P. T. Matsudaira, C. Kaiser, M. Krieger; Molecular cell biology, 5th edition; W. H. Freeman and company (2004)
3. G. Stuart, N. Sprutson, M. Hausser; Dendrites; Oxford University Press (2001)
4. R. W. Davies, B. J. Morris, G. L. Collingridge, S. P. Hunt; Molecular Biology of the Neuron, 2nd edition; Oxford University Press in Molecular and cellular neurobiology series (2004)
5. S. J. Moss, J. Henley, R. W. Davies, G. L. Collingridge, S. P. Hunt; Receptor and Ion-Channel Trafficking, Cell biology of ligand-gated and voltage-sensitive ion channels; Oxford University Press in Molecular and cellular neurobiology series (2002)
6. J. S. Newman, K. E. Thomas-Alyea; Electrochemical systems, 3rd edition; Electrochemical Society Series, Wiley Interscience (2004)
7. C. Holm, P. Kekicheff, R. Podgornik; Electrostatic effects in soft matter and biophysics, Kluwer Academic Publishers in cooperation with NATO Scientific Affairs Division (2001)
8. V. I. Kalikmanov; Statistical Physics of Fluids – Basic concepts and applications; Springer (2001)
9. D. Henderson; Fundamentals of inhomogenous fluids; Marcel Dekker (1992)
10. B. E. Conway, R. G. Barradas; Chemical Physics of ionic solutions; John Wiley & Sons (1966)
11. J. P. Hansen, I. R. McDonald; Theory of simple liquids; Academic Press (1976)
12. M. P. Das, F. Green; Condensed matter theories; Nova Science (2001)
13. J. W. Tester, M. Modell; Thermodynamics and its applications, 3rd edition; Prentice Hall (1997)
14. L. L. Lee; Molecular thermodynamics of electrolyte solutions; World Scientific (2008)
15. K. S. Pitzer; Thermodynamics; McGraw-Hill (1995)
16. J. F. Zemaitis Jr., D. M. Clark, M. Rafal, N. C. Scrivner; Handbook of aqueous electrolyte solutions ; DIPPR and AIChE Press (1986)
17. Y. Y. Akhadov; Dielectric properties of binary solutions – A data handbook; Pergamon Press (1981)
18. J. Barthel, R. Buchner, M. Münsterer; Electrolyte data collection – Dielectric properties of water and aqueous electrolyte solutions; DECHEMA Chemistry Data Series, vol. XII, part 2 (1995)
19. V. M. M. Lobo; Handbook of electrolyte solutions; Elsevier Publishers (1989)
20. O. Söhnel, P. Novotný; Densities of aqueous solutions of inorganic substances; Elsevier (1985)
21. D. D. Wagman, W. H. Evans, V. B. Parker, R. H. Schumm, I. Halow; Selected values of chemical thermodynamic properties; NBS technical notes 270-3, 270-4

Dissertation

22. J. Benda; Single Neuron Dynamics – Models linking theory and experiment; Humboldt University in Berlin (2002)

Papers on models of neurons

23. P. A. Rhodes, R. Llinas; A model of thalamocortical relay cells; Journal of Physiology, 565(3), 765 – 781, 2005
24. L. K. Purvis, R. J. Butera; Ionic current model of a hypoglossal motoneuron; Journal of Neurophysiology, 93, 723 – 733, 2005
25. A. J. Trevelyan, J. J. Jack; Detailed passive cable models of layer 2/3 pyramidal cells in rat visual cortex at different temperatures; Journal of Physiology, 539(2), 623 – 636, 2001
26. J. Benda, A. V. M. Hertz; A universal model of spike-frequency adaptation; Neural Computation, 15, 2523 – 2564, 2003
27. R. Amir, M. Devor; Electrical excitability of the soma of sensory neurons is required for spike invasion of the soma but not for through conduction; Biophysical Journal, 84, 2181 – 2191, 2003

Papers on signal propagation in dendrites

28. H. Kawaguchi, K. Fukunishi; Dendrite classification in rat hippocampal neurons according to signal propagation properties; Experimental Brain Research, 122, 378 – 392, 1998
29. G. Buzsaki, A. Kandel; Somatodendritic backpropagation of action potentials in cortical pyramidal cells of the awake rat; Journal of Neurophysiology, 79, 1587 – 1591, 1998
30. S. Antic, G. Major, D. Zecevic; Fast optical recordings of membrane potential changes from dendrites of pyramidal neurons; Journal of Neurophysiology 82, 1615 – 1621, 1999
31. D. A. Hoffman, J. C. Magee, C. M. Colbert, D. Johnston; K+ channel regulation of signal propagation in dendrites of hippocampal pyramidal neurons; Nature, 387, 869 – 875, 1997

Papers on the repartition, role and regulation of actin in neurons

32. F. Doussau, G. J. Augustine; The actin cytoskeleton and neurotransmitter release: an overview; Biochimie, 82, 353 – 363, 2000
33. F. Capani, M. E. Martone, T. J. Deerinck, M. H. Ellisman; Selective localization of high concentrations of F-actin in subpopulations of dendritic spines in rat central nervous system: a three-dimensional electron microscopic study; Journal of Computational Neurology, 435, 156 – 170, 2001

34. F. Capani, M. H. Ellisman, M. E. Martone; Filamentous actin is concentrated in specific subpopulations of neuronal and glial structures in rat central nervous system, Brain Research, 923, 1 – 11, 2001

35. T. Furuyashiki, Y. Arakawa, S. Takemoto-Kimura, H. Bito, S. Narumiya; Multiple spatiotemporal modes of actin reorganization by NMDA receptors and voltage-gated Ca^{2+} channels; Proceedings of the National Academy of Science USA, 99(22), 14458 – 14463, 2002

36. D. W. Allison, V. I. Gelfand, I. Spector, A. M. Craig; Role of actin in anchoring postsynaptic receptors in cultured hippocampal neurons: differential attachment of NMDA versus AMPA receptors; Journal of Neuroscience, 18(7), 2423 – 2436, 1998

37. E. A. Nimchinsky, B. L. Sabatini, K. Svoboda; Structure and function of dendritic spines; Annual Review in Physiology, 64, 313 – 353, 2002

38. C. Dillon, Y. Goda; The actin cytoskeleton: integrating form and function at the synapse; Annual Review in Neuroscience, 28, 25 – 55, 2005

39. Y. Fukazawa, Y. Saitoh, F. Ozawa, Y. Ohta, K. Mizuno, K. Inokuchi; Hippocampal LTP is accompanied by enhanced F-actin content within the dendritic spine that is essential for late LTP maintenance in vivo; Neuron, 38, 447 – 460, 2003

40. B. Qualmann, T. M. Boeckers, M. Jeromin, E. D. Gundelfinger, M. M. Kessels; Linkage of the actin cytoskeleton to the postsynaptic density via direct interactions of Abp1 with ProSap/Shank family; Journal of Neuroscience, 24(10), 2481 – 2495, 2004

41. A. W. McGee, D. S. Bredt; Assembly and plasticity of the glutamatergic postsynaptic specialization; Current Opinion in Neurobiology, 13, 111 – 118, 2003

42. T. G. Oertner, A. Matus; Calcium regulation of actin dynamics in dendritic spines; Cell Calcium, 37, 477 – 482, 2005

43. R. Yuste, A. Majewska, K. Holthoff; From form to function: calcium compartmentalization in dendritic spines; Nature Neuroscience, 3(7), 653 – 659, 2000

44. B. W. Bernstein, J. R. Bamburg; Actin-ATP hydrolysis is a major energy drain for neurons; Journal of Neuroscience, 23(1), 1 – 6, 2003

Papers on electrical properties of DNA, actin filaments and microtubules

45. M. Troll, D. Roitman, J. Conrad, B. H. Zimm; Electrostatic interactions between ions and DNA estimated with an electrolyte tank; Macromolecules, 19, 1186 – 1194, 1986

46. C. F. Anderson, M. T. Record Jr.; Ion distribution around DNA and other cylindrical polyions: theoretical descriptions and physical implications; Annual Reviews in Biophysics and Biophysical Chemistry, 19, 423 – 465, 1990

47. H. F. Cantiello, C. Patenaude, K. Zaner; Osmotically induced electrical signals from actin filaments; Biophysical Journal 59, 1284 – 1289, 1991

48. E. C. Lin, H. F. Cantiello; A novel method to study the electrodynamic behavior of actin filaments, Evidence for cable-like properties of actin; Biophysical Journal, 65, 1371 – 1378, 1993

49. J. X. Tang, P. A. Janmey; The polyelectrolyte nature of F-actin and the mechanism of actin bundle formation; Journal of biological chemistry, 271(15), 8556 – 8563, 1996

50. V. A. Bloomfield; DNA condensation by multivalent cations; Biopolymers: Nucleic Acid Science, 44(3), 269 – 282, 1997

51. W. Xian, J. X. Tang, P. A. Janmey, W. H. Braunlin; The polyelectrolyte behavior of actin filaments: a ^{25}Mg NMR study; Biochemistry, 38, 7219 – 7226, 1999

52. J. Gartzke, K. Lange; Cellular target of weak magnetic fields: ionic conduction along actin filaments of microvilli; American Journal of Physiology, 283, 1333 – 1346, 2002

53. D. D. Georgiev, S. N. Papaioanou, J. F. Glazebrook; Neuronic system inside neurons: molecular biology and biophysics of neuronal microtubules; Biomedical Reviews, 15, 67 – 75, 2004

54. J. A. Tuszynski, S. Portet, J. M. Dixon, C. Luxford, H. F. Cantiello; Ionic wave propagation along actin filaments; Biophysical Journal 86, 1890 – 1903, 2004

55. J. A. Tuszynski, J. A. Brown, E. Crawford, E. J. Carpenter, M. L. A. Nip, J. M. Dixon, M. V. Sataric; Mathematical and computer modeling, 1 – 16, 2005

56. T. E. Angelini, L. K. Sanders, H. Liang, W. Wriggers, J. X. Tang, G. C. L. Wong; Structure and dynamics of condensed multivalent ions within polyelectrolyte bundles: a combined X-ray diffraction and solid-state NMR study; Journal of Physics: Condensed matter, 17, S1123 – S1135, 2005

57. T. E. Angelini, H. Liang, W. Wriggers, G. C. L. Wong ; Direct observation of counterion organization in F-actin polyelectrolyte bundle; European Physical Journal E, 16, 389 – 400, 2005

Papers on models of signal propagation in neurons

58. C. Ripoll, V. Norris, M. Thellier; Ion condensation and signal transduction; BioEssays, 26, 549 – 557, 2004

59. N. Qian, T. J. Sejnowski; An electro-diffusion model for computing membrane potentials and ionic concentrations in branching dendrites, spines and axons; Biological Cybernetics, 62, 1 – 15, 1989

60. M. Leonetti; On biomembrane electrodiffusive models; European Physical Journal B, 2, 325 – 340, 1998

61. A. Nygren, A. Halter; A general approach to modeling conduction and concentration dynamics in excitable cells of concentric cylindrical geometry; Journal Theoretical Biology 199, 329 – 358, 1999

62. M. Leonetti and E. Dubois-Violette; Theory of electrodynamic instabilities in biological cells; Physical Review Letters, 81(9), 1977 – 1980, 1998

63. T. Euler, W. Denk; Dendritic processing; Current Opinion in Neurobiology, 11, 415 – 422, 2001

64. S. Coombes; From periodic traveling waves to traveling fronts in the spike-diffuse-spike model of dendritic waves; Mathematical Biosciences, 170, 155 – 172, 2001

Papers on the Poisson – Boltzmann theory

65. R. M. Fuoss, A. Katchalsky, S. Lifson; The potential of an infinite rod-like molecule and the distribution of counterions; Proceedings of the National Academy of Sciences USA, 37, 579 – 589, 1951

66. J. R. Philip, R. A. Wooding; Solution of the Poisson – Boltzmann equation about a cylindrical particle; Journal of Chemical Physics, 52(2), 953 – 959, 1969

67. C. W. Outhwaite; A modified Poisson – Boltzmann equation for the ionic atmosphere around a cylindrical wall; Journal of the Chemical Society – Faraday Trans. 2, 82, 789 – 794, 1986

68. T. Das, D. Bratko, L. B. Bhuiyan, C. W. Outhwaite; Polyelectrolyte solutions containing mixed valency ions in the cell model: a simulation and modified Poisson – Boltzmann study; Journal of Chemical Physics, 107(21), 9197 – 9207, 1997

69. I. Borukhov, D. Andelman, H. Orland; Steric effects in electrolytes: a modified Poisson – Boltzmann equation; Physical Review Letters, 79(3), 435 – 438, 1997

70. L. Lue, N. Zoeller, D. Blankschtein ; Incorporation of non-electrostatic interactions in the Poisson – Boltzmann equation; Langmuir, 15, 3726 – 3730, 1999

71. V. Vlachy; Ionic effects beyond Poisson – Boltzmann theory; Annual Review of Physical Chemistry 50, 145 – 165, 1999

72. M. Deserno, C. Holm, S. May; The fraction of condensed counterions around a charged rod: comparison of Poisson – Boltzmann theory and computer simulations; Macromolecules, 33, 199 – 207, 2000

73. M. Quesada – Perez, E. Gonzalez – Tovar, A. Martin – Molina, M. Lozada – Cassou, R. Hidalgo – Alvarez ; Overcharging in colloids : beyond the Poisson – Boltzmann approach ; ChemPhysChem, 4, 234 – 248, 2003

Papers on the density functional theory

74. A. G. Moreira, R. R. Netz; Strong – coupling theory for counterion distributions; Europhysics Letters, 52(6), 705 – 711, 2000

75. R. R. Netz; Electrostatics of counter – ions at and between planer charged walls: from Poisson – Boltzmann to the strong – coupling theory; European Physical Journal E, 5, 557 – 574, 2001

76. M. C. Barbosa, M. Deserno, C. Holm; A stable local density functional approach to ion-ion correlations; Europhysics Letters, 52(1), 80 – 86, 2000

77. D. Antypov, M. C. Barbosa, C. Holm ; Incorporation of excluded-volume correlations into Poisson – Boltzmann theory; Physical Review E, 71, 061106-1 – 061106-10, 2005

78. Y. X. Yu, J. Wu, G. H. Gao; Density-functional theory of spherical electric double layers and ζ potentials of colloidal particles in restricted primitive model electrolyte solutions; Journal of Chemical Physics, 120(15), 7223 – 7233, 2004

79. C. N. Patra, A. Yethiraj; Density functional theory for the non-specific binding of salt to polyelectrolytes: thermodynamic properties; Biophysical Journal, 78, 699 – 706, 2000

80. C. N. Patra, S. K. Ghosh; Structure of electric double layers: a self-consistent weighed-density-functional approach; Journal of Chemical Physics, 117(19), 8938 – 8943, 2002

81. C. N. Patra, L. B. Bhuiyan; The effect of ionic size on polyion – small ion distributions in a cylindrical double layer; Condensed matter physics, 8(2,42), 425 – 446, 2005

Papers on hypernetted chain theory

82. M. Lozada – Cassou; Hypernetted chain theory for the distribution of ions around a cylindrical electrode; Journal of Physical Chemistry, 87, 3729 – 3732, 1983
83. E. Gonzales – Tovar, M. Lozada – Cassou, D. Henderson; Hypernetted chain theory for the distribution of ions around a cylindrical electrode. II. Numerical solution for a model cylindrical polyelectrolyte; Journal of Chemical Physics, 83(1), 361 – 372,1985
84. R. Messina, E. Gonzalez – Tovar, M. Lozada – Cassou, C. Holm ; Overcharging: the crucial role of excluded volume; Europhysics Letters, 60(3), 383 – 389, 2002
85. R. Kjellander, T. Akesson, B. Jonsson, S. Marcelja; Double layer interactions in mono- and di-valent electrolytes: a comparison of the anisotropic hypernetted chain theory and Monte-Carlo simulations; Journal of Chemical Physics, 97(2), 1424 – 1431, 1992

Papers on counterion condensation

86. G. S. Manning; Limiting laws and counterion condensation in polyelectrolyte solutions, I. Colligative properties; Journal of Chemical Physics 51(3), 924 – 933, 1969
87. G. S. Manning; The molecular theory of polyelectrolyte solutions with applications to the electrostatic properties of polynucleotides; Quarterly Reviews in Biophysics 11(2), 179 – 246, 1978
88. B. H. Zimm, M. Le Bret; Counterion condensation and system dimensionality; Journal of Biomolecular Structure and Dynamics, 1, 461 – 471, 1983
89. M. Le Bret, B. H. Zimm; Distribution of counterions around a cylindrical polyelectrolyte and Manning's condensation theory; Biopolymers, 23, 287 – 312, 1984
90. R. D. Groot; Ion condensation on solid particles: theory and simulations; Journal of Chemical Physics, 95(12), 9191 – 9203, 1991
91. V. I. Perel, B. I. Shklovskii; Screening of a macroion by multivalent ions: a new boundary condition for the Poisson – Boltzmann equation and charge inversion; Physica A, 274(3,4), 446 – 453, 1999
92. B. I. Shklovskii; Screening of a macroion by multivalent ions: condensation induced inversion of charge; Physical Review E 60(5), 5802 – 5811, 1999
93. B. I. Shklovskii; Wigner crystal model of counterion induced bundle formation of rodlike polyelectrolytes; Physical Review Letters, 82(16), 3268 – 3271, 1999
94. A. Deshkovski, S. Obukhov, M. Rubinstein; Counterion phase transitions in dilute polyelectrolyte solutions; Physical Review Letters, 86(11), 2341 – 2344, 2001
95. A. G. Moreira, R. R. Netz; Counterions at charge-modulated substrates; Europhysics Letters, 57(6), 911 – 917, 2002

96. A. Y. Grosberg, T. T. Nguyen, B. I. Shklovskii ; Colloqium : The physics of charge inversion in chemical and biological systems; Reviews of Modern Physics, 74, 329 – 345, 2002

97. A. W. C. Lau, D. B. Lukatsky, P. Pincus, S. A. Safran; Charge fluctuations and counterion condensation; Physical Review E, 65, 051502-1 – 051602-7, 2002

98. D. B. Lukatsky, S. A. Safran, A. W. C. Lau, P. Pincus; Enhanced counterion localization induced by surface charge modulation; Europhysics Letters, 58(5), 785 – 791, 2002

99. M. L. Henle, C. D. Santangelo, D. M. Patel, P. A. Pincus; Distribution of counterions near discretely charged planes and rods; Europhysics Letters, 66(2), 284 – 290, 2004

100. C. C. Floeck, R. R. Netz; Counterions at disordered charged planar surfaces; Europhysics Letters, 70(3), 341 – 347, 2005

101. Z. J. Tan, S. J. Chen; Electrostatic correlations and fluctuations for ion binding to a finite length polyelectrolyte; Journal of Chemical Physics, 122, 044903-1 – 0444903-16, 2005

Papers on polymer solution theory

102. A. V. Dobrynin, R. H. Colby, M. Rubinstein; Scaling theory of polyelectrolyte solutions; Macromolecules, 28, 1859 – 1871, 1995

103. A. V. Dobrynin, M. Rubinstein; Counterion condensation and phase separation in solutions of hydrophobic polyelectrolytes; Macromolecules, 34, 1964 – 1972, 2001

104. R. de Vries; Flexible polymer-induced condensation and bundle formation of DNA and F-actin filaments; Biophysical Journal, 80, 1186 – 1194, 2001

105. F. Bordi, C. Cametti, A. Motta, G. Paradossi; Electrical conductivity of dilute and semi-dilute aqueous polyelectrolyte solutions: a scaling theory approach; Journal of Physical Chemistry B, 103, 5092 – 5099, 1999

106. F. Bordi, R. H. Colby, C. Cametti, L. De Lorenzo, T. Gili; Electrical conductivity of polyelectrolyte solutions in the semi-dilute and concentrated regime: the role of counterion condensation; Journal of Physical Chemistry B, 106, 6887 – 6893, 2002

107. F. Bordi, C. Cametti, T. Gili; Electrical conductivity of polyelectrolyte solutions in the presence of added salt: the role of solvent quality factor in light of a scaling approach; Physical Review E, 68, 011805-1 – 011805-12, 2003

108. M. Muthukumar; Theory of counterion condensation on flexible polyelectrolytes: adsorption mechanism; Journal of Chemical Physics, 120(19), 9343 – 9250, 2004

109. A. V. Dobrynin, M. Rubinstein; Theory of polyelectrolytes in solutions and at surfaces; Progress in Polymer Science, 30, 1049 – 1118, 2005

Paper on dielectric constant

110. P. Wang, A. Anderko; Computation of dielectric constants of solvent mixtures and electrolyte solutions; Fluid phase equilibria, 186, 103 – 122, 2001

Papers ionic radii

111. E. R. Nightingale; Phenomenological theory of ion salvation – Effective radii of hydrated ions; J. Phys. Chem. 63(9), 1381 – 1387, 1959

112. H. K. Roobottom, H. D. B. Jenkins, J. Passmore, L. Glasser; Thermochemical radii of complex ions; J. Chem. Educ. 76(11), 1570 – 1573, 1999
113. A.G. Volkov, S. Paula, D.W. Deamer; Two mechanisms of permeation of small neutral molecules and hydrated ions across phospholipid bilayers; Bioelectrochemsitry and Bioenergetics, 42, 153 – 160, 1997
114. M. Ito, P.G. Kostyuk and T. Oshima; Further study on anion permeability of inhibitory post-synaptic membrane of cat motoneurons; Journal of Physiology, 164, 150 – 156, 1962

Papers on multicomponent electrolytes

115. R. M. Rush, J. S. Johnson; Osmotic coefficients of synthetic sea-water solutions at 25°C; Journal of Chemical and Engineering Data, 11(4), 590 – 592, 1966
116. L. A. Bromley, D. Singh, P. Ray, S. Sridhar, S. M. Read; Thermodynamic properties of sea salt solutions; AIChE Journal, 20(2), 326 – 335, 1974
117. F. J. Millero, W. H. Leung ; The thermodynamics of seawater at one atmosphere; American Journal of Science, 276, 1035 – 1077, 1976

MIT Project on the Future of Natural Gas

Appendix E

The Ammonia Industry in the United States

*Ammonia's role as link between natural gas and agriculture
and its impact on the ethanol cycle*

INTRODUCTION

Ammonia is a simple chemical of molecular formula NH_3. It is one of the most widely produced chemicals in the world because it is the principal source of nitrogen for the whole chemical industry. It is usually synthesized by reacting nitrogen N_2 and hydrogen H_2 under high temperatures and pressures. Note that sodium nitrate is mined in Chile, which constitutes an alternative source of fixed nitrogen. Unfortunately the production and reserves are too small compared to the global demand for fixed nitrogen.

The production and commercialization of ammonia is included in the study on the future of natural gas because it is the largest industrial consumer of natural gas. Indeed in the United States in 2007 the manufacturing of ammonia represented 5.7 % of industrial consumption and 1.6 % of total consumption, even though domestic production accounted for only 60 % of domestic consumption [1]. Moreover ammonia and its derivatives are one of the major groups of fertilizers and play an essential role in the debates on biofuels and emissions of carbon dioxide.

The main uses of ammonia are in decreasing importance:

- fertilizer or precursor for the other fertilizers containing nitrogen
- ingredient in the fabrication of explosives
- ingredient in the manufacturing of various chemicals, fibers and plastics
- industrial solvent or refrigerating agent.

In the United States the fertilizer segment accounts for aapproximately 80% of the total consumption hence the present study examines it in great detail. But before delving into the details, let us provide an overview of the other segments [2].

The second biggest segment of the ammonia market is the fabrication of explosives. Ammonia is processed into ammonium nitrate that is mixed with fuel oil to yield a blasting agent merely called ANFO, ammonium nitrate / fuel oil. ANFO is cheap, stable in ambient conditions and insensitive to shocks. It is the explosive of choice in the mining, quarrying and construction industries; consequently it represents about 70% of the total explosives used in the United States [3].

The last two segments of the ammonia market are small overall but are very important for the chemical industry. First it is a widely used solvent and refrigerant in industrial processes [4]. Second it is the precursor for most of the chemicals containing nitrogen, such as nitric acid, melamine, hydrogen cyanide or acrylonitrile. In turn these are used in the production of numerous plastics and fibers. Thus ammonia is a basic feedstock for the fiber and plastics industries [4].

AMMONIA AND DERIVED FERTILIZERS

Modern agricultural practices still prescribe rotating between crops that work the soil out, such as corn or wheat, and crops that regenerate the soil, such as soybeans. Nevertheless the rotation is not sufficient to achieve high yields so exogenous nutrients are routinely added. The nutrients that constrain the growth of plants and their productivity are nitrogen, phosphorous and potassium. Thus commercial fertilizers supplement the soil in one of these ingredients or in a combination of them. The present study focuses on nitrogen and its main vector ammonia and its derivatives.

The fertilizers containing nitrogen are all derived from ammonia. Together they account for about 80% of the total consumption of ammonia.

Table 1: Ammonia and its agricultural derivatives

Product	Quantity	Proportion
Anhydrous Ammonia	3,160	26.2%
Aqua Ammonia (NH_4OH)	71	0.6%
Urea	2,380	19.8%
Ammonium Nitrate	325	2.7%
Urea-ammonium Nitrate Solutions	3,260	27.1%
Ammonium Sulfate	262	2.2%
Sodium Nitrate	13	0.1%
Other single nutrient forms	328	2.7%
Multinutrient products	2,240	18.6%
Total	12,039	100%

The source is the US Geological Survey – 2007 Minreals Yearbook – Nitrogen [2].

The multinutrient products are mainly monoammonium and diammonium phosphate.
The quantity is in thousands of metric tons of nitrogen. To obtain the corresponding quantity of ammonia, the numbers should be multiplied by 17/14.

Thus the quantity of ammonia consumed as direct and indirect fertilizer amounts to 14.6 million metric tons and represents 79 % of the total consumption of ammonia in 2007 [5].

The total quantities of fertilizers used hence the total quantity of ammonia consumed depend on the total acreage planted and on the choice of crops. Corn is the large scale crop that requires the highest quantity of fertilizer; wheat ranks second.

The consumption of the various fertilizers derived from ammonia depends on the price-to-effective-nitrogen content ratio, on the ease of a storage and application to the soil and on the ability of soil to absorb nitrogen. The distribution has stabilized in the last decades and is expected to shift only slowly.

- Anhydrous Ammonia
- Aqua Ammonia (NH4OH)
- Urea
- Ammonium Nitrate
- Urea-ammonium Nitrate Solutions
- Ammonium Sulfate
- Sodium Nitrate
- Other single nutrient forms
- Multinutrient products
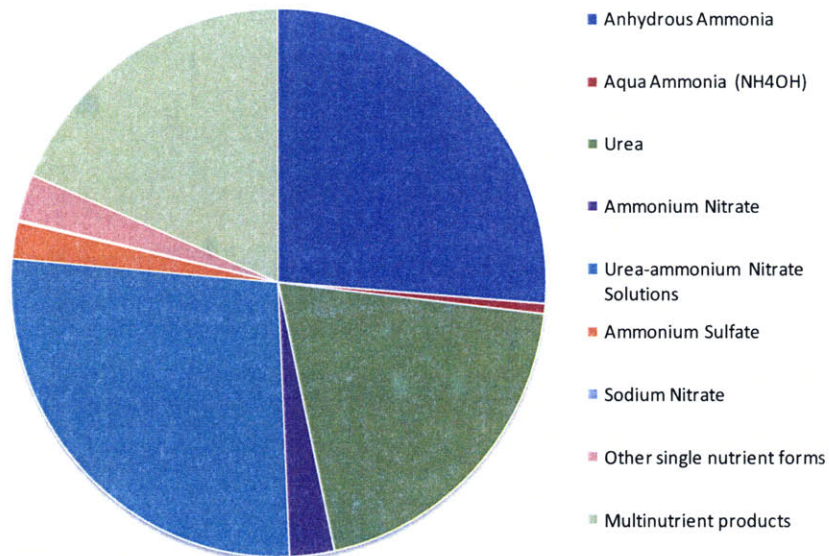
Figure 1: Distribution of ammonia and its agricultural derivatives (2007)

MANUFACTURING

Ammonia is produced at industrial scale by reacting nitrogen gas, N_2, with hydrogen gas, H_2 at very high temperatures and pressures: 350°C – 550°C and 8 – 40 atm depending on the catalyst used. The process was developed by Fritz Haber and Carl Bosch at the beginning of the XXth century and has been steadily improved since the

1950's [4]. The source of nitrogen gas is almost always air; the sources of hydrogen gas are often natural gas or gasified coal but oil, petroleum coke and the electrolysis of water are sometimes employed. The source of energy depends on the particulars of the plant and of its environment. In the United States, the second biggest producer in the world, natural gas is the main source of hydrogen and energy; in China, the biggest producer in the world, coal is the main source of energy and hydrogen. The source of hydrogen gas and energy are the main components of the cost of making ammonia, ranging between 70% and 95% of the total cost [4].

In the United States ammonia can be produced at 24 plants. One plant makes use of petroleum coke, one makes use of coal gasification and the rest are based on natural gas. One plant based on natural gas is under construction and production is planned to start in 2010. The most common process is given in Appendix 1. Only 22 plants currently produce ammonia. The 2 others are idle because they are not profitable at current prices for ammonia and natural gas. The list of plants, their capacity, efficiency and status is in Appendix 2.

In the United States natural gas is the main driver of the cost of producing ammonia. Currently it represents about 90% of the manufacturing costs [2]. Consequently the efficiency of a plant is measured as the quantity of natural gas required to produce a metric ton of ammonia. The average efficiency for the American plants is 38 GJ/metric ton. The older plants, built in the 1960's and 1970's have efficiencies of about 42 GJ/metric ton in spite of upgrades; the most recent ones built in the 1990's have efficiencies of about 28 GJ/metric ton, close to the current state of the art of 27 GJ/metric ton [6]. Even though the ability to distribute ammonia efficiently to customers matters, the current high prices of natural gas have forced numerous old and inefficient plants to close; the majority of these plants were small, owned and operated by cooperatives, and supplied only the very local market [2,7]. The 4 idle plants are not closed yet because they belong to large corporations that still ponder whether to modernize or to close them; they currently serve as storage and distribution sites.

DISTRIBUTION OF AMMONIA AND ITS AGRICULTURAL DERIVATIVES

At ambient pressure, ammonia's boiling point is – 33.3°C, which makes transportation from the manufacturing plants to the final customer difficult. To reduce the cost of distribution several methods have been developed:

   a. The first method is to further process ammonia by installing another plant nearby. Indeed several midsized ammonia plants are part of a larger industrial

complex that process all or part of their output into urea, nitric acid, ammonium nitrate, urea-ammonium nitrate solution, etc. The ammonia derivatives are either solids or liquids, which makes their transportation by barge, rail or truck much easier hence much cheaper.

Four ammonia plants, three of which are in activity, are owned by companies specialized in explosives. Their output is almost entirely converted in to ammonium nitrate then mixed with fuel oil to yield ANFO. Even though the recent high prices for fertilizers have pushed the companies to sell part of their production of ammonium nitrate as fertilizer, their role in the fertilizer market is negligible.

One ammonia plant is part of an industrial complex that makes plastics. Again the output of the plant is used almost entirely in the production of plastics. However the company does offer to sell fertilizers. But because the plant is on the east coast, it is too far away from the main market for fertilizers and is confined to the local market. Thus this plant has minimal impact on the fertilizer industry.

b. The second method designed to transport ammonia is to use dedicated pipelines. Two such pipelines have been built to connect the manufacturing plants to the plants producing commercial fertilizers or to the final agricultural customers. They are roughly parallel and span most of the Midwest. The western one originates in northern Texas and Oklahoma and runs north-east. The eastern one originates near New Orleans, first runs north then meanders through the Midwest; it can receive imported ammonia.

Figure 2: Ammonia Pipelines (the owners have changed)

The two pipelines together connect 9 of the 21 plants producing ammonia for the fertilizer market with storage and distribution terminals and with other processing plants throughout the Midwest. The cost of moving one metric ton of ammonia from one end to the other is about $30; in general the cost is roughly proportional to the distance travelled [8].

c. The companies that do not have access to the pipeline transport their ammonia over long distances by rail and usually own a fleet of competent cars. Rail is usually more expensive than pipelines because the competent cars are costly to purchase and maintain [9].

d. Trucks with refrigerated and pressurized tanks are used to move ammonia by road. This means is very expensive because the quantities involved are small [9].

Thus the four methods to transport ammonia are to further process ammonia into liquid or solid fertilizers and to transport these; to make use of a dedicated pipeline; to ship it by rail in pressurized and refrigerated cars; to ship it in trucks with similar tanks. Every company uses a combination of these four methods. A classical strategy is as follows:

- Process part of the ammonia into a solid or liquid fertilizer and supply these to the local market by barge, rail or road.

- Transport the ammonia over long distances through the pipeline or by rail. At the destination, it is either stored or processed into other fertilizers.
- The delivery to the final customer is usually made by truck.

The structure of the distribution system and the prominent role of pipelines have two major consequences. First foreign ammonia usually arrives in the Gulf of Mexico and enters the eastern pipeline. Thus the imports of ammonia do not face obstacles in distribution and storage. Consequently the main Midwestern market does not distinguish between the two supplies and imports and domestic production are on the same level. Second about 60% of domestic production takes place in the states bordering the Gulf of Mexico and most imports are delivered there therefore the price of ammonia in the Gulf of Mexico has become the reference and determines the prices paid elsewhere.

DEMAND

Since 2000 the high and volatile prices of natural gas have rendered many plants unprofitable and forced the definitive closure of about 35% of the installed capacity. Indeed the prices of ammonia remained low because of readily available imports. Hence the current production capacity of the United States is well below its internal demand, which has turned the country into the biggest importer of ammonia in the world [7]. We examine in order the demand, the domestic supply and the foreign supply.

The demand curve results from the four distinct uses downstream: manufacturing of explosives, industrial solvent and refrigerant, manufacturing of fibers and plastics and fertilizers. These segments are quite different so their respective demands do not overlap. They are described below.

Demand for ANFO and other explosives has markedly increased in the past years because the boom in commodity prices spurred a dramatic increase in mining. The demand will be lower in the coming years but remain close to the current heights. This demand is at the top of the demand curve and price insensitive as mining companies absolutely need explosives in their current operations. Ammonia consumption by the manufacture of explosives is small when compared to fertilizers but large when compared to the two other segments. Part of this ammonia is bought on the open market, part is produced in integrated facilities that churn out the final product, usually ANFO; the ammonia produced by integrated facilities is effectively out of the market.

Annual consumption of ammonia for industrial use is tiny but this demand must be satisfied as industrial processes cannot be easily altered. The cost of ammonia for the operation of these processes is minimal therefore this demand is price insensitive and shares the top of the demand curve with the segment of explosives.

Demand for ammonia for the manufacturing of fibers and plastics is steady. It is also price sensitive because the various manufacturers have the ability to trade in the downstream products and can import intermediaries. Thus this segment is the second component of the demand curve.

Finally the agricultural segment is on the lowest part of the demand curve and because of its sheer size it is the swing segment that determines the prices on the open market. In recent years the high prices of cereals have prompted farmers to increase the surfaces cultivated. Furthermore the state and foreign incentives to produce biofuels have induced a shift in cultivation from less fertilizer demanding crops, such as soybeans, towards more fertilizer demanding crops, such as corn and wheat. Consequently yearly demand of ammonia for agricultural uses is expected to remain as high as in the previous years or to increase slightly. In recent years the monthly volatility of ammonia prices has increased dramatically because the high prices have prompted farmers to adopt opportunistic behavior, which has exaggerated the usual seasonal variations.

SUPPLY

Domestic production of ammonia can no longer fulfill demand, even if all plants function at full capacity. Currently three plants are idle because they cannot produce ammonia at competitive prices; two other plants are closed because the owners modify the process by substituting coal gasification and petroleum coke to natural gas as a source of hydrogen and energy. Thus 22 plants currently produce ammonia and they function at 80% of their capacity. These plants have been investigated to construct the ammonia domestic supply curve.

Two plants that produce ammonia for the ANFO explosive and one plant that produces ammonia for the manufacturing of fibers and plastics were left out of the supply curve because they are part of large integrated complexes. The ammonia produced by these plants does not enter the main market; ammonia produced by these plants is preferred to the one from the open market because there are no transportation costs. The demand satisfied by these three plants is simply subtracted from the total demand and the result is called general demand as this is the demand affecting the open market.

The domestic supply curve is constructed by determining the cost of producing ammonia at each plant then arranging the plants from the lowest cost producer to the highest cost producer. The cost of producing ammonia is the sum of the cost of operation and of the cost of natural gas. The cost of operation is taken to be the same for all plants, $50 per metric ton; the value was determined from the Kirk-Othmer Encyclopedia of Chemical Technology [4]. The cost of natural gas is the product of the price of a natural gas, $/GJ, and of the efficiency of the plant, GJ/metric ton. The efficiency of the plants was determined through several methods:

- The efficiency for the plant was given on the website of the company.
- The history of the plant was given on the website and a number was assigned depending on the last upgrade; the more recent the upgrade, the lower the amount of natural gas required per ton of ammonia.
- When absolutely no information was given, the plants kept idle were attributed poor efficiencies corresponding to the state-of-the-art in the 1970's when most plants were built; the remaining producing plants were given equal efficiencies and the values were determined so that the average efficiency over all plants is the same as the average efficiency of the United States, 38 GJ/metric ton.

Another plant receives an ad hoc treatment because it makes use of petroleum coke instead of natural gas. Its cost of operation is assumed to be the same as those of a natural gas plant and the efficiency is set at 28 GJ/metric ton, close to 27 GJ/metric ton, which is the best currently available; this reflects the low cost of the source of energy and hydrogen. One company produces natural gas from coal gasification and either sells it in the open market or uses it in the production of ammonia; the efficiency of this plant is unknown and has been set at 38 GJ/metric ton, the average for the United States, because the company can always arbitrate between selling natural gas or manufacturing ammonia so the price of natural gas has an impact on the production of ammonia.

In a nutshell the domestic supply curve is determined by the efficiency of natural gas utilization at the plants. Non-gas operating costs vary little in comparison with the cost of natural gas therefore they were taken to be the same for all plants and equal to $50 per metric ton. Distribution costs were ignored because all plants face the same difficulties and have adopted similar strategies hence the cost of transportation has little impact on the decision whether to operate a plant or not. The impact is reflected in the price difference between the local farmer's market and the Gulf of Mexico that serves as reference.

In 2007 almost all ammonia is imported from five countries:

- Trinidad and Tobago   56 %
- Canada   15 %
- Russia   12 %
- Ukraine   10 %
- Venezuela   4 %

Again the cost of production is affected by the cost of operation and the cost of natural gas as most plants in these countries make use of natural gas. In Canada the cost of operation is virtually the same as in the United States and average natural gas efficiency for the country is 33.1 GJ/metric ton; the price of natural gas is strongly tied to the price in the United States but usually slightly lower; for instance in 2007 the average industrial price for natural gas was $7.22 in the United States [1] and $5.85 in Canada [10]. Furthermore since most plants are near the border with the United States, transportation costs are approximately the same as for domestic plants hence there is no transportation penalty.

In Russia, Ukraine, Venezuela and Trinidad and Tobago the cost of operation is lower because the construction of plants is cheaper and because the other manufacturing costs are minimal. The foreign exchange rates have an impact too. For simplicity the cost of operation was set at $30/metric ton. The natural gas efficiency is set at 40.4 GJ/metric ton in Russia and Ukraine, which is the average value of the lower world tercile [6]; these countries have Soviet era plants that are usually inefficient. The natural gas efficiency is set at 38.6 GJ/metric ton in Venezuela and Trinidad and Tobago, which is the average world efficiency in the production of ammonia [6]; in these countries most plants have been built in the 1990's and 2000's so they are modern and efficient, albeit not as efficient as the ones in Canada or Western Europe where the high cost of natural gas encourages regular investments in plant optimization.

Ammonia from the last four countries is imported using pressurized and refrigerated tankers. Maritime freight rates incurred are $30/metric ton for Trinidad and Tobago, $35/metric ton for Venezuela and $87.5/metric ton for Russia and Ukraine [11].

A summary of the foreign supply is given in Appendix 3.

AMMONIA MARKETS

The domestic supply curve is combined with five foreign suppliers. The capacity of the foreign suppliers is set at the actual quantities imported in 2007; the cost of ammonia is

the one determined using the method described above. Domestic plants and foreign suppliers are ordered by increasing cost of production.

The domestic demand is assumed to be inelastic. The prices of agricultural crops are high so farmers have already decided how much to plant. Thus the quantities of fertilizer required are already determined and farmers have little flexibility. To the domestic demand were added the exports.

Indeed exports of ammonia from the United States have become minuscule and have little impact on the domestic industry. The whole production of a plant in Alaska used to be exported to South Korea and this constituted the largest portion of exports. Currently that plant is closed for want of natural gas and the exports have dwindled to negligible quantities.

The result of the crossing of the demand and supply curves is consistent with what was observed, i.e. imports are on the lower side of the supply curve, three domestic plants are idle and 22 produce at 80% of their stated maximum capacity. The detailed result is in Appendix 4.

On one side almost all American plants use natural gas as a source of hydrogen and energy so since 2000 soaring natural gas prices have considerably increased their cost of producing ammonia. On the other side, in Trinidad and Tobago, Russia, Ukraine and Venezuela, the industrial price of natural gas has remained low, low enough to compensate for the cost of maritime transportation and to yield significant profits. Thus until 2007 the price of ammonia did not rise as much as the cost of domestic production. The result was that inefficient plants became unprofitable and were forced to close. Between 2000 and 2008, the total number of plants has fallen from 40 to 25, with only 22 currently in operation; total capacity has fallen from 20 million metric tons to 12.4 million metric tons [12]. Consequently in 2007 domestic production represents only 59% of domestic consumption.

The evolution in the number of plants between1990 and 2007 is given below [12].
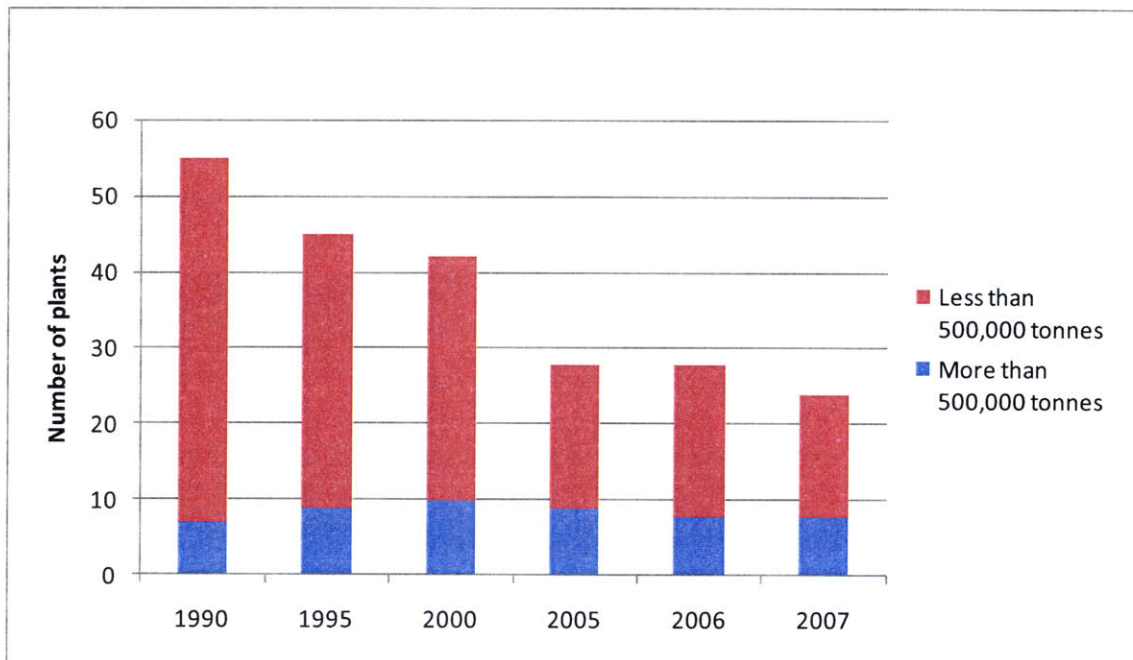
Figure 3: Number of ammonia plants in the U.S.

From 1990 to 2000, the ammonia industry was consolidating with small plants being closed and decommissioned and a few large plants being open. Production was on an upward trend. Between 2000 and 2007 the ammonia industry was in decline with many small plants were being closed and decommissioned and several large plants being idled for extended periods. Production has been on a marked downward trend.

Canadian plants are much more efficient than American plants in their use of natural gas and usually face similar prices for natural gas therefore ammonia produced in Canada is cheaper; consequently Canadian plants can export almost all their surplus to the United States [6]. Nevertheless the high cost of natural gas in Canada precludes the construction of additional plants. Thus Canadian imports are expected to remain the same in volume.

Trinidad and Tobago is the largest foreign supplier of ammonia to the United States. It is a Caribbean island with large reserves of natural gas; most of it is exported in liquefied form. The national gas company also provides cheap natural gas for local industrial use, prompting many foreign corporations to build plants and to export processed goods. The country gains by exporting products with a higher value added than mere natural gas. Ammonia is one of the industries that flourished under this policy. The companies building and operating the ammonia plants are the same as in the United States. Virtually all the ammonia produced in Trinidad and Tobago is exported to the United States. As the demand for ammonia increases in the United States, more plants are built in Trinidad and Tobago to fulfill this demand. The

phenomenon is that of delocalizing production close to a stable source of cheap natural gas.

Venezuela also has large reserves of natural gas that it aims at exporting. However political instability has discouraged investments both in the extraction of natural gas and in the production of ammonia. The situation is so dire that Venezuela exports the majority of its natural gas through the port terminals in Trinidad and Tobago. The production and exports of ammonia have remained essentially unchanged for years; all the surplus production is absorbed by the American market.

Russia and Ukraine have large chemical industries inherited from the Soviet era. They have large capacities for producing ammonia and use most of it internally or export it to Western Europe. Since 2001 they have started to export ammonia to the United States because the price of ammonia has risen to a level that compensated for the cost of transportation from the Black Sea to the Gulf of Mexico. Their share of total imports has grown overall but it is unsteady because local producers constantly weigh the opportunity of exporting to Western Europe, the Middle East or the United States. Unlike Canada, Trinidad and Tobago and Venezuela, there is spare capacity in Russia and Ukraine so these countries constitute an important adjustment factor.

In the business as usual view the demand for fertilizers and consequently for ammonia is forecasted to remain stable or to increase slightly in the coming years. The price of ammonia is expected to remain high so no domestic plant is expected to close. A large brand new plant is scheduled to start producing in 2010 and it is located on the eastern pipeline close to New Orleans; it is supposed to be state-of-the-art so it will be able to produce competitively; it also has agreements with established companies in order to commercialize its production. Thus domestic production will increase from 2010 onwards and displace part of the imports. The imports displaced first should be those from Ukraine because the price of natural gas in Ukraine is bound to increase as a consequence of the repeated energy quarrels with Russia.

In the medium term the fate of the ammonia industry in the United States depends on the willingness of the corporations to modernize their plants and make them more efficient in their use of natural gas; they should be able to become fully competitive with imports and reclaim part of the domestic market. The high or volatile price of natural gas discourages the construction of new facilities so 30% to 40% of domestic consumption would be satisfied by imports. Failing to modernize plants would result in progressive loss competitiveness, gradual closure of unprofitable plants and in ever higher imports.

Canada and Trinidad and Tobago will remain very important stable suppliers of ammonia. The supply from Venezuela is unpredictable because it is tied to the political fate of the country. Russia and Ukraine will remain swing foreign suppliers because of the inherently opportunistic behavior of the local companies.

ETHANOL AND THE AMMONIA MARKET

The business as usual view of the ammonia market does not take into account the development of ethanol as a fuel for transportation. Currently 155 million barrels of ethanol are produced and used in transportation, which represents 4.5% of total motor gasoline consumption in the United States [13]. Almost all ethanol is manufactured by grinding and fermenting corn then distilling the broth into ethanol. Therefore a mandated increase in the proportion of ethanol to be used for transportation – for instance 15% or 20% of transportation fuel must be ethanol – would have a dramatic impact on the corn market and consequently on the ammonia market since corn is the crop requiring most fertilizer; the proportions are given on a per volume basis.

To quantify the relationship between the consumption of ethanol and ammonia, the study examines the impact of a mandate that 15% or 20% of all transportation fuel consumed in the United States be renewable, i.e. is derived from ethanol as ethanol is the only scalable option in the near term. An important assumption underpins this work: the tariffs on ethanol are to remain high and effectively discourage imports. The full analysis is available in Appendix 5. The main results are discussed below:

- With a 15% or 20% mandate, the manufacturing of ethanol would require an additional 139.5 or 206.5 million metric tons of corn. In 2007 62.0 million metric tons of corn were exported. Thus a mandated increase in the use of ethanol has the potential to reduce to zero the exports of corn. However this is unlikely because the United States are by far the biggest exporter of corn with 60% of world exports and any significant drop in exports would dramatically increase the price of corn prompting farmers to increase cultivation. Nevertheless the policy would create tension enormous tension on corn prices worldwide and would upset the main corn importers: Japan, Taiwan and South Korean followed by Middle Eastern countries. Argentina, the second biggest corn exporter would respond to the high prices by expanding its production but it would be unable to compensate for a significant drop in American exports.
- It is very difficult to forecast the reduction in exports induced by a 15% or a 20% mandate. Therefore the study adopts a scenario in which the proportion of corn

exports diverted to domestic ethanol production is fixed at 25% of the additional demand for corn. Once this parameter is set, it follows that the domestic production of corn in the United States would have to increase by 42% or 62%. It follows that 27.3 or 40.5 million acres are required to produce the additional quantity of corn, corresponding to a 32 % or 47 % increase in the surfaces devoted to corn. This would represent a major shift in cultivation patterns, which have been stable for decades; it would also put an end to the practice of rotating between corn, a crop that depletes the soil of nutrients, and alfalfa or soybean, two crops that replenish soil with nutrients; abandoning rotations would severely degrade the quality of soil in time.

- Growing these large additional quantities of corn, while not sacrificing other crops, would require the utilization of an additional 2.1 or 3.1 million metric tons of ammonia, representing an increase of respectively 13.3 % or 19.7 %. In both cases the additional demand for ammonia will be only partly satisfied by the new plant scheduled to start operating in 2010; two outcomes are possible: either the large increase in domestic demand prompts the modernization and reopening of the idle plants, which would limit imports; or all the additional ammonia would have to be imported from Russia, Ukraine and Trinidad and Tobago, which would represent a considerable increase in imports. Note that if such a mandate is enacted and the second scenario occurs, the idle plants would miss a golden opportunity to modernize and restart production and would be condemned to close definitively.

- A mandate for ethanol to become a significant proportion of total motor fuel would have an impact on the market for natural gas too. The distillation of ethanol requires 10.7 MJ per liter; the ammonia entering in the growing of corn contributes 1.5 MJ per liter. Thus the manufacture of a liter of ethanol requires a total of 12.2 MJ of natural gas. The main consequence is that a 15 % or a 20 % mandate would induce an additional consumption of natural gas amounting to 682 PJ or 1009 PJ and representing 9.5 % or 14.0 % of the total natural gas used by the American industry.

ETHANOL AND THE EMISSIONS OF CARBON DIOXIDE

One of the arguments in favor of expanding the use of ethanol is that part of its carbon content is derived from the atmosphere through corn. Thus net emissions from the combustion of ethanol should be lower than the emissions from the combustion of gasoline. This assertion is investigated using the simple cycle shown below.
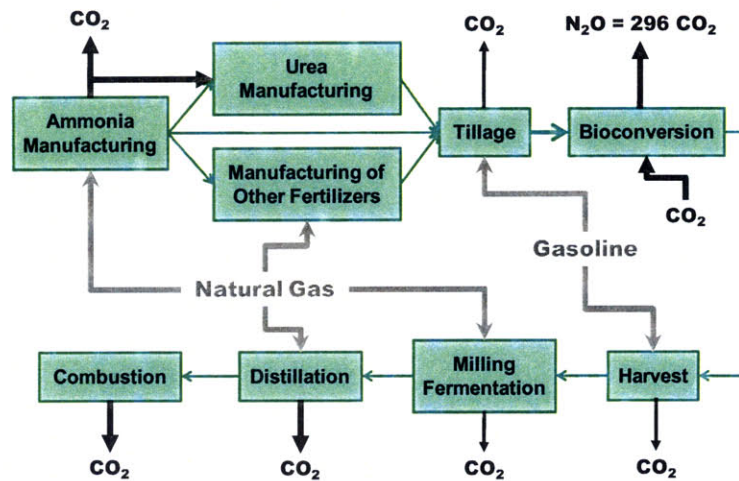
Figure 4: Cycle of ethanol and ammonia

The main emissions of carbon dioxide stem from the manufacturing of ammonia, the distillation of ethanol and final combustion. Furthermore the absorption of ammonia into soil is very effective albeit not complete; the consequence is the emission 1% to 4% of nitrogen as nitrous oxide, a greenhouse gas estimated to be 296 times more efficient than carbon dioxide [14]. Nitrous oxide also reacts with ozone however its overall impact on the ozone layer is unknown. Furthermore tillage and harvesting also result in emissions of carbon dioxide because agricultural machinery is powered by gasoline; the milling and fermentation of corn use some natural gas and electricity which translates into more emissions of carbon dioxide. Nevertheless the emissions from these last operations are negligible when compared to the main ones.

The main absorption of carbon dioxide from the atmosphere stems from the growth of corn plants; moreover emissions of carbon dioxide are markedly reduced when the manufacturing of urea takes place near an ammonia plant because part of the carbon dioxide in the waste stream is used as feedstock in the production of urea.

The calculations take into account the emissions from the production of ammonia, from the incomplete absorption of fertilizers, from the distillation of ethanol and from its combustion; they also include the recycling of carbon dioxide into urea and the absorption of carbon dioxide by the growth of corn plants. Calculations are detailed in Appendix 6.

The main finding is that the use of ethanol as a motor fuel increases the overall emissions of greenhouse gases. Indeed an average car using gasoline would emit about 23 kg of carbon dioxide per 100 km whereas using ethanol it would emit between 26 kg and 32 kg per 100 km. This comparison with gasoline is confirmed by another comparison with natural gas: burning 1 GJ of natural gas approximately yields 50 kg of

carbon dioxide whereas burning 1 GJ of ethanol yields between 75 kg and 94 kg of carbon dioxide.

For ethanol the first contributor to the emissions of carbon dioxide is, as expected, the direct combustion; the second is the distillation of ethanol; the third is the nitrous oxide emitted because of the incomplete absorption of nutrients; the emissions resulting from the manufacturing of ammonia come a distant fourth. The emissions of carbon dioxide are given as a range because the emissions of nitrous oxide are not well known; the literature gives a range of 1 % – 4 % of total nitrogen applied to the field. The other figures are reliable.

A further source of uncertainty is the amount of carbon dioxide captured from the atmosphere by a corn field; the estimate is unreliable because it depends on what happens to the field after the harvest:

- The field can be ploughed with all the stover and left to rest. The practice is called conservative tillage. The least carbon dioxide is reemitted because the stover rots and is incorporated in the soil.
- Cattle or other ruminants may be brought for grazing; afterwards the field is ploughed. More carbon dioxide equivalent is emitted than previously because the metabolism of cows generates methane, which is 25 times more potent than carbon dioxide as a greenhouse gas.
- Most stover is collected and used as fodder. The field is ploughed to aerate it. The soil is allowed rest for a few months. Little carbon dioxide is incorporated into the soil. The overall carbon balance of the soil is close to zero. This is the most common practice.
- Corn stover may be collected and used as primitive fuel. The field is repeatedly ploughed in depth and allowed little rest before new sowing. This practice is called intensive tillage. Hardly any carbon dioxide is incorporated to the soil. The carbon balance is negative.

These practices vary hugely from one region to another; they also vary in time. No aggregate figures are available from USDA or another government agency. Hence the average figure for the capture of carbon dioxide by the corn crop – 486 kg per acre of corn – is an estimate based on a few field studies from Canada [15]. Nevertheless this source of uncertainty does not have a large impact on the final figures because the sensitivity is low, i.e. increasing the amount of carbon dioxide absorbed by 50 kg/acre results in reducing overall emissions of carbon dioxide by 0.7 kg every 100 km. Furthermore a safe assumption is that a large increase in the production of corn in the

United States will result in tillage becoming more intensive and in less carbon dioxide captured in soil because intensive tillage increases yields in the short run.

CONCLUSION

The production of ammonia in the United States uses large quantities of natural gas both as a source of hydrogen and as a source of energy. Therefore natural gas represents 80 % to 90 % of the cost of manufacturing ammonia and the price of ammonia is strongly correlated to the price of natural gas. Furthermore ammonia is the base ingredient for all nitrogenous fertilizers, which are used in large quantities on cereal and fruit crops. Thus ammonia is the main link between natural gas and agriculture with the consequence that 10 % to 30 % of the cost of producing cereals and fruits can be attributed to natural gas.

The United States is the second largest consumer of ammonia in the world but only the fourth largest producer; as a result it is the largest importer of ammonia. The current situation results from the combination of several unfavorable factors:

- Most American plants are inefficient in their use of natural gas.
- The price of natural gas has been high and volatile since the turn of the century.
- Ammonia can be imported from several countries that produce it at low cost.

Domestic ammonia prices have not risen as fast the price of natural gas hence numerous plants have become unprofitable and have been forced to close sometimes temporarily but more often definitively. Domestic production accounted for only 62 % of domestic consumption in 2007.

The high prices of ammonia have not compelled farmers to reduce their use of nitrogenous fertilizers because the prices of cereals have risen in parallel. In particular the production of corn, the crop requiring most fertilizer, has increased in recent years because of mandates promoting the use of ethanol as motor fuel in combination with gasoline. A short analysis shows that approximately half of the energy in a gallon of ethanol originates in the natural gas consumed by the distillation of corn and by the manufacturing of the ammonia required to grow the corresponding corn grains. Furthermore a mandate requiring that 20 % of motor fuel by volume be ethanol would require a 62 % increase in the production of corn from the level of 2007; the exports of corn would collapse; in parallel industrial consumption of natural gas would increase by 14 %.

A second analysis compared the emissions of greenhouse gases resulting from the combustion of natural gas, gasoline, ethanol and E85. The results show that the combustion of one gigajoule of ethanol yields approximately three times as much carbon dioxide as the combustion of one gigajoule of natural gas. Moreover the overall emissions of carbon dioxide from motor fuels are lower for gasoline than for ethanol or E85 on a per mile basis. The main uncertainty factor in the analysis is the net amount of carbon dioxide absorbed by an acre of corn; however sensitivity analysis shows that the impact of this factor is limited and hardly influences the final figures.

The first main conclusion from this study is that the American ammonia industry has suffered in the past decade from the high prices of natural gas and foreign competition. The decline seems to have ceased recently because the prices of ammonia have increased considerably. The second main conclusion is that substituting ethanol to gasoline as a motor fuel shifts the dependence from oil to natural gas and barely alleviates; it results overall in more energy consumption and more emissions of greenhouse gases; it also rocks domestic agriculture and cereal markets; it encourages the most intensive and least sustainable agricultural practices.

BIBLIOGRAPHY

1. EIA Natural Gas Summary (*tonto.eia.doe.gov/dnav/ng/ng_sum_lsum_dcu_nus_a.htm*)
2. USGS 2007 Minerals Yearbook – Nitrogen
3. Britannica Online: article on explosives, section on modern high explosives
4. Kirk-Othmer Encyclopedia of Chemical Technology – Ammonia
5. USGS Mineral Commodity Study 2009 – Nitrogen
6. Natural Resources Canada – Benchmarking Energy Efficiency and Carbon Dioxide Emissions
7. USDA – Impact of Rising Natural Gas Prices on U.S. Ammonia Supply
8. NuStar Energy (*www.nustarenergy.com/Customers/Pages/PipelineTariffs.aspx*)
9. United Nations Industrial Development Organization – International Fertilizer Development Center: Fertilizer Manual, Kluwer Academic Publishers, 1998
10. Natural Resources Canada – Review of 2007/2008 North American Natural Gas Demand
11. Potash Corporation – N-P-K Outlook 2006 and 2009 Q1 Market Analysis
12. USGS Minerals Yearbook – Nitrogen (from 1991 to 2007)
13. EIA – Petroleum Supply
14. P. J. Crutzen, A. R. Mosier, K. A. Smith, W. Winiwarter, Atmospheric Chemistry and Physics Discussions 7, 11191 - 11205, 2007
15. Ontario Corn Producers Association (*www.ontariocorn.org/envt/envclim.html*)

APPENDIX 1
COMMON AMMONIA MANUFACTURING PROCESS

Natural Gas → **Compression and Heating** → **Desulfurization** → **Primary Reforming** (Steam, Q)

from 1 atm to 30 – 40 atm
from 25°C to 350 - 400°C

from 1 – 5 ppm to less than 1 ppm
typically done on a bed of ZnO

750 – 800°C and catalysts using nickel or precious metals

CO_2 ↑ **CO_2 scrubbing** ← Water ↑ **Cooling and Bulk Water Removal** ← **Shift Conversion** ← **Secondary Reforming** (Air)

Absorber – stripper system (<1000 ppm)

Water condensation close to 25°C

$CO \rightarrow CO_2$ in two steps

1000 – 1200°C and partial combustion of remaining alkanes

H_2 ↓ **Methanation** → **Desiccation** → **Compression and Heating** → **Ammonia Synthesis**

To remove residual CO and CO_2 (nickel catalysts)

Molecular sieves reduce water content to < 1 ppm

8 – 40 atm and 350 – 550°C

Iron or ruthenium catalysts

CO_2 from scrubbing can be recycled and used in other processes (synthesis of urea)

NH_3 at − 33°C ← **Refrigeration**

NH_3

Anhydrous NH_3	**NH_4NO_3**	**HNO_3**	**Explosives**
NH_3 solutions	**$(NH_4)_2SO_4$**	**Animal Feed**	
Aqueous NH_4OH	**Urea**	**Melamine**	
Other fertilizers	**$(NH_3)_2HPO_4$**	**Acrylonitrile**	
Industrial Solvent	**$NH_3H_2PO_4$**	**HCN**	

APPENDIX 2
AMMONIA PLANTS IN THE UNITED STATES

US average efficiency for ammonia plants			38.0 GJ/metric ton

Company	Location	Capacity	Efficiency	
Agrium Inc.	Borger, TX	490	40.0	no information about efficiency
	Kenai, AK	280	40.0	closed - production using coal gasification planned in 2012
CF Industries, Inc.	Donaldsonville, LA	2,040	38.0	no information about efficiency
Coffeyville Resources, LLC	Coffeyville, KS	400	X	production with petroleum coke not natural gas – integrated facility
Dakota Gasification Co.	Beulah, ND	360	38.0	production with gas from coal gasification
Dyno Nobel Inc.	Cheyenne, WY	175	X	production chiefly used to manufacture explosives
	St. Helens, OR	100	X	no information on efficiency - integrated manufacturing
Green Valley Chemical Corp.	Creston, IA	35	38.3	32,000 cubic feet of gas per short ton of NH3 - close to US average
Honeywell International Inc.	Hopewell, VA	530	39.0	no information on ammonia plant
Koch Nitrogen Co.	Beatrice, NE	265	40.0	no information on ammonia plant
	Dodge City, KS	280	40.0	no information on ammonia plant
	Enid, OK	930	40.0	no information on ammonia plant
	Fort Dodge, IA	350	40.0	no information on ammonia plant
	Sterlington, LA	1,110	43.0	closed - no information on efficiency
LSB Industries, Inc.	Cherokee, AL	160	38.0	ammonia used as precursor for fertilizers, nitric acid and explosives
	Pryor, OK	300	42.0	idle plant - no information on efficiency
Mosaic Co., The	Faustina, LA	510	38.0	no information on ammonia plant
PCS Nitrogen, Inc., LP	Augusta, GA	690	37.0	given on website
	Geismar, LA	480	X	production of ammonia suspended indefinitely
	Lima, OH	585	37.0	given on website
	Memphis, TN	370	X	idle since 2003 – not listed on company website – condemned ?
Rentech Energy Midwest Corp.	East Dubuque, IL	260	39.0	no information on efficiency
US TransCarbon	Faustina, LA	1,200	27.0	starts producing in 2010
Terra Industries Inc.	Beaumont, TX	230	42.0	sold to Eastman Chemical – production using petroleum coke in 2011
	Donaldsonville, LA	450	38.0	swing producer – closed in 2003, modernized in 2007, restarted in 2008
	Port Neal, IA	340	28.5	rebuilt in 1995 – state of the art then
	Verdigris, OK	950	34.0	regularly upgraded plant
	Woodward, OK	400	30.0	modernized in the 1990's
	Yazoo City, MS	450	34.0	modernized in the 2000's
Total Capacity		12,440		
Active Capacity		10,750		
Idle Capacity		1,690		
Average Efficiency			38.0	

The capacity is in thousands of metric tons. The efficiency is in GJ of natural gas per metric tons.
The main source is the US Geological Survey, 2007 Minerals Yearbook – Nitrogen. It is updated using the company websites.

Company	Location	Distribution			
		Pipeline	River	Rail and road	Maritime
Agrium Inc.	Borger, TX	X			
	Kenai, AK				X
CF Industries, Inc.	Donaldsonville, LA	X	X	X	
Coffeyville Resources, LLC	Coffeyville, KS			X	
Dakota Gasification Co.	Beulah, ND			X	
Dyno Nobel Inc.	Cheyenne, WY			integrated	
	St. Helens, OR			integrated	
Green Valley Chemical Corp.	Creston, IA			X	
Honeywell International Inc.	Hopewell, VA			integrated	
Koch Nitrogen Co.	Beatrice, NE	X		X	
	Dodge City, KS			X	
	Enid, OK	X		X	
	Fort Dodge, IA			X	
	Sterlington, LA	X		X	
LSB Industries, Inc.	Cherokee, AL		mostly integrated		
	Pryor, OK			X	
Mosaic Co., The	Faustina (Donaldsonville), LA	X	X	X	
PCS Nitrogen, Inc., LP	Augusta, GA			X	
	Geismar, LA		X	X	
	Lima, OH			X	
	Memphis, TN		X	X	
Rentech Energy Midwest Corp.	East Dubuque, IL			X	
US TransCarbon	Faustina, LA	X	X	X	
Terra Industries Inc.	Beaumont, TX			X	
	Donaldsonville, LA	X	X	X	
	Port Neal, IA	X		X	
	Verdigris, OK	X		X	
	Woodward, OK			X	
	Yazoo City, MS		X	X	

There are two large pipelines for ammonia:
- The western one originates in Texas and Oklahoma and runs far to the west of the Mississippi river. It can transport only domestic ammonia.
- The eastern one originates near New Orleans and runs on just west to the Mississippi river. It can transport imported ammonia.

Both pipelines connect plants, storage sites and distribution terminals. They cover the whole Midwest.

APPENDIX 3
IMPORTS OF AMMONIA IN 2007

	Prices of Natural Gas	Plant Efficiency	Manufacturing Costs	Maritime Freight Rates	Cost of Imported Ammonia	Total Production
Trinidad & Tobago	2.50	38.6	30	30.0	157	6,200
Russia	1.00	40.4	30	87.5	158	12,800
Ukraine	5.20	40.4	30	87.5	328	5,100
Canada	5.85	33.1	50	0.0	244	5,000
Venezuela	1.00	38.6	30	35.0	104	1,400

Numbers from 2007.

Price of Natural Gas	$/GJ
Average Plant Efficiency	GJ/tonne NH3 LHV
Manufacturing Costs	$/tonne NH3
Maritime Freight Rates	$/tonne NH3 delivered to the Gulf of Mexico
Cost of Imported Ammonia	$/tonne NH3 in the Gulf of Mexico

Maritime freight rates are from Potash Corporation, Overview of Nitrogen Markets.
They are subject to large changes in short periods.

Prices of natural gas are from Natural Resources Canada, Review of 2007/2008 North American natural gas demand
and from Potash Corporation, The N-P-K Outlook 2006 and from the 2009 Q1 Market Analysis.
Some of these prices are further quotes from Fertecon, a consultancy specialized in fertilizer markets.

Manufacturing costs are from the Kirk-Othmer Encyclopedia of Chemical Technology.

Average plant efficiencies are adapted from a study by the Canadian Industry Program for Energy Conservation:
Benchmarking Energy Efficiency and Carbon Dioxide Emissions.

APPENDIX 4
AMMONIA MARKET CLEARING

		Efficiency	Cost of a tonne of ammonia	Capacity	Production	Cumulative Production
Domestic Price of	Venezuela		104	270	270	270
Natural Gas ($/GJ)	Trinidad & Tobago		157	4,360	4,360	4,630
7.07	Russia		158	1,640	1,640	6,270
	Canada		244	920	920	7,190
Manufacturing Cost	Coffeyville, KS	28.0	248	400	412	7,602
of Ammonia ($/tonne)	Port Neal, IA	28.5	252	340	350	7,952
50.00	Woodward, OK	30.0	262	400	412	8,364
	Verdigris, OK	34.0	290	950	979	9,343
	Yazoo City, MS	34.0	290	450	464	9,806
Total Demand	Augusta, GA	37.0	312	690	711	10,517
18,633	Lima, OH	37.0	312	585	603	11,119
	Donaldsonville, LA	38.0	319	2,040	2,101	13,221
General Demand	Beulah, ND	38.0	319	360	371	13,591
17,804	Cherokee, AL	38.0	319	160	165	13,756
	Faustina, LA	38.0	319	510	525	14,282
Production Level	Donaldsonville, LA	38.0	319	450	464	14,745
103%	Creston, IA	38.3	321	35	36	14,781
	East Dubuque, IL	39.0	326	260	268	15,049
	Ukraine		328	350	350	15,399
	Enid, OK	40.0	333	930	958	16,357
	Borger, TX	40.0	333	490	505	16,862
	Beatrice, NE	40.0	333	265	273	17,134
	Dodge City, KS	40.0	333	280	288	17,423
	Fort Dodge, IA	40.0	333	350	361	17,783
	Beaumont, TX	42.0	347	230	237	18,020
	Pryor, OK	42.0	347	300	309	18,329
	Sterlington, LA	42.0	347	1,110	1,143	19,473
	Domestic Production for General Market			10,243		
	Imports			7,540		
	General Demand Satisfied			17,783		
	Total Domestic Production			11,073		
	Total Demand Satisfied			18,613		

The quantities of ammonia are given in thousands of metric tons.

The general demand is the total demand without the consumption for plastics and part of the consumption for explosives because the corresponding plants are part of integrated facilities that use the output internally. This ammonia is effectively out of the market.

APPENDIX 5
ETHANOL, CORN AND AMMONIA

Natural Gas needed to produce 1 kg of ethanol	whole process including fertilizer and electricity	19.5	MJ/kg EtOH	from Jeremy Johnson's thesis
	only processing of corn	13.5	MJ/kg EtOH	
Ethanol Yield	volume of ethanol per unit weight of corn	2.7	gal/bushel	from USDA - ers.usda.gov/AmberWaves/April06/Features/Ethanol.htm
		0.4	L/kg	
Corn Yield	corn grain per unit surface	150.7	bushel/acre	2007 statistics
		3,828.0	kg/acre	from nass.usda.gov
Nitrogen Use	ammonia equivalent per unit surface	77.1	kg/acre	from ers.usda.gov/Data/FertilizerUse

Increases in

Ethanol Production	1,000	L	
Corn Consumption	2,485	kg	25% Percentage coming from the reduction in exports
Corn Cultivation	0.49	acres	
Ammonia Use	37.5	kg	
Natural Gas through NH3	1,502	MJ	assuming domestic production
Natural Gas from distillation	10,652	MJ	
Total Natural Gas	12,153	MJ	
Elasticity	12.2	MJ/L	Elasticity of natural gas consumption with respect to ethanol production

US Motor Gasoline consumption	3,389	mm barrels	2007	EIA
US Fuel Ethanol consumption	155	mm barrels	2007	EIA

Fuel EtOH under 5% mandate	169	mm barrels	mandate is by volume
Fuel EtOH under 10% mandate	339	mm barrels	
Fuel EtOH under 15% mandate	508	mm barrels	
Fuel EtOH under 20% mandate	678	mm barrels	

Additional corn consumption

				Corn cultivation in 2007 (higher than usual)	86,520,000	acres
5% mandate	5,611	ktonnes	1.7%	Corn production in 2007 (record production)	331,177	ktonnes
10% madate	72,571	ktonnes	21.9%	Corn exports in 2007 (record export year)	62,000	ktonnes
15% mandate	139,531	ktonnes	42.1%			
20% mandate	206,491	ktonnes	62.4%			

Additional corn cultivation

5% mandate	1,099,348	acres	1.3%
10% madate	14,218,606	acres	16.4%
15% mandate	27,337,864	acres	31.6%
20% mandate	40,457,122	acres	46.8%

Percentage relative to corn cultivation

Additional ammonia use

Ammonia consumption in 2007   15,800   ktonnes

5% mandate	84,760	tonnes	0.5%
10% madate	1,096,255	tonnes	6.9%
15% mandate	2,107,749	tonnes	13.3%
20% mandate	3,119,244	tonnes	19.7%

Percentage relative to ammonia consumption

Additional nat. gas through NH3

5% mandate	3,390,390	GJ
10% madate	43,850,182	GJ
15% mandate	84,309,974	GJ
20% mandate	124,769,765	GJ

Additional nat. gas from distillation

5% mandate	24,047,797	GJ
10% madate	311,026,214	GJ
15% mandate	598,004,631	GJ
20% mandate	884,983,048	GJ

Total consumption of natural gas in 2007   25,035,132,014   GJ
Total industrial consumption of natural gas in 2007   7,196,261,823   GJ

Total additional natural gas

5% mandate	27,438,187	GJ	0.38%
10% madate	354,876,396	GJ	4.93%
15% mandate	682,314,605	GJ	9.48%
20% mandate	1,009,752,814	GJ	14.03%

Percentages relative to industrial gas consumption

APPENDIX 6
COMPARISON OF CARBON DIOXIDE EMISSIONS

Production and utilization of 1000 L of ethanol

Production of NH_3	Natural gas consumption	1,502	MJ				
	CO2 generation	76	kg				
Production of urea	CO2 consumption	14	kg				

The production of fertilizers containing nitrogen consumes a negligible amount of natural gas and emits a negligible amount of carbon dioxide.

Application of fertilizer to soil	Amount of NH_3 equivalent	37.5	kg	ers.usda.gov/Data/FertilizerUse	
	Number of moles of N	2.208	kmoles		
	Emissions of N_2O - low hyp.	0.011	kmoles	1% of N applied emitted as N_2O	P. J. Crutzen, A. R. Mosier, K. A. Smith, W. Winiwarter, Atmospheric Chemistry and Physics Discussions 7, 11191 - 11205, 2007
	Emissions of N_2O - high hyp.	0.044	kmoles	4% of N applied emitted as N_2O	
	Equiv. CO_2 emitted - low hyp.	144	kg	$CO_2 = 296\ N_2O$ as a greenhouse gas	
	Equiv. CO_2 emitted - high hyp.	575	kg		
Plant growth	Net CO2 absorbed from atm.	486	kg	www.ontariocorn.org/envt/envclim.html	
Distillation of ethanol	Natural Gas Consumption	10,652	MJ		
	CO_2 Emission	536	kg		

Combustion of ethanol	Volume of ethanol	1,000	L	Energy density	23.4	MJ/L	source: www.ior.com.au/ecflist.html
	Number of moles of ethanol	17	kmoles	Total energy	23,400	MJ	source: www.ior.com.au/ecflist.html
	CO_2 emitted	1,507	kg				

Final Results	Natural gas consumed	12,153	MJ	underestimated because only the production of NH_3 and urea is accounted for
	CO_2 emitted - low hyp.	1,763	kg	underestimated the consumption of gasoline and other fossil fuels in farming and transportation is neglected
	CO_2 emitted - high hyp.	2,195	kg	
CO_2 Emitted by direct combustion of the natural gas		612	kg	

Based on 1 GJ of natural gas	Natural gas consumed	1,000	MJ	Energy from ethanol	1,000	MJ
	CO_2 emitted by dir. comb.	50	kg	CO_2 emitted - low hyp.	75	kg
Ethanol intermediation	CO_2 emitted - low hyp.	145	kg	CO_2 emitted - high hyp.	94	kg

	CO2 emitted - high hyp.		181	kg					
Tank of average car		40	L						
Efficiency of average car		10	L/100 km						
Distance travelled with full tank		400	km						
		249	miles						
Energy densities	Gasoline	34.2	MJ/L	source: www.ior.com.au/ecflist.html					
	Ethanol	23.4	MJ/L	source: www.ior.com.au/ecflist.html					
	E80	32.0	MJ/L	80% gasoline + 20% ethanol by volume					
Distance travelled with full tank	Gasoline	400	km		www.ior.com.au/ecflist.html				
	Ethanol	274	km		www.eia.doe.gov/oiaf/1605/coefficients.html				
	E80	375	km		CO_2 emissions	gasoline	19.564	lb CO_2 / gal	
$CO2$ emissions from full tank	Gasoline	94	kg				2.344	kg CO_2 / L	
	Ethanol	71	kg	low hyp.		ethanol	1.763	kg CO_2 / L	low hyp.
		88	kg	high hyp.			2.195	kg CO_2 / L	high hyp.
	E80	89	kg	low hyp.					
		93	kg	high hyp.					
CO2 emissions per 100 km	Gasoline	23	kg						
	Ethanol	26	kg	low hyp.					
		32	kg	high hyp.					
	E80	24	kg	low hyp.					
		25	kg	high hyp.					